NOTE TO USERS

This reproduction is the best copy available.

uOttawa

L'Université canadienne
Canada's university

FACULTÉ DES ÉTUDES SUPÉRIEURES ET POSTOCTORALES

uOttawa

L'Université canadienne
Canada's university

FACULTY OF GRADUATE AND POSDOCTORAL STUDIES

Emélie Braschi

AUTEUR DE LA THÈSE / AUTHOR OF THESIS

Ph.D. (Biochemistry)

GRADE / DEGREE

Department of Biochemistry, Microbiology and Immunology

FACULTÉ, ÉCOLE, DÉPARTEMENT / FACULTY, SCHOOL, DEPARTMENT

Characterization of the First Mitochondrial SUMO E3 Ligase, MAPL

TITRE DE LA THÈSE / TITLE OF THESIS

Heidi McBride

DIRECTEUR (DIRECTRICE) DE LA THÈSE / THESIS SUPERVISOR

CO-DIRECTEUR (CO-DIRECTRICE) DE LA THÈSE / THESIS CO-SUPERVISOR

Steffany Bennett

John Copeland

Douglas Gray

Eric Shoubridge

Gary W. Slater

Le Doyen de la Faculté des études supérieures et postdoctorales / Dean of the Faculty of Graduate and Postdoctoral Studies

Characterization of the first Mitochondrial SUMO E3 Ligase, MAPL

By

Emélie Braschi

A thesis submitted to the Faculty of Graduate and Postdoctoral Studies

in partial fulfillment of the requirement for the degree of

Doctor of Philosophy

Department of Biochemistry, Microbiology and Immunology

University of Ottawa

Ottawa, Ontario, Canada

Your file Votre référence
ISBN: 978-0-494-69135-9
Our file Notre référence
ISBN: 978-0-494-69135-9

Abstract

Mitochondrial dynamics play essential roles in a number of physiological processes, including metabolism, the cell cycle, cell stresses and migration. In these instances, mitochondrial morphology, distribution, and function are tightly coordinated by signalling cascades. However, it has been unclear how cellular signalling cascades intersect with the mitochondrial machinery. Many signalling switches utilize post-translational modifications to dynamically alter function, and we have shown that the division rates of mitochondria can be regulated by the conjugation of Drp1 with the Small Ubiquitin Like Modifier 1, SUMO1 (1). This modification functions in concert with phosphorylation events, making Drp1 a central candidate for the regulation of mitochondrial dynamics through signaling pathways.

In the first aim of this thesis, I demonstrated that MAPL is a novel mitochondrial SUMO E3 ligase, which modifies Drp1 as well as other mitochondrial substrates. In order to understand the global impact of mitochondrial SUMOylation on mitochondrial fission and other processes, the second objective of this manuscript was to identify the binding partners and substrates of MAPL. To this end, I performed an affinity column which successfully identified a number of MAPL interacting partners, and using a large-scale SUMOylation assay on isolated mitochondria, I have characterized the mitochondrial SUMO proteome.

One interacting partner of MAPL identified using affinity chromatography was Vps35, a component of the retromer coat complex. In the third objective of this thesis, I examined whether Vps35 regulates the formation of a novel aspect of mitochondrial dynamics: Mitochondrial Derived Vesicles, MDVs. Our lab has recently shown that MAPL is incorporated in small vesicular profiles that are targeted to peroxisomes. These vesicular

profiles contain selected proteins and are formed independently of Drp1, the known mitochondrial fission GTPase. I have shown that the retromer complex is required for the transport of MAPL MDVs to peroxisomes, providing new insights into the mechanism of MDV formation.

The work presented in this thesis makes important and novel contributions to our understanding of the mechanisms of mitochondrial SUMOylation, and in establishing the role of MDVs in cellular biology.

Acknowledgments

I would like to thank my supervisor, H. McBride for her support during my doctoral studies, and lab members, especially R. Zunino, L. Xu, and M. Neuspiel for giving me advice and training. Margaret Neuspiel, a former PhD student in H. McBride's lab, also built the foundations of this project since she first discovered Mitochondrial Derived Vesicles and did the initial characterization of MAPL. I would also like to thank my thesis advisory committee members, D. Gray and R. Screaton, as well as L. Pellegrini and B. Raught for their insights and comments, and V. Gayon, and R. Milne for critically reading this thesis.

Table of Contents

ABSTRACT II

ACKNOWLEDGMENTS IV

TABLE OF CONTENTS V

LIST OF ABBREVIATIONS VIII

LIST OF FIGURES XI

LIST OF TABLES XII

CHAPTER I GENERAL INTRODUCTION 13

I.1 HISTORICAL PERSPECTIVE 13
I.1.1 THE MITOCHONDRIA, AN ORGANELLE SPECIALIZED IN PRODUCING ENERGY 13
I.1.2 DISCOVERY OF MITOCHONDRIAL DYNAMICS 14
I.1.3 HYPOTHESIS 19
I.2 MITOCHONDRIAL DYNAMICS AND CELLULAR FUNCTION 20
I.2.1 METABOLISM 20
I.2.2 THE CELL CYCLE 30
I.2.3 CELL STRESSES 38
I.2.4 MITOCHONDRIAL QUALITY CONTROL 45
I.2.5 MITOCHONDRIA AND LOCALIZED ENERGY REQUIREMENTS 51
I.3 RETHINKING OUR VIEW OF THE MITOCHONDRIA 59
I.3.1 COMPLEX REGULATION OF DRP1 BY SIGNALING CASCADES 61
I.3.2 MITOCHONDRIAL SUMOYLATION MACHINERY, DISCOVERY OF MAPL 64
I.3.3 MITOCHONDRIAL DERIVED VESICLES 71
I.4 PROBLEM AND OBJECTIVES 72
I.5 REFERENCES 74

CHAPTER II MAPL IS A NEW MITOCHONDRIAL SUMO E3 LIGASE THAT REGULATES MITOCHONDRIAL FISSION 86

II.1 SIGNIFICANCE AND AUTHOR CONTRIBUTIONS 86
II.2 INTRODUCTION 87
II.3 RESULTS 88
II.4 MATERIAL AND METHODS 100
II.4.2 QUANTIFICATION AND STATISTICAL ANALYSIS 106
II.5 DISCUSSION 106
II.6 REFERENCES 108

CHAPTER III MAPL INTERACTING COLUMN AND MITOCHONDRIA SUMO PROTEOME 110

III.1 SIGNIFICANCE AND AUTHOR CONTRIBUTIONS 110
III.2 INTRODUCTION 110
III.3 RESULTS 111
III.3.1 MAPL AFFINITY COLUMN 111
III.3.2 MITOCHONDRIAL SUMO PROTEOME 118
III.4 MATERIALS AND METHODS 123
III.5 DISCUSSION 127
III.5.1 MAPL AFFINITY COLUMN 127
III.5.2 MITOCHONDRIAL SUMO PROTEOME 128
III.5.3 CURRENT AND FUTURE DIRECTIONS 131
III.6 REFERENCES 133

CHAPTER IV VPS35 MEDIATES THE VESICULAR TRANSPORT BETWEEN THE MITOCHONDRIA AND PEROXISOMES 134

IV.1 SIGNIFICANCE AND AUTHOR CONTRIBUTIONS 134
IV.2 INTRODUCTION 134
IV.3 RESULTS 135
IV.4 MATERIALS AND METHODS 150
IV.5 DISCUSSION 157
IV.6 REFERENCES 160

CHAPTER V GENERAL CONCLUSION 163

V.1 THE EMERGING MITOCHONDRIA 163
V.1.1 FROM IN-VITRO ASSAYS TO MITOCHONDRIAL DYNAMICS 163
V.1.2 MITOCHONDRIA AS SIGNALING ORGANELLES 165
V.1.3 DISCOVERY OF MAPL AND MDVS 167
V.2 MAPL IS THE FIRST MITOCHONDRIAL SUMO E3 LIGASE 169
V.2.1 INSIGHTS FROM THE CHARACTERIZATION OF MAPL, ITS SUBSTRATES, AND PARTNERS 169
V.2.2 PHYSIOLOGICAL ROLES OF MITOCHONDRIAL SUMOYLATION 171
V.3 MITOCHONDRIAL DERIVED VESICLES 178
V.3.1 DIFFERENT CARGOS, DIFFERENT FATES 178
V.3.2 MITOCHONDRIAL TO PEROXISOME TRANSPORT 181
V.4 SUMO, MAPL AND MDVS 187
V.4.1 MEMBRANE REMODELING 188
V.4.2 APOPTOSIS 195
V.4.3 CONCLUSION 199
V.5 REFERENCES 201

APPENDIX 1 CURRICULUM VITAE .....

APPENDIX 2 CARGO-SELECTED TRANSPORT FROM THE MITOCHONDRIA TO PEROXISOMES IS MEDIATED BY VESICULAR CARRIERS .....

APPENDIX 3 TRANSLOCATION OF SENP5 FROM THE NUCLEOLI TO THE MITOCHONDRIA MODULATES DRP1-DEPENDENT FISSION DURING MITOSIS .....

APPENDIX 4 PARKIN SELECTIVELY MODULATES THE DELIVERY OF OXIDIZED CARGO TO THE LYSOSOMES THROUGH A NOVEL VESICULAR TRANSPORT PATHWAY.....

List of Abbreviations

AIF	Apoptosis Inducing Factor
AMP	adenosine monophosphate
AMPK	activates the adenosine monophosphate kinase
Apaf1	Apoptotic protease activating factor 1
APC	Adenomatosis Polyposis Coli
Arp2/3	Actin Related Protein 2/3
ATP	Adenosine Tri-Phosphate
Bak	Bcl_2-killer 1
BAM	Beside a Membrane
BAR	Bin, Amphiphysin, Rvs
Bax	Bcl_2 associated X protein
Bcl_2	B-cell lymphoma 2
BMH	Bis-maleimidohexane
BSA	Bovine Serum Albumin
CaMKIα	Ca^{2+}/Calmodulin-dependent protein Kinase I α
CapZ	Capping protein muscle Z-line
CCCP	Carbonyl Cyanide-p-Trifluoromethoxyphenylhydrazone
Cdc42	Cell division cycle 42
Cdk	Cyclin Dependent Kinase
CKI	Cyclin dependent Kinase Inhibitor
DNA	Deoxyribonucleic acid
Drp1	Dynamin Related Protein 1
EEA1	Early Endosome Antigen 1
EGFR	Epidermic growth factor receptor
EndoG	Endonuclease G
ERK	Extracellular signal regulated kinase
Fis1	Mitochondrial Fission Protein 1
FKBP38	FK506 binding protein 8
FOXO	Forkhead Box sub-group O
FRPA	Fluorescence Recovery After Photobleaching
GED	GTPase Effector Domain
GFP	Green Fluorescent Protein
GLO-1	Gut granule Loss 1
GOLPH3	Golgi pPhosphoprotein 3
GSK3β	Glycogen Synthase Kinase β
GTP	Guanosine triphosphate
GTPase	guanine tri-phosphatase
HeLa	Henrietta Lacks
IAP	Inhibitors of Apoptosis
IgA	Polymeric immunoglobulin A
IGF-1	Insulin like Growth Factor 1

IQGAP1	IQ motif containing GTPase activating protein 1
IRF3	Interferon Regulatory Factor 3
JNK	c-Jun n-terminal Kinase
KAP1	Kinesin Associate Protein 1
Lamp1	Lysosomal Associated Protein 1
MAPL	Mitochondrial Anchored Protein Ligase
MARCHV	Membrane Associate Ring Finger 5
MAVS	Mitochondrial Antiviral Signaling Protein
mDia1	Diaphanous homologue 1
MDV	Mitochondrial Derived Vesicles
MEF	Mouse Embryonic Fibroblasts
Mfn	mitofusin
Miro	Mitochondrial Rho-1
MLC	Myosin Light Chain
MLCK	Myosin Light Chain Kinase
MOMP	Mitochondrial Outer Membrane Permeabilization (MOMP
mtDNA	mitochondrial DNA
mTOR	mammalian Target of Rapamycin
MycBP2	Myc binding protein 2
Myo2	Myosin 2
NF-kB	Nuclear Factor kappa-light-chain-enhancer of activated B cells
NGF	Nerve Growth Factor
NRF1	Nuclear Respiratory Factor 1
NT	Non targeted
Opa1	Optic Atrophy 1
Pam	Peptidylglycine alpha-amidating monooxygenase
PARL	Presenilin Associated Rhomboid Like Protease
PEG	Polyethylene glycol
PGC1α	Peroxisome Proliferator α Coactivator 1
PI3K	phosphoinositide 3-kinase
PIAS	Protein Inhibitor of Activated STAT
pIgR	Polymeric immunoglobulin receptor
Pin-1	Pin-formed 1
PKA	cAMP dependent kinase
PML	Promyelocytic Leukemia
PMS	Post-mitochondrial supernatant
PX	phox homology
Rac1	Ras-related C3 botulinum toxin substrate 1
RanBP2	Ran binding protein 2
RhoA	Ras homolog gene family, member A
RIG-1	RNA receptor retinoid inducible gene 1
RING	Really Interesting New Gene
RNA	Ribonucleic acid
RNAi	Ribonucleic acid interference
ROS	Reactive Oxygen Species
RPM-1	Presynaptic Morphology 1

SENP5	Sentrin Specific Peptidase
SH3	Src homology 3
sHeLa	spinner HeLa
shRNA	short-hairpin RNAI
SIM	SUMO Interaction Motifs
SIMH	Stress Induced Mitochondrial Hyperfusion (SIMH) involves
Siz1/2	SAP and Miz-finger containing
Slp-2	Sloppy paired 2
SNX	Sorting Nexin 9
SUMO E1	SUMO activating enzyme
SUMO E2	SUMOconjugating enzyme
SUMO E3	SUMO ligase
SUMO	Small Ubiquitin Like Modifier
TCA	Tricarboxylic Acid
Tet	Tetracyclin
TGFβ	Transforming Growth Factor β
TOPORS	Topoisomerase I binding arginine/serine-rich
tRNA	transfer RNA
Ubc9	Ubiquitin Conjugating Enzyme 9
Vdac	Voltage Dependent Anion Channel 1
Vps	Vacuolar Protein Factor
WAVE1	WASP family verprolin homologous protein 1
WCE	Whole cell extract
YFP	Yellow Fluorescent Protein

List of Figures

Figure I-1 Mitochondria are shaped by fusion and fission events 15
Figure I-2 Core proteins involved in mitochondrial fusion and fission 18
Figure I-3 Transient fragmentation in response to hyperglycemia 24
Figure I-4 Mitochondrial fragmentation in chronic hyperglycemia 29
Figure I-5 Mitochondrial dynamics and the G1 to S phase transition 33
Figure I-6 Mitochondrial fragmentation during mitosis 37
Figure I-7 Mitochondrial dynamics and cellular stresses 39
Figure I-8 Parkin and mitochondrial quality control 49
Figure I-9 Coordination of mitochondrial dynamics, transport and function 58
Figure I-10 Positioning and morphology of mitochondria respond to cellular signals 60
Figure I-11 Drp1 is regulated by different signaling cascades 63
Figure I-12 : Downstream effects of SUMOylation 66
Figure I-13 Enzymatic cascade of the SUMOylation reaction 67
Figure I-14 Topology of MAPL 70

Figure II-1 MAPL has SUMO E3 ligase activity in vitro 90
Figure II-2 MAPL SUMOylates native mitochondrial substrates 92
Figure II-3 Silencing of MAPL reduces total SUMO1 conjugates. 94
Figure II-4 MAPL SUMOylates DRP1 and modulates mitochondrial dynamics. 96
Figure II-5 MAPL forms a complex with Drp1 99

Figure III-1 MAPL affinity column 113
Figure III-2 Confirmation of the MAPL affinity column by western blot analysis 116
Figure III-3 Confirmation of interacting partners by co-immunoprecipitation 117

Figure IV-1 MAPL and Vps35 are in a complex 138
Figure IV-2 Vps35 is recruited to emerging MDVs enriched for MAPL 141
Figure IV-3 Specificity of theVps35 antibody 142
Figure IV-4 Vps35 recruitment to mitochondria is MAPL-independent 144
Figure IV-5 Lysosomal contamination of the mitochondrial preparations 145
Figure IV-6 Vps35 is required for the formation of MAPL MDVs 148
Figure IV-7 Vps26A is required for the formation of MAPL MDVs 149

Figure V-1 SENP5 is recruited to the mitochondria during mitosis 173
Figure V-2 SUMOylation of Drp1 175
Figure V-3 SUMOylation and cell death 177
Figure V-4 MDVs enriched for specific cargo have specific fates 180
Figure V-5 The retromer complex 183
Figure V-6 MAPL and migration 194
Figure V-7 MAPL and cell death 198
Figure V-8 MAPL is an attractive modulator of cellular signaling 200

List of Tables

Table III-1 MAPL affinity column 114
Table III-2 Mitochondrial SUMO proteome, compiled from two independent experiments 121
Table III-3 Mitochondria SUMO proteome, compiled from three independent experiments 122

Chapter I General Introduction

I.1 Historical perspective

I.1.1 The mitochondria, an organelle specialized in producing energy

During our eventful, complicated and controversial evolution, our ancestor, an anaerobic archaea was faced with a tangible problem: about one billion years ago, cyanobacteria had mastered photosynthesis, and were slowly increasing the atmospheric oxygen concentrations. Unfortunately for us, poor little bacteria, oxygen was toxic, and little survived the shock. Our chances were looking quiet grim until one of us had the good idea to engulf an arrogant aerobic bacteria (1). The engulfed bacteria decreased our intracellular oxygen, giving us fresh strength, and who would not enjoy being spoon-fed pyruvate? Since our partnership was going so well, we continued to develop this mutually beneficial relationship (1). Compartmentalizing our energy production provided tangible benefits (2). Solutes and enzymes could now be concentrated, and toxic by-products were shielded from the rest of the cell (2). Eventually, the aerobic bacteria evolved to become the modern mitochondria (1).

Millions of years later, pioneer *in-vitro* studies using isolated mitochondria have provided invaluable insights into the mechanisms of energy production. We now understand the electron transport chain and oxidative phosphorylation. However, these Nobel Prize winning experiments also led to the misconception that mitochondria function as single

units, with little connection with the cellular environment. The discovery of mitochondrial dynamics in the early 1990's shook this conception of mitochondria.

I.1.2 Discovery of mitochondrial dynamics

I.1.2.1 Inter-mitochondrial genetic complementation and time-lapse microscopy

The idea that mitochondria are dynamic organelles originated with *S. cerevisiae* mating experiments, which demonstrated that mitochondrial proteins can be shared between individual mitochondria (3). Haploid yeast cells were tagged with different mitochondrial fluorescent markers. Their co-localization in zygotes following mating indicated the sharing of content (3). Pioneer studies, which detected *in-vivo* mitochondrial DNA (mtDNA) complementation in mice, then provided the evidence that mitochondrial fusion played an important physiological function (4). Mitochondria were rendered respiration-incompetent by deleting a portion of the mtDNA, containing genes encoding for mitochondrial transfer RNA (tRNA) (4). These mitochondria were introduced by electroporation into a zygote with *wild-type* mitochondria (4). The examination of cytochrome c oxidase function in the resulting mice showed that all mitochondria contained both mutated and *wild-type* mtDNA, indicating that individual mitochondria can exchange genetic material (4). Importantly, the *wild-type* mtDNA was able to rescue the mutated mtDNA, demonstrating that mtDNA complementation was an important physiological aspect of mitochondrial fusion (4). In addition, better microscopy techniques allowed for the visualization of live mitochondria using fluorescent proteins (5). Unexpectedly, far from being a static bean-shaped organelle, mitochondria formed a highly interconnected reticulum shaped by continuous fusion and fission events *(Figure 1.1)*.

Figure I-1 Mitochondria are shaped by fusion and fission events

Cos-7 cells were incubated with 50nM of the potentiometric dye, tetramethyl rhodamine ester (TMRE) (6). Stimulating fusion, or inhibiting fission leads to the formation of an interconnected network (bottom, left panel). On the other hand, stimulating fission, or inhibiting fusion leads to a fragmented phenotype (bottom, right panel). Harder and McBride, unpublished.

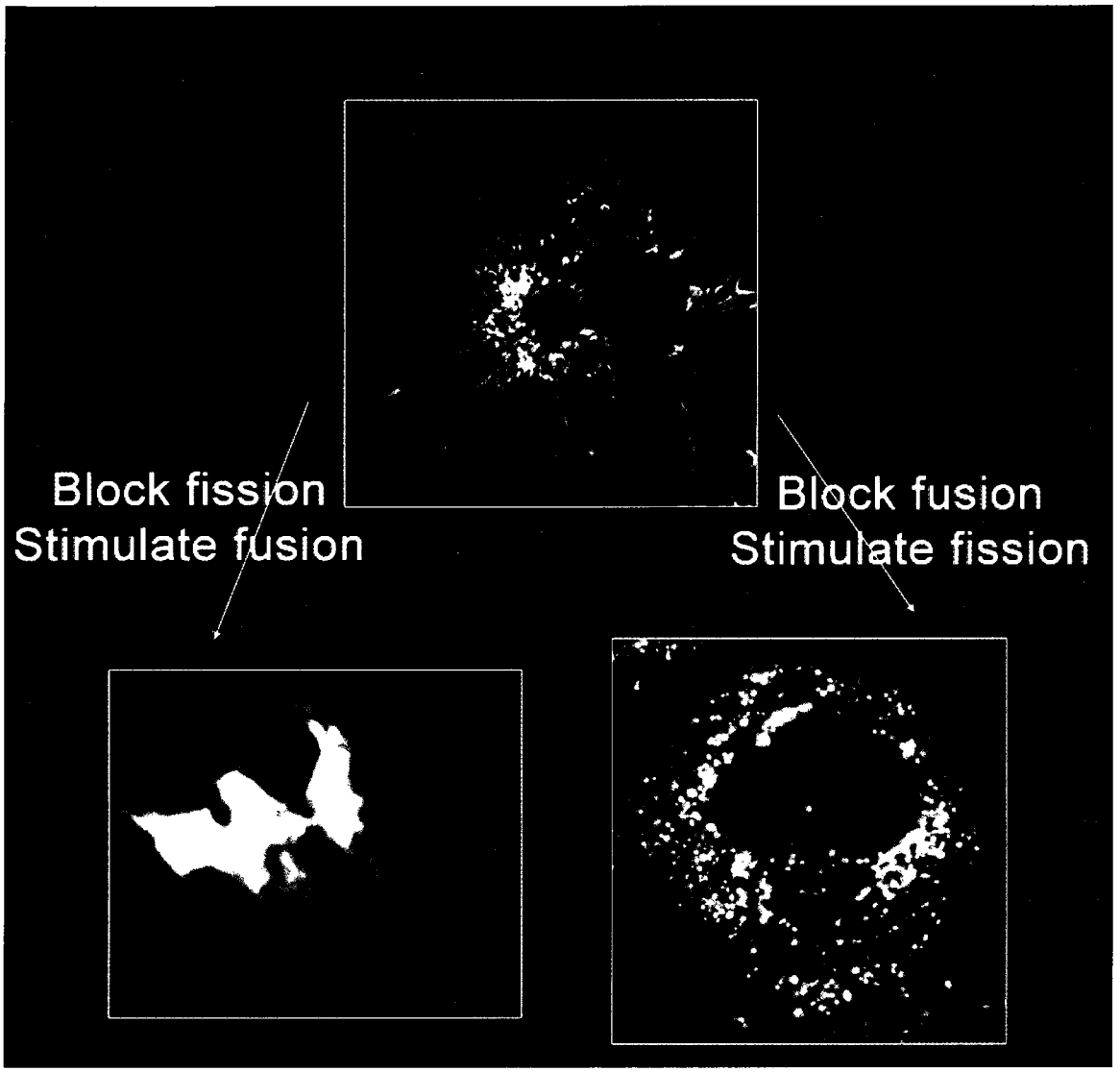
Block fission
Stimulate fusion
Block fusion
Stimulate fission

I.1.2.2 The mitochondrial fusion and fission machinery

Yeast genetic screens and mammalian studies led to the characterization of a novel class of mitochondrial proteins involved in regulating mitochondrial morphology. These proteins, which typically belong to the fusion or to the fission machinery, are summarized in *Figure 1.2*. Most of the discussion thereafter will focus on the mammalian proteins within the core machinery, and only these ones are depicted in *Figure 1.2*.

The fusion of the mitochondrial inner and outer membranes can be uncoupled (7). Outer membrane fusion depends on two guanine tri-phosphatases (GTPases), Miitofusin 1 and 2 (Mfn) (8). Human Mfn1 and 2 share 63% identity and the same domains, including coiled-coiled domains, which mediate homo-and heterodimeric interactions, transmembrane domains and a GTP-binding domain facing the cytoplasm (8). Inner membrane fusion is mediated by another GTPase, Optic Atrophy 1 (Opa1), and the Presenilin Associated Rhomboid Like Protease (PARL) (9). Highlighting the importance of mitochondrial fusion, the loss of Mfn1 or Mfn2 in mice leads to mid-gestational lethality due to specific, non-redundant placental defects (10). Bypassing the placental problems by using the Meox2-Cre, which expresses the Cre recombinase throughout the embryo, but not in the cell lineages that give rise to the placenta, leads to severe neurological defects in the Meox2-Cre/$Mfn2^{loxP}$. The mice die at days 1-17 after birth (11). The Meox2-Cre/$Mfn1^{loxP}$ mice are fully viable and fertile up to one year of age, but the loss of a single copy of Mfn2 leads to perinatal lethality (11). In addition, mutations in Mfn2 in human patients lead to a pathology of the longest motor and sensory nerves innervating the hands and feet, the Charcot Marie Tooth subtype 2A disease (12, 13). Mutations in Opa1 trigger the autosomal dominant Optic

Atrophy, an illness caused by the degeneration of retinal ganglion cells, leading to blindness (14, 15).

The core machinery regulating mitochondrial fission includes a GTPase, the Dynamin Related Protein 1 (Drp1), and the outer-membrane anchored, Mitochondrial Fission Protein 1 (Fis1) (9). Both of these proteins are also involved in regulating the fission of peroxisomes (16). Fis1 has been proposed to act as a mitochondrial receptor for the cytoplasmic Drp1 (17), but this is controversial and the recruitment of Drp1 to the mitochondria is still poorly understood (18). Drp1 assembles at fission sites into large oligomers, and GTP hydrolysis promotes mitochondrial scission (19-21). Like mitochondrial fusion, mitochondrial fission plays important physiological functions. The loss of Drp1 is embryonic lethal. Mice die at day 11.5-12.5, and suffer severe brain developmental abnormalities (22, 23). A mutation in Drp1 was also reported, with led to a dominant negative effect, and to severe developmental abnormalities in a new born, who died 37 days after birth (24).

Only proteins of the core machineries have been described above, and other proteins have been suggested to regulate mitochondrial fission or fusion (9). However, the list of core morphology proteins remains short. Future study will hopefully expand this list, in addition to uncovering regulators of the core morphology proteins.

Figure I-2 Core proteins involved in mitochondrial fusion and fission

A) Mfn1 and Mfn2 are fusion GTPases which can form homo and heterodimers. Opa1 is an inner membrane fusion GTPase, which modulates inner membrane fusion. Opa1 is partially regulated by the rhomboid like protease, PARL. Mouse *knock-out* phenotypes and human diseases linked to these proteins are shown. B) Fis1 is an outer-membrane integral protein, which might be involved in the recruitment of the cytosolic protein Drp1. Drp1 is a fission GTPase which assembles at fission sites. GTP hydrolysis triggers fission. Mouse *knock-out* phenotypes and human diseases linked to these proteins are shown.

A

FUSION

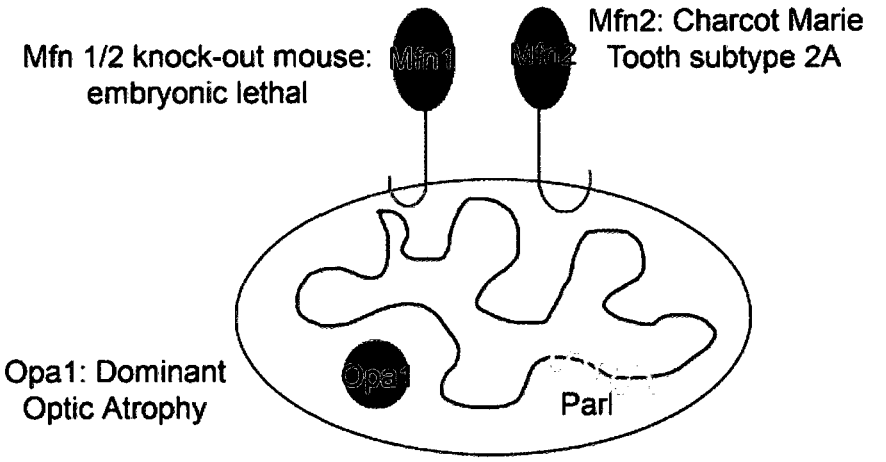

B

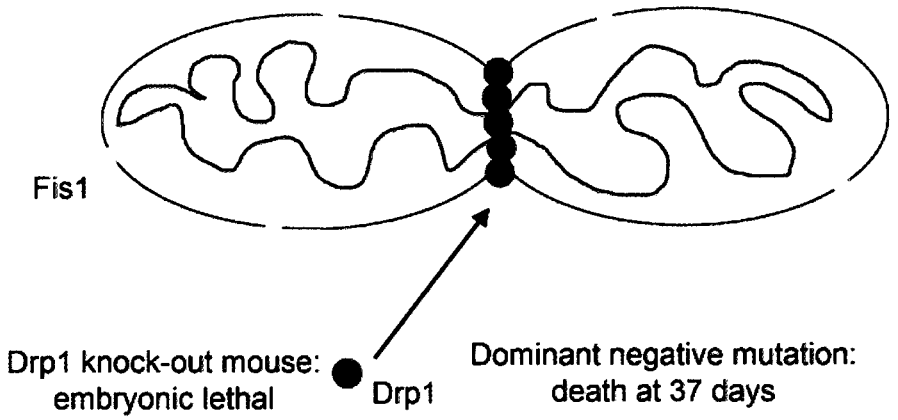

FISSION

I.1.3 Hypothesis

Enhancing fusion or decreasing fission leads to the same morphological state, a fused phenotype. On the other hand, decreasing fusion or enhancing fission, both lead to a fragmented phenotype. The importance of using both these processes to regulate mitochondrial morphology was therefore at first puzzling. Different hypotheses have been proposed. Fission could facilitate the proper positioning of the mitochondria in polarized cells and organelle biogenesis (25). In fact, mitochondrial morphology is tightly regulated during the cell cycle. In particular, mitochondria fragment during mitosis, a transition which could facilitate mitochondrial segregation between the two daughter cells (26).

Fusion could facilitate the distribution of proteins and mtDNA within the whole mitochondrial population. This would prevent the formation of malfunctioning, isolated mitochondria with depleted mtDNA or damaged proteins. Supporting this hypothesis, downregulating Mfn2 and Mfn1 strongly impairs oxidative phosphorylation and leads to mitochondrial heterogeneity, with some mitochondria being less polarized than others (27). In addition, the loss of Mfn2 in Purkinje cells leads to the formation of mitochondria devoid of mtDNA nucleoids (11).

Beyond biogenesis and the homogenization of the mitochondrial population, numerous studies have documented the central role played by mitochondrial dynamics within cellular physiology. Mitochondrial dynamics, by responding to cellular signaling, modulate metabolic transitions, responses to localization cues, and some mitochondrial proteins are emerging as signaling intermediates. Our lab has recently identified the Small Ubiquitin Like Modifier (SUMO) as an important post-translational modification of

mitochondrial proteins (28). *The hypothesis of my project was that the mitochondrial SUMOylation machinery may play a central role in propagating signals between diverse cellular signaling cascades and the mitochondria.*

In the rest of this introduction, I will provide evidence supporting the importance of mitochondrial dynamics in the regulation of metabolism, the cell cycle and cell stresses. I will then discuss novel results indicating that sub-populations of mitochondria with specific cargo can be generated to facilitate mitochondrial quality control. This section will be followed by an examination of the mechanisms to coordinate mitochondrial dynamics, movement, and function. These complex processes will lead me into the discussion of signaling cascades involved in the regulation of mitochondrial dynamics. Finally, the last section will describe a novel phenomenon in mitochondrial dynamics: the discovery of Mitochondrial Derived Vesicles (MDV).

I.2 Mitochondrial dynamics and cellular function

I.2.1 Metabolism

I.2.1.1 Fragmentation and calcium transients

The β-cell is a sensor for circulating nutrients, including glucose, amino acids and fatty acids (29). It plays a central role in adjusting insulin secretion in response to these cues. Glucose is transported inside the cell through glucose transporters, and is then metabolized to pyruvate (29). Pyruvate is further oxidized in the mitochondria, generating a burst of Adenosine Tri-Phosphate (ATP). Increased ATP concentrations lead to the closure of ATP-

sensitive K^+ channels, depolarizing the plasma membrane and opening of voltage dependent Ca^{2+} channels (29). Cytoplasmic Ca^{2+} activates signal transduction cascades, leading to the release of insulin granules (29). In addition, Ca^{2+} further increases the rates of mitochondrial oxidative phosphorylation, providing the energy necessary for insulin granule secretion (29).

In fact, in isolated mitochondria, a sub-micromolar increase in calcium leads to the activation of the Ca^{2+}-dependent enzymes of the Krebs cycle, activating mitochondrial metabolism. Three metabolic enzymes are activated by Ca^{2+}; activation is either achieved by a calcium-dependent dephosphorylation step or by direct binding of Ca^{2+} to the enzymes. Metabolite transporters can also be regulated by calcium (30). Importantly, to respond to Ca^{2+} levels, the mitochondria are positioned in strategifc localization, in close proximity to the sources of intracellular Ca^{2+}. They form intimate contact sites with the endoplasmic reticulum, for example (31). Upon cell stimulation, the mitochondria are exposed to the Ca^{2+} emanating from the microenvironment of the open inositol triphosphate-gated channels, which is much higher then in the cytoplasm (32). Importantly, these signaling events are qualitatively different from mitochondrial Ca^{2+} overloads, which can lead to cell death by necrosis or apoptosis (33).

Evidence suggests that mitochondrial fission might play a specific role to regulate calcium homeostasis in insulin-releasing cells (34). Manipulating the mitochondrial network in the pancreatic β cell line INS-1E by inducing fragmentation by overexpressing Fis1, or by reducing fusion by overexpressing a dominant-negative Mfn1, leads to a similar phenotype with 50-60% of fragmented mitochondria (34). However, the overexpression of Fis1 but not of the dominant-negative Mfn1 impairs insulin secretion (34). Fragmentation induced by Fis1 blocks glucose-stimulated mitochondrial calcium transients, leading to a reduction in

ATP production (34). This in turns affects the release of insulin-containing granules (34). This result indicates that it is not the sustained fragmentation *per se*, which triggers the pathological state, but rather that it is a downstream effect of overexpressing Fis1 specifically, or of inducing mitochondrial fission (34). Interestingly, a role for fission in calcium homeostasis has already been proposed. Fission prevents the propagation of mitochondrial calcium transients, which can have a protective function (35), and mitochondria in Fis1 overexpressing cells have a delayed uptake of Ca^{2+} entering across the plasma membrane (36).

I.2.1.2 Fragmentation and cristae morphology

Mitochondrial fragmentation following high glucose can also have important functions in non-insulin releasing cells. In rat liver cells and rat myoblasts, hyperglycemic conditions trigger mitochondrial fragmentation, a step necessary to increase mitochondrial metabolism (37). Inhibiting mitochondrial fission by using a dominant-negative form of Drp1 prevents high glucose-induced oxygen consumption (37). Importantly, preventing pyruvate uptake does not stop mitochondrial fragmentation, indicating that yet unknown signaling events coordinate pyruvate uptake and mitochondrial morphology in order to maximize metabolism in response to glucose (37). Fragmentation, which could be triggered by decreased fusion, increased fission or both, could favor an increase in metabolism by regulating inner membrane morphology (37).

Different regions within the inner membrane have been described: the inner boundary membrane, closer to the outer membrane, and the cristae membrane, which forms folds within the matrix space and concentrates the proteins involved in oxidative phosphorylation (38). The inner boundary membrane is attached to cristae by narrow

openings, called cristae junctions (38). Early studies performed in the 1960s by electron microscopy led to the discovery that the mitochondrial inner membrane can switch between different morphologies (39, 40). Two main states were described, a "condensed" state, with a compact matrix and an "orthodox" state, with a bigger matrix volume (39, 40). Importantly, the morphology of the inner membrane is mediated by inner membrane fusion and fission events, which depend on the respiratory state of the mitochondria, indicating that these are regulated processes (39, 40). For example, the condensed state has been associated with increased oxidative phosphorylation (41). In other words, the dynamic structure of the inner membrane could facilitate rapid responses to environmental changes (41). Since mitochondrial morphology has been shown to regulate the remodeling of cristae (42), an attractive hypothesis is that mitochondrial dynamics modulate cristae morphology to respond to metabolic demands (37) *(Figure 1.3)*.

Figure I-3 Transient fragmentation in response to hyperglycemia

In response to high glucose, signaling cascades lead to mitochondrial fragmentation through the activation of fission, or a reduction of fusion. Fragmentation facilitates pyruvate uptake and might promote changes in cristea morphology to facilitate metabolism. Importantly, these changes are transient.

Transient hyperglycemia

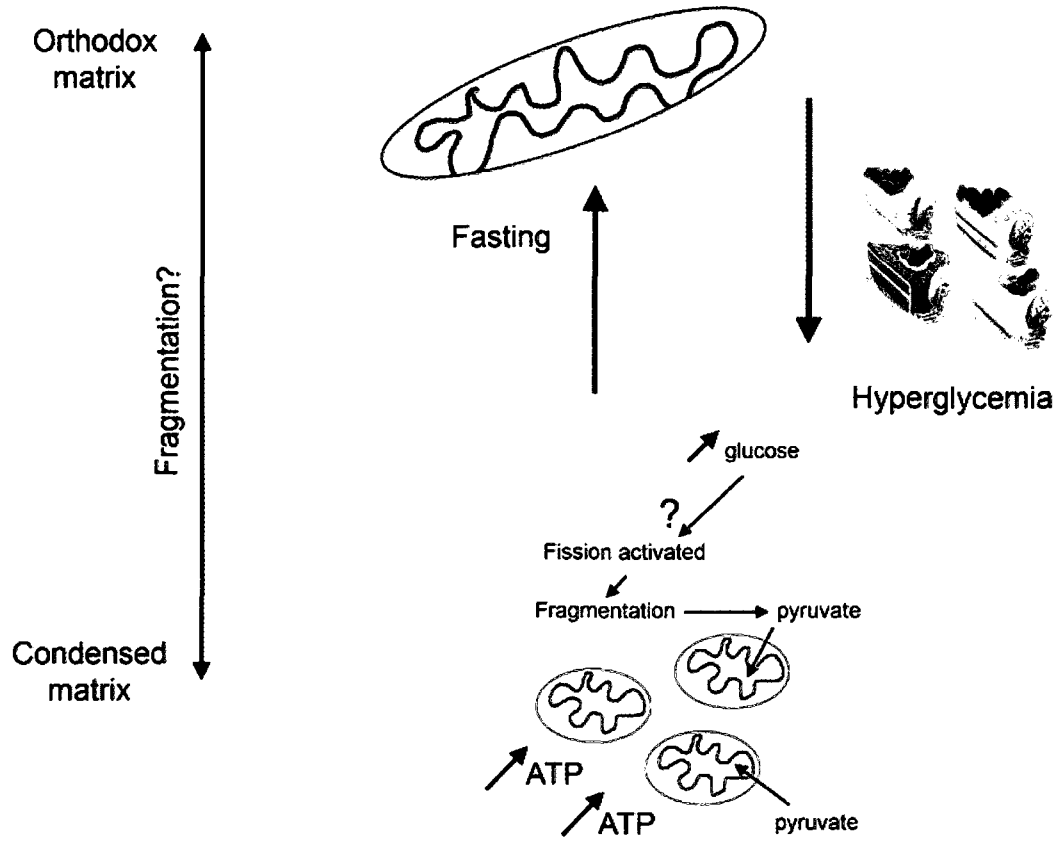

Fragmentation is transient:
Increased pyruvate uptake

I.2.1.3 Mfn2 and diabetes

Given the role of mitochondrial dynamics during metabolism, it is not surprising that morphology defects have been linked to diabetes. For example, β-cells from diabetic Zucker rats have abnormally fragmented mitochondria prior to the onset of diabetes (43), and obese patients with type 2 diabetes have fragmented skeletal muscle mitochondria (44). However, it is unclear whether mitochondrial fragmentation is the consequence or the cause of β-cell dysfunction.

One mechanism, which has been proposed to explain mitochondrial fragmentation in obesity and diabetes, is a loss of Mfn2 expression caused by the reduction in the levels of the Peroxisome Proliferator α Coactivator 1 (PGC1α) in these patients. PGC1α is a transcription factor, which regulates the expression of mitochondrial proteins, including Mfn2 (45). In fact, Mfn2 is downregulated in the Zucker rat model of type 2 diabetes (46), and when compared to healthy subjects, skeletal muscle cells of obese subjects have reduced levels of Mfn2 specifically, since there are no differences in total mitochondrial mass (45).

The loss of both Mfn1 and Mfn2 leads to severe defects, including reduced cell proliferation and a significant decrease in cellular respiration (27). Reductions of Mfn2 protein levels, on the other hand, lead to a milder reduction in glucose utilization, and oxygen consumption (46). Interestingly, the downregulation of Mfn2 in myotubes increases the efficiency of oxidative phosphorylation, since these mitochondria exhibit virtually no proton leak (46). This is an interesting observation, since it suggests that when Mfn2 is partially downregulated, for the same production of ATP, the cell needs to utilize less glucose. If the input of calories and the consumption of ATP remain constant, this could

favor the accumulation of glucose, and could play a role in the early steps of insulin resistance (47).

Nevertheless, a sustained decrease in Mfn2 appears detrimental to the organism. In diabetic subjects, the rates of oxidative phosphorylation are insufficient to sustain normal metabolic functions, since the levels of plasma lactate are increased, indicating an increase in glycolysis (47). The reduced rates of oxidative phosphorylation can be explained by different mechanisms. In fibroblasts, the loss of Mfn2 disrupts the interactions between the endoplasmic reticulum and the mitochondria, reducing the efficiency of mitochondrial Ca^{2+} uptake in response to inositol triphosphate (48, 49). This in turn could reduce the efficiency of oxidative phosphorylation.

In addition, Mfn2 appears to regulate the expression of respiratory chain complexes. The downregulation of Mfn2 reduces the expression of the subunits of complexes I, II, III and V, essentially inhibiting oxidative phosphorylation (50). On the other hand, overexpressing Mfn2 enhances the expression of complex I, IV, and V, increases membrane potential, and rates of glucose utilization (50). Interestingly, the function of Mfn2 as a regulator of metabolism can be separated from its role as a fusion GTPase. A mutant of Mfn2 that lacks fusion activity retains the ability to increase mitochondrial membrane potential and glucose utilization when overexpressed (50). This suggests that Mfn2 can regulate mitochondrial function through fusion independent pathways, and that changes in the expression of respiratory chain complexes are not the indirect consequence of changes in mitochondrial morphology. Although no differences in the levels of PGC1α could be detected in this study (50), Mfn2 heterozygous mice show a greater induction of PGC1α expression than *wild-type* mice in skeletal muscles cells following hypoglycemia, indicating

that the effect of Mfn2 on the expression of respiratory complexes might be mediated in part through PGC1α (51).

It is likely that this function of Mfn2 as a regulator of mitochondrial gene expression is not shared with Mfn1. Indeed, the overexpression of Mfn1 leads to reduced ATP content, increased lactate production, and impaired glucose-stimulated insulin secretion (34). Interestingly, it has previously been suggested that Mfn2 possesses specific signaling functions (52). The high levels of homology between Mfn1 and 2 and their ability to form homotypic and heterotypic dimers have led to the hypothesis that they fulfill redundant functions within the cell (53). However, Mfn1 has fast rates of nucleotide hydrolysis and a low affinity for GTP, suggesting that it functions as a mechanoenzyme (52). On the other hand, Mfn2 has low rates of hydrolysis and a high affinity for GTP, which are the characteristics of a regulatory enzyme. In the GTP-bound form, it could act as a docking site for downstream effectors, currently unknown (52).

I.2.1.4 Conclusion

Changes in mitochondrial morphology seem to correlate with β-cell dysfunction. Since mitochondrial fragmentation is usually associated with cell death, it has been proposed that mitochondrial fragmentation *per se* could cause β-cell dysfunction and apoptosis. However, the studies presented above show that much care should be taken when interpreting mitochondrial phenotypes.

Although mitochondrial fragmentation triggered by the overexpression of fission proteins, or by the inhibition of fusion proteins, appears morphologically similar, the downstream cellular consequences can be different (34). In addition, emerging studies illustrate the multiple functions of mitochondrial morphology proteins, and introduce the

idea that they can act as signaling intermediates (46). The challenge is to discover downstream signaling events and to understand the coordination between upstream signaling cascades, mitochondrial dynamics, and function.

Finally, the modulation of the fission and fusion machineries by cellular signaling following a physiological stimulus can develop into a pathological state. For example, fragmentation is a physiological response to hyperglycemia (37). However, the persistence of the hyperglycemic state in diabetic patients leads to a reduction in PGC1α, triggering a loss of Mfn2 expression (45). Improper fusion or the loss of Mfn2-mediated signaling, could then lead to a reduction in the cell's oxidative capacity and eventually cell death. In other words, both physiological and pathological situations are characterized by fragmented mitochondria *(Figure 1.4)*.

Figure I-4 Mitochondrial fragmentation in chronic hyperglycemia

Although both physiological (left) and pathological (right) situations lead to fragmented mitochondria, fragmentation is transient in physiological conditions, but permanent in the pathological state. Permanent fragmentation could be caused by impaired levels of PGC1α, triggering a loss of Mfn2 and decreased mitochondrial fusion. Decreased fusion and signaling activity of Mfn2 could lead to impaired oxidative phosphorylation and to the accumulation of damage, eventually triggering cell death.

Chronic hyperglycemia

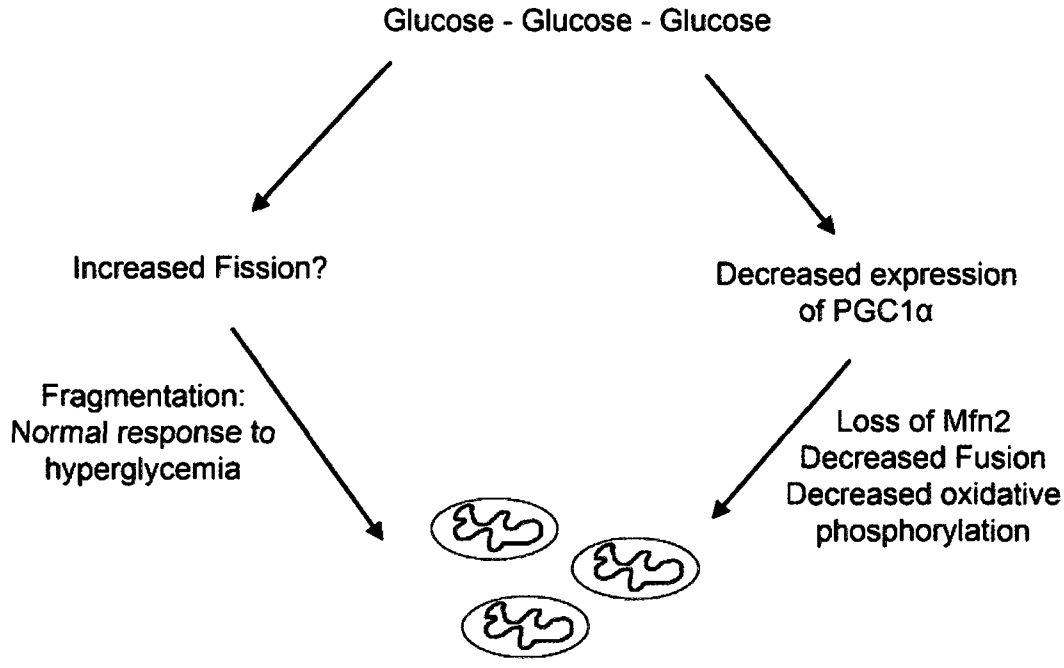

Fragmention is permanent:
Accumulation of damaged proteins?
Loss of mitochondrial function
Death

I.2.2 The cell cycle

In early G_1, the transcription of mitochondrial genes is repressed as the levels of cyclin D1 increase (54). The activation of cyclin D1/Cyclin-Dependent Kinase 4 (Cdk4) triggers the phosphorylation and subsequent degradation of the Nuclear Respiratory Factor 1 (NRF1), which regulates the transcription of mitochondrial genes (54). Oxidative phosphorylation is therefore reduced during G_1 (54, 55). Past the restriction point, mitochondrial oxidative phosphorylation is enhanced, due to a modest increase in mass and a significant increase in oxygen consumption (55), and the mitochondria fuse into a network (56). These events are required for the buildup of cyclin E and entry into S phase (56). Since cyclin D1 levels remain high throughout the G_1/S transition, the increase in mitochondrial respiration is probably triggered by a cyclin D1-independent event. Importantly, inducing the formation of a mitochondrial network in cells arrested at G_0, by inhibiting the function of Drp1 using a pharmalogical agent, triggers entry into S phase, bypassing the requirement for growth factors (56). It is unclear whether the increased oxidative phosphorylation resulting from the fused network is sufficient to trigger S phase entry. If this were the case, artificially enhancing mitochondrial function using creatine should trigger cell cycle entry (57). Alternatively, the fused reticulum could trigger downstream signaling events leading to S phase entry. In fact, although the need for respiring mitochondria for S phase entry has been documented (56), it is unclear whether it is the increase in oxidative phosphorylation, or the changes in mitochondrial dynamics, or both, which lead to cyclin E buildup. If changes in mitochondrial dynamics are important for the regulation of the G_1/S transition, this raises the possibility that cell-cycle kinases regulate the fusion or fission machineries *(Figure 1.5)*.

Beyond complex morphological changes, the mitochondria also appear to act as cell cycle check points during the G_1/S transition. In particular, overexpressing Mfn2 leads to a decrease in serum-induced proliferation without affecting cell death (58). In the same study, the authors detected a Ras-binding domain in Mfn2. The Ras-binding domain, but not mitochondrial localization, appears important for the Mfn2 triggered growth arrest (58). These results support the idea that Mfn2 has a fusion independent role during the cell cycle (58). The authors proposed that the overexpression of Mfn2 sequesters Ras and abolishes downstream signaling cascades (58). Ras-mediated signaling in response to growth factors leads to the transcriptional activation of cyclin D1. One could therefore postulate that in early G_1, a mitochondrial-specific signal is transmitted to Mfn2, leading to the release of Ras, increased cyclin D1 levels and cell cycle progression (50). Since cyclin D1 represses the transcription of mitochondrial genes, a feedback loop in early G_1 could be established between Mfn2, Ras, and cyclin D1. Past the restriction point, oxidative phosphorylation is increased, and since the overexpression of Mfn2 increases respiration, unknown mechanisms could activate Mfn2. Active Mfn2 would also participate in the formation of the mitochondrial network characteristic of the G_1/S transition.

Studies in *D. melanogaster* have demonstrated other roles for the mitochondria during G_1 through metabolic intermediates. A first mutation in the gene encoding for cytochrome c oxidase subunit V leads to a drop in cellular ATP and cell cycle arrest during G_1 (59). The increase in adenosine monophosphate (AMP) activates the adenosine monophosphate kinase (AMPK), leading to a p53-dependent cyclin E degradation. Importantly, the levels of ATP remain high enough to permit cellular survival, growth and differentiation (59).

In addition, the same group reported the disruption of Complex 1 in *D. melanogaster* also leads to G_1 arrest. In this case, the ATP levels remain normal but Reactive Oxygen Species (ROS) levels are increased (60). This leads to the activation of the c-Jun n-terminal Kinase (JNK), and of the transcription factor Forkhead Box sub-group O (FOXO). Increased transcription of Dacapo, the p27 Cyclin-dependent Kinase Inhibitor (CKI) homologue, triggers a G_1 cell cycle arrest (60). These examples are important since they illustrate that the cell is able to respond to mitochondrial dysfunction and to block the cell cycle specifically, although the mitochondrial function remains sufficient to sustain cell growth and differentiation. They also illustrate that mitochondrial retrograde signaling, both through metabolic intermediates, and proteins like Mfn2, are integral components of cell cycle check points *(Figure 1.5)*.

Figure I-5 Mitochondrial dynamics and the G1 to S phase transition

In early G_1, cyclin D1 represses the transcription of mitochondrial genes, leading to low levels of oxidative phosphorylation. Following the restriction point, cyclin D1 is degraded, the mitochondria form a network and oxidative phosphorylation is increased. These are important for the buildup of cyclin E and entry into S phase. Potential mitochondrial checkpoints are indicated.

Early G1:

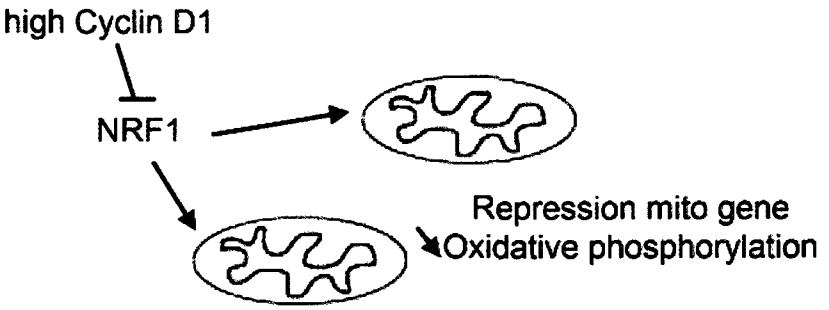

Late G1:

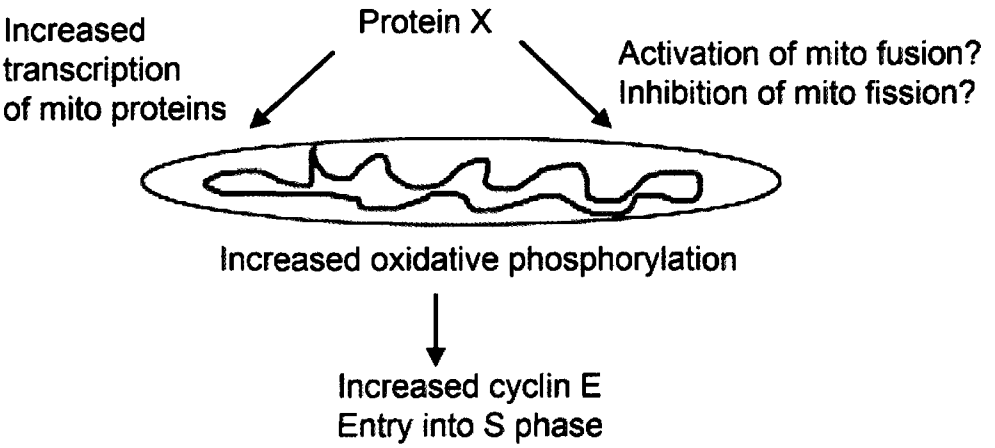

Mitochondrial checkpoints:

Mfn2 upregulation leads to G1 arrest
Decreased ATP levels lead to a p53-dependent G1 arrest
Increased ROS levels lead to a p27-dependent G1 arrest

I.2.2.1 The G2/M transition

Following fusion in late G_1, the mitochondria fragment during mitosis. This event is regulated by the phosphorylation of Drp1 on Ser585 by Cyclin B/ Cdk1 (26). The phosphorylation site is in the GTPase Effector Domain of Drp1 (GED), a domain important for intramolecular interactions (26). However, phosphorylation does not seem to impair GTPase activity and it is unclear how phosphorylation leads to mitochondrial fission (26). Phosphorylation could increase the affinity of Drp1 for other factors that would facilitate its recruitment to the mitochondria. Alternatively, phosphorylation could promote a second post-translational modification, like ubiquitination or SUMOylation, which would then enhance its fission activity. In fact, recent work in our lab has shown that the Sentrin-Specific Peptidase 5 (SENP5), which regulates the deSUMOylation of Drp1 (61), is primarily nucleolar during interphase but becomes mitochondrial at G_2/M (62). The recruitment of SENP5 to the mitochondria correlates with increased rates of Drp1 cycling on the mitochondria, and mitochondrial fission (62). Therefore, during mitosis, changes in the deSUMOylation/SUMOylation cycle of Drp1 could promote mitochondrial fission (62), and the phosphorylation of Drp1 could play a role in the regulation of this cycle. Interestingly, the downregulation of SENP5 leads to a cell cycle arrest at G_2/M, precisely when it should translocate to the mitochondria. It is therefore possible that the deSUMOylation of mitochondrial substrates during G_2/M functions as a cell cycle check point.

In addition, the fragmentation of the mitochondria during mitosis could facilitate the proper positioning of mitochondria within the two daughter cells. Unexpectedly, when HeLa cells were transfected with a phospho-defective mutant of Drp1, the mitochondria remained tubular and the cell cycle proceeded normally (26). However, recent papers have highlighted

the importance of the cellular context when looking at the effects of Drp1. In fact, although primary Mouse Embryonic Fibroblasts (MEFs) isolated from DRP1 *knock-out* animals show up to a seventeen-fold reduction in proliferation rates (23), MEFs immortalized with the large T-antigen grow at the same rate as their *wild-type* counterparts (22). ATP levels in *wild-type* compared to *knock-out* MEFs were similar in both studies, indicating that differential energy production cannot explain these differences in proliferation. In addition, silencing Drp1 with RNAi in HeLa cells, an immortalized cell line, leads to slower rates of proliferation. These cells also have inefficient oxidative phosphorylation, which might explain their growth defects (63). In other words, it remains unclear whether the fragmentation of mitochondria at G_2/M facilitates the positioning of the mitochondria in the two daughter cells, and whether it functions as a mitotic checkpoint. In addition, the prolonged overexpression of a dominant negative form of Drp1 causes a p53-dependent buildup of cyclin E in HCT116 cells, leading to delayed S phase entry (26). It is therefore possible that the proliferation defects in cells lacking Drp1 are due to defects in the G_1/S transition, as opposed to the activation of a mitotic checkpoint *(Figure 1.6)*.

I.2.2.2 Conclusion

Mitochondrial dynamics respond to the progression of the cell cycle. During the G_1/S transition, mitochondrial dynamics appear to synchronize mitochondrial metabolism and G_1 progression (56). During mitosis, the significance of mitochondrial fragmentation remains elusive. The discovery of specific chemical modulators of mitochondrial proteins might be essential to dissect the role of mitochondrial dynamics during the cell cycle. In fact, acute versus chronic changes in mitochondrial fission can have opposite effects on cell cycle progression (56). In addition, during mitosis, the complexity of the Drp1 fission cycle in

mammalian cells, and the absence of an established *in-vitro* model to study Drp1-mediated fission, makes it difficult to dissect the specific roles of signaling cascades in the regulation of the fission activity of Drp1. Finally, different cell types and transformed versus untransformed cells seem to respond differently to the loss of Drp1 (23). However, despite these limitations, these results highlight the tight regulation of mitochondrial dynamics by signaling cascades. Importantly, mitochondrial dynamics might participate in the synchronization of mitochondrial function with the cell cycle.

Figure I-6 Mitochondrial fragmentation during mitosis

During mitosis, SENP5 is recruited to the mitochondria, which leads to a loss of mitochondrial SUMOylation. In addition, CyclinB/Cdk1 phosphorylates Drp1. Both of these events probably coordinate the Drp1-induced mitotic fragmentation. Potential G_2/M mitochondrial checkpoints are indicated.

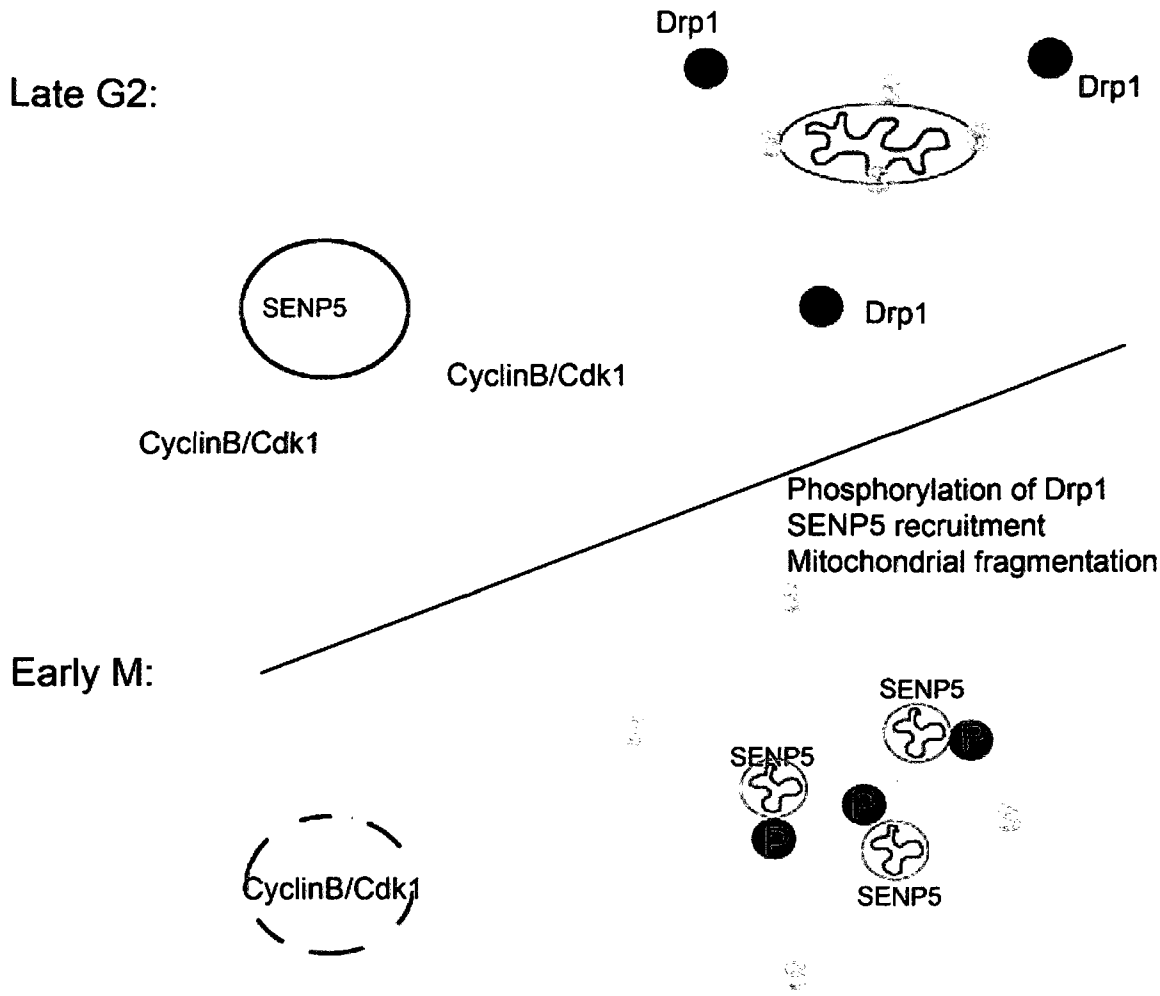

Mitochondrial check points:

The downregulation of SENP5 leads to a G2/M arrest

I.2.3 Cell stresses

I.2.3.1 Mild stress triggers hyperfusion of the reticulum

Following mild stress triggered by ultraviolet irradiation, actinomycin D, cycloheximide, serum, or amino acid deprivation, the mitochondria fuse into a highly interconnected network. This process, called Stress Induced Mitochondrial Hyperfusion (SIMH) involves an increase in mitochondrial fusion and requires Opa1, Mfn1 and Stromatin like protein 2 (Slp-2) although it occurs independently of Mfn2 (64). Slp-2 is a recently identified Mfn2-interacting protein (65). Interestingly, the *knock-down* of Slp-2 does not lead to a reduction in steady state mitochondrial fusion, although it prevents SIMH, indicating a specific role in stress-induced fusion (64). Slp-2 prevents the cleavage of Opa1 under stress conditions, such that the long isoform, which is essential for fusion, is retained (64).

Importantly, SIMH appears to be a survival response to mild and specific stresses. In fact, rendering cells incompetent for SIMH by *knocking-down* Mfn1 increases their sensitivity to Actinomycin D and ultraviolet stresses, but not to staurosporine treatment, a stress which does not induce SIMH (64). Interestingly, SIMH leads to increased ATP production, which might be important for cellular survival (64), but stresses that do not induce SIMH, such as staurosporine, do not promote cellular ATP production (64).

Stress-induced fusion could enhance survival by distributing damaged proteins and mtDNA throughout the reticulum. SIMH could function as a protective mechanism in mild stress conditions, when repair is possible, or for specific stresses leading to the depletion of cellular ATP *(Figure 1.7)*.

Figure I-7 Mitochondrial dynamics and cellular stresses

A) Mild, specific stresses induce mitochondrial fusion. One mechanism includes the prevention of Opa1 cleavage by Slp-2. Fusion is protective, and the downregulation of Mfn1 decreases fusion and survival. B) Stronger apoptotic signals do not trigger fusion, and the downregulation of Mfn1 has no effect on survival.

A

ultra-violet radiation
cyloheximide
serum deprivation
amino acids

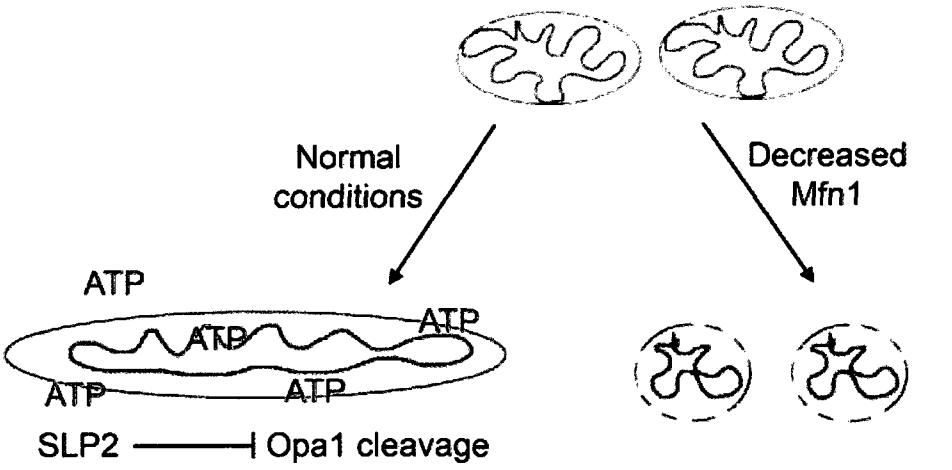

Elongation:
Increased ATP
Increased survival

No elongation:
decreased survival

B

Staurosporine

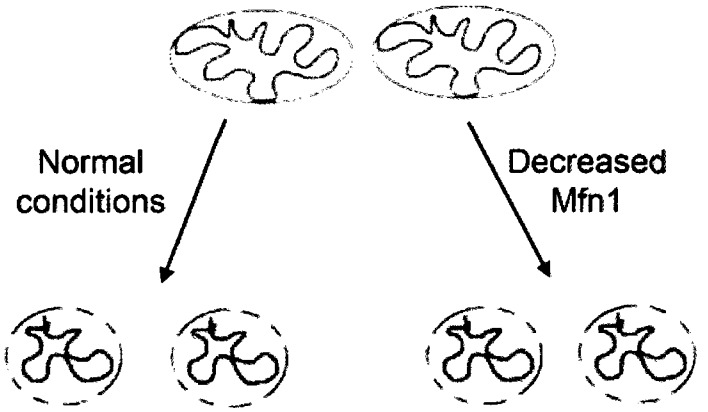

Fragmentation and cytochrome c release

I.2.3.2 Apoptosis and mitochondrial fragmentation

Overview of the mitochondrial cell death pathways

A number of the cellular changes associated with apoptosis are triggered directly or indirectly by caspases (66). Caspases are proteases, which are synthesized as inactive zymogens (66). Activation can be triggered either by cleavage from another upstream caspase, in a caspase cascade, or induced by cross-activation (66). At the plasma membrane, ligand binding to death receptors like the Fas or Trail receptors triggers oligomerization of the receptors (66). The initiator caspase 8 associated with the cytoplasmic tails, come in close proximity and mutually cleave and activate each other thanks to their low intrinsic protease activity. This pathway is commonly called the extrinsic pathway. In the intrinsic pathway, another initiator caspase, caspase 9, is activated within the apoptosome (67). The apoptosome is constituted of the Apoptotic protease activating factor 1 (Apaf1) and cytochrome c, a protein normally part of the mitochondria electron transport chain where it acts as a redox intermediate. In the cytoplasm, cytochrome c binds Apaf1, triggering its oligomerization and the recruitment of procaspase 9 molecules. Active caspase 9 cleaves and activates downstream executioner caspases such as caspase 3 (68).

Cytochrome c is not the only protein to be released from the mitochondria during cell death. Other released proteins include Smac/Diablo, the Apoptosis Inducing Factor (AIF) and the Endonuclease G (EndoG) (69). Smac/Diablo inhibits the activity of the Inhibitors of Apoptosis (IAPs), a family of proteins which bind and sequester caspases (70). These proteins function as safety nets in the case of a transient leakage of the mitochondria. EndoG and AIF translocate to the nucleus, triggering chromatin condensation and DNA fragmentation (69).

In other words, the mitochondria's involvement during apoptosis includes the release of cytochrome c, essential for the activation of caspase 9, factors that inhibit anti-apoptotic proteins, and proteins involved in the degradation of DNA (71). Cytochrome c, AIF, and EndoG are intermembrane space proteins (71). For their release into the cytoplasm, the mitochondrial outer membrane must therefore be permeabilized (71). This event, triggered by the activation of the pro-apoptotic B-cell lymphoma 2 (Bcl_2) family members, such as the Bcl_2 associated X protein (Bax) and Bcl_2-killer 1 (Bak), is usually referred to as the Mitochondrial Outer Membrane Permeabilization (MOMP) (71). The composition of the permeability transition pore remains controversial (71).

Following an apoptotic stimulus, activated Bax and Drp1 translocate to the mitochondria in enrichments that co-localize with Mfn2 (72). Translocation is followed by the fragmentation of the mitochondrial reticulum (72), and cytochrome c release, although the exact order of these events is controversial (73). Numerous studies have shown that promoting fusion or inhibiting fission delays apoptosis. The downregulation of Drp1 and Fis1, or the overexpression of Mfn1 and Mfn2 delays caspase activation for a number of pro-apoptotic signals (18, 52, 74, 75). However, unlike caspase inhibition, preventing mitochondrial fragmentation delays, but does not inhibit cell death (76). In fact, the inhibition of Drp1 prevents the release of cytochrome c but does not affect the release of other pro-apoptotic molecules including Smac/Diablo and AIF (76).

Controversial role of fragmentation during cell death

The role of mitochondrial fragmentation during cell death is controversial. For example, it is unclear whether mitochondria actively fragment to promote cell death or whether fragmentation is simply a consequence of cell death. For example, the recruitment

of Drp1 during apoptosis could regulate active mitochondrial fission. On the other hand, mitochondrial fragmentation could result from the loss of Opa1, which can occur prior to fragmentation (77). Opa1 depletion blocks fusion, which could promote the fragmentation of the reticulum during cell death (78). Another possibility is that fragmentation *per se* does not promote cell death but that since the factors that mediate mitochondrial fission in healthy cells are also responsible for cytochrome c release in dying cells, their activation could alter mitochondrial dynamics. For example, the apoptotic protein Bax modulates mitochondrial fusion in steady state by regulating the distribution of Mfn2 (79), and Drp1 has been suggested to fulfill a fission-independent apoptotic function (80).

Interestingly, a fused reticulum triggered by the manipulation of different proteins can confer a more or less stringent protection against cell death. The downregulation of both Fis1 and Drp1 lead to similar long, tubular mitochondria, although the downregulation of Fis1 is significantly more protective against various apoptotic stimuli than the downregulation of Drp1 (18). In addition, although the inhibition of Fis1 prevents Bax activation, the inhibition of Drp1 does not (18). This indicates that the protection conferred by the downregulation of Fis1 is not only a consequence of the fused reticulum and supposes another function of Fis1 during cell death, currently unknown.

Finally, new studies using Drp1 *knock-out* animals and MEFs have shown that the role of mitochondrial dynamics in cell death is tissue and context specific. Using Large T-antigen transformed MEFs, one study showed that following apoptotic stimuli, Bax recruitment to the mitochondria, cytochrome c release, caspase activation, and phosphatidylserine exposure were delayed, whereas the release of Smac/Diablo was unaffected (22). On the other hand, a study using primary MEFs showed no differences in

the rates of caspase activation or annexin V staining, although the authors did document delayed caspase 3 activation in the neural tube *in-vivo* (23). Both studies reported mitochondrial fragmentation during cell death, but as a late event (22), which could reflect the loss of intermembrane space fusion proteins like Opa1. It therefore appears that Drp1-dependent protection against cell death is tissue and cell type-specific, and also depends on cellular transformation. This indicates that the activation or inactivation of specific signaling cascades determines the protection conferred by mitochondrial fusion during cell death. The challenge will be to isolate these pathways to better understand the cellular specificity of fusion-induced resistance to apoptosis.

Physiological functions attributed to mitochondrial fragmentation during cell death

Actively fragmenting the mitochondria during cell death could fulfill different functions. Fragmentation could be a pro-survival mechanism. Following increased concentrations of calcium, mitochondrial fragmentation limits the propagation of the Ca^{2+} into the whole reticulum, restricting calcium overload to a few mitochondria (35). However, this is likely a specific mechanism for a particular type of insult, since the same study reported that the overexpression of Drp1 increases the sensitivity to staurosporine-induced apoptosis (35).

Another possibility is that fragmentation promotes cristae remodeling. Most of the cytochrome c resides within mitochondrial cristae, and inner membrane remodeling could be necessary to release this pool. In fact, inhibiting fission by using a dominant-negative form of Drp1 prevents apoptosis-induced cristae remodeling (42). In addition, the incubation of mitochondria with pro-apoptotic Bcl_2 family members leads to the disassembly of Opa1

oligomers, and to a subtle opening in cristae junctions sufficient for the release of cytochrome c (81), although it is unclear whether fragmentation promotes this event.

Finally, fragmentation could promote the formation of mitochondrial microdomains. Fragmentation could increase mitochondrial surface and concentrate specific lipids on the outer mitochondrial membrane, facilitating the recruitment of pro-apoptotic proteins (82). Drp1 has been shown to regulate mitochondrial membrane fluidity by unknown mechanisms (63), which could become important during cell death (82).

I.2.3.3 Conclusion

The response of mitochondria to cellular stress is complex and two specific stages have been documented so far. A mild stress triggers mitochondrial fusion (64), whereas a prolonged or more severe stress leads to apoptosis and mitochondrial fission (72). The role of mitochondrial dynamics during apoptosis is still poorly understood, and much of the controversy might stem from differences in cellular environments and cell type specificity (22). Importantly, signaling pathways might coordinate morphological changes, and the differential response of mitochondria to these signaling cascades could influence survival. For example, following a mild stress, survival will depend on the ability of the mitochondria to promote fusion (64). Future studies will hopefully unravel the complex responses of mitochondria to cell stresses.

I.2.4 Mitochondrial quality control

I.2.4.1 Cytokinesis

Microtubules, actin and intermediate filaments

The cytoskeleton is composed of three components: microfilaments, microtubules and intermediate filaments (83). The building blocks of microfilaments are globular actin monomers (G-actin), which can polymerize into filaments (F-actin) (83). Monomers are arranged head to tail and therefore give rise to a polarized filament with distinct ends (83). Microtubules are made from tubulin monomers, which also have distinguishable ends: the "minus" end is attached to the microtubule organizing centre, whereas the "plus" end radiates towards the periphery (83). Unlike microtubule and actin, the basic units of intermediate filaments consist of tissue specific molecules, which polymerize into non-polar filaments: for example, keratin in epithelial cells, or neurofilaments in neurons (83).

Two main mechanisms are used in the cell to generate force: motor proteins and actin polymerization (83). Motor proteins include the actin-dependent myosins and the microtubule-dependent kinesins (plus end directed) and dyneins (minus end directed) (83). Motor proteins possess a heavy chain, for binding filaments and hydrolysing ATP, and light chains to interact with cargos or adaptor proteins (83). Finally, the Actin Related Protein 2/3 (Arp2/3) complex mediates actin polymerization-based movement, by stimulating the nucleation of new filaments to generate secondary F-actin filaments (83). In mammalian cells, the mitochondria use microtubules for long distance traveling (83), whereas short range movement can occur along actin microfilaments with myosin motors (84).

Cytokinesis and quality control

In *S. cerevisiae* cells, movement occurs mostly along F-actin filaments, aligned into bundles in the long axis of the cell (85). Anterograde movement is towards the bud tip, and retrograde transport towards the mother cell (85). Controversies exist as to which types of locomotion is used for transport (85). The myosin protein 2 (Myo2), has been shown to regulate the transport of organelles, including mitochondria (86). However, mutations that decrease the motor's step size, does not affect mitochondrial motility (87). Instead, Myo2 was suggested to act as a retention protein, to anchor mitochondria to the bud tip (87).

An interesting alternative has been proposed, which relies on another mechanism to generate force: actin polymerization (83). For anterograde transport, the mitochondria would use the Arp2/3 complex to promote actin nucleation (88), and the mitochore, composed of three integral outermembrane proteins would act as a scaffold, to attach the mitochondria to the actin cables (89). Inhibition of any of these proteins leads to defects in mitochondria morphology, and to the inhibition of mitochondrial movement (89). However, these proteins are also essential for the import of some proteins, and they could simply be required for the import of proteins required for movement (90, 91).

An attractive hypothesis related to the non-motor based mitochondrial movement is that it provides a means for quality control (89). According to this model, during retrograde transport the mitochondria bind to actin cables and are passively transported toward the mother cell tip (92). However, anterograde movement occurs against the retrograde movement of the actin cables, using the nucleation of actin cables by Arp2/3. The most metabolically active mitochondria would therefore be preferentially transferred to the bud (89). Damaged, carbonylated proteins accumulate with replicative age, but are selectively

retained in the mother cell during division, and not inherited in the daughter cell (93). Similarly, Apr2/3 mediated anterograde movement could promote the retention of damaged mitochondria in the mother cell (89). The mechanism by which "damaged" mitochondria are recognized for passive transport back to the mother are unknown but could reflect either changes in a metabolic sensor that affect the Arp2/3 nucleation, or diminishing local ATP concentrations that render active transport impossible.

I.2.4.2 Fission and autophagy

A recent study has elegantly demonstrated that fission can produce metabolically different organelles (94). The authors hypothesized that if fusion is a selective process, mitochondria with low fusion capacities could be identified (94). Using a photoactivable Green Fluorescent Protein (GFP), they were able to highlight a subpopulation of mitochondria that retained the activated GFP, and were therefore not fusing with the rest of the reticulum (94). Importantly, these had reduced potential and the probability that they would fuse with another mitochondria was significantly lower than that of a hyperpolarized mitochondria. Interestingly, mitochondria with lower potential had decreased levels of Opa1, which could explain their exclusion from the rest of the reticulum (94). Low-expressing Opa1 mitochondria were eventually targeted for autophagy (94).

This study illustrates that fission can be a selective process, since it can lead to two populations of mitochondria: a hyperpolarized mitochondria and a mitochondria with low potential and low levels of Opa1. It is unclear whether Opa1 is specifically segregated prior to the fission event or whether Opa1 is selectively degraded in low potential mitochondria post-fission.

A recent study suggests that Parkin might be involved in the selection of damaged mitochondria to be targeted for mitophagy (95). Parkin is a cytosolic protein, with some association with the endoplasmic reticulum and the mitochondria (95). In an elegant study, Narendra *et al.*, showed that decoupling the mitochondria using Carbonyl Cyanide-m-Chlorophenyl hydrazone (CCCP) triggers the recruitment of Parkin to the mitochondria (95). Closer examination in HeLa cells revealed that Parkin was selectively recruited to mitochondria with low potential. This was not simply caused by fragmentation, since Parkin was still recruited to mitochondria unable to fragment due to the overexpression of a dominant negative form of Drp1 (95). Strikingly, HeLa cells transfected with Parkin and treated with CCCP, became devoid of mitochondria as assessed by electron microscopy (95). Supporting these observations, the cells were able to grow on glucose media but not on galactose-only media, indicating that they had lost their oxidative phosphorylation capacity (95). Importantly, the downregulation of proteins regulating autophagy prevented the degradation of mitochondria, indicating that Parkin mediates the delivery of damaged mitochondria to lysosomes (95) *(Figure 1.8)*.

Figure I-8 Parkin and mitochondrial quality control

Fission can be a selective process, creating two asymmetric mitochondria: one with high potential, and another with low potential. The daughter mitochondrion with the lower potential remains isolated from the rest of the reticulum due to low levels of Opa1. These mitochondria are then selectively removed by autophagy. Importantly, Parkin plays an important role in selecting damaged cargo for autophagy.

Asymetric Drp1
mediated fission

Recruitment of Parkin
to damaged mitochondria

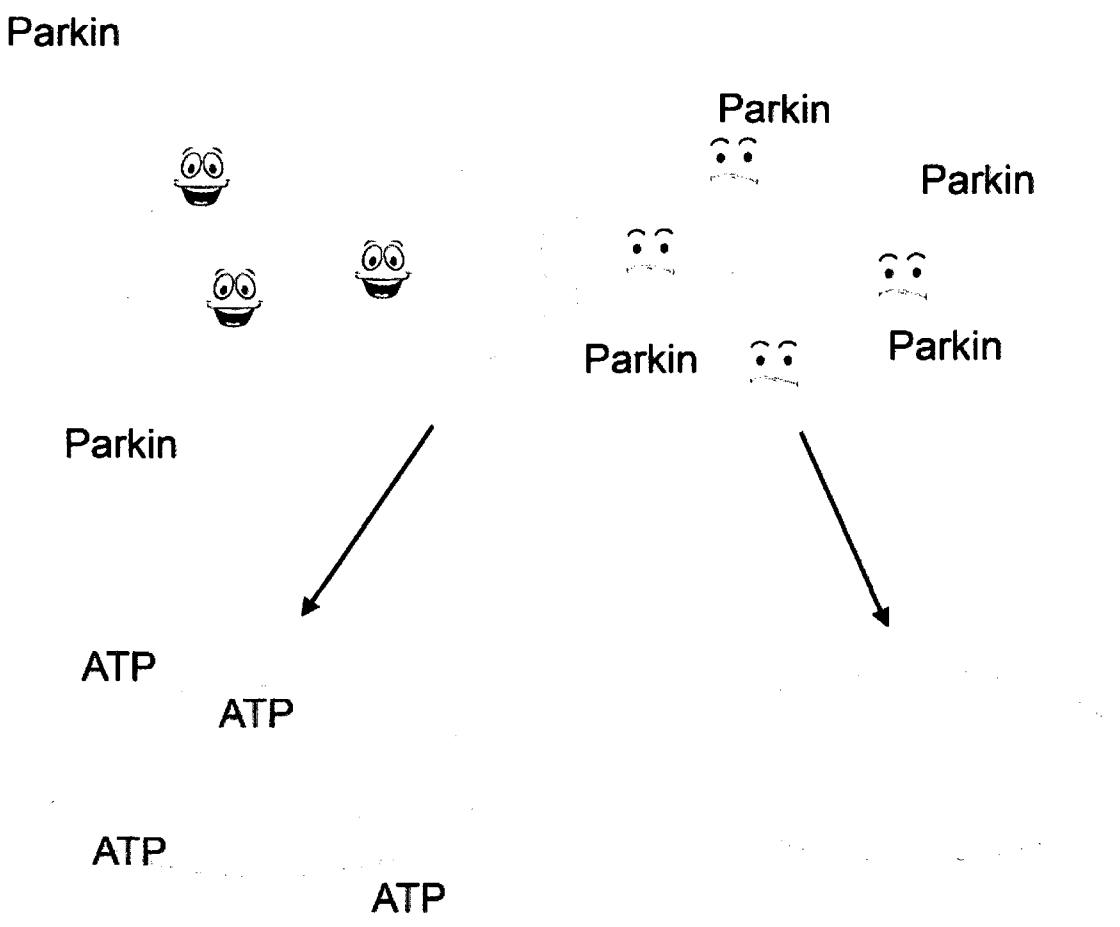

Healthy mitochondria
High potential
Re-fuses into the network

Damaged mitochondria
Low potential
Low levels of Opa1
Discarded by autophagy

A

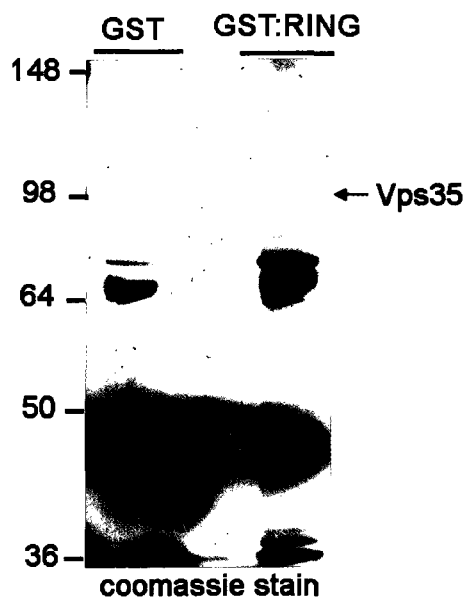

B

Peptides	Mascot Score	P-value
R.ILVGTNLVR.L	68	0.00069
K.AELAELPLR.L	52	0.026
R.LSQLEGVNVER.Y	59	0.0057
K.IPVDTYNNILTVLK.L	83	2.00E-05
R.SEDPDQQYLILNTAR.K	81	2.70E-05
K.ENDAVTIQVLNQLIQK.I	96	8.10E-07
K.LFDIFSQQVATVIQSR.Q	86	9.40E-06
K.IREDLPNLESSEETEQINK.H	70	0.00031

C

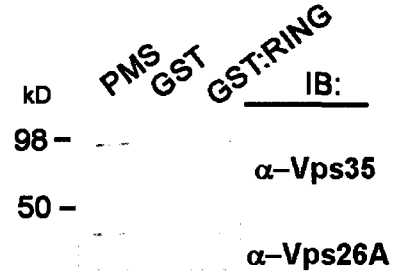

D

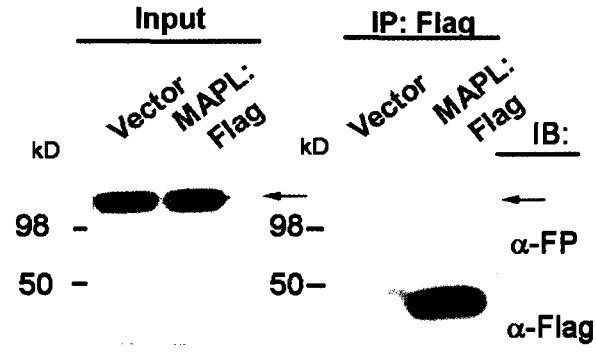

E

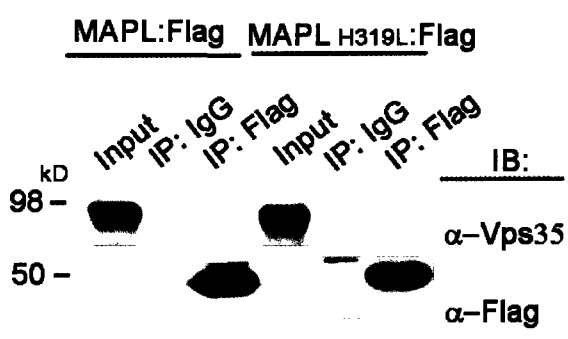

F

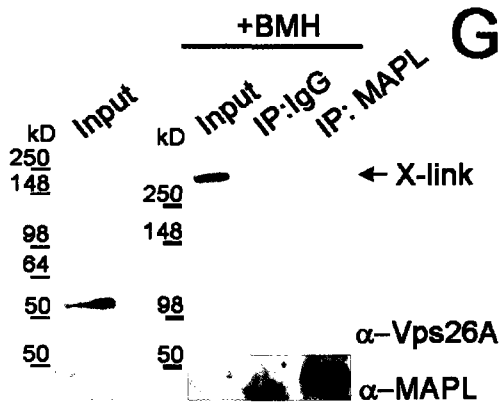

G

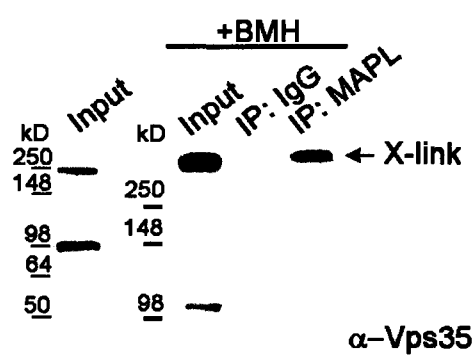

Parkin functions in a novel vesicular pathway governing mitochondrial quality control.

Vincent Soubannier[1], Gian-Luca McLelland[2], Emelie Braschi[1], Peter Rippstein[1], Brett Kaufman[2], Eric A. Shoubridge[2], Edward A. Fon[2], and Heidi M. McBride[1] *

[1]University of Ottawa Heart Institute, Lipoproteins and Atherosclerosis Group, 40 Ruskin St., Ottawa, Ontario, K1Y 1V1, Canada.

[2]Montreal Neurological Institute, McGill University, 3801 University Ave., Montreal, Québec, H3A 2B4, Canada.

Summary: Mitochondrial vesicles target lysosomes.

Summary

Interference with the mechanisms that govern mitochondrial quality control have been increasingly linked with neurodegenerative diseases. However, the mechanisms that govern mitochondrial protein and lipid turnover are poorly understood. We have identified a novel mitochondrial quality control pathway characterized by mitochondria derived vesicles (MDVs). MDVs are induced by oxidative stress and are delivered to lysosomes. Their biogenesis can be reconstituted *in vitro* and is independent of Drp1-induced mitochondrial fission. Remarkably, the amount of cargo removed by the MDV pathway is comparable to the rates of degradation mediated by mitochondrial proteases. MDVs are selectively enriched for oxidized proteins, whose identity was dependent upon the type of mitochondrial stress. In particular, the induction of MDVs by intrinsic mitochondrial damage required the selective recruitment of parkin to the vesicles during budding. These data are the first to characterize a novel vesicle transport route between the mitochondria and lysosomes, providing new insights into the pathogenesis of Parkinson's disease.

Highlights.

- This is the first report of a novel mitochondrial vesicle transport route that delivers oxidized cargo to lysosomes, playing an important role in quality control.
- The cell-free reconstitution of vesicle budding from mitochondria demonstrates cargo specificity and differential regulation of cargo incorporation depending upon the type of stress.
- This study demonstrates that the Parkinson's disease protein parkin is required for the formation of vesicles carrying matrix cargo upon internal mitochondrial oxidative stress, placing this new pathway as a therapeutic target for the treatment of parkinson's disease.

Introduction.

Mitochondrial respiration is the source of many reactive oxygen species, peroxides and nitric oxides, which can lead to the oxidation of mitochondrial protein, lipids and the introduction of mutations within the mitochondrial genome. Thus, the removal of oxidized components is essential for the maintenance of mitochondrial function. Dysfunction in mitochondrial quality control has long been implicated in aging and neurodegenerative diseases such as Parkinson's disease (PD). PD is characterized by the degeneration of midbrain dopamine neurons leading to progressive motor impairment (Lang and Lozano, 1998a; Lang and Lozano, 1998b). The first clues that mitochondrial dysfunction was involved in PD stem from the discovery that neurotoxins such as MPTP and rotenone, which are potent mitochondrial complex I inhibitors could recapitulate pathological and clinical features of PD (Betarbet et al., 2000; Langston et al., 1983). These neurotoxins lead to the generation of ROS and are used widely as animal models of PD (Terzioglu and Galter, 2008). However useful as a model, it is unlikely that such toxins are directly responsible for the vast majority of PD cases, raising questions as to the role of mitochondrial dysfunction in the disease. Many of these doubts have now been quelled by work implicating PD genes in mitochondrial function. In particular, parkin, an E3 ubiquitin ligase and PINK1, a mitochondrially-localized protein kinase, each responsible for autosomal recessive forms of PD, have been intimately linked with mitochondrial dynamics and quality control. Most notably, in *Drosophila*, parkin and PINK1 function in common pathway to regulate mitochondrial morphology (Bueler, 2009; Poole et al., 2008), whereas in mammalian cells PINK1 is required to target parkin to depolarized mitochondria, leading to their autophagic

clearance (Narendra et al., 2008; Vives-Bauza et al., 2009). Thus, the recent convergence of genetic and neurotoxin studies has strongly implicated mitochondrial dysfunction in PD. However, many of the basic mechanisms governing mitochondrial quality control and their role in neurodegeneration remain largely unknown.

The three known means controlling mitochondrial protein turnover are the mitochondrial proteases, proteasome-mediated degradation and mitochondrial autophagy (mitophagy). Proteases of the AAA ATPase family are localized both within the matrix and intermembrane space and play essential roles in the degradation of unfolded and unassembled proteins (Arnold and Langer, 2002). In the yeast *saccharomyces cerevisiae* it has been shown that protease dependent turnover of pre-existing and newly imported proteins reaches 6-12% of the total mitochondrial protein per hour (Augustin et al., 2005). These proteins are degraded into peptides within the mitochondria which are released into the cytosol for final degradation by the proteasome. Since the proteases degrade unfolded proteins, it is likely that oxidized proteins would become unfolded, thereby presenting them to the proteases. This has been shown to be true for the LON protease-mediated degradation of oxidized aconitase (Bota and Davies, 2002).

In selected cases, mitochondrial outer membrane proteins have been shown to be ubiquitinated and targeted to the proteasome. This process has not been linked to ROS or oxidation, rather it allows the regulated turnover of individual proteins. For example, the ubiquitination of the Bcl-2 family member Mcl-1 by MULE during the initiation of cell death selectively removes the anti-apoptotic protein from the organelle (Warr et al., 2005; Zhong et al., 2005). Similarly in yeast, the protease-dependent degradation of the fusion GTPase Fzo1 leads to the fragmentation of mitochondria during G1 arrest and upon addition of the mating pheromone (Neutzner and Youle, 2005). It is not yet clear how these integral membrane, tail-anchored proteins are extracted from the mitochondria and delivered to the proteasome, leaving open the possibility for an outer mitochondrial membrane associated degradation pathway (OMMAD) (Neutzner et al., 2007).

The final mechanism for mitochondrial turnover is through mitophagy, where whole organelles are engulfed by the autophagosome and targeted to the lysosomes for degradation. This process is most evident during reticulocyte maturation, where all of the mitochondria are removed in a programmed process requiring specific proteins like the BH3-containing proteins Nix and BNIP3 (Chen et al., 2008; Sandoval et al., 2008; Schweers et al., 2007). It has recently

been shown that DRP1-dependent mitochondrial fission is important for targeting respiration-incompetent mitochondria to the autophagosome (Narendra et al., 2008; Twig et al., 2008); providing the first evidence that autophagy can specifically target dysfunctional and fragmented organelles. Mitophagy has been shown to be induced by ROS accumulation, which is linked to respiration-incompetence, making this an obvious pathway to clear the damaged organelles. Indeed, the selective targeting of depolarized mitochondria to the autophagosome by parkin and PINK1 further supports the specificity of autophagic turnover, and the involvement of this pathway in PD (Narendra et al., 2008; Vives-Bauza et al., 2009).

Together these three processes are thought to comprise the mechanisms that govern mitochondrial quality control. However, we have recently discovered a new process in mitochondrial cell biology, characterized by the ability of mitochondria to generate mitochondrial derived vesicles (MDVs) (Andrade-Navarro et al., 2009; Neuspiel et al., 2008). MDVs are formed in a manner independent from the fission GTPase DRP1, and ultrastructural analysis of cells transfected with a SUMO E3 ligase MAPL has shown budding profiles on the mitochondrial surface consistent with vesicle formation (Braschi et al., 2009; Neuspiel et al., 2008). Most critically, MDVs show evidence of cargo selectivity, where for example, the vesicles may carry a protein like MAPL, but lack the outer mitochondrial membrane import receptor Tom20. We initially characterized a number of distinct MDV pools in the cell and demonstrated that one population of MDVs carrying MAPL target the peroxisomes (Neuspiel et al., 2008). In the current study we have determined that MDVs are generated as an early response to oxidative stress and are enriched in oxidized proteins. Moreover, upon internal oxidative stress there is a specific induction of double membrane bound mitochondrial matrix-containing MDVs, which requires the recruitment of parkin. We propose that MDVs comprise a novel pathway in mitochondrial quality control that functions to selectively remove oxidized cargo for delivery to the lysosomes. More broadly, the requirement for parkin in this pathway suggests a central role for MDV-related transport defects in PD, helping to explain the accumulation of mitochondrial damage during disease progression.

Results

Mitochondrial Derived Vesicles transport to lysosomes is an early response to oxidative stress.

Our earlier study identified at least two populations of MDVs, one carried a newly identified outer membrane protein called MAPL (mitochondrial anchored protein ligase) and was targeted to peroxisomes; however, the fate of other MDVs remained unknown (Neuspiel et al., 2008). We hypothesized that at least some of the MDVs we had observed may represent a pathway for the removal of damaged proteins and lipids from the mitochondrial reticulum. To test this, we treated cells with a sub-toxic dose of ROS-generating enzyme glucose oxidase to induce protein oxidation(Das et al., 2005). Upon this oxidative stress, we observed that mitochondria produce MDVs as an early response, before the fragmentation of the mitochondrial network, characteristic of mitochondrial dysfunction (Figure 1A). The formation of these structures occurred even upon silencing of DRP1, confirming that they were not fragmented mitochondria and that this process was independent of mitochondrial fission (Neuspiel et al., 2008). The quantification of MDVs confirmed a significant ($p<0.05$) increase in MDV formation upon ROS production by glucose oxidase (Figure 1B) and that this increase occurred even in the presence of the dominant interfering mutant of the mitochondrial fission GTPase Drp1 (DRP1 (K38E)) (Figure 1C). The quantification indicates that the formation of MDVs is a significant first-line response of mitochondria to oxidative stress.

To determine whether these vesicles were targeted for degradation, we treated cells expressing DRP1(K38E) with glucose oxidase (Figure 1Di,ii) and examined whether the MDVs co-localized with lysosomal markers. To ensure that we followed MDVs rather than mitochondrial fragments, the structures must have shown evidence of cargo selectivity in addition to their independence on DRP1. In this case, we examined structures that were positive for the outer membrane marker Tom20, but negative for the ectopically expressed matrix protein OCT-DsRed (Harder et al., 2004). Using these parameters, we identified Tom20 positive MDVs induced after treatment with glucose oxidase, and shown that a population of these that co-localized with lysosomes, as indicated by Lamp1 immunostaining (Figure 1C).

Reconstitution of MDV formation *in vitro*.

To characterize the formation of MDVs biochemically, we reconstituted their formation from bovine heart mitochondria. Isolated mitochondria were incubated for 60 min at 37°C in the

presence of cytosol and an energy regenerating mixture, then separated by centrifugation. The post-mitochondrial supernatant was then treated with trypsin to remove any background signal resulting from broken mitochondria. The trypsin-resistant proteins incorporated within MDVs were examined by Western blot (Figure 2). The assay was stimulated by the presence of cytosol, with peak activity at 3 mg/ml (Figure 2A,B), and was time-dependent (Figure 2C,D). To quantify the relative enrichment of each mitochondrial protein within the supernatant fractions, we compared the signal intensity relative to that found in the initial mitochondrial fraction. The data reveal that VDAC (ratio of 0.9) is more enriched in vesicles compared to the complex III subunit core 2 (ratio of 0.2) (Figure 2B,D). The differential enrichment of cargo found within the supernatant fraction provides evidence for cargo selectivity in this *in vitro* reconstitution assay. When comparing the amount of protein found in the vesicles relative to that present in the starting mitochondria (Figure 2A,C), our data indicate that approximately 0.1 - 5% of mitochondrial proteins are released from the organelles per hour, with Core 2 at the lower end and VDAC showing a more abundant incorporation. This represents a significant amount of mitochondrial protein turnover, similar to the 6-12% calculated protein turnover through mitochondrial proteases (Augustin et al., 2005).

The basal reaction, performed at 37°C, for 60 minutes in the absence of cytosol, was energy-independent, since apyrase treatment was not inhibitory (Figure 2E). In fact, the addition of apyrase stimulated the reaction, which may reflect increased mitochondrial stress. The reaction was also stimulated by addition of non-hydrolysable forms of both ATP and GTP, indicating that nucleoside triphosphate-binding factors stimulate vesicle formation. (Figure 2E). Indeed, that GTPgS treatment stimulated MDV formation was consistent with the evidence that this process is DRP1-independent. DRP1 would require GTP hydrolysis for the fission of membranes, a process known to be inhibited by non-hydrolysable analogues of GTP. The energy independence of MDV formation is consistent with a number of budding processes, including shiga toxin entry and reconstituted coat-dependent vesicle budding reactions (Matsuoka et al., 1998; Romer et al., 2007; Spang et al., 1998).

To test whether vesicle formation can be stimulated *in vitro* as it was in intact cells (Figure 1), we incubated isolated mitochondria under a number of conditions inducing various types of stress (Figure 3). Xanthine in the presence of xanthine oxidase was used as an external ROS generator, and antimycin A was used to inhibit complex III, leading to internal ROS. The

data show that ROS induced stress simulated MDV production in a temperature-dependent manner (Figure 3A). However, where xanthine oxidase led to VDAC enriched MDVs, antimycin A treatment led to the enrichment of the complex III component, core 2 (Figure 3A). The inhibition of mitochondrial ribosomes with chloramphenicol stimulated VDAC-containing vesicles without enrichment of core2, and the inhibition of the ATP synthase with oligomycin had no effect, further indicating that the reaction is ATP independent (Figure 3A). Again, the basal reaction was also stimulated by ATPγS, as seen in Figure 2E. Importantly, the basal reaction and the stimulatory effects of antimycin A, xanthine oxidase and GTPγS were all inhibited in the presence of N-ethylmaleimide, a non-specific alkylator of free cysteine residues (Figure 3B). NEM sensitivity is a hallmark feature of all cell-free membrane transport assays and indicates the requirement for a cysteine-containing enzyme in the budding process (Block et al., 1988).

To further characterize the cargo incorporated into MDVs under oxidative stress, we tested for the presence of multiple proteins within the trypsinized post-mitochondrial supernatants of various treatments (Figure 3C). Although components of OXPHOS complexes II, III and IV are differentially incorporated within these MDVs under various treatments, proteins of complex I and V were excluded (Figure 3C). The matrix enzyme pyruvate dehydrogenase was also enriched in MDVs upon the induction of damage, indicating that soluble matrix cargo is also incorporated. We probed the reactions with antibodies against the nucleoid protein TFAM (Figure 3D) (Kaufman et al., 2007), and performed PCR reactions to amplify mtDNA within the supernatants (Figure 3E). Under the conditions examined, we found no evidence that mtDNA is incorporated within MDVs.

Given the stimulation of MDV formation upon oxidative stress, we tested whether there is enrichment for oxidized protein within the cargo. The MDVs were incubated in presence of DNPH to derivatize the carbonyl groups, a signature of oxidation, which were detected by Western blot analysis (Figure 3F). Loading equivalent protein amounts of mitochondria and vesicle fractions, the data show that the MDVs are enriched in oxidized cargo relative to the parent mitochondria, both in the basal conditions (Figure 3F, left panel), and upon treatment with antimycin A (Figure 3F, right panel). Taken together, the reconstitution experiments confirm and extend the data obtained in cells, demonstrating that MDVs are stimulated under conditions of stress and are selectively enriched for oxidized cargo.

Ultrastructural analysis of the initial mitochondria used in the *in vitro* assay revealed the presence of 70-100 nm vesicular structures still attached to a few mitochondria (Figure 4A). In most cases, the presence of both membranes is clearly visible (Figure 4A, left and middle panels), often with a constriction site evident (Figure 4A, middle panel, arrow). We also observed the outer membrane forming protrusions with constrictions at their base, consistent with the formation of single membrane bound vesicles (Figure 4A left panel, arrow). Examination of the post-mitochondrial supernatant from xanthine oxidase treatment revealed primarily single membrane bound vesicles (Figure 4B left panel), consistent with the preferential enrichment of VDAC in this fraction. In contrast, treatment with antimycin A, which was enriched for the complex III component core2, revealed two populations of vesicles, one with a single membrane, and a second containing a double membrane (Figure 4B, right panels). These ultrastructural analyses prove that both single and double membrane bound vesicles are being actively formed during the reaction.

To further isolate the MDVs and determine their density, vesicles generated by antimycin A treatment were separated using a discontinuous sucrose gradient. A light fraction containing VDAC appears at the 20/30% sucrose interface, and a heavy fraction containing both core2 and VDAC sediments at the 30/40% interface, along with the ER contaminants (Figure 4c). These conditions of separation and purification of the fractions allowed us to omit the pre-treatment of samples with trypsin, allowing us to investigate the incorporation of the outer membrane protein import receptor Tom20. Tom20 was present in the heavy membrane vesicles, but was poorly enriched relative to VDAC in the light membrane fraction (Figure 4C). Ultrastructural analysis of the light membrane fractions isolated at 20/30% sucrose confirmed the presence of single membrane vesicles, and the heavy membrane fraction isolated at 30/40% sucrose revealed the presence of double membrane bound vesicles (Figure 4D). These data directly demonstrate that the trypsin-resistant proteins found within the supernatants of the budding reaction are contained within regular, membrane bound vesicle structures. Together with the specific enrichment of cargo, these data confirm that MDVs reflect a *bona fide* vesicle intermediate rather than a non-specific disruption of the mitochondria.

Parkin is required for antimycinA induced MDVs.

These data infer the existence of machinery capable of sorting mitochondrial proteins within the bilayer and generating the vesicle. The question of how cargo may be recognized then

becomes an essential aspect of this process. We considered that there may be local regions of the mitochondria where proteins become oxidized, which could function as exit sites for MDVs. To date, the only candidate protein able to recognize uncoupled mitochondria is parkin. As an E3 ubiquitin ligase already implicated in mitochondrial quality control, we considered it a candidate regulator of this early response to oxidative stress. To examine the potential role for parkin in MDV formation, we incubated transfected HeLa cells expressing GFP-parkin and OCT-DsRed2 with CCCP, glucose oxidase, and antimycin A for analysis by confocal microscopy. These cells were also infected with adenovirus expressing DRP1 (K38E) in order to prevent mitochondrial fragmentation and follow only the MDV population. As previously shown, GFP-parkin is cytosolic in untreated cells and is efficiently recruited to the entire population of mitochondria upon depolarization with 10 μM CCCP treatment (Figure 5, CCCP). Upon treatment with glucose oxidase, Tom20 vesicles are visible that lack OCT-DsRed2 (Figure 5, GO, open arrowheads), yet GFP-parkin remains cytosolic with no visible recruitment to mitochondria or MDVs. However, following treatment with 100 μM antimycin A, we observed the selective recruitment of GFP-parkin to MDVs enriched for the mitochondrial matrix marker OCT-DsRed2, yet devoid of Tom20 (Figure 5A (Anti A, arrows)). In contrast to the effects of CCCP, the antimycin A-induced recruitment of parkin was MDV-specific, with no parkin found on mitochondria *per se*. These data show that in addition to its recruitment to depolarized mitochondria; parkin is recruited to MDVs carrying matrix, oxidized (Figure 3F) cargo. We followed the fate of MDVs positive for OCT-DsRed2 and confirmed that they are also targeted to the lysosomes (Supplemental Figure 1A). Given the established delivery of whole mitochondria to the autophagosome for degradation, we tested whether MDV delivery to lysosomes involved the activation of autophagy. Biochemical experiments showed that neither GO nor antimycin A treatments induced the activation of LC3, an early marker of autophagy (Supplementary Figure 1B), suggesting that the vesicular delivery of oxidized cargo to lysosomes is likely an LC3-independent mechanism.

We further investigated the recruitment of endogenous parkin on MDVs formed *in vitro* from bovine heart mitochondria after induction of oxidative stress using antimycin A. Vesicles were separated on a discontinuous sucrose gradient and western blot analysis of the MDV fractions revealed a shift of cytosolic parkin, found at the bottom of gradient under basal conditions, into the vesicle fraction found at the 30/40% interface in presence of antimycin A

(Figure 6). Therefore, the *in vitro* assay confirmed that endogenous parkin is recruited to antimycin A-induced MDVs.

Finally, in order to assess the function of parkin in MDV formation, we took advantage of the fact that HeLa cells do not express parkin. We then quantified the number of DsRed2-positive MDVs generated upon antimycin A (*versus* vehicle control) treatment in the presence or absence of transfected GFP-parkin (Figure 7A). Control cells treated with antimycin A did not see a significant change in either Tom20 or OCT-DsRed2 containing MDVs (Figure 7B). However, treatment of cells expressing GFP-parkin with 40 μM antimycin A generated a significant increase in MDVs specifically carrying OCT-DsRed2, without an accompanying change in Tom20 positive MDVs ($p<0.05$). These data provide further evidence for the specificity of MDV formation and indicate that parkin-GFP is a rate-limiting component of matrix-enriched MDV formation upon antimycin A treatment.

Discussion

These data are the first to outline a novel mechanism for mitochondrial quality control that shows a very high level of specificity for the selective removal of damaged proteins. The combined use of confocal and EM imaging with the biochemical reconstitution of MDV formation have established the existence of a novel intracellular transport route between mitochondria and lysosomes. Quantitatively, the amount of protein incorporated into the vesicles *in vitro* is similar to the amount of proteins degraded by the mitochondrial protease systems per hour (Augustin et al., 2005). We suggest that MDV-based transport of damaged cargo to lysosomes plays a role in the steady-state removal of oxidized mitochondrial respiratory complexes, integral membrane proteins, soluble proteins and lipids. One implication of this work is that MDVs provide a unique vehicle for the efficient removal of entire OXPHOS complexes. This quality control strategy would provide the dual advantage of circumventing the need for proteases to degrade individual respiratory complex subunits with the potential buildup of toxic proteolytic intermediates, while sparing an otherwise healthy mitochondrion from complete engulfment and destruction by mitophagy. In fact, the early removal of oxidized proteins could prevent the activation of mitophagy, which targets whole mitochondria only after they have become terminally respiration-incompetent (Twig et al., 2008). In this way, MDV

transport to lysosomes would complement the established mechanisms for mitochondrial turnover and appear to function independently of the autophagic machinery.

We propose that the existence of a selective pathway for the delivery of damaged mitochondrial cargo to lysosomes likely plays a crucial role in the protection of the mitochondrial reticulum from oxidative stress, mitochondrial impairment and cell degeneration. This point is highlighted by the involvement of parkin. Mitochondrial impairment has long been associated with the pathogenesis of PD in the form of reduced complex I activity (Schapira et al., 1990) and accumulation of mtDNA mutations in dopaminergic brain regions in PD patients (Bender et al., 2006). Although we have demonstrated a role for parkin in the generation of antimycin A-induced vesicles, we did not see any incorporation of complex I in these conditions. The reduced complex I activity observed in PD models may reflect an overall imbalance in mitochondrial quality control and increased ROS generation from *any* of the OXPHOS complexes. In this way, targeting this complex with drugs may reveal a sensitivity to damage that leads to PD.

Despite the accumulated evidence the cellular mechanisms responsible for mitochondrial dysfunction in PD remain unclear. By implicating parkin in the MDV pathway, this study provides a novel framework for understanding the role of mitochondrial quality control in PD. Indeed, by taking part in the removal of oxidized, damaged respiratory complexes and other proteins through the MDV pathway, parkin may help maintain mitochondrial integrity through both the preservation of a functional electron transport chain and the protection of the mitochondrial genome from oxidative damage. Previous studies have implicated the PD genes in the regulation of mitochondrial morphology, where the parkinson's phenotype in the fly could be rescued by restoring the mitochondrial reticulum (Deng et al., 2008; Exner et al., 2007; Lutz et al., 2009; Mortiboys et al., 2008; Poole et al., 2008). However this study, along with the recent reports of parkin involvement in mitochondrial turnover (Narendra et al., 2008; Vives-Bauza et al., 2009), suggest that observed changes in morphology may be secondary to changes in mitochondrial integrity (McBride, 2008).

Cargo selectivity and transport of MDVs.

One of the essential conclusions from this study is that the cargo incorporation into MDVs is highly selective. The data show that ROS generated within the OXPHOS chain enriches MDVs for subunits of complexes II, III and IV, yet complex I, V and mtDNA nucleoids

are excluded. The exposure to ROS generated outside mitochondria leads to vesicles enriched for VDAC, but lacking complex III. Despite the differential cargo incorporation, MDVs appear to be of uniform size, as indicated by the ultrastructural analysis and by the distinct sedimentation peaks identified on sucrose gradients. The exclusion of the large complexes I, V and mtDNA could be due to size limitations, or perhaps they may be incorporated with different triggers. The average size of a nucleoid has been shown to be almost 70nm, which could be too large for this pathway.

Although the vesicles examined in this study were targeted to lysosomes, we have previously shown that MDVs carrying MAPL are delivered to peroxisomes (Andrade-Navarro et al., 2009; Neuspiel et al., 2008). The diversity of MDVs makes it difficult to know how many there are in any given cell since we are limited in our microscopic techniques and can only follow one or two species at a time, which likely underestimates the true number of MDVs that are produced under a given oxidative stress condition. However, these data point to the emerging concept in mitochondrial biology; that MDVs have the potential to carry a number of different proteins to different intracellular destinations in a selective manner. One implication of this transport process is the observation that many mitochondrial proteins localize to other sub-cellular locations. Certainly, a number of these are due to cryptic import signals, like those present in Bcl-2 (Annis et al., 2004; Nguyen et al., 1993) and Fis1 (Delille and Schrader, 2008), but this is not evident in all cases. For example, it has been shown that complex V, the F_1F_0-ATP synthase, is dually-localized to the plasma membrane of endothelial cells, where it plays a role in HDL metabolism (Chi and Pizzo, 2006; Martinez et al., 2003). This complex *must* be assembled within the mitochondrial inner membrane, since it contains two subunits encoded by the mtDNA. Although complex V was absent from the vesicles induced by antimycin A, we cannot exclude that in certain cell types with unique triggers, that a vesicular transport route may carry this complex, either directly or indirectly, to the cell surface.

The contribution of MDVs and parkin to mitochondrial integrity.

This study is the first to document MDVs as a mechanism regulating the removal of oxidized proteins from mitochondria. With our current tools it is difficult to predict the global impact of this pathway in maintaining mitochondrial integrity *in vivo*, however a number of points can be made from the data presented here. The primary observation that MDV formation is an early response to oxidative damage places this process within a hierarchy of cellular

responses. Our biochemical studies show that even under basal conditions, vesicles carrying oxidized proteins are removed from mitochondria (Figure 3F), indicating that this is an ongoing process to maintain mitochondrial integrity. In addition, we consistently observe low numbers of vesicles in untreated cells, even in the absence of parkin (Figure 7B). This demonstrates that although parkin plays a significant role in at least one class of MDVs, it is not an essential component for the entire pathway. Indeed, parkin was required specifically to generate vesicles triggered from intrinsic mitochondrial ROS, and was not recruited to the vesicles formed upon cytosolic ROS. This indicates a complex set of machineries that are responsive to distinct molecular cues, initiated either internally or externally relative to mitochondria, capable of identifying oxidized or otherwise damaged proteins, and laterally enriching them within the mitochondrial membranes in order to form a vesicle.

Although we have shown that, in the case of treatment with antimycin A, parkin is selectively recruited to matrix-enriched MDVs, the receptor(s), accessory factors and target substrates involved in this pathway remain unknown. The PD gene *PINK1*, which encodes a mitochondrial kinase, was recently shown to be necessary for parkin recruitment to mitochondria depolarized by CCCP (Vives-Bauza et al., 2009). Whether or not PINK1 and other PD genes are also involved in the MDV pathway identified here remains to be determined. More universally, given the involvement of parkin, we consider it possible that a number of ubiquitin E3 ligases could play distinct roles in the formation of different populations of vesicles. Taking the ubiquitination of cell surface receptors for lysosomal sorting as precedent (Katzmann et al., 2002), it is possible that ubiquitination may function as a mechanism to segregate proteins for their incorporation into the vesicle. In this way, parkin may not play a role in glucose oxidase-induced vesicles, but would be essential only for those formed in response to intrinsic ROS damage. Clearly there will be a great deal of future work required to elucidate the components of this novel interorganellar signaling pathway, in order to identify the determinants of MDV formation, cargo incorporation and selective delivery to the target organelle.

MDVs and mitophagy: redundant pathways ensuring mitochondrial health?

The relationship between parkin, mitophagy and MDV formation appears to be complex. Uncoupling the entire mitochondrial reticulum has been shown to lead to a complete recruitment of parkin to the mitochondria (Narendra et al., 2008), a finding that has been replicated in this study. However, the study by Narendra *et al.* showed that the delivery of mitochondria to

lysosomes was through an autophagic pathway, which does not appear to be the case for parkin-positive MDVs induced by antimycin A. Where the global loss of mitochondrial membrane potential would lead to complete mitochondrial recruitment of parkin, local oxidative stress may restrict its recruitment to specific mitochondrial domains, which are eventually incorporated into vesicles. The common underlying mechanism of parkin recruitment appears to be based upon changes in mitochondrial function, which could translate as either global or local changes in the redox status within the intermembrane space. For example, potential alterations in disulfide bridging could activate parkin recruitment factors, like PINK1, leading to increased kinase activity on the cytosolic side of the outer membrane. A complex set of disulfide-relay chaperones exist within the intermembrane space that may be involved in this type of redox sensing, including Erv1and Mia40 (Koehler and Tienson, 2009). The selective participation of parkin in this novel vesicular pathway not only adds another layer of regulation to the expanding role for parkin in mitochondrial homeostasis, but highlights a requirement for future study to resolve some of the discrepancies in the literature concerning parkin and mitochondrial dynamics, as well as to tease apart the role for parkin in mitochondrial quality control.

Regardless of the precise mechanism involved in the generation of parkin-positive MDVs, we do not consider it surprising that the early MDV response to oxidative stress may function prior to the activation of autophagy. This would represent a distinct quality control process that operates when the majority of the mitochondrial reticulum remains intact and actively respiring. This scenario is in contrast to treatment with CCCP, where mitochondrial ATP production would be abolished. Although MDV biogenesis and mitophagy may represent two mitochondrial degradation pathways that are active under distinct cellular conditions, the differential requirement for autophagy in the delivery of mitochondrial proteins to the lysosomes may in fact ensure redundancy in mitochondrial turnover mechanisms. This redundancy may be what allows PD patients to survive relatively symptom-free until the onset of disease, which can be in later years. This opens the door for the identification of therapeutic interventions that may accelerate the turnover of mitochondrial proteins that would be of benefit to patients suffering from a number of neurodegenerative diseases.

Experimental Procedures

Antibodies and Reagents

Antibodies were purchased from the following providers: anti-Core2, anti-VDAC, anti-Cox1, anti-PDH, anti-NDUFA6, anti-su30kD, anti-F_1 β, Mitoscience (Eugene, Oregon, USA); anti-TFAM (Brett A. Kaufman), anti-Tom20, anti-parkin, anti-Lamp1 (Santa Cruz Biotechnology). Oxyblot reagents were purchased from Chemicon International - California, USA and used following the manufacturers instructions. Dextran 647 was purchased from Invitrogen.

Cell Culture

HeLa were maintained in Dulbecco's Modified Eagle Medium (Gibco Invitrogen) supplemented with 10% fetal bovine serum, penicillin and streptomycin.

DNA Constructs

DRP1(K38E)-CFP was previously described (Harder et al., 2004). The matrix marker pOCT-DsRed construct contains the first 32 amino acids of ornithine carbamyl transferase fused to DsRed2.

Loading of cells with Dextran 647

Cells were briefly washed with DMEM media without fetal bovine serum before incubation with Dextran 647 at 1mg/ml for 30 min. Cells were then washed and incubated with DMEM supplemented with 10% fetal bovine serum for 3h

Microscopy and Mitochondrial cargo selection

Confocal images were obtained with a 100X objective NA1.4 on an Olympus IX81 inverted microscope with appropriate lasers (633 nm for mitotracker 633, 543 nm for DsRed2), using Olympus FV1000 confocal scanning microscope. .

Purification of Mitochondria from Cow Heart

Fresh cow heart was cut into small pieces and washed a number of times in ice cold PBS. The volume equivalent of heart tissue was measured and then homogenized with 2 times the tissue volume of Mitochondrial Isolation Buffer (MIB; 220 mM mannitol, 68mM sucrose, 80 mM KCl, 0.5 mM EGTA, 2mM magnesium acetate, 20 mM Hepes pH 7.4) and in presence of protease inhibitor cocktail (Roche Diagnostics), using quick pulses in a Waring blender. The lysate was

centrifuged twice at 3,000 x g at 4°C for 20 minutes to remove nuclei and unbroken cells. The supernatant was then centrifuged at 10,000 x g for 20 minutes at 4°C. The supernatant was kept as the cytosolic fraction. The pellet was washed with 0.5 L of MIB buffer and centrifuged again at 10,000 x g for 20 minutes at 4°C. The mitochondrial pellet was finally re-suspended in a minimum volume of MIB buffer and the protein concentration was determined by Bradford assay.

In vitro reconstitution of MDV formation.

Five milligrams of purified cow heart mitochondria were washed 3 times in 1 mL of MIB buffer by centrifugation at 10,000 x g at 4°C. The first wash was performed in presence of protease inhibitor cocktail (Roche Diagnostics). Bovine heart cytosol was cleared by ultracentrifugation at 200,000 x g for 40 min at 4°C. The washed mitochondria were mixed with bovine heart cytosol at increasing concentrations and incubated at 37°C for 60 minutes in the presence of an energy regenerating mixture containing 1 mM ATP, 5 mM Succinate, 80 μM ADP, 2 mM K_2HPO_4, pH 7.4. We tested the effect of a panel of damage by adding to the assay either: 50 μM antimycin A, 50 μg/ml chloramphenicol, 100 μM GTPγS, 200 μM xanthine and 0.4U xanthine oxidase, 20 mM NEM, all from Sigma. Following the reaction, the intact, "donor" mitochondria were removed from the mixture by two sequential centrifugations at 10,000 x g at 4°C. The supernatants containing the light membrane fraction were then treated with 0.5 mg/ml trypsin for 10 minutes at 4°C. After trypsin treatment, loading buffer was added and the samples were separated by SDS-PAGE, transferred to nitrocellulose membranes and blotted.

mtDNA extraction

800 μl of vesicles were isolated from the budding assay and divided in two halves. The first half was treated by trypsin and analyzed by western blot to estimate protein cargo selection. To estimate the mtDNA content of the second half, calcium concentration was first adjusted to 2 mM. The supernatants were then incubated 20 min at 4°C in presence of 10 U of DNAse I to degrade unprotected mtDNA. The reaction was quenched by using 15% TCA and the precipitate was pelleted by centrifugation at 17,000 x g for 5 min. The pellet was re-suspended in 400 μl of 100 mM Tris pH 8.5, 0.2% SDS, 5 mM EDTA, 200 mM NaCl, and incubated overnight with 10 μl of Qiagen proteinase K solution in a 55°C waterbath. Then, 50 μl of 4 M potassium acetate at pH 4.5-5 was added and the solution was incubated for 10 min on ice, followed by centrifugation

at 17,000 x g for 5 min. Finally, the supernatant were submitted to isopropanol precipitation and the pellet was used as a template for PCR reaction using primer recognizing bovine CoxI sequence (CoxI-FWD 5'-CCAAGATGCAACATCACCAA-3'; CoxI-REV 5'-CTGGGATTGCGTCTGTTTTT-3').

Sucrose gradient fractionation

All steps were carried out at 4°C. The supernatants obtained from budding reactions were adjusted to 40% (in absence of cytosol) or 50% sucrose (in presence of cytosol) in mitochondrial isolation buffer (220 mM mannitol, 68mM sucrose, 80 mM KCl, 0.5 mM EGTA, 2mM magnesium acetate, 20 mM Hepes pH 7.4) and loaded on the bottom of a discontinuous sucrose gradient with steps at 40%, 30%, 20%, and buffer. Samples were subjected to centrifugation at 150,000 x g for 6 hours and fractions were collected for analysis as indicated.

Electron Microscopy

Isolated mitochondria from bovine heart and the supernatant resulting from the *in vitro* mitochondrial budding reaction were fixed in 1.6% glutaraldehyde in PBS pH 7.4 prior to centrifugation at 10,000 x g or 200,000 x g, respectively. The fixed mitochondrial pellet was resuspended in 0.3% low-melting agarose, recentrifuged and the resulting pellet cut into 1mm pieces. The fixed supernatant material was similarly isolated by centrifugation and carefully scraped from the bottom of the centrifuge tubes. Both mitochondrial pellet & supernatant samples were then postfixed in 1% osmium tetroxide in 0.1M na cacodylate buffer, en bloc stained in 3% aqueous uranyl acetate, dehydrated in ascending ethanol and embedding in Spurr epoxy resin. Ultra thin sections were cut on a Reichert Ultracut E ultramicrotome and counter stained with lead citrate. Digital images were taken using a JEOL 1230 TEM at 60 kV adapted with a 2,000 by 2,000 pixel bottom mount CCD digital camera (Hamamatsu, Japan) and AMT software.

Induction of oxidative stress or membrane depolarization in GFP-parkin-expressing HeLa cells

HeLa cells were transiently transfected with pOCT-DsRed2 and pEGFP-parkin plasmids, and infected with adenovirus coding for DRP1(K38E)-CFP. Cells were treated for two hours with either 10 μM CCCP, 100 μM antimycin A or 0.025U glucose oxidase. Untreated cells were used as a control. Cells were then fixed and immunostained against TOM20, then incubated with an

Alexa Fluor 647-conjugated goat anti-rabbit secondary antibody (Molecular Probes). Confocal images were captured as previously described.

MDV quantification for GFP-parkin-expressing HeLa cells

HeLa cells were transiently transfected with pOCT-DsRed2 and either pEGFP-parkin or empty pEGFP-C3 plasmids, and infected with adenovirus coding for DRP1(K38E)-CFP. Cells at 90% confluency were treated with 40 μM antimycin A or control vehicle for two hours, then immediately fixed and immunostained against TOM20, and incubated with a DyLight 649 goat anti-rabbit secondary antibody (Jackson Laboratories). Triple-channel images (excitation wavelengths of 488 nm, 543 nm and 633 nm) were acquired through a 100X,1.4 N.A. lens on a Zeiss LSM 510 confocal microscope. Two types of MDVs were quantified based on cargo selectivity (either TOM20-positive or OCT-DsRed2-positive signals, but not both) in three independent, blinded experiments using only images from the channels corresponding to OCT-DsRed2 and TOM20. >20 cells were counted per condition per experiment. After data gathering, cells negative for GFP or GFP-parkin were not included in the statistical analysis (total GFP-positive cells always remained >20 in every condition for every experiment). Statistical significance was determined by two-way ANOVA followed by a post-hoc analysis (Prism 5, GraphPad Software). Differences were considered significant if $p<0.05$.

Acknowledgements

This work was supported by a Heart and Stroke Foundation of Ontario Grant-In-Aid to H.M.M., and a Neurosciences Canada Brain Repair Group Grant to H.M.M and E.A.F. The Ernest and Margaret Ford Endowed Research Fellowship in Cardiology supported V.S., and a CIHR Doctoral Research Award supports E.B. E.A.F. is supported by a Fonds de la Recherche en Santé du Québec chercheur-boursier senior Award. E.A.S. is a Howard Hughes International Research Scholar.

References

Andrade-Navarro, M. A., Sanchez-Pulido, L., and McBride, H. M. (2009). Mitochondrial vesicles: an ancient process providing new links to peroxisomes. Curr Opin Cell Biol *21*, 560-567.

Annis, M. G., Yethon, J. A., Leber, B., and Andrews, D. W. (2004). There is more to life and death than mitochondria: Bcl-2 proteins at the endoplasmic reticulum. Biochim Biophys Acta *1644*, 115-123.

Arnold, I., and Langer, T. (2002). Membrane protein degradation by AAA proteases in mitochondria. Biochim Biophys Acta *1592*, 89-96.

Augustin, S., Nolden, M., Muller, S., Hardt, O., Arnold, I., and Langer, T. (2005). Characterization of peptides released from mitochondria: evidence for constant proteolysis and peptide efflux. J Biol Chem *280*, 2691-2699.

Bender, A., Krishnan, K. J., Morris, C. M., Taylor, G. A., Reeve, A. K., Perry, R. H., Jaros, E., Hersheson, J. S., Betts, J., Klopstock, T., *et al.* (2006). High levels of mitochondrial DNA deletions in substantia nigra neurons in aging and Parkinson disease. Nat Genet *38*, 515-517.

Betarbet, R., Sherer, T. B., MacKenzie, G., Garcia-Osuna, M., Panov, A. V., and Greenamyre, J. T. (2000). Chronic systemic pesticide exposure reproduces features of Parkinson's disease. Nat Neurosci *3*, 1301-1306.

Block, M. R., Glick, B. S., Wilcox, C. A., Wieland, F. T., and Rothman, J. E. (1988). Purification of an N-ethylmaleimide-sensitive protein catalyzing vesicular transport. Proc Natl Acad Sci U S A *85*, 7852-7856.

Bota, D. A., and Davies, K. J. (2002). Lon protease preferentially degrades oxidized mitochondrial aconitase by an ATP-stimulated mechanism. Nat Cell Biol *4*, 674-680.

Braschi, E., Zunino, R., and McBride, H. M. (2009). MAPL is a new mitochondrial SUMO E3 ligase that regulates mitochondrial fission. EMBO Rep *10*, 748-754.

Bueler, H. (2009). Impaired mitochondrial dynamics and function in the pathogenesis of Parkinson's disease. Exp Neurol *218*, 235-246.

Chen, M., Sandoval, H., and Wang, J. (2008). Selective mitochondrial autophagy during erythroid maturation. Autophagy *4*, 926-928.

Chi, S. L., and Pizzo, S. V. (2006). Cell surface F1Fo ATP synthase: a new paradigm? Ann Med *38*, 429-438.

Das, A., Hazra, T. K., Boldogh, I., Mitra, S., and Bhakat, K. K. (2005). Induction of the human oxidized base-specific DNA glycosylase NEIL1 by reactive oxygen species. J Biol Chem *280*, 35272-35280.

Delille, H. K., and Schrader, M. (2008). Targeting of hFis1 to peroxisomes is mediated by Pex19p. J Biol Chem *283*, 31107-31115.

Deng, H., Dodson, M. W., Huang, H., and Guo, M. (2008). The Parkinson's disease genes pink1 and parkin promote mitochondrial fission and/or inhibit fusion in Drosophila. Proc Natl Acad Sci U S A *105*, 14503-14508.

Exner, N., Treske, B., Paquet, D., Holmstrom, K., Schiesling, C., Gispert, S., Carballo-Carbajal, I., Berg, D., Hoepken, H. H., Gasser, T., *et al.* (2007). Loss-of-function of human PINK1 results in mitochondrial pathology and can be rescued by parkin. J Neurosci *27*, 12413-12418.

Harder, Z., Zunino, R., and McBride, H. (2004). Sumo1 conjugates mitochondrial substrates and participates in mitochondrial fission. Curr Biol *14*, 340-345.

Katzmann, D. J., Odorizzi, G., and Emr, S. D. (2002). Receptor downregulation and multivesicular-body sorting. Nat Rev Mol Cell Biol *3*, 893-905.

Kaufman, B. A., Durisic, N., Mativetsky, J. M., Costantino, S., Hancock, M. A., Grutter, P., and Shoubridge, E. A. (2007). The mitochondrial transcription factor TFAM coordinates the assembly of multiple DNA molecules into nucleoid-like structures. Mol Biol Cell *18*, 3225-3236.

Koehler, C. M., and Tienson, H. L. (2009). Redox regulation of protein folding in the mitochondrial intermembrane space. Biochim Biophys Acta *1793*, 139-145.

Lang, A. E., and Lozano, A. M. (1998a). Parkinson's disease. First of two parts. N Engl J Med *339*, 1044-1053.

Lang, A. E., and Lozano, A. M. (1998b). Parkinson's disease. Second of two parts. N Engl J Med *339*, 1130-1143.

Langston, J. W., Ballard, P., Tetrud, J. W., and Irwin, I. (1983). Chronic Parkinsonism in humans due to a product of meperidine-analog synthesis. Science *219*, 979-980.

Lutz, A. K., Exner, N., Fett, M. E., Schlehe, J. S., Kloos, K., Lammermann, K., Brunner, B., Kurz-Drexler, A., Vogel, F., Reichert, A. S., *et al.* (2009). Loss of parkin or PINK1 function increases Drp1-dependent mitochondrial fragmentation. J Biol Chem *284*, 22938-22951.

Martinez, L. O., Jacquet, S., Esteve, J. P., Rolland, C., Cabezon, E., Champagne, E., Pineau, T., Georgeaud, V., Walker, J. E., Terce, F., *et al.* (2003). Ectopic beta-chain of ATP synthase is an apolipoprotein A-I receptor in hepatic HDL endocytosis. Nature *421*, 75-79.

Matsuoka, K., Orci, L., Amherdt, M., Bednarek, S. Y., Hamamoto, S., Schekman, R., and Yeung, T. (1998). COPII-coated vesicle formation reconstituted with purified coat proteins and chemically defined liposomes. Cell *93*, 263-275.

McBride, H. M. (2008). Parkin mitochondria in the autophagosome. J Cell Biol *183*, 757-759.

Mortiboys, H., Thomas, K. J., Koopman, W. J., Klaffke, S., Abou-Sleiman, P., Olpin, S., Wood, N. W., Willems, P. H., Smeitink, J. A., Cookson, M. R., and Bandmann, O. (2008). Mitochondrial function and morphology are impaired in parkin-mutant fibroblasts. Ann Neurol *64*, 555-565.

Narendra, D., Tanaka, A., Suen, D. F., and Youle, R. J. (2008). Parkin is recruited selectively to impaired mitochondria and promotes their autophagy. J Cell Biol *183*, 795-803.

Neuspiel, M., Schauss, A. C., Braschi, E., Zunino, R., Rippstein, P., Rachubinski, R. A., Andrade-Navarro, M. A., and McBride, H. M. (2008). Cargo-selected transport from the mitochondria to peroxisomes is mediated by vesicular carriers. Curr Biol *18*, 102-108.

Neutzner, A., and Youle, R. J. (2005). Instability of the mitofusin Fzo1 regulates mitochondrial morphology during the mating response of the yeast Saccharomyces cerevisiae. J Biol Chem *280*, 18598-18603.

Neutzner, A., Youle, R. J., and Karbowski, M. (2007). Outer mitochondrial membrane protein degradation by the proteasome. Novartis Found Symp *287*, 4-14; discussion 14-20.

Nguyen, M., Millar, D. G., Yong, V. W., Korsmeyer, S. J., and Shore, G. C. (1993). Targeting of Bcl-2 to the mitochondrial outer membrane by a COOH-terminal signal anchor sequence. J Biol Chem *268*, 25265-25268.

Poole, A. C., Thomas, R. E., Andrews, L. A., McBride, H. M., Whitworth, A. J., and Pallanck, L. J. (2008). The PINK1/Parkin pathway regulates mitochondrial morphology. Proc Natl Acad Sci U S A *105*, 1638-1643.

Romer, W., Berland, L., Chambon, V., Gaus, K., Windschiegl, B., Tenza, D., Aly, M. R., Fraisier, V., Florent, J. C., Perrais, D., *et al.* (2007). Shiga toxin induces tubular membrane invaginations for its uptake into cells. Nature *450*, 670-675.

Sandoval, H., Thiagarajan, P., Dasgupta, S. K., Schumacher, A., Prchal, J. T., Chen, M., and Wang, J. (2008). Essential role for Nix in autophagic maturation of erythroid cells. Nature *454*, 232-235.

Schapira, A. H., Cooper, J. M., Dexter, D., Clark, J. B., Jenner, P., and Marsden, C. D. (1990). Mitochondrial complex I deficiency in Parkinson's disease. J Neurochem *54*, 823-827.

Schweers, R. L., Zhang, J., Randall, M. S., Loyd, M. R., Li, W., Dorsey, F. C., Kundu, M., Opferman, J. T., Cleveland, J. L., Miller, J. L., and Ney, P. A. (2007). NIX is required for programmed mitochondrial clearance during reticulocyte maturation. Proc Natl Acad Sci U S A *104*, 19500-19505.

Spang, A., Matsuoka, K., Hamamoto, S., Schekman, R., and Orci, L. (1998). Coatomer, Arf1p, and nucleotide are required to bud coat protein complex I-coated vesicles from large synthetic liposomes. Proc Natl Acad Sci U S A *95*, 11199-11204.

Terzioglu, M., and Galter, D. (2008). Parkinson's disease: genetic versus toxin-induced rodent models. Febs J *275*, 1384-1391.

Twig, G., Elorza, A., Molina, A. J., Mohamed, H., Wikstrom, J. D., Walzer, G., Stiles, L., Haigh, S. E., Katz, S., Las, G., *et al.* (2008). Fission and selective fusion govern mitochondrial segregation and elimination by autophagy. Embo J *27*, 433-446.

Vives-Bauza, C., Zhou, C., Huang, Y., Cui, M., de Vries, R. L., Kim, J., May, J., Tocilescu, M. A., Liu, W., Ko, H. S., *et al.* (2009). PINK1-dependent recruitment of Parkin to mitochondria in mitophagy. Proc Natl Acad Sci U S A.

Warr, M. R., Acoca, S., Liu, Z., Germain, M., Watson, M., Blanchette, M., Wing, S. S., and Shore, G. C. (2005). BH3-ligand regulates access of MCL-1 to its E3 ligase. FEBS Lett *579*, 5603-5608.

Zhong, Q., Gao, W., Du, F., and Wang, X. (2005). Mule/ARF-BP1, a BH3-only E3 ubiquitin ligase, catalyzes the polyubiquitination of Mcl-1 and regulates apoptosis. Cell *121*, 1085-1095.

Figure legends

Figure 1: ROS stimulates the formation of mitochondrial vesicles.

a) HeLa cells were untreated (top left), or incubated with 0.025U of glucose oxidase for the indicated time prior to labeling with MitofluorRed 633. Representative images of each condition are shown, with the vesicles circled. Scale bars : 5 microns. b) and c) Boxplot representations of the numbers of vesicles. The numbers of vesicles were counted from 50 cells in each of 3 independent experiments. d) i) and ii) HeLa cells co-transfected with DRP1(K38E)-CFP and with the matrix OCT-DsRed2 marker (labeled red) were either left untreated (i) or incubated with glucose oxidase (GO) for one hour (ii) prior to fixation and labeling Tom20 (green) and Lamp1(purple). Representative confocal images are shown and circles within the boxed region highlight the co-localization of Tom20-positive vesicles (green) with lysosomes (purple), which lack OCT-DsRed2 (red). Scale bars, 2 microns.

Figure 2: Reconstitution of MDV formation.

a) Titration of cytosol with 5 mg of isolated mitochondria at 37°C for 60 minutes in the presence of an ATP regenerating system. Mitochondria were removed by centrifugation and 10% of the supernatant loaded onto an SDS-PAGE gel for transfer and western blotting, as indicated. 20 μg of starting mitochondria were loaded as an input control. b) The relative intensities of the cargo within the supernatant was quantified relative to that found within the 20μg of starting mitochondria. Standard errors were calculated from three different gels loaded with the same reaction. The data is representative of at least 2 independent experiments. c) Time course of MDV formation under minimal conditions in the absence of cytosol. The reaction was incubated at 37°C for the indicated times in the presence of an ATP regenerating system and the supernatants were separated by SDS-PAGE and transferred for western blots as shown. and d) quantification of c), as in b). e) Isolated mitochondria were incubated with an ATP regenerating system for 60 minutes at 37°C in the presence of 0.1 mM of GTPγS or ATPγS as indicated; or with 5 U of Apyrase and in absence of the ATP regenerating system. The data is representative of at least 3 independent experiments.

Figure 3: *In vitro* formation of MDVs show differential cargo selectivity.

a) Isolated mitochondria were incubated in the absence of cytosol, with an energy regenerating system, for 60 minutes at 37°C under the indicated conditions (for details see materials and methods). A second reaction was performed in the presence of xanthine oxidase (XO) at 4°C to examine the temperature dependence (last lane). At the exposures shown here, the VDAC western blot does not detect the signal within the 20μg of starting mitochondria. Longer exposures reveal the presence of VDAC in the mitochondria, yet the signals observed within the supernatant became saturated (data not shown). The data is representative of at least 3 independent experiments. b) As in a) except that 20 mM of NEM was added when indicated. c) As in b), the supernatants were separated by SDS-PAGE and transferred for western blots as shown. d) and e) Reactions were done as in b) and extraction of mtDNA was performed as described in materials and methods. f) Reactions were performed as in a) except that the supernatants were not submitted to trypsin treatment. Twenty micrograms of the MDVs and of the mitochondria they budded from were used. The detection of protein oxidation was performed using the oxyblot system.

Figure 4: Sucrose fractionation and EM analysis of MDVs.

a) EM sections of isolated mitochondria from bovine heart showing vesicular profiles. Scale bars are 100 nm. b) Supernatants obtained from reactions treated with either XO or Antimycin A were fixed in 1.6% glutaraldehyde and isolated by high speed centrifugation . The pellet was prepared for EM sectioning and representative images are shown as indicated. Scale bars are all 100 nm. c) Supernatants obtained from reactions treated with Antimycin A were fractionated on a discontinuous sucrose gradient. After centrifugation, fractions were collected and analyzed by western-blot as indicated. d) EM analysis of fractions obtained in c). Scale bars are 100 nm.

Figure 5: Inhibition of complex III with antimycin A recruits parkin selectively to matrix-positive, TOM20-negative MDVs.

HeLa cells transiently expressing GFP-parkin, OCT-DsRed2 and DRP1(K38E)-CFP were imaged after no treatment (top-left panels), or treatment with 0.025U glucose oxidase (GO, top-right panles), 10 μM CCCP (bottom-left panels) or 100 μM antimycin A (anti A, bottom-right panels) for two hours. White boxes are expanded at the right of every image, with the channels

split. Arrows indicate OCT-DsRed2-positive/TOM20-negative MDVs that colocalize with GFP-parkin, while the triangle indicates GFP-parkin colocalizing with a possible MDV budding event. Open arrowheads indicate GO-stimulated TOM20-positive/OCT-DsRed2-negative MDVs that do not colocalize with GFP-parkin. Scale bars indicate 30 microns.

Figure 6: Endogenous parkin is recruited to vesicles *in vitro*.

Supernatants obtained from reactions performed in presence of 3 mg/ml of cytosol using mitochondria incubated in basal conditions or treated with antimycin A were fractionated on a discontinuous sucrose gradient. After centrifugation, fractions were collected and analyzed by western-blot as indicated.

Figure 7: Parkin induces the biogenesis of matrix-positive, TOM20-negative in response to antimycin A.

a) HeLa cells transiently expressing GFP-parkin, OCT-DsRed2 and DRP1(K38E)-CFP were treated with 40 μM antimycin A (anti A) or control vehicle (veh) for two hours, then fixed and immunostained against TOM20. Typical confocal images of the GFP-parkin signal are shown in the leftmost panels, with the centre panels corresponding to the merged (GFP-parkin, OCT-DsRed2 and TOM20) images. White boxes are expanded in the rightmost panels, with the channels split. Arrows indicate MDVs positive for both GFP-parkin and OCT-DsRed2 but not TOM20, and the triangle indicates an OCT-DsRed2-positive MDV that is not associated with GFP-parkin or TOM20. Scale bars indicate 30 microns. b, c) The amount of (b) TOM20-positive/OCT-DsRed2-negative and (c) OCT-DsRed2-positive/TOM20-negative MDVs in HeLa cells from (a) expressing either GFP or GFP-parkin were quantified, and analyzed by two-way ANOVA followed by a post-hoc analysis. Data are displayed as mean + SEM from three independent experiments. "*" indicates statistically significant ($p<0.05$) differences.

Supplementary Figure 1:

a) HeLa cells infected with DRP1(K38E)-CFP adenovirus were co-transfected with GFP-parkin and OCT-DsRed2 and incubated for 2h with 30 μM antimycinA after Dextran 647 loading. A representative image is shown, with OCT-DsRed2 vesicles co-localizing with GFP-parkin and Dextran 647 (arrows) or not (circle). Scale bars : 5 microns. b) LC3-GFP stable HeLa cells were incubated with 0.025U of glucose oxidase, 30 μM antimycinA for 2 hours or 50 μM rapamycin

for 4 hours as a positive control. Cell extracts were obtained with RIPA buffer and analyzed by western blotting, as indicated. Autophagy activation was revealed by the GFP cleavage.

Figure 1:

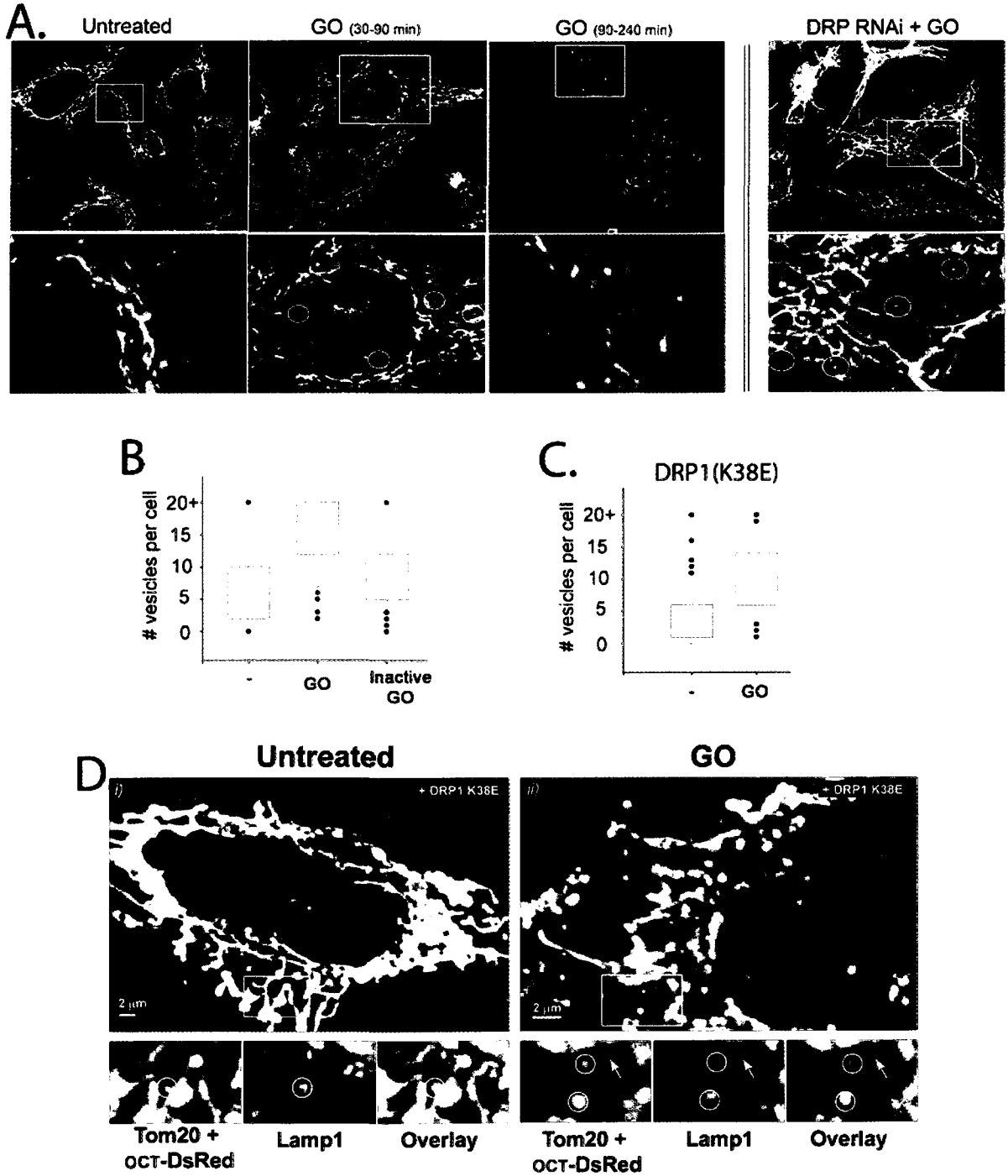

Soubannier et al, Figure 1

Figure 2

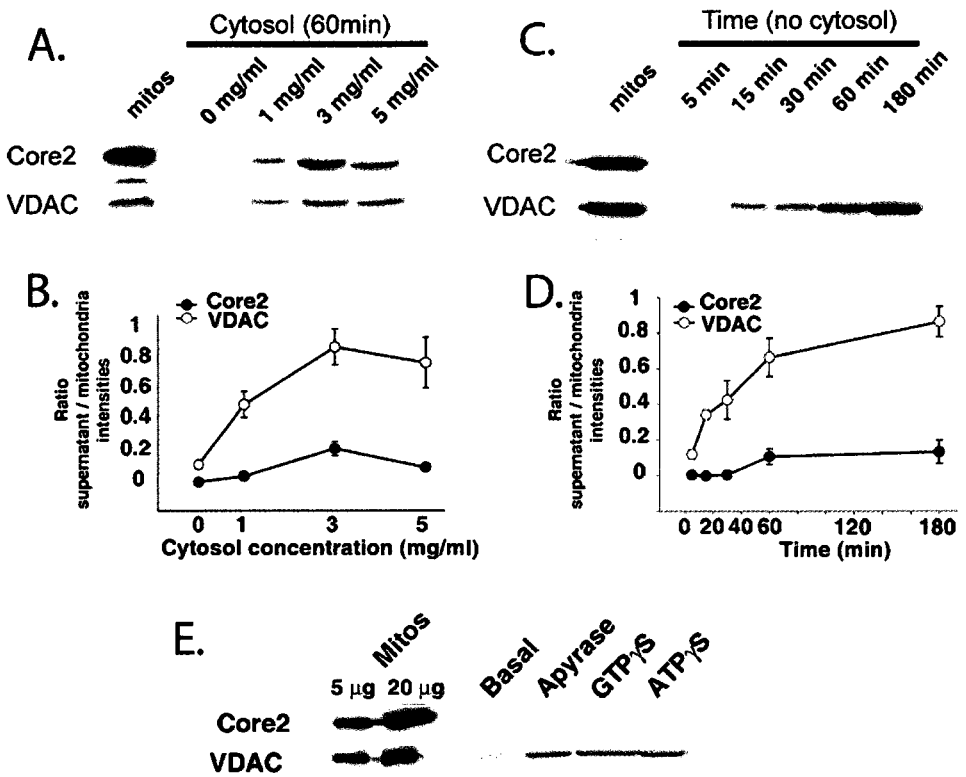

Soubannier et al. Figure 2

Figure 3

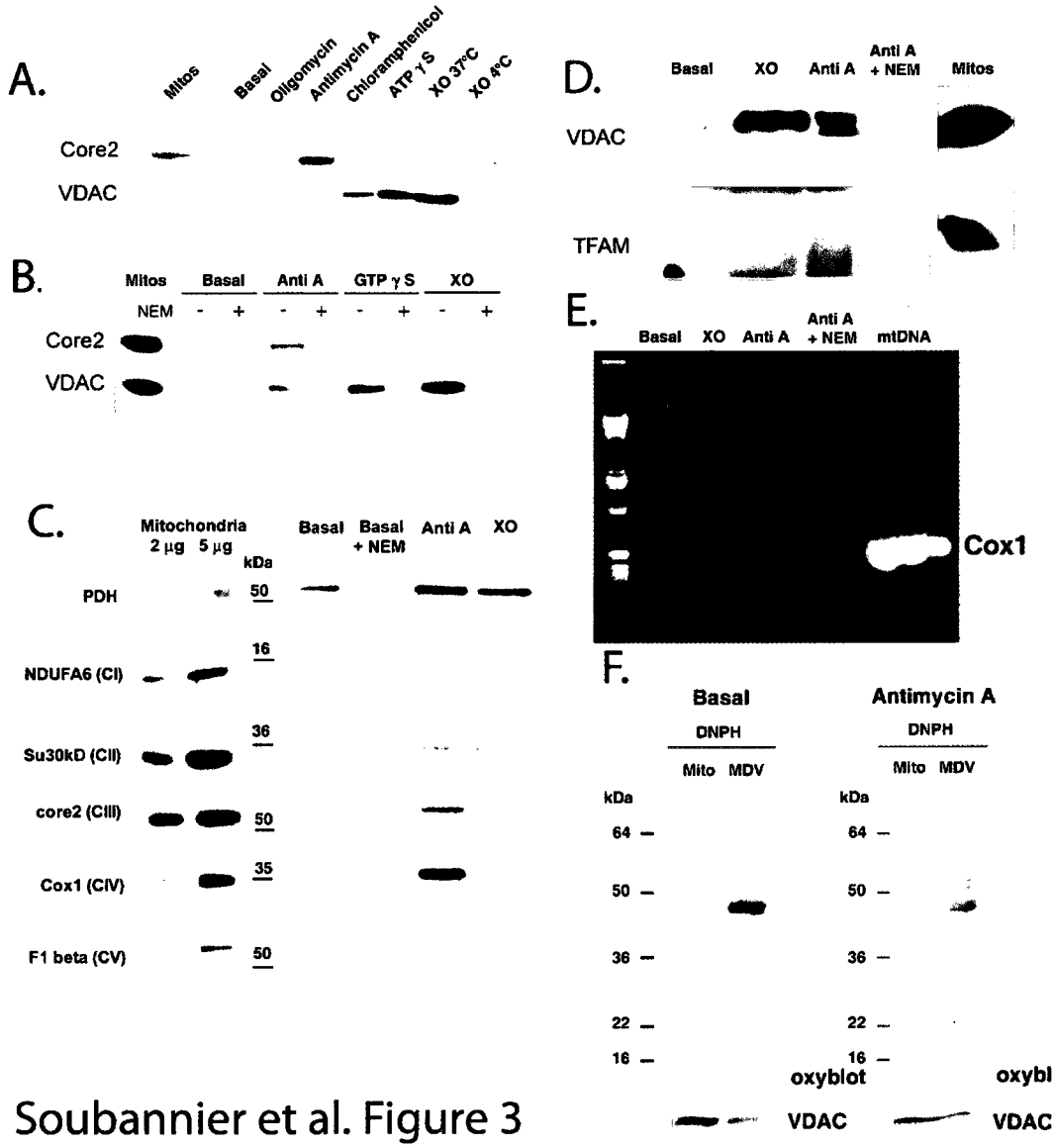

Soubannier et al. Figure 3

Figure 4

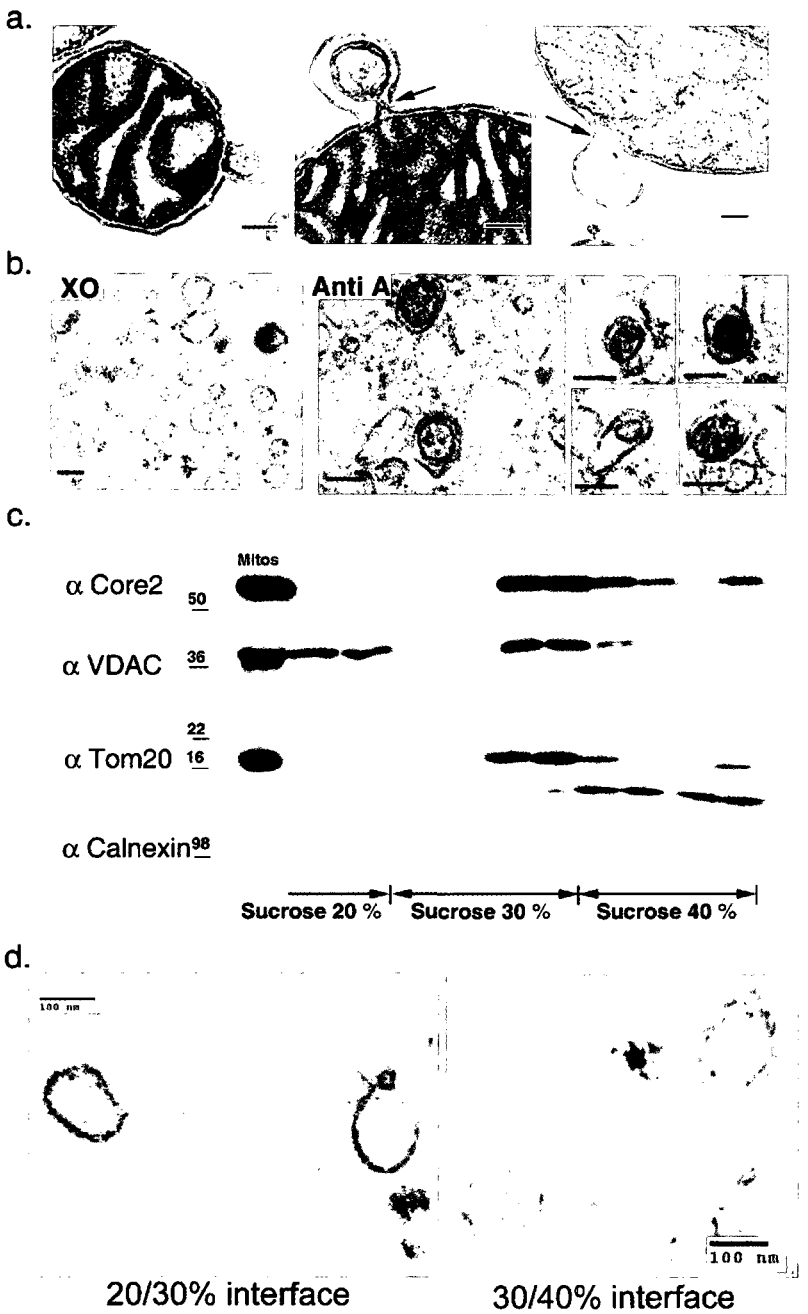

Soubannier et al., Figure 4

Figure 5

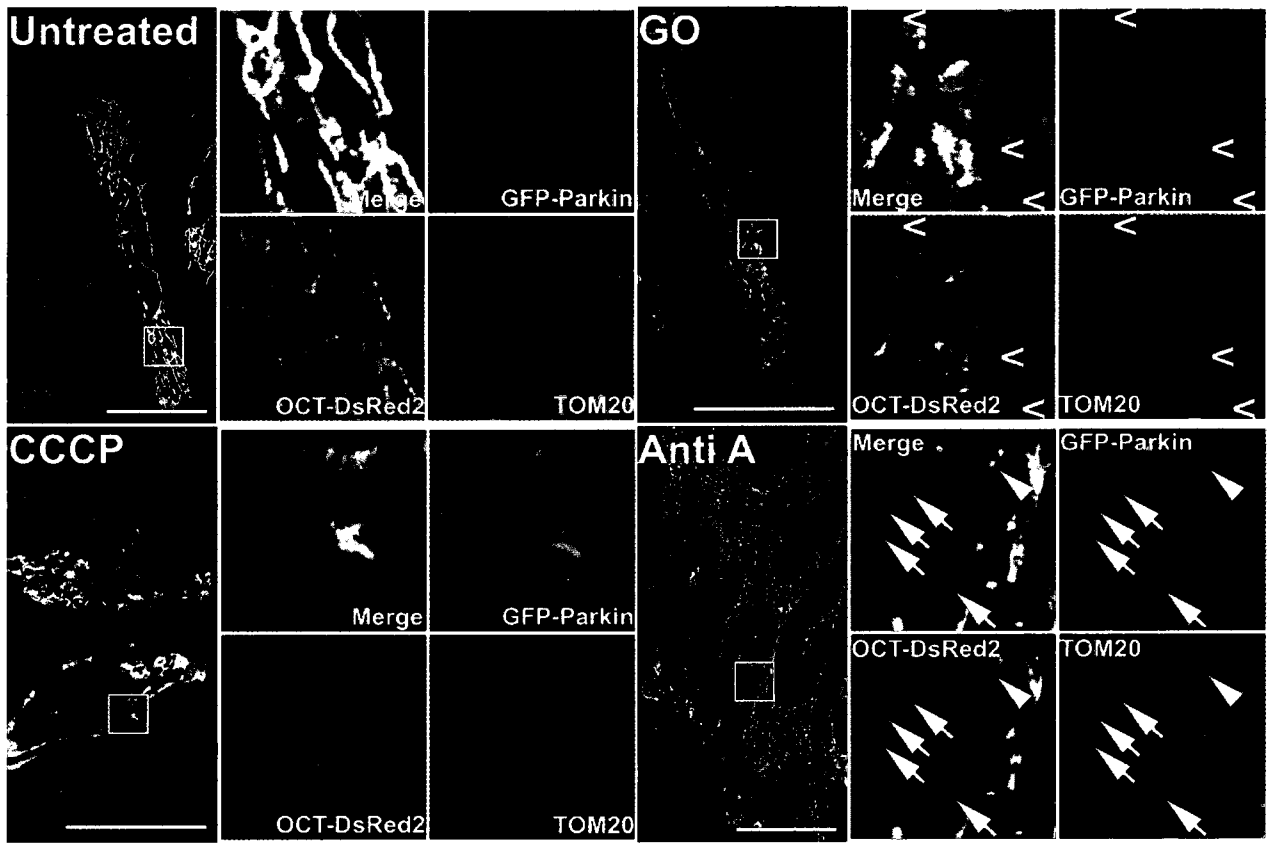

Soubannier et al., Figure 5

Figure 6

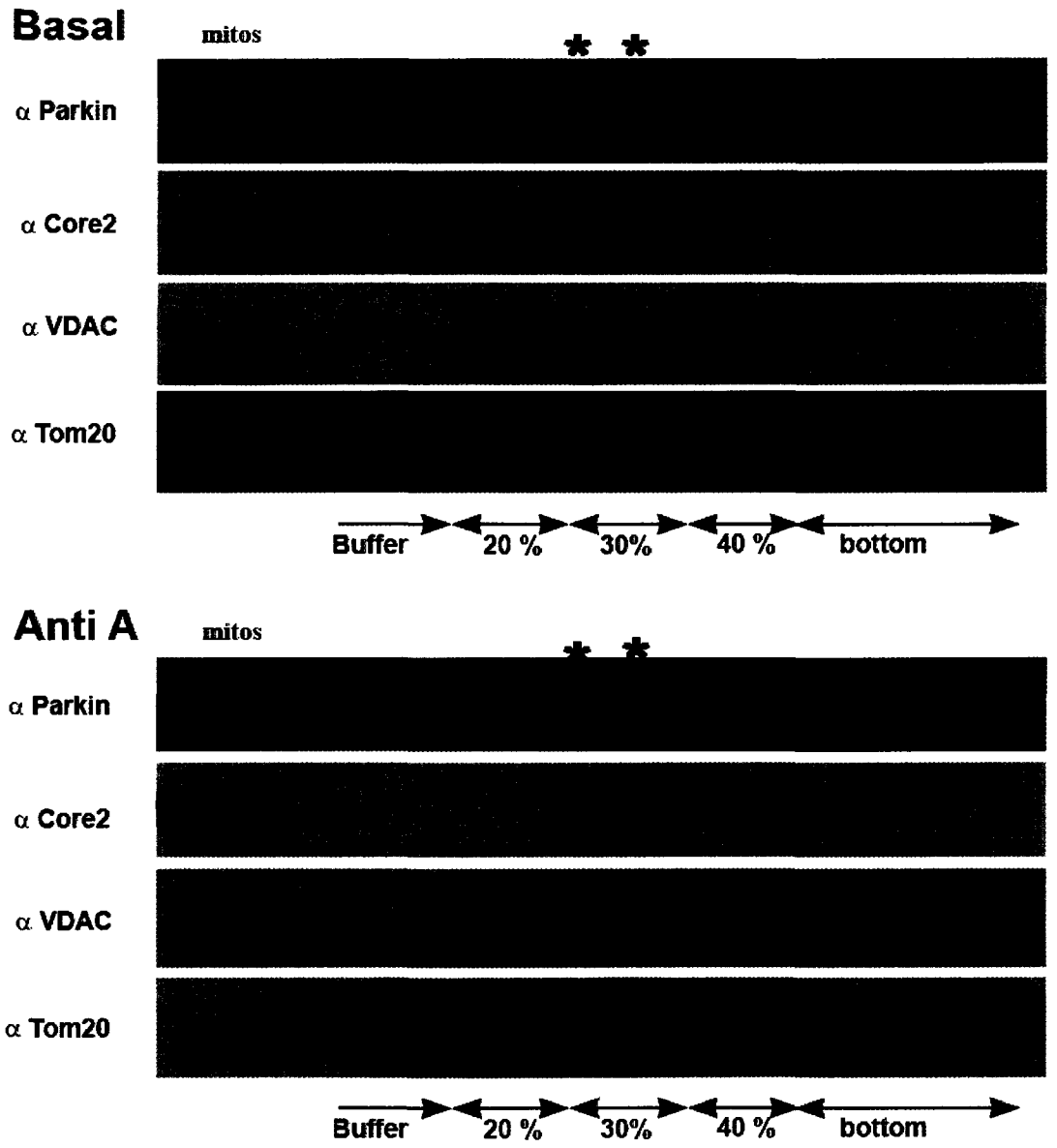
Basal
mitos
α Parkin
α Core2
α VDAC
α Tom20
Buffer
20 %
30%
40 %
bottom
Anti A
mitos
α Parkin
α Core2
α VDAC
α Tom20
Buffer
20 %
30%
40 %
bottom

Figure 7

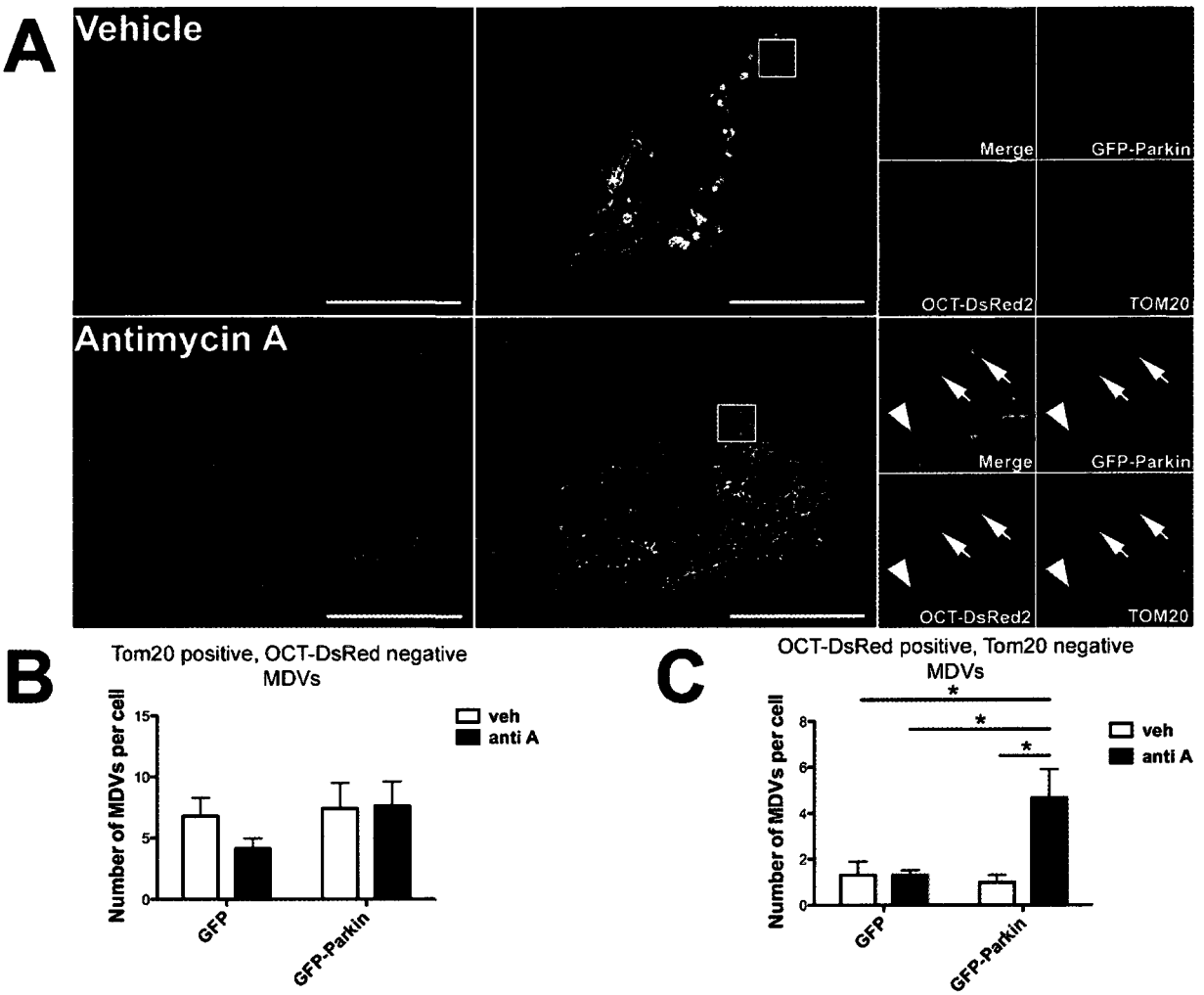

Soubannier et al., Figure 7

Supplementary Figure 1

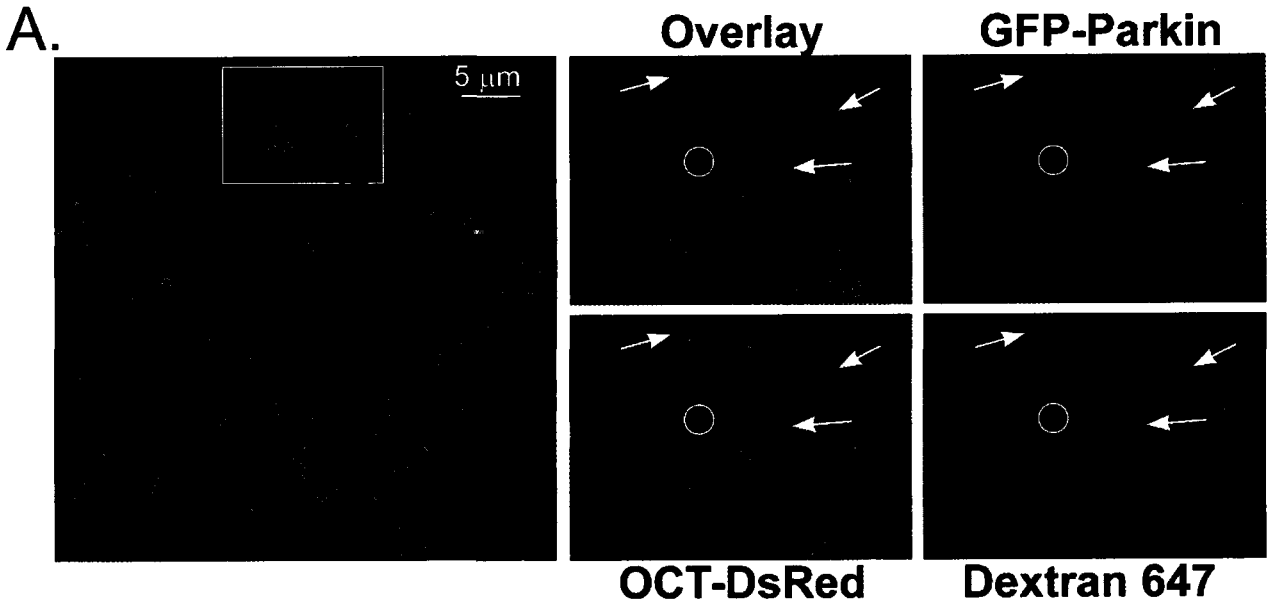

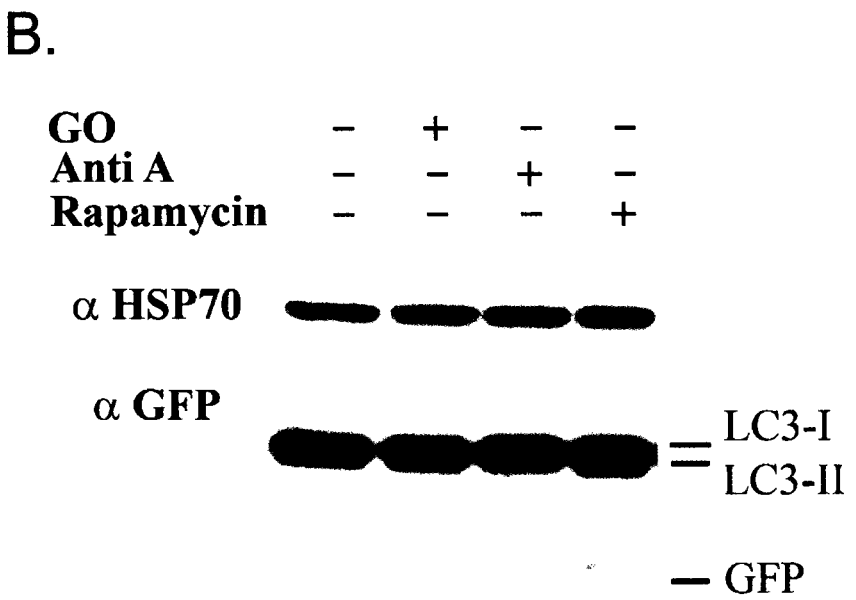

Soubannier et al., Suppl Figure 1

I.2.4.3 Quality control mechanisms in neurons

Asymmetrical fission could play an important role in complex cell types like neurons. In fact, in neurons, mitochondria form a heterogeneous population, different mitochondria being more or less hyperpolarized, and moving at different rates, and, although axonal mitochondria appear uniformly distributed along the axon, careful analysis shows that some travel fast whereas others are almost stationary (96). Importantly, the velocity of movement is linked to potential. Antimycin A, which blocks complex III activity, leading to mild damage and a mild loss of potential, increases transport towards the cell body, where the damaged mitochondria are thought to be degraded (96). Supporting the hypothesis that mild damage triggers retrograde transport, 80% of mitochondria with low potential are transported towards the cell soma (96). One could postulate that mild damage triggers asymmetrical fission, with the damaged daughter mitochondria being transported to the cell body, whereas the other mitochondria would continue to fulfill its function in the axon.

The coupling of transport and mitochondrial function has been proposed to be regulated by motors. In particular, a dynein light chain, Tctex1 was shown to interact with the Voltage Dependent Anion Channel 1 (Vdac1) (97). Since Vdac1 is thought to be a member of the permeability transition pore, Tctex1 could potentially regulate dynein binding to low potential mitochondria to promote retrograde transport (97). In other words, mitochondrial dynamics, function, and transport could coordinately act as quality control mechanism.

I.2.4.4 Conclusion

These studies elegantly illustrate that material can be specifically selected to be removed from the mitochondrial reticulum (98). In addition, damaged mitochondria can be targeted for selected transport towards the cell soma in neurons (96). The discovery of the mechanisms involved in cargo recognition and selection will have important implications in neurodegenerative diseases. Mice lacking autophagic genes have severe neurodegeneration defects, indicating that autophagy plays a central role in neuronal homeostasis (99, 100). In addition, Parkin, is the protein product of Park2, a gene whose function is commonly lost in familial Parkinson's disease (95). A malfunctioning mitochondrial quality control mechanism and the resulting accumulation of damaged mitochondrial proteins could lead to high ROS, triggering global cellular damage. Finally, an attractive hypothesis is that selective fission is not restricted to autophagy and could play a role to select the fittest mitochondria, as has been suggested in the yeast system during cytokinesis (89), or in creating specialized mitochondria geared to respond to the needs of specific sub-cellular environments.

I.2.5 Mitochondria and localized energy requirements

I.2.5.1 Actin remodeling

In addition to regulating mitochondrial function, mitochondrial dynamics facilitate the positioning of mitochondria at sites of high ATP consumption. For example, mitochondria cluster at the synapse, a site of high energy demand (101). In addition, one

study in lymphocytes has elegantly demonstrated the essential role of mitochondrial dynamics during cell migration (102).

During chemotaxis, lymphocytes polarize to migrate towards the chemoattractant (102). The machinery for actin polymerization is concentrated in the anterior part of the cell, called the leading edge (102). The posterior part of the cell, called the uropod, contains adhesion molecules, the microtubule organizing center, and the majority of cellular organelles and cytosol (102). Mitochondria are specifically transported to the uropod, unlike the endoplasmic reticulum, which remains evenly localized in the cytoplasm (102). Polarization and migration depend on the polymerization of actin at the leading edge (103); the microtubule organizing centre directs vesicular traffic, in addition to maintaining polarization (104). Mitochondria repositioning depends on the integrity of microtubules, but not of the actin cytoskeleton (102).

Importantly, the formation of a mitochondrial network by overexpressing Opa1, promoting fusion, or overexpressing a dominant negative form of Drp1, inhibiting fission, prevents migration (102). Since the global levels of ATP are unchanged, mitochondrial fragmentation seems to be required for the positioning of mitochondria in specific sub-cellular domains at the uropod needing high levels of ATP (102). Supporting this hypothesis, using creatine to enhance mitochondrial oxidative phosphorylation, rescues the migration defects triggered by Opa1 overexpression (102).

Myosins move along actin filaments in an ATP dependent manner, and, by contracting actin filaments, provide the tension for cellular movements (105). The activity of Myosins is controlled by the phosphorylation of the Myosin Light Chain (MLC) by the Myosin Light Chain Kinase (MLCK) (105). Interestingly, immunofluorescence studies

indicate that MLC phosphorylation is more intense at the uropod than at the leading edge (102). In addition, when mitochondrial ATP production is inhibited by oligomycin treatment, MLC phosphorylation is lost at the uropod specifically (102). This indicates that mitochondrial ATP is required for the proper activity of the MLCK at specific sub-cellular sites.

Although it is still unknown whether mitochondrial remodeling and transport are essential in all migrating cells, this same study did report similar morphological changes in a number of cell types, including Jurkat T cells, human peripheral blood T-cells, differentiated HL-60 myelocytic cells (neutrophil-like), and MCF7 cells (breast cancer cells) stimulated with insulin like growth factor 1 (IGF-1) (102).

Another study in neurons has demonstrated a specific requirement for mitochondrial ATP and the activation of MLCK (106). A mutation in Drp1 in *D. melanogaster* leading to decreased synaptic mitochondria was shown to affect high frequency stimulation specifically (106). Defects were traced to a specific pool of vesicles, the reserve pool, which are usually used under intense stimulation (106). Increasing ATP levels by directly supplying the synapse with ATP, rescued the defects triggered by the mutated Drp1, whereas drugs inhibiting mitochondrial calcium uptake had no effect (106). This indicates that mitochondrial ATP production is required for the proper unloading of the vesicles (106). Importantly, when the synapses of Drp1 mutants were filled with ATP and supplied with MLCK inhibitors, unloading of the reserve pool vesicle was prevented (106), demonstrating that mitochondrial ATP is important for the activation of the myosin complex. In these two studies, the challenge will be to understand which signals coordinate

migration or high frequency stimulation, to changes in mitochondrial dynamics and transport.

I.2.5.2 Synaptic function

Synaptic mitochondria are important for neuronal function

The neurons are morphologically complex cells with distinct microenvironments, at the synapse or the cell body, separated by long distances. Mitochondria are present in the cell body, but accumulate where the demands for ATP are high, at motile growth cones (107), synapses (108), nodes of Ranvier (109) and myelination boundaries (110). In addition, mitochondria move to dendritic protrusions following synaptic stimulation and during spine remodeling (111). In this highly complex cell type, mitochondrial dynamics seem to be critical for the creation of small mitochondria that are more easily transported within dendrites or axons.

Highlighting the importance of mitochondrial dynamics in neurons, mutations in MFN2 and OPA1 lead to neurodegenerative disorders (12, 13). In addition, in rat hippocampal neurons, the overexpression of a dominant negative form of Drp1 reduces the amount of mitochondria in dendrites and leads to a reduction in the numbers of dendrites by 79% (112). On the other hand, the overexpression of *wild-type* Drp1 increases the amounts of mitochondria in the dendrites, leading to a two-fold increase in the density of dendrititic spines, and to a higher number of functional pre-synaptic terminals (112).

Indeed, mitochondria are not only essential for the formation of dendritic spines, they are also a limiting factor, which might be linked to the availability of ATP, since improving mitochondrial respiration with creatine also improves synaptic density (112). Interestingly, mitochondria with high membrane potential have a high colocalization with

intermediate filaments (113). Since intermediate filaments are not normally used for transport, it is possible that once mitochondria have reached their localization, other signaling events trigger hyperpolarization (113). One way in which this can be achieved is through the modulation of oxidative phosphorylation by Ca^2 (114). Finally, the ability of mitochondria to store Ca^{2+} might have an important function during specific forms of synaptic activations, which require Ca^{2+} release from the mitochondria (115).

Regulation of mitochondrial dynamics, transport, and function by signaling cascades

In addition to mitochondrial fission, mitochondrial transport plays an important role in neuronal homeostasis. For axonal traveling, the mitochondria use microtubules (84). In *D. Melanogaster*, the best studied adaptors for these long range movements are Milton and Mitochondrial Rho-1 (Miro) (116). Miro is an outer membrane mitochondrial protein, which possesses two GTPase domains and two calcium binding domains (116). Miro regulates mitochondrial transport by binding to Milton, a kinesin heavy chain binding protein (117). The downregulation of either Milton or Miro stops anterograde mitochondrial axonal transport, and the axon terminals become devoid of mitochondria (118)

Interestingly, repetitive depolarization triggers the formation of new dendritic spines, and the relocalization of dendritic mitochondria into dendritic protrusions (112), a short range movement which relies on the actin filaments and is dependent on the WASP family verprolin homologous protein 1 (WAVE1) (111). WAVE1 is recruited to the mitochondria after neuronal stimulation (111), and its ability to regulate Arp2/3 dependent actin polymerization modulates short-range mitochondrial movement (111).

In addition, the mitochondria can respond to extracelluar signals by locally altering their transport and by undergoing docking interactions with the actin cytoskeleton. For example, localized, short term Nerve Growth Factor (NGF) signaling in chick embryonic neurons triggers the accumulation of mitochondria at the synaptic terminal, in a phosphoinositide 3-kinase (PI3K) dependent manner (119, 120). Latrunculin B, which depolymerizes actin, does not interrupt general mitochondrial movement although the mitochondria fail to accumulate upon NGF stimulation (119, 120).

A signaling cascade downstream of NGF leads to the expression of p35, a neuronal-specific activator of Cdk5 (121). Interestingly, Cdk5 has been implicated in both mitochondrial dynamics and transport. Cdk5 is an upstream regulator of mitochondrial fission (122). Cdk5 also activates the Glycogen Synthase Kinase β (GSK3β), which triggers the release of kinesins from membrane bound organelles (123, 124), although a direct role for GSK3β in mitochondrial transport specifically has not been demonstrated. Cdk5 could therefore coordinate mitochondrial fission and transport in response to cellular signaling. In addition to activating Cdk5, NGF signaling could also activate the Ras homolog gene family, member A (RhoA), downstream of PI3K. RhoA promotes mitochondrial docking to the actin cytoskeleton through the Diaphanous homologue 1 (mDia1) (125). In other words, NGF signaling could trigger the release of mitochondria from microtubules, in a Cdk5 dependent manner (121), and modulate mitochondrial docking through RhoA activation (125).

Finally, mitochondrial movement is also coupled to Ca^{2+} concentrations. The overexpression of Miro enhances mitochondrial movement at resting Ca^{2+} concentrations, but promotes mitochondrial arrest at higher, yet physiological Ca^{2+} levels (126). Although

the mechanisms are unclear, Ca^{2+} binding to Miro alters Miro-kinesin interactions (127, 128). When ATP levels are low, Ca^{2+} transport is compromised and cytosolic Ca^{2+} increase, which would promote the arrest of mitochondria to replenish the ATP supplies (126).

I.2.5.3 Conclusion

The coordination of mitochondrial dynamics, transport and function can be achieved by signaling cascades and second messengers like calcium. Signaling cascades are also critical to regulate the release of mitochondria from microtubules and their docking to the actin cytoskeleton for short-distance movement (103). The importance of these signaling networks is especially apparent when mitochondrial ATP is essential in specific subcellular compartments, for example in migrating cells or in neurons *(Figure 1.9)*. These provide interesting systems to dissect the complex integration of mitochondria within cellular processes.

Figure I-9 Coordination of mitochondrial dynamics, transport and function

A) Mitochondrial transport and dynamics are tightly coupled. B) Following frequent depolarization, mitochondria are recruited to dendritic protrusions by docking to the actin cytoskeleton through Wave1. C) NGF stimulation triggers the activation of Cdk5 and PI3K. Cdk5 might mediate the unloading of mitochondria at the nerve terminal by regulating GSK3β activity. PI3K activates mDia which promotes the docking of the mitochondria to the actin cytoskeleton. D) Low ATP promotes the accumulation of calcium. Mitochondrial transport is stopped following calcium binding to Miro, and the mitochondria can increase cellular ATP.

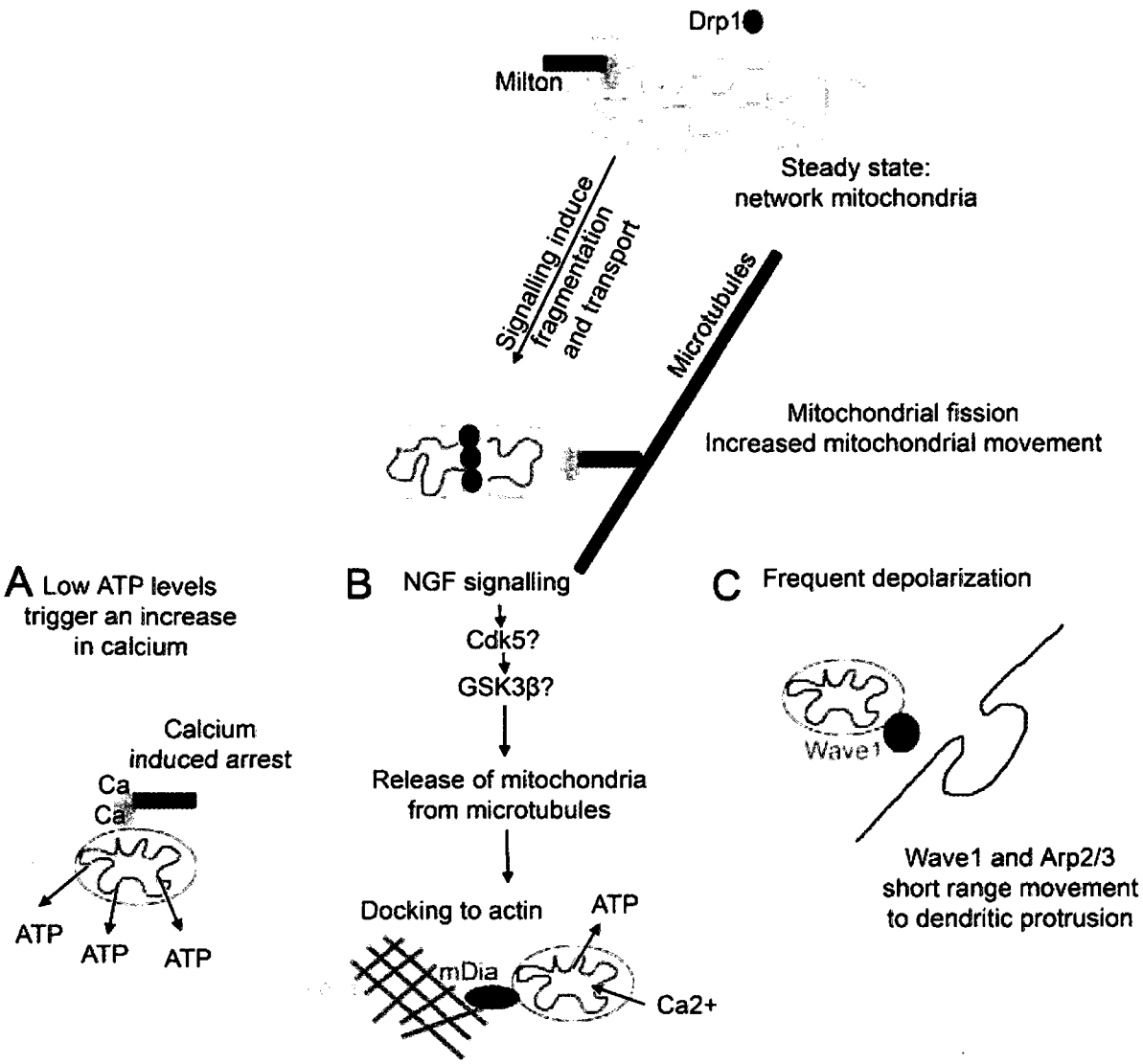
Drp1
Milton
Steady state:
network mitochondria
Signalling induce
fragmentation
and transport
Microtubules
Mitochondrial fission
Increased mitochondrial movement
A Low ATP levels
trigger an increase
in calcium
Calcium
induced arrest
Ca
Ca
ATP
ATP
ATP
B NGF signalling
Cdk5?
GSK3β?
Release of mitochondria
from microtubules
Docking to actin
ATP
mDia
Ca2+
C Frequent depolarization
Wave1
Wave1 and Arp2/3
short range movement
to dendritic protrusion

I.3 Rethinking our view of the mitochondria

The roles of mitochondria in metabolism, migration, the cell cycle, mild cellular stresses and apoptosis demonstrate that mitochondria are active cellular players. They respond to cellular signaling and modulate their morphology and oxidative capacities in response to different cellular environments. Mitochondrial dynamics are also tightly coupled to mitochondrial transport *(Figure 1.10).* Given the importance of mitochondrial fission and fusion, signaling cascades could exert a direct control over mitochondrial morphology by targeting the core fission and fusion machineries. In fact, the numerous post-translational modifications of Drp1 support this hypothesis.

Figure I-10 Positioning and morphology of mitochondria respond to cellular signals

Figure taken from: Soubannier V., McBride HM. (2009) Positioning mitochondrial plasticity within cellular signaling cascades. *Biochim Biophys Acta.* 1793(1):154-70, with permission.

(1) Mitochondrial dynamics are modulated by signaling cascades, (2) Mitochondrial movement along microtubules is important for their transport at sites of high energy demands, (3) Once the mitochondria have reached a specific sub-cellular localization, they might use the actin cytoskeleton for short range movements, (4) Finally, second messengers like the calcium ion can modulate mitochondrial output.

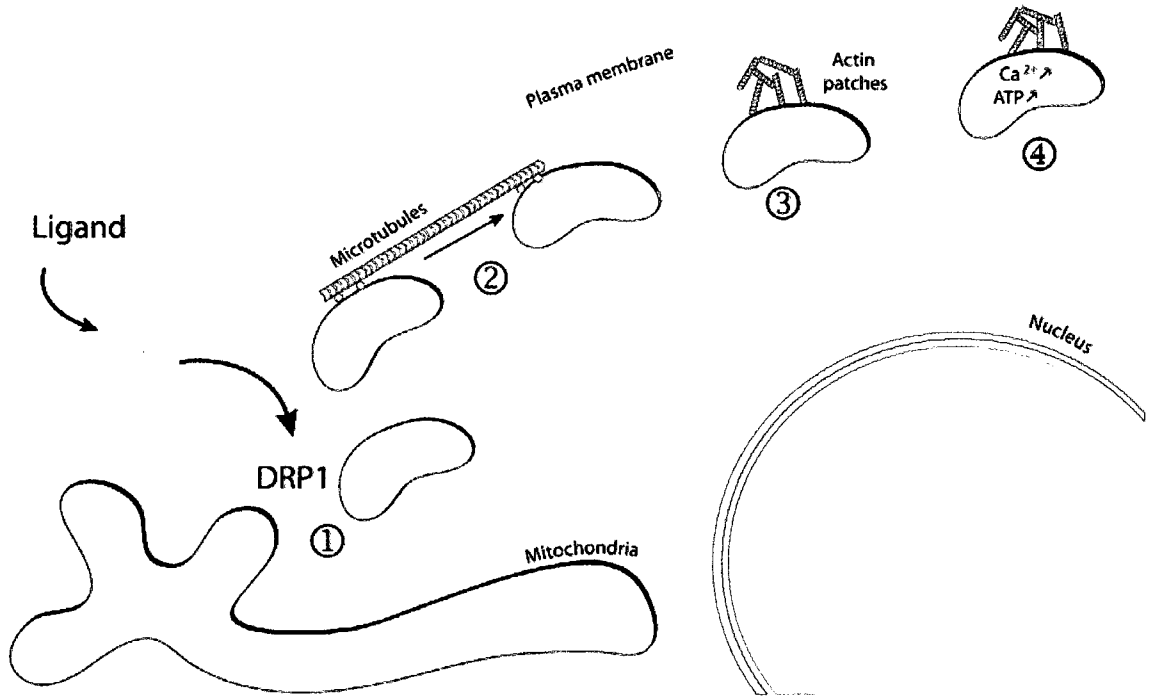
Ligand
Plasma membrane
Microtubules
②
Actin
patches
③
Ca 2+↗
ATP↗
④
Nucleus
DRP1
①
Mitochondria

I.3.1 Complex regulation of Drp1 by signaling cascades

Drp1 is regulated by different signaling cascades through post-translational modifications *(Figure 1.11)*. The known mechanisms to regulate the activity of Drp1 include the modulation of its recruitment to the mitochondria, or the change in its GTPase activity. Drp1 has an N-terminal GTP binding domain and a C-terminal GTPase effector domain (GED). This domain folds to interact with the GTP-binding domain, and can also interact with the GED domain of other Drp1 molecules (129, 130). Modulating Drp1's intra-molecular interactions by post-translationally modifying the GED domain can affect GTPase activity (131, 132).

The mitochondrial-anchored ubiquitin E3 ligase Membrane Associated Ring Finger 5 (MARCHV) regulates the recruitment of Drp1 to the mitochondria, thereby controlling fission events, although it is not clear whether MARCHV directly ubiquitinates Drp1 (133). Drp1 is also phosphorylated by CyclinB/Cdk1 on Ser585 during mitosis to facilitate mitotic mitochondrial fragmentation (26). Phosphorylation by the cAMP-dependent kinase (PKA) on Ser637 promotes the formation of a network, and provides resistance against diverse apoptotic stimuli (131, 132). The fission activity of Drp1 is also modulated by calcium signaling. Drp1 is phosphorylated by the Ca^{2+}/Calmodulin-dependent protein Kinase I α (CaMKIα), at Ser637, following Ca^{2+} influx through voltage-dependent Ca^{2+}channels. In neurons, this increases the translocation of Drp1 to the mitochondria, and triggers mitochondrial fragmentation (134). On the other hand, increased Ca^{2+}concentrations caused by mitochondrial damage activate the phosphatase calcineurin. Dephosphorylation of Ser637 increases Drp1 recruitment to the mitochondria and leads to fragmentation (132). In

other words, both calcium-induced phosphorylation and dephosphorylation lead to mitochondrial fragmentation. Importantly, these two studies used different isoforms of Drp1, which might explain the contradictory results. Finally, nitric oxide produced by the β-amyloid protein leads to the S-nitrosylation of Drp1 and mitochondria fragmentation, which may contribute to neurodegeneration (135).

In addition to phosphorylation, ubiquitination and nitrosylation, we have demonstrated that mitochondrial proteins, including Drp1 are SUMOylated (28). The number of mitochondrial proteins, or of proteins peripherally associated with mitochondria which are SUMOylated raises the possibility that SUMOylation is an important mitochondrial post-translational modification (28).

Figure I-11 Drp1 is regulated by different signaling cascades

Drp1 is modified by a number of enzymes. Post-translational modifications include ubiquitination, SUMOylation, S-nitrosylation, and phosphorylation.

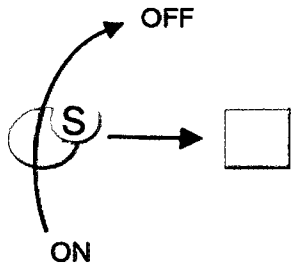

conformational change

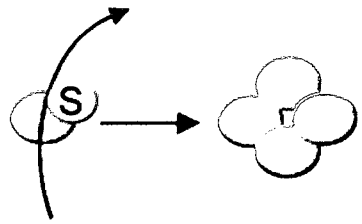

oligomer assembly

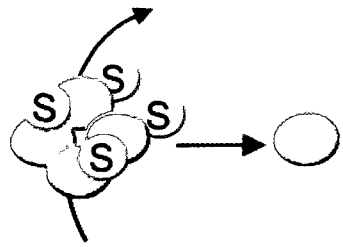

oligomer disassembly

I.3.2 Mitochondrial SUMOylation machinery, discovery of MAPL

I.3.2.1 SUMOylation, a conserved post translational modification

SUMO is an important cellular modifier, structurally very similar to ubiquitin (136). The conjugated SUMO can be recognized by SUMO Interaction Motifs (SIM), and can therefore lead to the formation of new binding interfaces. SUMOylation also triggers changes in protein conformation when the SUMOylated protein has an internal SIM (137) *(Figure 1.12)*. The enzymatic cascade leading to SUMOylation is similar to that of ubiquitination. The SUMO must first get cleaved at its C-terminus, unmasking a di-glycine motif. The active SUMO is then attacked by the cysteine residue of the SUMO-activating enzyme, or SUMO E1, in an ATP-dependent manner, which results in the formation of a thioester bond. The SUMO is then transferred to the Ubiquitin Conjugating Enzyme 9 (Ubc9), or SUMO E2. Ubc9 covalently conjugates SUMO onto the lysine residue of the substrate (137). This step is enhanced by a SUMO protein ligase, or SUMO E3 ligase, which provides specificity (137). The SUMO E3 ligase is not catalytic but rather acts as a scaffold, properly positioning the SUMO, the Ubc9 and the substrate (137). Importantly, SUMOylation is transient and SUMO proteases are responsible for the removal of SUMO, allowing rapid cycles of SUMOylation/deSUMOylation (137) *(Figure 1.3)*.

SUMOylation was historically described as a nuclear event involved in the regulation of complex assembly for nuclear transport and in the modulation of chromatin structure (138). As such, all known SUMO E3 ligases are primarily nuclear: the Really Interesting New Gene (RING) containing Protein Inhibitor of Activated STAT (PIAS) family is involved in senescence and is localized in Promyelocytic Leukemia (PML) bodies

(139), the Polycomb 2 is involved in the stable repression of gene transcription (140), the Ran binding protein 2 (RanBP2) is localized at the nuclear pore complex where it regulates nuclear trafficking (141), and the Kruppel-associated box domain-associated protein 1 (KAP1) represses transcription through the SUMOylation of its adjacent bromodomain (142). Importantly, although SUMO E3 ligases were originally identified as RING containing enzymes, most members do not have a RING domain (137).

Figure I-12 : Downstream effects of SUMOylation

SUMOylation can lead to different downstream signaling events. SUMOylation can induce conformational changes if the SUMOylated protein also possesses a SIM. SUMO can be recognized by other proteins containing SIMs, leading to oligomer assembly. On the other hand, SUMO can trigger the disassembly of cellular complexes.

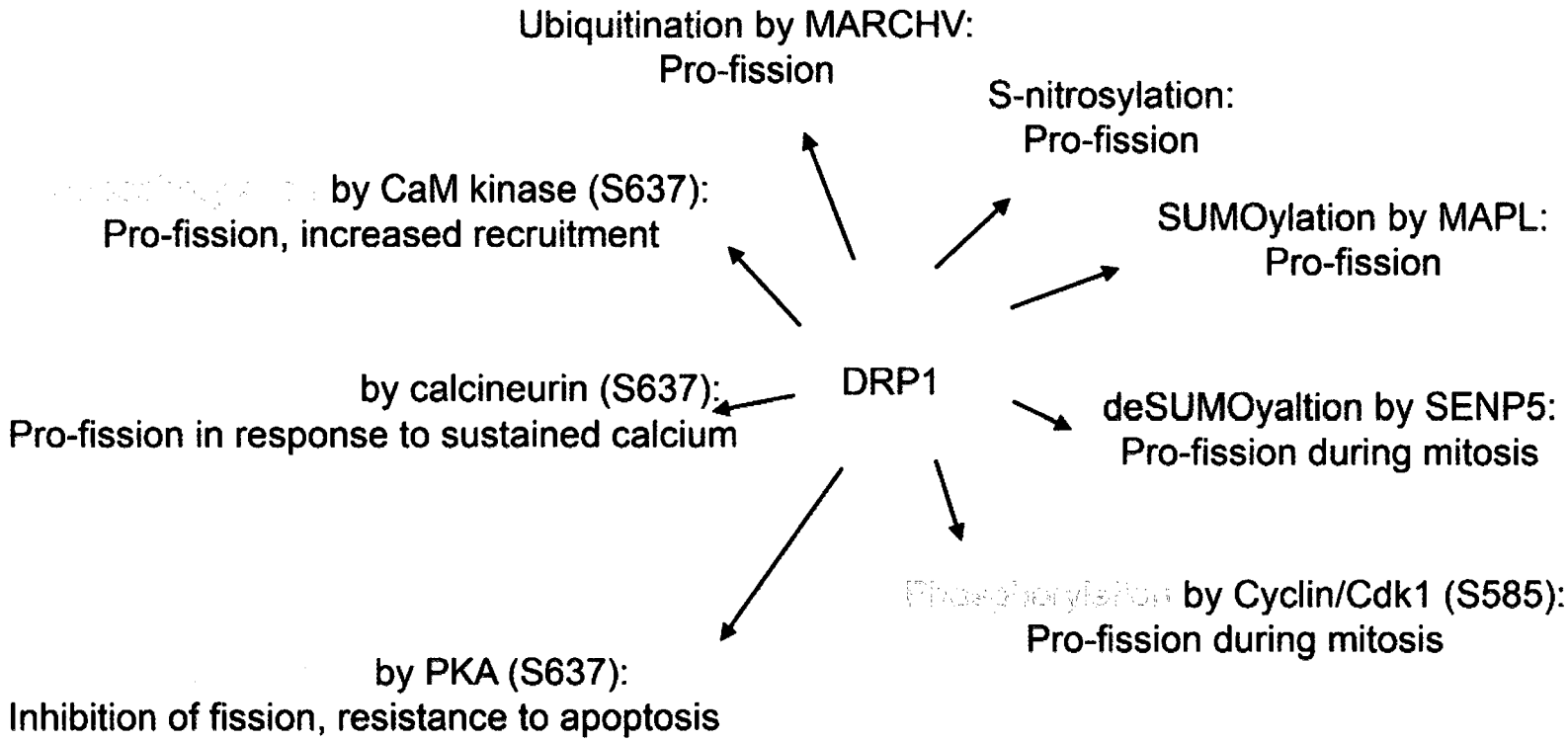
Ubiquitination by MARCHV:
Pro-fission
S-nitrosylation:
Pro-fission
by CaM kinase (S637):
Pro-fission, increased recruitment
SUMOylation by MAPL:
Pro-fission
by calcineurin (S637):
Pro-fission in response to sustained calcium
DRP1
deSUMOyaltion by SENP5:
Pro-fission during mitosis
by Cyclin/Cdk1 (S585):
Pro-fission during mitosis
by PKA (S637):
Inhibition of fission, resistance to apoptosis

Figure I-13 Enzymatic cascade of the SUMOylation reaction

Figure taken from: Geiss-Friedlander R and Melchior F (2007) Concepts in sumoylation: a decade on. *Nat Rev Mol Cell Biol.* 8(12):947-56, with permission.

SUMO is first cleaved at its C-terminus, uncovering a di-glycine motif. In an ATP-dependent reaction, the active SUMO is attached by a thioester bond to a cysteine residue to the SUMO activating enzyme, the Uba2/AOS1 dimer. The SUMO is then transferred to the SUMO conjugating enzyme Ubc9. Finally, Ubc9 covalently conjugates SUMO onto the lysine residue of the substrate with the help of a SUMO E3 ligase. SUMO proteases, by removing SUMO, allow rapid cycles of SUMOylation/deSUMOylation.

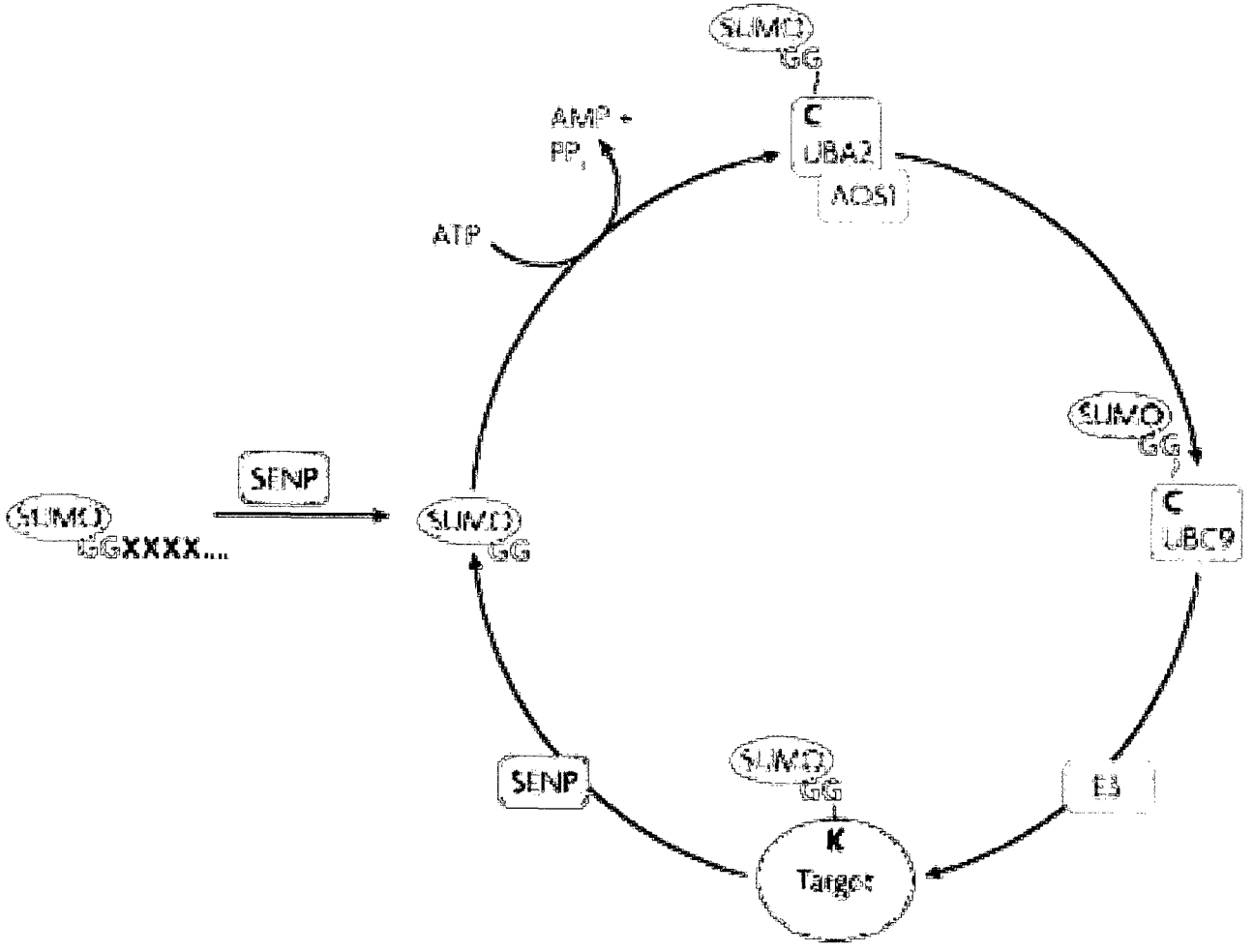

Nature Reviews | **Molecular Cell Biology**

Recent examples have highlighted the importance of SUMOylation in non-nuclear events (136). In particular, the SUMOylation of the septin GTPase is important for the disassembly of the septin rings in yeast (143). SUMOylation has also been implicated in the recycling of the kainate receptor (144), the activation of the voltage-gated K^+ channel (145), the regulation of the activity of an endoplasmic reticulum-localized phosphatase (146), and in the amplification of the Transforming Growth Factor β (TGFβ) signaling (147). In some of these cases, the SUMOylation events have been explained by the cytoplasmic migration of a nuclear SUMO E3 ligase. For example, the movement of the SAP and Miz-finger containing SUMO E3 ligase (Siz1/2) to the cytokinetic furrow during mitosis is required for the SUMOylation of septins in yeast (148). However, since the activity of SUMO E3 ligases is thought to be largely controlled by their localization it is also very likely that there are primarily cytoplasmic SUMO E3 ligases.

I.3.2.2 MAPL, a mitochondrial SUMO E3 ligase

Currently, the only known mitochondrial SUMO substrate is Drp1, but a number of other, unidentified mitochondrial proteins are SUMO substrates. SUMOylation enhances mitochondrial fission, a phenomenon which is prevented by a dominant negative form of Drp1 (28). In addition to the steady state function of Drp1 SUMOylation, Drp1 is SUMOylated in a Bax/Bak-dependent manner during apoptosis, an event which correlates with a drastic change in the dynamic behavior of Drp1 (149). Finally, the deSUMOylation of Drp1 by SENP5 during mitosis might be important to trigger mitochondrial mitotic fragmentation (62).

These examples illustrate a role for SUMOylation in mitochondrial dynamics. We therefore hypothesized that a mitochondrial SUMO E3 ligase might be responsible for the

SUMOylation of Drp1 and of other mitochondrial targets. In order to uncover potential mitochondrial SUMO E3 ligases, a bioinformatics approach was used (150). The human genome was screened for RING containing proteins with a transmembrane domain and a mitochondrial targeting sequence. Using this method, a new protein was uncovered: the Mitochondrial Anchored Protein Ligase (MAPL) (150). MAPL is mitochondrial, contains two transmembrane domains, a C-terminal RING finger domain, which faces the cytosol, and a Beside a Membrane (BAM) domain, localized in the intermembrane space (150) *(Figure 1.14)*. The overexpression of MAPL promotes Drp1-dependent mitochondrial fission, which is consistent with a potential role as a mitochondrial SUMO E3 ligase (150). In addition, the BAM domain, of unknown function, is conserved from prokaryotes to eukaryotes, the RING domain appearing in higher eukaryotes (151). The conservation of MAPL and its role in regulating mitochondrial fission made it an attractive protein for further studies.

Figure I-14 Topology of MAPL

Figure taken from: Andrade-Navarro MA, Sanchez-Pulido L, McBride HM. (2009) Mitochondrial vesicles: an ancient process providing new links to peroxisomes. Curr Opin Cell Biol. 21(4):560-7, with permission.

Cartoon representing the topology of MAPL in different species. In eukaryotes, the orthologs of MAPL are present in the sea urchin, insects, fish, mammals, plants, but not in fungi or nematode. The RING domain is only present in higher eukaryotes. There are five different prokaryotic configurations of MAPL. In *Flavobacterium* and *Desulfuromonadales*, the protein is composed just of the BAM and transmembrane domains. In *Dehalococcus* and *Reinekea*, the protein contains an additional domain, the LemA domain, of unknown functions. In *Reinekea* the BAM domain appears twice.

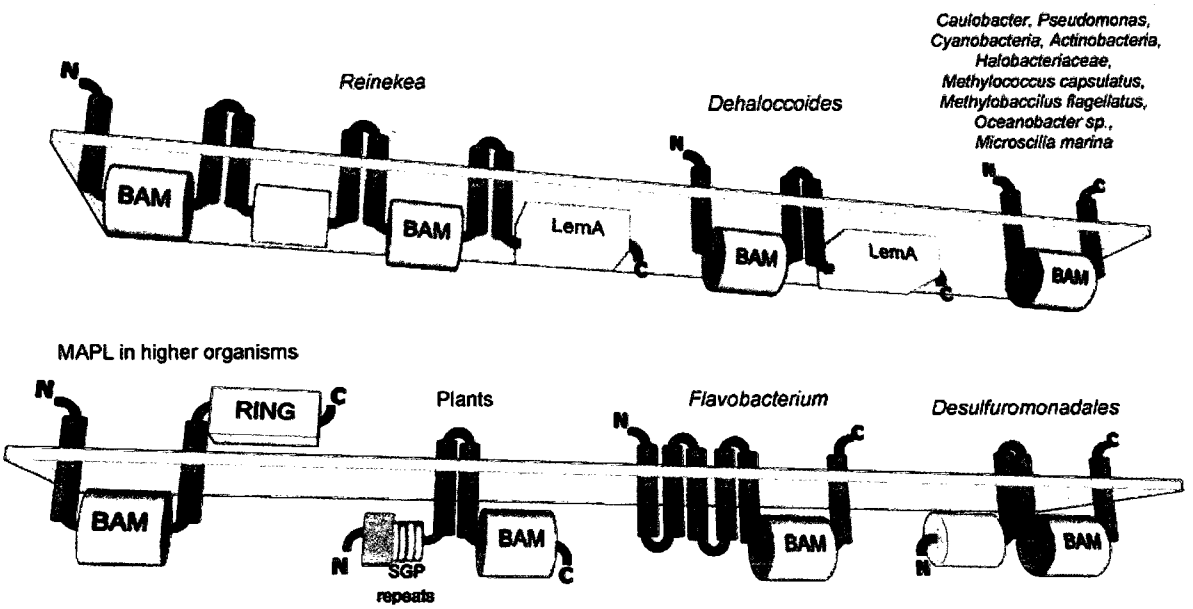
Caulobacter, Pseudomonas,
Cyanobacteria, Actinobacteria,
Halobacteriaceae,
Methylococcus capsulatus,
Methylobacillus flagellatus,
Oceanobacter sp.,
Microscilla marina
Reinekea
Dehaloccoides
N
BAM
BAM
LemA
C
N
BAM
LemA
C
N
C
BAM
MAPL in higher organisms
N
RING
C
Plants
Flavobacterium
Desulfuromonadales
BAM
N
SGP
repeats
BAM
C
N
BAM
C
N
C
BAM

I.3.3 Mitochondrial Derived Vesicles

The examination of cells transfected with MAPL:YFP by confocal and electron microscopy led to the identification of small structures that are enriched for MAPL (151). These structures, which we defined as Mitochondria Derived Vesicles (MDVs), are not usual fragments since they are uniform 70-100 nm structures, exhibit cargo specificity, and are formed independently of the fission machinery (151). Unexpectedly, MAPL positive MDVs are targeted to a subpopulation of peroxisomes, highlighting a previously uncharacterized communication pathway between these organelles (151).

MAPL is a positive regulator of mitochondrial fission (151), and since mitochondria and peroxisomes share the same fission machinery, including Fis1, Drp1, and the Mitochondria Fission Factor (Mff), it is possible that MAPL also regulates peroxisomal fission (16, 151, 152). However, MAPL is only targeted to a subpopulation of peroxisomes and it is therefore unlikely that its primary role is to regulate peroxisomal morphology. On the other hand, since mitochondria and peroxisomes share a number of metabolic functions (153), the transport of MAPL could coordinate the metabolic functions of these two organelles through SUMOylation. MDVs could also shuttle different enzymes or lipids (151). In fact, the mitochondria are unable to degrade very long fatty acids. If such lipids were to be misrouted and to enter the mitochondria, they could be shuttled back to peroxisomes though MDVs (151). Uncovering the machinery involved in the formation of MDVs will be an important step towards the understanding of the physiological function of this novel trafficking pathway.

I.4 Problem and Objectives

The mitochondria form an interconnected network, constantly remodeled by fusion and fission events. Highlighting the physiological importance of mitochondrial dynamics, the loss of the mitochondrial morphology proteins is embryonic lethal and mutations in their genes lead to human diseases (25). Changes in mitochondrial dynamics also play important roles in essential cellular events, including metabolism (37), the cell cycle (62), migration (102) and cellular stress (64). In addition, specific cellular functions of mitochondrial morphology proteins are emerging. Mfn2, but not Mfn1, is linked to β-cell dysfunction (50, 154). Mfn1, but not Mfn2, is required for stress induced hyperfusion (64). Fis1 seems to have a specific role in insulin secretion (34) and to play a role in cell death not shared by Drp1 (18). In fact, beyond their roles as modulators of morphology, these mitochondrial proteins now emerge as key players within cellular signaling networks. This is best highlighted by the complex functions of Mfn2 as a promoter of mitochondrial fusion, a regulator of metabolism, and of cell cycle progression (10, 50, 58, 154). The challenge is to dissect these different functions and to understand their coordination with mitochondrial morphology and cellular signaling.

Post-translational modifications have been shown to coordinate signaling cascades and mitochondrial morphology. So far, most of the attention has been focused on Drp1, which is SUMOylated (28), phosphorylated (132), ubiquitinated (133) and S-nitrosylated (135). However, in addition to Drp1, evidence points towards an important role for SUMOylation in mitochondrial function. Although we do not yet know whether this role is restricted to the control of mitochondrial morphology, the number of mitochondrial SUMO substrates indicates that mitochondrial SUMOylation might fulfill a much broader function.

The hypothesis of my project was that the mitochondrial SUMOylation machinery may play a central role in propagating signals between diverse cellular signaling cascades and the mitochondria.

- The first objective was to explore whether the RING domain of MAPL possesses SUMO or Ubiquitin E3 ligase activity. I have demonstrated that MAPL functions as a SUMO E3 ligase for a number of mitochondrial substrates, including Drp1.
- The second objective was to identify the interacting partners and substrates of MAPL. In addition to Drp1, there are a number of uncharacterized SUMO1 substrates. To better understand the physiological function of MAPL and of mitochondrial SUMOylation, we decided to isolate potential MAPL interacting partners using an affinity column approach, and to characterize the mitochondrial SUMO proteome.
- One of the substrates of MAPL, the Vacuolar Protein Factor 35 (Vps35) is a component of a coat complex, the retromer (155). I have shown that Vps35, regulates the vesicular transport of MAPL from the mitochondria to peroxisomes, providing important mechanistic insights into the formation of MDVs.

I.5 References

1. Gray, M.W., G. Burger, and B.F. Lang. 1999. Mitochondrial evolution. *Science* 283:1476-1481.
2. Searcy, D.G. 2003. Metabolic integration during the evolutionary origin of mitochondria. *Cell Res* 13:229-238.
3. Nunnari, J., W.F. Marshall, A. Straight, A. Murray, J.W. Sedat, and P. Walter. 1997. Mitochondrial transmission during mating in Saccharomyces cerevisiae is determined by mitochondrial fusion and fission and the intramitochondrial segregation of mitochondrial DNA. *Mol Biol Cell* 8:1233-1242.
4. Nakada, K., K. Inoue, T. Ono, K. Isobe, A. Ogura, Y.I. Goto, I. Nonaka, and J.I. Hayashi. 2001. Inter-mitochondrial complementation: Mitochondria-specific system preventing mice from expression of disease phenotypes by mutant mtDNA. *Nat Med* 7:934-940.
5. Cortese, J.D., L.A. Voglino, and C.R. Hackenbrock. 1998. Novel fluorescence membrane fusion assays reveal GTP-dependent fusogenic properties of outer mitochondrial membrane-derived proteins. *Biochim Biophys Acta* 1371:185-198.
6. Loew, L.M. 1993. Confocal microscopy of potentiometric fluorescent dyes. *Methods Cell Biol* 38:195-209.
7. Malka, F., O. Guillery, C. Cifuentes-Diaz, E. Guillou, P. Belenguer, A. Lombes, and M. Rojo. 2005. Separate fusion of outer and inner mitochondrial membranes. *EMBO Rep* 6:853-859.
8. Santel, A., and M.T. Fuller. 2001. Control of mitochondrial morphology by a human mitofusin. *J Cell Sci* 114:867-874.
9. Liesa, M., M. Palacin, and A. Zorzano. 2009. Mitochondrial dynamics in mammalian health and disease. *Physiol Rev* 89:799-845.
10. Chen, H., S.A. Detmer, A.J. Ewald, E.E. Griffin, S.E. Fraser, and D.C. Chan. 2003. Mitofusins Mfn1 and Mfn2 coordinately regulate mitochondrial fusion and are essential for embryonic development. *J Cell Biol* 160:189-200.
11. Chen, H., J.M. McCaffery, and D.C. Chan. 2007. Mitochondrial fusion protects against neurodegeneration in the cerebellum. *Cell* 130:548-562.
12. Zuchner, S., M. Noureddine, M. Kennerson, K. Verhoeven, K. Claeys, P. De Jonghe, J. Merory, S.A. Oliveira, M.C. Speer, J.E. Stenger, G. Walizada, D. Zhu, M.A. Pericak-Vance, G. Nicholson, V. Timmerman, and J.M. Vance. 2005. Mutations in the pleckstrin homology domain of dynamin 2 cause dominant intermediate Charcot-Marie-Tooth disease. *Nat Genet* 37:289-294.
13. Zuchner, S., and J.M. Vance. 2005. Emerging pathways for hereditary axonopathies. *J Mol Med* 83:935-943.

14. Delettre, C., G. Lenaers, L. Pelloquin, P. Belenguer, and C.P. Hamel. 2002. OPA1 (Kjer type) dominant optic atrophy: a novel mitochondrial disease. *Mol Genet Metab* 75:97-107.

15. Delettre, C., G. Lenaers, J.M. Griffoin, N. Gigarel, C. Lorenzo, P. Belenguer, L. Pelloquin, J. Grosgeorge, C. Turc-Carel, E. Perret, C. Astarie-Dequeker, L. Lasquellec, B. Arnaud, B. Ducommun, J. Kaplan, and C.P. Hamel. 2000. Nuclear gene OPA1, encoding a mitochondrial dynamin-related protein, is mutated in dominant optic atrophy. *Nat Genet* 26:207-210.

16. Kobayashi, S., A. Tanaka, and Y. Fujiki. 2007. Fis1, DLP1, and Pex11p coordinately regulate peroxisome morphogenesis. *Exp Cell Res* 313:1675-1686.

17. James, D.I., P.A. Parone, Y. Mattenberger, and J.C. Martinou. 2003. hFis1, a novel component of the mammalian mitochondrial fission machinery. *J Biol Chem* 278:36373-36379.

18. Lee, Y.J., S.Y. Jeong, M. Karbowski, C.L. Smith, and R.J. Youle. 2004. Roles of the mammalian mitochondrial fission and fusion mediators Fis1, Drp1, and Opa1 in apoptosis. *Mol Biol Cell* 15:5001-5011.

19. Smirnova, E., L. Griparic, D.L. Shurland, and A.M. van der Bliek. 2001. Dynamin-related protein Drp1 is required for mitochondrial division in mammalian cells. *Mol Biol Cell* 12:2245-2256.

20. Ingerman, E., E.M. Perkins, M. Marino, J.A. Mears, J.M. McCaffery, J.E. Hinshaw, and J. Nunnari. 2005. Dnm1 forms spirals that are structurally tailored to fit mitochondria. *J Cell Biol* 170:1021-1027.

21. Hoppins, S., L. Lackner, and J. Nunnari. 2007. The machines that divide and fuse mitochondria. *Annu Rev Biochem* 76:751-780.

22. Ishihara, N., M. Nomura, A. Jofuku, H. Kato, S.O. Suzuki, K. Masuda, H. Otera, Y. Nakanishi, I. Nonaka, Y. Goto, N. Taguchi, H. Morinaga, M. Maeda, R. Takayanagi, S. Yokota, and K. Mihara. 2009. Mitochondrial fission factor Drp1 is essential for embryonic development and synapse formation in mice. *Nat Cell Biol* 11:958-966.

23. Wakabayashi, J., Z. Zhang, N. Wakabayashi, Y. Tamura, M. Fukaya, T.W. Kensler, M. Iijima, and H. Sesaki. 2009. The dynamin-related GTPase Drp1 is required for embryonic and brain development in mice. *J Cell Biol.*

24. Waterham, H.R., J. Koster, C.W. van Roermund, P.A. Mooyer, R.J. Wanders, and J.V. Leonard. 2007. A lethal defect of mitochondrial and peroxisomal fission. *N Engl J Med* 356:1736-1741.

25. Chan, D.C. 2006. Mitochondria: dynamic organelles in disease, aging, and development. *Cell* 125:1241-1252.

26. Taguchi, N., N. Ishihara, A. Jofuku, T. Oka, and K. Mihara. 2007. Mitotic phosphorylation of dynamin-related GTPase Drp1 participates in mitochondrial fission. *J Biol Chem* 282:11521-11529.

27. Chen, H., A. Chomyn, and D.C. Chan. 2005. Disruption of fusion results in mitochondrial heterogeneity and dysfunction. *J Biol Chem* 280:26185-26192.

28. Harder, Z., R. Zunino, and H. McBride. 2004. Sumo1 conjugates mitochondrial substrates and participates in mitochondrial fission. *Curr Biol* 14:340-345.

29. Wiederkehr, A., and C.B. Wollheim. 2006. Minireview: implication of mitochondria in insulin secretion and action. *Endocrinology* 147:2643-2649.

30. Rizzuto, R., and T. Pozzan. 2006. Microdomains of intracellular Ca2+: molecular determinants and functional consequences. *Physiol Rev* 86:369-408.

31. Rizzuto, R., P. Pinton, W. Carrington, F.S. Fay, K.E. Fogarty, L.M. Lifshitz, R.A. Tuft, and T. Pozzan. 1998. Close contacts with the endoplasmic reticulum as determinants of mitochondrial Ca2+ responses. *Science* 280:1763-1766.

32. Rizzuto, R., M. Brini, M. Murgia, and T. Pozzan. 1993. Microdomains with high Ca2+ close to IP3-sensitive channels that are sensed by neighboring mitochondria. *Science* 262:744-747.

33. Orrenius, S., B. Zhivotovsky, and P. Nicotera. 2003. Regulation of cell death: the calcium-apoptosis link. *Nat Rev Mol Cell Biol* 4:552-565.

34. Park, K.S., A. Wiederkehr, C. Kirkpatrick, Y. Mattenberger, J.C. Martinou, P. Marchetti, N. Demaurex, and C.B. Wollheim. 2008. Selective actions of mitochondrial fission/fusion genes on metabolism-secretion coupling in insulin-releasing cells. *J Biol Chem* 283:33347-33356.

35. Szabadkai, G., A.M. Simoni, M. Chami, M.R. Wieckowski, R.J. Youle, and R. Rizzuto. 2004. Drp-1-dependent division of the mitochondrial network blocks intraorganellar Ca2+ waves and protects against Ca2+-mediated apoptosis. *Mol Cell* 16:59-68.

36. Frieden, M., D. James, C. Castelbou, A. Danckaert, J.C. Martinou, and N. Demaurex. 2004. Ca(2+) homeostasis during mitochondrial fragmentation and perinuclear clustering induced by hFis1. *J Biol Chem* 279:22704-22714.

37. Yu, T., J.L. Robotham, and Y. Yoon. 2006. Increased production of reactive oxygen species in hyperglycemic conditions requires dynamic change of mitochondrial morphology. *Proc Natl Acad Sci U S A* 103:2653-2658.

38. Zick, M., R. Rabl, and A.S. Reichert. 2009. Cristae formation-linking ultrastructure and function of mitochondria. *Biochim Biophys Acta* 1793:5-19.

39. Hackenbrock, C.R. 1966. Ultrastructural bases for metabolically linked mechanical activity in mitochondria. I. Reversible ultrastructural changes with change in metabolic steady state in isolated liver mitochondria. *J Cell Biol* 30:269-297.

40. Hackenbrock, C.R. 1968. Ultrastructural bases for metabolically linked mechanical activity in mitochondria. II. Electron transport-linked ultrastructural transformations in mitochondria. *J Cell Biol* 37:345-369.

41. Mannella, C.A., D.R. Pfeiffer, P.C. Bradshaw, Moraru, II, B. Slepchenko, L.M. Loew, C.E. Hsieh, K. Buttle, and M. Marko. 2001. Topology of the mitochondrial inner membrane: dynamics and bioenergetic implications. *IUBMB Life* 52:93-100.

42. Germain, M., J.P. Mathai, H.M. McBride, and G.C. Shore. 2005. Endoplasmic reticulum BIK initiates DRP1-regulated remodelling of mitochondrial cristae during apoptosis. *Embo J* 24:1546-1556.

43. Bindokas, V.P., A. Kuznetsov, S. Sreenan, K.S. Polonsky, M.W. Roe, and L.H. Philipson. 2003. Visualizing superoxide production in normal and diabetic rat islets of Langerhans. *J Biol Chem* 278:9796-9801.

44. Kelley, D.E., J. He, E.V. Menshikova, and V.B. Ritov. 2002. Dysfunction of mitochondria in human skeletal muscle in type 2 diabetes. *Diabetes* 51:2944-2950.

45. Cartoni, R., B. Leger, M.B. Hock, M. Praz, A. Crettenand, S. Pich, J.L. Ziltener, F. Luthi, O. Deriaz, A. Zorzano, C. Gobelet, A. Kralli, and A.P. Russell. 2005. Mitofusins 1/2 and ERRalpha expression are increased in human skeletal muscle after physical exercise. *J Physiol* 567:349-358.

46. Bach, D., S. Pich, F.X. Soriano, N. Vega, B. Baumgartner, J. Oriola, J.R. Daugaard, J. Lloberas, M. Camps, J.R. Zierath, R. Rabasa-Lhoret, H. Wallberg-Henriksson, M. Laville, M. Palacin, H. Vidal, F. Rivera, M. Brand, and A. Zorzano. 2003. Mitofusin-2 determines mitochondrial network architecture and mitochondrial metabolism. A novel regulatory mechanism altered in obesity. *J Biol Chem* 278:17190-17197.

47. Zorzano, A., M. Liesa, and M. Palacin. 2009. Role of mitochondrial dynamics proteins in the pathophysiology of obesity and type 2 diabetes. *Int J Biochem Cell Biol* 41:1846-1854.

48. Merkwirth, C., and T. Langer. 2008. Mitofusin 2 builds a bridge between ER and mitochondria. *Cell* 135:1165-1167.

49. de Brito, O.M., and L. Scorrano. 2008. Mitofusin 2 tethers endoplasmic reticulum to mitochondria. *Nature* 456:605-610.

50. Pich, S., D. Bach, P. Briones, M. Liesa, M. Camps, X. Testar, M. Palacin, and A. Zorzano. 2005. The Charcot-Marie-Tooth type 2A gene product, Mfn2, up-regulates fuel oxidation through expression of OXPHOS system. *Hum Mol Genet* 14:1405-1415.

51. Soriano, F.X., M. Liesa, D. Bach, D.C. Chan, M. Palacin, and A. Zorzano. 2006. Evidence for a mitochondrial regulatory pathway defined by peroxisome proliferator-activated receptor-gamma coactivator-1 alpha, estrogen-related receptor-alpha, and mitofusin 2. *Diabetes* 55:1783-1791.

52. Neuspiel, M., R. Zunino, S. Gangaraju, P. Rippstein, and H. McBride. 2005. Activated mitofusin 2 signals mitochondrial fusion, interferes with Bax activation, and reduces susceptibility to radical induced depolarization. *J Biol Chem* 280:25060-25070.

53. Koshiba, T., S.A. Detmer, J.T. Kaiser, H. Chen, J.M. McCaffery, and D.C. Chan. 2004. Structural basis of mitochondrial tethering by mitofusin complexes. *Science* 305:858-862.

54. Wang, C., Z. Li, Y. Lu, R. Du, S. Katiyar, J. Yang, M. Fu, J.E. Leader, A. Quong, P.M. Novikoff, and R.G. Pestell. 2006. Cyclin D1 repression of nuclear respiratory

factor 1 integrates nuclear DNA synthesis and mitochondrial function. *Proc Natl Acad Sci U S A* 103:11567-11572.

55. Schieke, S.M., J.P. McCoy, Jr., and T. Finkel. 2008. Coordination of mitochondrial bioenergetics with G1 phase cell cycle progression. *Cell Cycle* 7:1782-1787.

56. Mitra, K., C. Wunder, B. Roysam, G. Lin, and J. Lippincott-Schwartz. 2009. A hyperfused mitochondrial state achieved at G1-S regulates cyclin E buildup and entry into S phase. *Proc Natl Acad Sci U S A* 106:11960-11965.

57. Walsh, B., M. Tonkonogi, K. Soderlund, E. Hultman, V. Saks, and K. Sahlin. 2001. The role of phosphorylcreatine and creatine in the regulation of mitochondrial respiration in human skeletal muscle. *J Physiol* 537:971-978.

58. Chen, K.H., X. Guo, D. Ma, Y. Guo, Q. Li, D. Yang, P. Li, X. Qiu, S. Wen, R.P. Xiao, and J. Tang. 2004. Dysregulation of HSG triggers vascular proliferative disorders. *Nat Cell Biol* 6:872-883.

59. Mandal, S., P. Guptan, E. Owusu-Ansah, and U. Banerjee. 2005. Mitochondrial regulation of cell cycle progression during development as revealed by the tenured mutation in Drosophila. *Dev Cell* 9:843-854.

60. Owusu-Ansah, E., A. Yavari, S. Mandal, and U. Banerjee. 2008. Distinct mitochondrial retrograde signals control the G1-S cell cycle checkpoint. *Nat Genet* 40:356-361.

61. Zunino, R., A. Schauss, P. Rippstein, M. Andrade-Navarro, and H.M. McBride. 2007. The SUMO protease SENP5 is required to maintain mitochondrial morphology and function. *J Cell Sci* 120:1178-1188.

62. Zunino, R., E. Braschi, L. Xu, and H.M. McBride. 2009. Translocation of SenP5 from the nucleoli to the mitochondria modulates DRP1-dependent fission during mitosis. *J Biol Chem* 284:17783-17795.

63. Benard, G., N. Bellance, D. James, P. Parrone, H. Fernandez, T. Letellier, and R. Rossignol. 2007. Mitochondrial bioenergetics and structural network organization. *J Cell Sci* 120:838-848.

64. Tondera, D., S. Grandemange, A. Jourdain, M. Karbowski, Y. Mattenberger, S. Herzig, S. Da Cruz, P. Clerc, I. Raschke, C. Merkwirth, S. Ehses, F. Krause, D.C. Chan, C. Alexander, C. Bauer, R. Youle, T. Langer, and J.C. Martinou. 2009. SLP-2 is required for stress-induced mitochondrial hyperfusion. *Embo J* 28:1589-1600.

65. Hajek, P., A. Chomyn, and G. Attardi. 2007. Identification of a novel mitochondrial complex containing mitofusin 2 and stomatin-like protein 2. *J Biol Chem* 282:5670-5681.

66. Hengartner, M.O. 2000. The biochemistry of apoptosis. *Nature* 407:770-776.

67. Zou, H., Y. Li, X. Liu, and X. Wang. 1999. An APAF-1.cytochrome c multimeric complex is a functional apoptosome that activates procaspase-9. *J Biol Chem* 274:11549-11556.

68. Wang, X. 2001. The expanding role of mitochondria in apoptosis. *Genes Dev* 15:2922-2933.

69. Susin, S.A., H.K. Lorenzo, N. Zamzami, I. Marzo, B.E. Snow, G.M. Brothers, J. Mangion, E. Jacotot, P. Costantini, M. Loeffler, N. Larochette, D.R. Goodlett, R. Aebersold, D.P. Siderovski, J.M. Penninger, and G. Kroemer. 1999. Molecular characterization of mitochondrial apoptosis-inducing factor. *Nature* 397:441-446.

70. Dubrez-Daloz, L., A. Dupoux, and J. Cartier. 2008. IAPs: more than just inhibitors of apoptosis proteins. *Cell Cycle* 7:1036-1046.

71. Tsujimoto, Y., T. Nakagawa, and S. Shimizu. 2006. Mitochondrial membrane permeability transition and cell death. *Biochim Biophys Acta* 1757:1297-1300.

72. Karbowski, M., Y.J. Lee, B. Gaume, S.Y. Jeong, S. Frank, A. Nechushtan, A. Santel, M. Fuller, C.L. Smith, and R.J. Youle. 2002. Spatial and temporal association of Bax with mitochondrial fission sites, Drp1, and Mfn2 during apoptosis. *J Cell Biol* 159:931-938.

73. Yamaguchi, R., and G. Perkins. 2009. Dynamics of mitochondrial structure during apoptosis and the enigma of Opa1. *Biochim Biophys Acta* 1787:963-972.

74. Olichon, A., L. Baricault, N. Gas, E. Guillou, A. Valette, P. Belenguer, and G. Lenaers. 2003. Loss of OPA1 perturbates the mitochondrial inner membrane structure and integrity, leading to cytochrome c release and apoptosis. *J Biol Chem* 278:7743-7746.

75. Sugioka, R., S. Shimizu, and Y. Tsujimoto. 2004. Fzo1, a protein involved in mitochondrial fusion, inhibits apoptosis. *J Biol Chem* 279:52726-52734.

76. Estaquier, J., and D. Arnoult. 2007. Inhibiting Drp1-mediated mitochondrial fission selectively prevents the release of cytochrome c during apoptosis. *Cell Death Differ* 14:1086-1094.

77. Pellegrini, L., and L. Scorrano. 2007. A cut short to death: Parl and Opa1 in the regulation of mitochondrial morphology and apoptosis. *Cell Death Differ* 14:1275-1284.

78. Arnoult, D., A. Grodet, Y.J. Lee, J. Estaquier, and C. Blackstone. 2005. Release of OPA1 during apoptosis participates in the rapid and complete release of cytochrome c and subsequent mitochondrial fragmentation. *J Biol Chem* 280:35742-35750.

79. Karbowski, M., K.L. Norris, M.M. Cleland, S.Y. Jeong, and R.J. Youle. 2006. Role of Bax and Bak in mitochondrial morphogenesis. *Nature* 443:658-662.

80. Cassidy-Stone, A., J.E. Chipuk, E. Ingerman, C. Song, C. Yoo, T. Kuwana, M.J. Kurth, J.T. Shaw, J.E. Hinshaw, D.R. Green, and J. Nunnari. 2008. Chemical inhibition of the mitochondrial division dynamin reveals its role in Bax/Bak-dependent mitochondrial outer membrane permeabilization. *Dev Cell* 14:193-204.

81. Yamaguchi, R., L. Lartigue, G. Perkins, R.T. Scott, A. Dixit, Y. Kushnareva, T. Kuwana, M.H. Ellisman, and D.D. Newmeyer. 2008. Opa1-mediated cristae opening is Bax/Bak and BH3 dependent, required for apoptosis, and independent of Bak oligomerization. *Mol Cell* 31:557-569.

82. Kuwana, T., M.R. Mackey, G. Perkins, M.H. Ellisman, M. Latterich, R. Schneiter, D.R. Green, and D.D. Newmeyer. 2002. Bid, Bax, and lipids cooperate to form supramolecular openings in the outer mitochondrial membrane. *Cell* 111:331-342.

83. Boldogh, I.R., and L.A. Pon. 2007. Mitochondria on the move. *Trends Cell Biol* 17:502-510.

84. Hollenbeck, P.J., and W.M. Saxton. 2005. The axonal transport of mitochondria. *J Cell Sci* 118:5411-5419.

85. Frederick, R.L., and J.M. Shaw. 2007. Moving mitochondria: establishing distribution of an essential organelle. *Traffic* 8:1668-1675.

86. Itoh, T., E.A. Toh, and Y. Matsui. 2004. Mmr1p is a mitochondrial factor for Myo2p-dependent inheritance of mitochondria in the budding yeast. *Embo J* 23:2520-2530.

87. Boldogh, I.R., S.L. Ramcharan, H.C. Yang, and L.A. Pon. 2004. A type V myosin (Myo2p) and a Rab-like G-protein (Ypt11p) are required for retention of newly inherited mitochondria in yeast cells during cell division. *Mol Biol Cell* 15:3994-4002.

88. Boldogh, I.R., H.C. Yang, W.D. Nowakowski, S.L. Karmon, L.G. Hays, J.R. Yates, 3rd, and L.A. Pon. 2001. Arp2/3 complex and actin dynamics are required for actin-based mitochondrial motility in yeast. *Proc Natl Acad Sci U S A* 98:3162-3167.

89. Boldogh, I.R., and L.A. Pon. 2006. Interactions of mitochondria with the actin cytoskeleton. *Biochim Biophys Acta* 1763:450-462.

90. Meisinger, C., M. Rissler, A. Chacinska, L.K. Szklarz, D. Milenkovic, V. Kozjak, B. Schonfisch, C. Lohaus, H.E. Meyer, M.P. Yaffe, B. Guiard, N. Wiedemann, and N. Pfanner. 2004. The mitochondrial morphology protein Mdm10 functions in assembly of the preprotein translocase of the outer membrane. *Dev Cell* 7:61-71.

91. Meisinger, C., S. Pfannschmidt, M. Rissler, D. Milenkovic, T. Becker, D. Stojanovski, M.J. Youngman, R.E. Jensen, A. Chacinska, B. Guiard, N. Pfanner, and N. Wiedemann. 2007. The morphology proteins Mdm12/Mmm1 function in the major beta-barrel assembly pathway of mitochondria. *Embo J* 26:2229-2239.

92. Fehrenbacher, K.L., H.C. Yang, A.C. Gay, T.M. Huckaba, and L.A. Pon. 2004. Live cell imaging of mitochondrial movement along actin cables in budding yeast. *Curr Biol* 14:1996-2004.

93. Aguilaniu, H., L. Gustafsson, M. Rigoulet, and T. Nystrom. 2003. Asymmetric inheritance of oxidatively damaged proteins during cytokinesis. *Science* 299:1751-1753.

94. Twig, G., A. Elorza, A.J. Molina, H. Mohamed, J.D. Wikstrom, G. Walzer, L. Stiles, S.E. Haigh, S. Katz, G. Las, J. Alroy, M. Wu, B.F. Py, J. Yuan, J.T. Deeney, B.E. Corkey, and O.S. Shirihai. 2008. Fission and selective fusion govern mitochondrial segregation and elimination by autophagy. *Embo J* 27:433-446.

95. Kitada, T., S. Asakawa, N. Hattori, H. Matsumine, Y. Yamamura, S. Minoshima, M. Yokochi, Y. Mizuno, and N. Shimizu. 1998. Mutations in the parkin gene cause autosomal recessive juvenile parkinsonism. *Nature* 392:605-608.

96. Miller, K.E., and M.P. Sheetz. 2004. Axonal mitochondrial transport and potential are correlated. *J Cell Sci* 117:2791-2804.

97. Schwarzer, C., S. Barnikol-Watanabe, F.P. Thinnes, and N. Hilschmann. 2002. Voltage-dependent anion-selective channel (VDAC) interacts with the dynein light chain Tctex1 and the heat-shock protein PBP74. *Int J Biochem Cell Biol* 34:1059-1070.

98. Todde, V., M. Veenhuis, and I.J. van der Klei. 2009. Autophagy: principles and significance in health and disease. *Biochim Biophys Acta* 1792:3-13.

99. Hara, T., K. Nakamura, M. Matsui, A. Yamamoto, Y. Nakahara, R. Suzuki-Migishima, M. Yokoyama, K. Mishima, I. Saito, H. Okano, and N. Mizushima. 2006. Suppression of basal autophagy in neural cells causes neurodegenerative disease in mice. *Nature* 441:885-889.

100. Komatsu, M., S. Waguri, T. Chiba, S. Murata, J. Iwata, I. Tanida, T. Ueno, M. Koike, Y. Uchiyama, E. Kominami, and K. Tanaka. 2006. Loss of autophagy in the central nervous system causes neurodegeneration in mice. *Nature* 441:880-884.

101. Kaasik, A., V. Veksler, E. Boehm, M. Novotova, A. Minajeva, and R. Ventura-Clapier. 2001. Energetic crosstalk between organelles: architectural integration of energy production and utilization. *Circ Res* 89:153-159.

102. Campello, S., R.A. Lacalle, M. Bettella, S. Manes, L. Scorrano, and A. Viola. 2006. Orchestration of lymphocyte chemotaxis by mitochondrial dynamics. *J Exp Med* 203:2879-2886.

103. Pollard, T.D., and G.G. Borisy. 2003. Cellular motility driven by assembly and disassembly of actin filaments. *Cell* 112:453-465.

104. Etienne-Manneville, S. 2004. Actin and microtubules in cell motility: which one is in control? *Traffic* 5:470-477.

105. Tan, J.L., S. Ravid, and J.A. Spudich. 1992. Control of nonmuscle myosins by phosphorylation. *Annu Rev Biochem* 61:721-759.

106. Verstreken, P., C.V. Ly, K.J. Venken, T.W. Koh, Y. Zhou, and H.J. Bellen. 2005. Synaptic mitochondria are critical for mobilization of reserve pool vesicles at Drosophila neuromuscular junctions. *Neuron* 47:365-378.

107. Morris, R.L., and P.J. Hollenbeck. 1993. The regulation of bidirectional mitochondrial transport is coordinated with axonal outgrowth. *J Cell Sci* 104 (Pt 3):917-927.

108. Bindokas, V.P., C.C. Lee, W.F. Colmers, and R.J. Miller. 1998. Changes in mitochondrial function resulting from synaptic activity in the rat hippocampal slice. *J Neurosci* 18:4570-4587.

109. Fabricius, C., C.H. Berthold, and M. Rydmark. 1993. Axoplasmic organelles at nodes of Ranvier. II. Occurrence and distribution in large myelinated spinal cord axons of the adult cat. *J Neurocytol* 22:941-954.

110. Bristow, E.A., P.G. Griffiths, R.M. Andrews, M.A. Johnson, and D.M. Turnbull. 2002. The distribution of mitochondrial activity in relation to optic nerve structure. *Arch Ophthalmol* 120:791-796.

111. Sung, J.Y., O. Engmann, M.A. Teylan, A.C. Nairn, P. Greengard, and Y. Kim. 2008. WAVE1 controls neuronal activity-induced mitochondrial distribution in dendritic spines. *Proc Natl Acad Sci U S A* 105:3112-3116.

112. Li, Z., K. Okamoto, Y. Hayashi, and M. Sheng. 2004. The importance of dendritic mitochondria in the morphogenesis and plasticity of spines and synapses. *Cell* 119:873-887.

113. Wagner, O.I., J. Lifshitz, P.A. Janmey, M. Linden, T.K. McIntosh, and J.F. Leterrier. 2003. Mechanisms of mitochondria-neurofilament interactions. *J Neurosci* 23:9046-9058.

114. McCormack, J.G., A.P. Halestrap, and R.M. Denton. 1990. Role of calcium ions in regulation of mammalian intramitochondrial metabolism. *Physiol Rev* 70:391-425.

115. Yang, F., X.P. He, J. Russell, and B. Lu. 2003. Ca2+ influx-independent synaptic potentiation mediated by mitochondrial Na(+)-Ca2+ exchanger and protein kinase C. *J Cell Biol* 163:511-523.

116. Klopfenstein, D.R., and R.D. Vale. 2004. The lipid binding pleckstrin homology domain in UNC-104 kinesin is necessary for synaptic vesicle transport in Caenorhabditis elegans. *Mol Biol Cell* 15:3729-3739.

117. Fransson, S., A. Ruusala, and P. Aspenstrom. 2006. The atypical Rho GTPases Miro-1 and Miro-2 have essential roles in mitochondrial trafficking. *Biochem Biophys Res Commun* 344:500-510.

118. Stowers, R.S., L.J. Megeath, J. Gorska-Andrzejak, I.A. Meinertzhagen, and T.L. Schwarz. 2002. Axonal transport of mitochondria to synapses depends on milton, a novel Drosophila protein. *Neuron* 36:1063-1077.

119. Chada, S.R., and P.J. Hollenbeck. 2004. Nerve growth factor signaling regulates motility and docking of axonal mitochondria. *Curr Biol* 14:1272-1276.

120. Chada, S.R., and P.J. Hollenbeck. 2003. Mitochondrial movement and positioning in axons: the role of growth factor signaling. *J Exp Biol* 206:1985-1992.

121. Harada, T., T. Morooka, S. Ogawa, and E. Nishida. 2001. ERK induces p35, a neuron-specific activator of Cdk5, through induction of Egr1. *Nat Cell Biol* 3:453-459.

122. Meuer, K., I.E. Suppanz, P. Lingor, V. Planchamp, B. Goricke, L. Fichtner, G.H. Braus, G.P. Dietz, S. Jakobs, M. Bahr, and J.H. Weishaupt. 2007. Cyclin-dependent kinase 5 is an upstream regulator of mitochondrial fission during neuronal apoptosis. *Cell Death Differ* 14:651-661.

123. Morfini, G., G. Szebenyi, H. Brown, H.C. Pant, G. Pigino, S. DeBoer, U. Beffert, and S.T. Brady. 2004. A novel CDK5-dependent pathway for regulating GSK3 activity and kinesin-driven motility in neurons. *Embo J* 23:2235-2245.

124. Morfini, G., G. Szebenyi, R. Elluru, N. Ratner, and S.T. Brady. 2002. Glycogen synthase kinase 3 phosphorylates kinesin light chains and negatively regulates kinesin-based motility. *Embo J* 21:281-293.

125. Minin, A.A., A.V. Kulik, F.K. Gyoeva, Y. Li, G. Goshima, and V.I. Gelfand. 2006. Regulation of mitochondria distribution by RhoA and formins. *J Cell Sci* 119:659-670.

126. Saotome, M., D. Safiulina, G. Szabadkai, S. Das, A. Fransson, P. Aspenstrom, R. Rizzuto, and G. Hajnoczky. 2008. Bidirectional Ca2+-dependent control of mitochondrial dynamics by the Miro GTPase. *Proc Natl Acad Sci U S A* 105:20728-20733.

127. Wang, X., and T.L. Schwarz. 2009. The mechanism of Ca2+ -dependent regulation of kinesin-mediated mitochondrial motility. *Cell* 136:163-174.

128. Macaskill, A.F., J.E. Rinholm, A.E. Twelvetrees, I.L. Arancibia-Carcamo, J. Muir, A. Fransson, P. Aspenstrom, D. Attwell, and J.T. Kittler. 2009. Miro1 is a calcium sensor for glutamate receptor-dependent localization of mitochondria at synapses. *Neuron* 61:541-555.

129. Prakash, B., G.J. Praefcke, L. Renault, A. Wittinghofer, and C. Herrmann. 2000. Structure of human guanylate-binding protein 1 representing a unique class of GTP-binding proteins. *Nature* 403:567-571.

130. Schumacher, B., and P. Staeheli. 1998. Domains mediating intramolecular folding and oligomerization of MxA GTPase. *J Biol Chem* 273:28365-28370.

131. Chang, C.R., and C. Blackstone. 2007. Cyclic AMP-dependent protein kinase phosphorylation of Drp1 regulates its GTPase activity and mitochondrial morphology. *J Biol Chem* 282:21583-21587.

132. Cribbs, J.T., and S. Strack. 2007. Reversible phosphorylation of Drp1 by cyclic AMP-dependent protein kinase and calcineurin regulates mitochondrial fission and cell death. *EMBO Rep* 8:939-944.

133. Karbowski, M., A. Neutzner, and R.J. Youle. 2007. The mitochondrial E3 ubiquitin ligase MARCH5 is required for Drp1 dependent mitochondrial division. *J Cell Biol* 178:71-84.

134. Han, X.J., Y.F. Lu, S.A. Li, T. Kaitsuka, Y. Sato, K. Tomizawa, A.C. Nairn, K. Takei, H. Matsui, and M. Matsushita. 2008. CaM kinase I alpha-induced phosphorylation of Drp1 regulates mitochondrial morphology. *J Cell Biol* 182:573-585.

135. Cho, D.H., T. Nakamura, J. Fang, P. Cieplak, A. Godzik, Z. Gu, and S.A. Lipton. 2009. S-nitrosylation of Drp1 mediates beta-amyloid-related mitochondrial fission and neuronal injury. *Science* 324:102-105.

136. Geiss-Friedlander, R., and F. Melchior. 2007. Concepts in sumoylation: a decade on. *Nat Rev Mol Cell Biol* 8:947-956.

137. Meulmeester, E., and F. Melchior. 2008. Cell biology: SUMO. *Nature* 452:709-711.

138. Seeler, J.S., and A. Dejean. 2003. Nuclear and unclear functions of SUMO. *Nat Rev Mol Cell Biol* 4:690-699.

139. Johnson, E.S., and A.A. Gupta. 2001. An E3-like factor that promotes SUMO conjugation to the yeast septins. *Cell* 106:735-744.

140. Kagey, M.H., T.A. Melhuish, and D. Wotton. 2003. The polycomb protein Pc2 is a SUMO E3. *Cell* 113:127-137.

141. Pichler, A., A. Gast, J.S. Seeler, A. Dejean, and F. Melchior. 2002. The nucleoporin RanBP2 has SUMO1 E3 ligase activity. *Cell* 108:109-120.

142. Ivanov, A.V., H. Peng, V. Yurchenko, K.L. Yap, D.G. Negorev, D.C. Schultz, E. Psulkowski, W.J. Fredericks, D.E. White, G.G. Maul, M.J. Sadofsky, M.M. Zhou, and F.J. Rauscher, 3rd. 2007. PHD domain-mediated E3 ligase activity directs intramolecular sumoylation of an adjacent bromodomain required for gene silencing. *Mol Cell* 28:823-837.

143. Johnson, E.S., and G. Blobel. 1999. Cell cycle-regulated attachment of the ubiquitin-related protein SUMO to the yeast septins. *J Cell Biol* 147:981-994.

144. Martin, S., A. Nishimune, J.R. Mellor, and J.M. Henley. 2007. SUMOylation regulates kainate-receptor-mediated synaptic transmission. *Nature* 447:321-325.

145. Benson, M.D., Q.J. Li, K. Kieckhafer, D. Dudek, M.R. Whorton, R.K. Sunahara, J.A. Iniguez-Lluhi, and J.R. Martens. 2007. SUMO modification regulates inactivation of the voltage-gated potassium channel Kv1.5. *Proc Natl Acad Sci U S A* 104:1805-1810.

146. Dadke, S., S. Cotteret, S.C. Yip, Z.M. Jaffer, F. Haj, A. Ivanov, F. Rauscher, 3rd, K. Shuai, T. Ng, B.G. Neel, and J. Chernoff. 2007. Regulation of protein tyrosine phosphatase 1B by sumoylation. *Nat Cell Biol* 9:80-85.

147. Kang, J.S., E.F. Saunier, R.J. Akhurst, and R. Derynck. 2008. The type I TGF-beta receptor is covalently modified and regulated by sumoylation. *Nat Cell Biol* 10:654-664.

148. Takahashi, Y., M. Iwase, A.V. Strunnikov, and Y. Kikuchi. 2008. Cytoplasmic sumoylation by PIAS-type Siz1-SUMO ligase. *Cell Cycle* 7:1738-1744.

149. Wasiak, S., R. Zunino, and H.M. McBride. 2007. Bax/Bak promote sumoylation of DRP1 and its stable association with mitochondria during apoptotic cell death. *J Cell Biol* 177:439-450.

150. Neuspiel, M., A.C. Schauss, E. Braschi, R. Zunino, P. Rippstein, R.A. Rachubinski, M.A. Andrade-Navarro, and H.M. McBride. 2008. Cargo-selected transport from the mitochondria to peroxisomes is mediated by vesicular carriers. *Curr Biol* 18:102-108.

151. Andrade-Navarro, M.A., L. Sanchez-Pulido, and H.M. McBride. 2009. Mitochondrial vesicles: an ancient process providing new links to peroxisomes. *Curr Opin Cell Biol* 21:560-567.

152. Camoes, F., N.A. Bonekamp, H.K. Delille, and M. Schrader. 2009. Organelle dynamics and dysfunction: A closer link between peroxisomes and mitochondria. *J Inherit Metab Dis* 32:163-180.

153. Poirier, Y., V.D. Antonenkov, T. Glumoff, and J.K. Hiltunen. 2006. Peroxisomal beta-oxidation--a metabolic pathway with multiple functions. *Biochim Biophys Acta* 1763:1413-1426.

154. Bach, D., D. Naon, S. Pich, F.X. Soriano, N. Vega, J. Rieusset, M. Laville, C. Guillet, Y. Boirie, H. Wallberg-Henriksson, M. Manco, M. Calvani, M. Castagneto, M. Palacin, G. Mingrone, J.R. Zierath, H. Vidal, and A. Zorzano. 2005. Expression of Mfn2, the Charcot-Marie-Tooth neuropathy type 2A gene, in human skeletal muscle: effects of type 2 diabetes, obesity, weight loss, and the regulatory role of tumor necrosis factor alpha and interleukin-6. *Diabetes* 54:2685-2693.

155. Bonifacino, J.S., and J.H. Hurley. 2008. Retromer. *Curr Opin Cell Biol* 20:427-436.

Chapter II MAPL is a new mitochondrial SUMO E3 ligase that regulates mitochondrial fission

II.1 Significance and author contributions

The research presented in the following chapter characterizes the first mitochondrial SUMO E3 ligase, MAPL. We also demonstrate that MAPL SUMOylates the fission GTPase Drp1, in addition to other mitochondrial proteins. The identification of MAPL reinforces the importance of mitochondrial SUMOylation and will provide invaluable tools to dissect this process. This work resulted in a first author manuscript published in EMBO report: Braschi E., Zunino R., McBride H.M (2009) MAPL is a new mitochondrial SUMO E3 ligase that regulates mitochondrial fission. *EMBO Rep.* 10(7):748-54.

I performed most of the experimental work. A technician in the laboratory of Dr. McBride, R. Zunino, is responsible for the *in-vivo* evidence that Drp1 is SUMOylated by MAPL, a result presented in *Figure 2.4B*. V. Soubannier and P. Rippstein (University of Ottawa Heart Institute, Canada) are responsible for the isolation and preparation of the bovine mitochondrial samples for electron microscopy. Finally, I wrote the majority of this manuscript in conjunction with my supervisor, and would like to thank B. Raught (Ontario Cancer Institute, Toronto, Canada) and R. Screaton (Apoptosis Research Centre, Ottawa, Canada) for their critical comments on the manuscript.

II.2 Introduction

Post-translational modifications, including the conjugation of the SUMO to it substrates, allows the rapid response to dynamic changes in cellular signals. The SUMOylation of protein targets leads to diverse consequences, including the formation or disassembly of protein complexes, the regulation of protein localization, and the modulation of other post-translational modifications such as phosphorylation and ubiquitination (1, 2). SUMOylation is a multi-step process involving an E1 heterodimer, an E2 ligase and a SUMO E3 ligase which is thought to provide specificity and enhance the reaction rate of the final step (1). All SUMO E3 ligases characterized to date are localized primarily within the nucleus. These include the PIAS family (3, 4), polycomb2 (5), and RanBP2 (6). Initially, SUMO E3 ligases were identified by the presence of a conserved RING finger domain, however, at least two family members do not require this domain for their SUMOylation activity (6, 7). As a result, SUMO E3 ligases are defined by their ability to 1) bind Ubc9, 2) bind SUMO1, and 3) enhance the transfer of SUMO from Ubc9 onto a substrate. As with the SUMO proteases, each of the SUMO E3 ligases has been shown to function on multiple substrates, so the pairing of the substrate to the E3 ligase is restricted by their subcellular localizations.

Although most SUMO substrates have been studied in the nucleus, there are a number of essential targets localized in the cytosol and associated to other intracellular organelles (2, 8-12). We have previously identified SUMOylation as a post-translational modification for a number of mitochondrial proteins (13-15). In particular, we have shown that the SUMOylation of the fission GTPase Drp1 regulates mitochondrial dynamics both in steady state and during cell death (13, 14). Specifically the increase in Drp1 SUMOylation

leads to an increase in Drp1 protein levels, and in addition, SUMOylated Drp1 is more stably associated with the membrane (14). Importantly, the abundance of mitochondrial SUMOylated substrates suggests that SUMOylation plays a more global role in mitochondrial processes. We were therefore interested in identifying a SUMO E3 ligase involved in the regulation of mitochondrial SUMOylation. Here, we show that MAPL (16), functions as a SUMO E3 ligase involved in the conjugation of specific mitochondrial targets, including Drp1.

II.3 Results

MAPL was first identified as a novel mitochondrial outer membrane protein whose expression led to an increase in mitochondrial fragmentation in a RING-finger dependent manner (16). Since the SUMOylation of Drp1 is known to enhance fission, we tested whether the RING-domain of MAPL exhibits SUMO E3 ligase activity upon mitochondrial substrates. We first examined whether MAPL possessed SUMO1 E3 ligase activity *in-vitro*. Incubation of a biotinylated peptide containing the SUMO1 consensus sequence ΨKxE with 500 nM of the recombinant RING finger domain of MAPL ($MAPL_{(257-352)}$), the E1 heterodimer and Ubc9, led to the conjugation of His_6:SUMO1 *(Figure 2.1)*. This conjugation was significantly increased over the minimal reaction observed with only the E1 heterodimer and Ubc9. In addition, the reaction was ATP-, temperature- and dose-dependent *(Figure 2.1 A, B)*.

The RING-finger domain of MAPL was previously reported to function as an E3 ubiquitin ligase *in-vitro* (17). We also observed auto-ubiquitination activity with

GST:MAPL$_{(257-352)}$, however, the reaction required the presence of 30 μM RING domain, and increased levels of both the E1 and Ubc4 *(Figure 2.1 C)*.

Figure II-1 MAPL has SUMO E3 ligase activity in vitro

A) Biotinylated peptides containing either the SUMO1 consensus sequence (lanes 1-3, 5) or a scrambled sequence (lane 4) were incubated in the indicated conditions. Following the reaction, the biotinylated peptide was isolated and isolates probed for the association of conjugated His-SUMO1. The addition of 500nM $MAPL_{(257-352)}$ (lane 1) significantly enhances the conjugation of SUMO1 by Ubc9 (compare with lane 5) in a temperature (lane 2) and ATP dependent manner (lane 3). B) The same reaction conditions were used as in lane 1 A) but with increasing amounts of $MAPL_{(257-352)}$, as indicated. C) GST-$MAPL_{(257-352)}$was used in an in vitro auto-ubiquitination assay. In the presence of 30 uM GST-$MAPL_{(257-352)}$, 0.5 uM of ubiquitin E1, 5 uM of Ubc4 and 10 uM ubiquitin, the RING domain of MAPL facilitates the conjugation of ubiquitin (lane 1) in an ATP (lane 2) and RING (lane 3) dependent manner. In the presence of 500 nM GST-$MAPL_{(257-352)}$, 50 nM of ubiquitin E1, 250 nM of Ubc4 and 10 uM ubiquitin, the RING domain of MAPL does not facilitate the conjugation of ubiquitin (lane 4). D) Following the transfection of HeLa cells with MAPL:Flag and Ubc9:YFP, cell lysates were immunoprecipitated with either anti-Flag coupled resin or mouse IgG, as indicated.

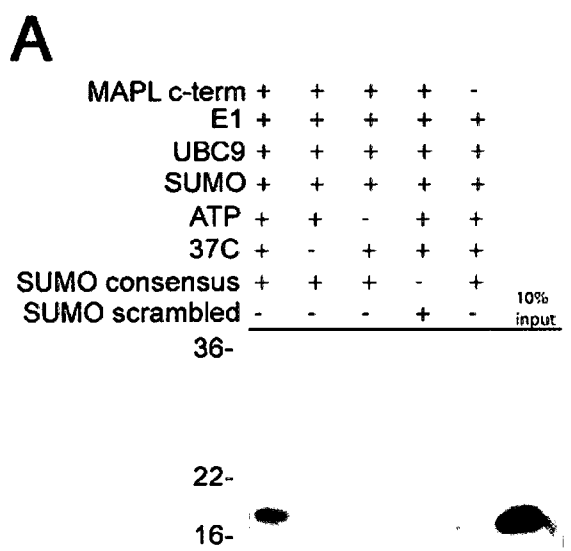
A
MAPL c-term + + + + -
E1 + + + + +
UBC9 + + + + +
SUMO + + + + +
ATP + + - + +
37C + - + + +
SUMO consensus + + + - +
SUMO scrambled - - - + -
10% input
36-
22-
16-

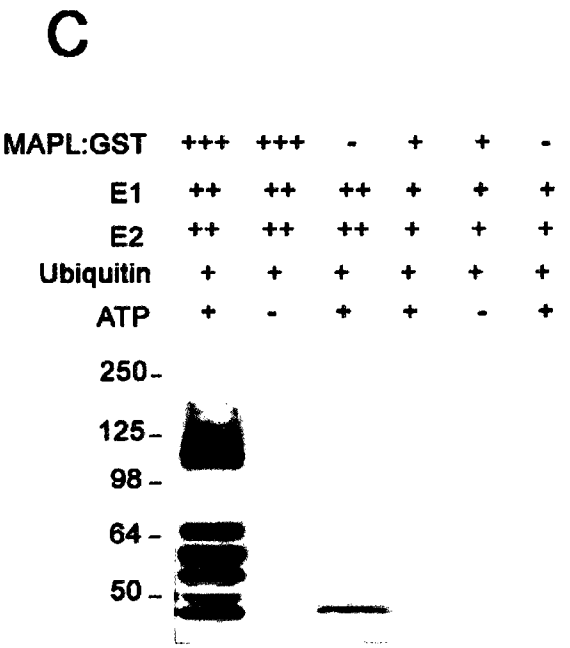
C
MAPL:GST +++ +++ - + + -
E1 ++ ++ ++ + + +
E2 ++ ++ ++ + + +
Ubiquitin + + + + + +
ATP + - + + - +
250-
125-
98-
64-
50-

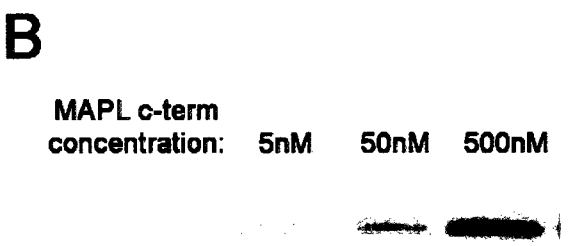
B
MAPL c-term concentration: 5nM 50nM 500nM

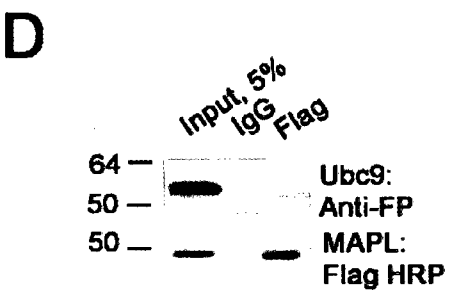
D
Input, 5%
IgG
Flag
64 —
50 —
50 —
Ubc9: Anti-FP
MAPL: Flag HRP

In lower concentrations of E1 and E2, 100 nM of $MAPL_{(257-352)}$ is sufficient to sustain a robust SUMOylation reaction, but even 500 nM of $GST:MAPL_{(257-352)}$ is not enough to support the ubiquitination reaction *(Figure 2.1 C, right 3 lanes)*. Therefore, although it is possible for MAPL to facilitate ubiquitin conjugation in vitro, under physiological concentrations MAPL preferentially acts as a SUMO E3 ligase. In addition to the conjugation assays described so far, all known SUMO E3 ligases interact directly with the E2 enzyme Ubc9 (18). To confirm whether MAPL could also bind Ubc9, HeLa cells were transfected with both Ubc9:YFP and MAPL:Flag, solubilized and immunoprecipitates were examined by western blot *(Figure 2.1 D)*. The data show that a fraction of Ubc9:YFP is precipitated with MAPL:Flag, consistent with the evidence that they function within the same enzymatic cascade.

Since MAPL is a mitochondrial anchored protein, we tested whether the RING domain of MAPL could mediate the SUMOylation of mitochondrial targets on intact organelles. As revealed by electron microscopy and western blot analysis, highly purified mitochondria were isolated from bovine heart *(Figure 2.2 A,B)* and used as substrate for in vitro SUMOylation reactions. The addition of excess E1 heterodimer and Ubc9 enzymes along with His_6:SUMO1 to mitochondria isolated from bovine heart resulted in the efficient conjugation of a number of mitochondrial targets in an ATP-dependent manner *(Figure 2.2 C, compare lanes 1 and 2)*. This result is consistent with our previous report that there are multiple mitochondrial SUMO1 conjugates (13), and highlights the presence of an active, endogenous SUMO E3 ligase on the mitochondria. The basal reaction was enhanced by 1.5 fold upon addition of 500 nM $MAPL_{(257-352)}$ (student's t-test, $n=10$, $p<0.05$) *(Figure 2.2 C, compare lanes 1 and 3, quantified in Figure 2.2 F)*.

Figure II-2 MAPL SUMOylates native mitochondrial substrates.

The purity of isolated bovine heart mitochondria was visualized by A) electron microscopy (scale bar represents 10 microns) and B) western blot analysis. C) Isolated mitochondria from bovine heart were incubated with 50 nM SUMO E1, 250 nM Ubc9 and 10 uM his-SUMO1 under the conditions indicated. The addition of 500 nM $MAPL_{(257-352)}$ increased the efficiency of SUMO1 conjugation (lane 1) in an ATP dependent manner (lane 2). D) Isolated mitochondria from bovine heart were incubated in the presence of 50 nM Ubiquitin E1, 250 nM Ubc4, 10 uM Ubiquitin under the conditions indicated. Addition of 500 nM MAPL(257-352) is indicated. E) Isolated mitochondria from bovine heart were incubated in the presence of 0.5uM Ubiquitin E1, 5 uM Ubc4, 10 uM Ubiquitin under the conditions indicated. Addition of 30 uM $MAPL(257_{-352})$ is indicated. F) Quantification of the increase in the SUMOylation/Ubiquitination reactions due to the addition of exogenous MAPL (lanes 1 versus 3 in C, D and E). Standard errors are represented.

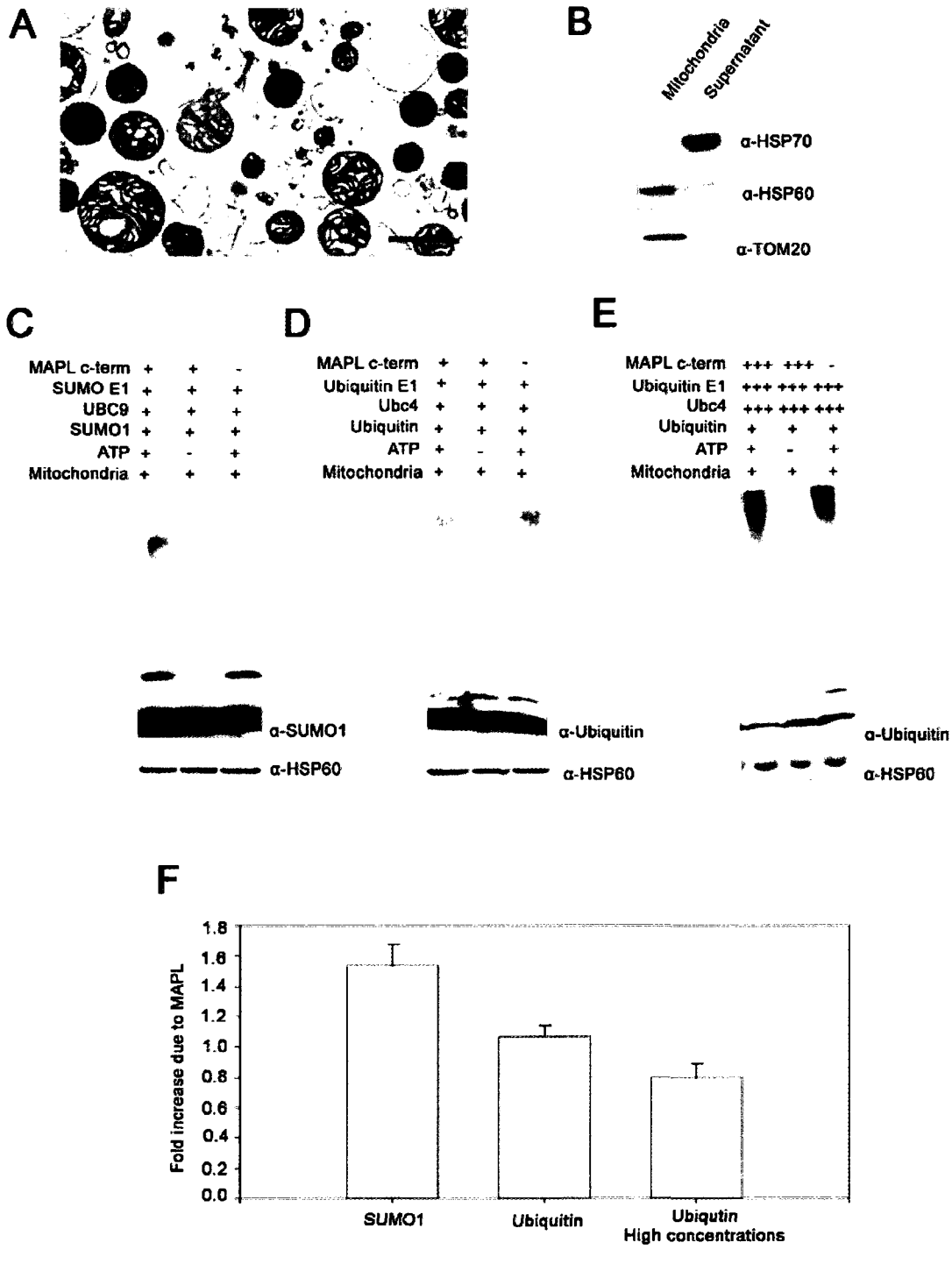
A
B
Mitochondria
Supernatant
α-HSP70
α-HSP60
α-TOM20
C
MAPL c-term + + -
SUMO E1 + + +
UBC9 + + +
SUMO1 + + +
ATP + - +
Mitochondria + + +
α-SUMO1
α-HSP60
D
MAPL c-term + + -
Ubiquitin E1 + + +
Ubc4 + + +
Ubiquitin + + +
ATP + - +
Mitochondria + + +
α-Ubiquitin
α-HSP60
E
MAPL c-term +++ +++ -
Ubiquitin E1 +++ +++ +++
Ubc4 +++ +++ +++
Ubiquitin + + +
ATP + - +
Mitochondria + + +
α-Ubiquitin
α-HSP60
F
Fold increase due to MAPL
1.8
1.6
1.4
1.2
1.0
0.8
0.6
0.4
0.2
0.0
SUMO1
Ubiquitin
Ubiqutin
High concentrations

Isolated mitochondria were also able to support the ubiquitination of substrates in an ATP-dependent manner *(Figure 2.2 D)*. This is most likely driven, at least in part, by a previously identified mitochondrial ubiquitin E3 ligase, MARCHV (19-21). However, the addition of 500nM $MAPL_{(257-352)}$ to the ubiquitination reaction on isolated mitochondria did not result in an increase in the basal ubiquitination reaction observed during the 90 minute incubation (student's t -test, n=6, $p>0.05$) *(Figure 2.2 D, compare lanes 1 and 3)*. Importantly, increasing the concentrations of E1, E2 and $MAPL_{(257-352)}$ to the levels which permitted the self-ubiquitination reaction in *Figure 2.1C* did not result in an increase in the basal ubiquitination reaction *(Figure 2.2 E,F)* (student's t-test, n=5, $p>0.05$). This indicates that MAPL preferentially functions as a SUMO1 E3 ligase activity not only on synthetic peptides, but also on native mitochondrial targets.

We then turned our attention to the activity of MAPL in intact cells by downregulating the expression of MAPL. Stable cell lines transfected with shRNA directed against MAPL enabled us to reduce the levels of MAPL by 58% compared to a scrambled control *(Figure 2.3 A, B)*. This decrease in MAPL levels led to a concomitant 46% (student's t-test, n=3, $p<0.05$) decrease in the levels of endogenous SUMO1 conjugates *(Figure 2.3 A)*, but the levels of ubiquitinated proteins remained unchanged *(Figure 2.3 B)*. To control that this effect was not due to off-target silencing, we used a pooled siRNA mixture to silence MAPL in HeLa cells *(Figure 2.3 C)*. The data show that a 58% silencing of MAPL led to a 24% reduction in SUMO conjugates (student's t-test, n=3, $p<0.05$). This further supports the evidence that MAPL predominantly functions as a SUMO E3 ligase under physiological conditions.

Figure II-3 Silencing of MAPL reduces total SUMO1 conjugates.

A) HeLa cells transfected with either shRNA vector alone (shvector) or with MAPL-specific shRNA (shMAPL), were selected in the presence of 5 ug/ml puromycin. Total lysates were probed for SUMO1. The graph represents the average from three independent experiments. B) As in A), but the extracts were probed with anti-ubiquitin antibodies. The graph represents the average from three independent experiments. C) HeLa cells were transfected with either a pooled siRNA mixture directed against MAPL or a control siRNA. Total lysates were probed for SUMO1. The data are plotted from the average of three independent experiments. D) Isolation of the nuclear, cytosolic and mitochondrial fractions of HeLa cells stably transfected with a shRNA directed against MAPL or a control shRNA. A 40% reduction in the expression of MAPL leads to a 30% reduction in total SUMO1 conjugates, 38% reduction in nuclear SUMO1 conjugates, 20% reduction in cytosolic SUMO1 conjugates and a 53% reduction in mitochondrial SUMO1 conjugates.

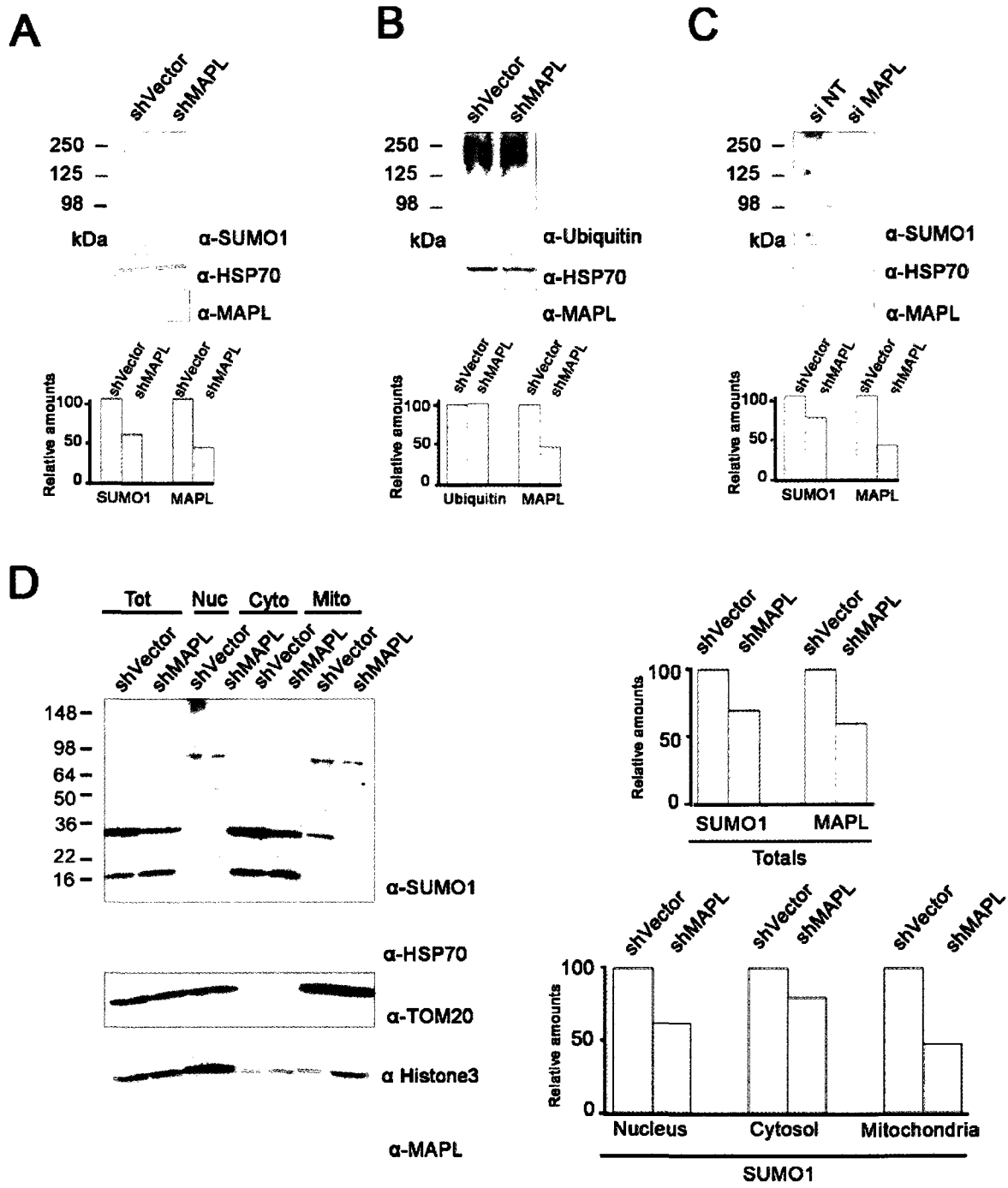
A
shVector
shMAPL
250 –
125 –
98 –
kDa
α-SUMO1
α-HSP70
α-MAPL
Relative amounts
100
50
0
SUMO1
MAPL
B
shVector
shMAPL
250 –
125 –
98 –
kDa
α-Ubiquitin
α-HSP70
α-MAPL
Relative amounts
100
50
0
Ubiquitin
MAPL
C
si NT
si MAPL
250 –
125 –
98 –
kDa
α-SUMO1
α-HSP70
α-MAPL
Relative amounts
100
50
0
SUMO1
MAPL
D
Tot
Nuc
Cyto
Mito
shVector
shMAPL
148 –
98 –
64 –
50 –
36 –
22 –
16 –
α-SUMO1
α-HSP70
α-TOM20
α Histone3
α-MAPL
Relative amounts
100
50
0
SUMO1
MAPL
Totals
Nucleus
Cytosol
Mitochondria
SUMO1

Finally, to determine whether the silencing of MAPL primarily affected mitochondrial SUMO1 substrates, we isolated the nuclear, cytosolic and mitochondrial fractions of HeLa cells stably transfected with shRNA directed against MAPL or a control shRNA *(Figure 2.3 D)*. The data show that although the reduction of MAPL expression leads to a decrease in SUMO1 conjugates in all three fractions, the greatest loss of SUMO1 conjugates occurs on the mitochondria. Since the SUMOylation of Drp1 has been shown to stabilize the protein and stimulate mitochondrial fission (13-15), we next tested whether silencing of MAPL leads to the destabilization of Drp1. The downregulation of MAPL by 46%, led to a 17% decrease in the Drp1 levels *(Figure 2.4 A)*. This decrease in the Drp1 protein levels, although statistically significant ($p<0.05$), did not lead to significant changes in mitochondrial morphology (16).

To test whether this loss of Drp1 is associated with a direct reduction in its SUMO1 conjugation, cells expressing His_6:SUMO1 and Drp1:YFP were solubilized and all SUMO1 conjugates were isolated using Nickel-Nitrilotriacetic Acid (Ni-NTA) agarose beads (*Figure 2.4 B)*. Examination of the total extracts show that the transfection levels of His_6:SUMO1 were similar since a number of conjugate bands are of equal intensity *(Figure 2.4 B asterisk)*. However, the high molecular weight conjugation pattern for SUMOylation is reduced upon the silencing of MAPL. Isolation of these conjugates further confirms the reduction in SUMOylation. The ratio of Drp1 in the total extracts to that found in the His_6:SUMO1 isolates is reduced from 1 to 0.3 *(Figure 2.4 B)*. The molecular weight of Drp1:YFP is shifted in the His_6:SUMO1 column, consistent with an Sodium Dodecyl Sulfate (SDS)-resistant His_6:SUMO1 conjugate *(Figure 2.4 B arrow)*.

Figure II-4 MAPL SUMOylates DRP1 and modulates mitochondrial dynamics.

A) HeLa cells were stably transfected with either shRNA vector alone (shvector) or MAPL-specific shRNA (shMAPL) .Total lysates were analyzed by blots with the indicated antibodies. The graph represents the quantification from four independent experiments. Standard errors are represented. B) Vector or shMAPL expressing HeLa cells were transfected with DRP1-YFP and His6-SUMO1, harvested and SUMO1 conjugates were isolated using NTA-agarose. Western blots of SUMO1, Drp1-FP and controls are indicated. SUMO conjugates in the totals were separated using a 4-20% SDS-PAGE gradient (left), and the SUMO:His6 isolates were separated on a 6% SDS-PAGE gel (right). The ratio of SUMOylated DRP1 is reduced from 1 to 0.3 in the MAPL silenced cells compared to the control cells. C) Endogenous DRP1 was immunoprecipitated from HeLa cells and used as the substrate in an in vitro SUMO assay. In the presence 50 nM SUMO E1, 250 nM Ubc9 and 10 uM his-SUMO1, the addition of 500nM of $MAPL_{(257-352)}$ led to the formation of a higher molecular weight band. Quantification reveals that the presence of ATP and MAPL (lane 1), led to an increase in the signal (asterisk) relative to the background (lane 3) by 37% in the SUMO1 blot, and 47% in the DRP1 blot. In the absence of ATP (lane 2) there is no detectible increase in the SUMO1 signal, with the DRP1 antibody detecting a 19% increase. D) HeLa cells transfected with the indicated constructs were seeded together, and 50% PEG 5000 was added for 60 s after a 1-h preincubation with cycloheximide. Images of both fluorophores were taken from fixed cells after 4 h and 6 h. E) Quantification of the percentage of heterokaryons with complete fusion of mitochondria. The graph represents the average and standard error of 3 independent experiments.

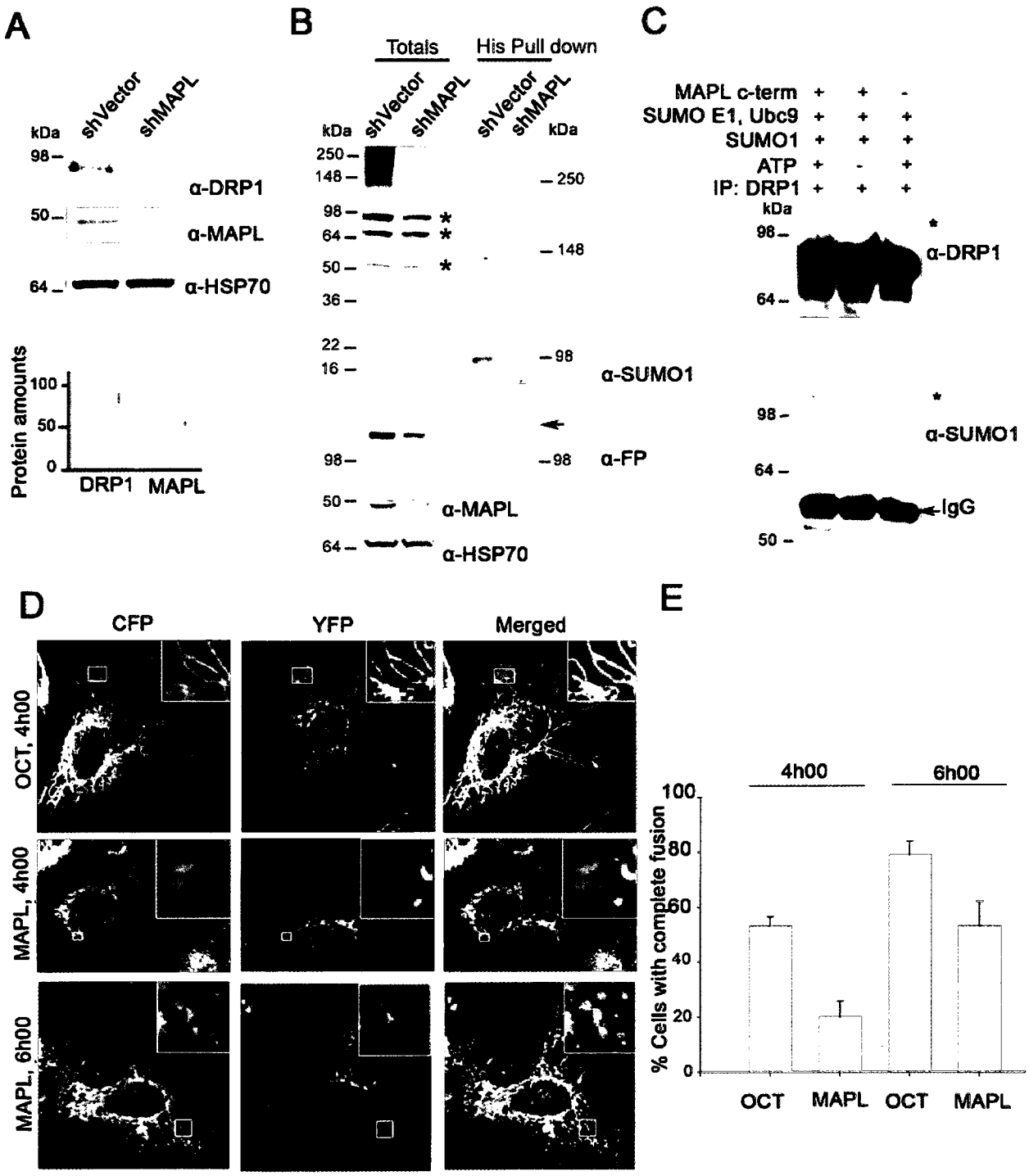
A
shVector
shMAPL
kDa
98
50
64
α-DRP1
α-MAPL
α-HSP70
Protein amounts
100
50
0
DRP1
MAPL
B
Totals
His Pull down
shVector
shMAPL
shVector
shMAPL
kDa
kDa
250
148
98
64
50
36
22
16
98
50
64
250
148
98
98
α-SUMO1
α-FP
α-MAPL
α-HSP70
C
MAPL c-term + + -
SUMO E1, Ubc9 + + +
SUMO1 + + +
ATP + - +
IP: DRP1 + + +
kDa
98
64
α-DRP1
98
α-SUMO1
64
IgG
50
D
CFP
YFP
Merged
OCT, 4h00
MAPL, 4h00
MAPL, 6h00
E
4h00
6h00
100
80
60
40
20
0
% Cells with complete fusion
OCT
MAPL
OCT
MAPL

To show that recombinant MAPL can SUMOylate Drp1 directly, we isolated endogenous Drp1 from HeLa cell extracts by immunoprecipitation and used this as a substrate in the in vitro SUMOylation assay *(Figure 2.4 C)*. In a reaction containing the E1 and E2 SUMO conjugating enzymes and His_6:SUMO1, $MAPL_{(257-352)}$ was able to enhance the conjugation of SUMO1 to the immunoprecipitated Drp1 in an ATP-dependent manner *(Figure 2.4 C, compare lanes 1 and 2)*. In addition to the *in-vitro* reaction, immunoprecipitation of endogenous MAPL also revealed a fraction of Drp1 present in the precipitates *(Figure 2.5)*, consistent with the evidence that MAPL SUMOylates Drp1. Taken together, our data show that the overexpression of MAPL stimulates fission (16), that the silencing of MAPL leads to a reduction in Drp1 levels and SUMO conjugates and that MAPL SUMOylates Drp1 in vitro.

Finally, the fragmented phenotype observed upon the overexpression of MAPL can be explained by the stabilization and activation of Drp1 fission activity. However, it is also clear that there are a number of unidentified SUMO1 targets on the mitochondria. We therefore decided to test whether the rates of fusion may also be affected by the increased mitochondrial SUMOylation. To directly assess the fusion capacity of mitochondria in cells overexpressing MAPL, we employed a Polyethylene glycol (PEG) fusion assay (22). Mitochondria from heterokaryons transfected with matrix marker proteins alone were 53.3% fused within 4 hours *(Figure 2.4 D,E)*. In contrast, cells expressing CFP:MAPL and MAPL:YFP showed significantly less mitochondrial fusion at 4 hours, with only 20% of cells having completely mixed mitochondrial contents (student's t-test, $n=3$, $p<0.05$). However, by 6 hours after cell fusion, there was no longer a significant difference between the control and MAPL overexpressing cells (79% for cells overexpressing the markers, and

53.3% for MAPL overexpressing cells (student's t-test, n=3, $p>0.05$) *(Figure 2.4 D,E)*. This indicates that in addition to promoting fission, MAPL leads to a reduction in fusion rates.

Figure II-5 MAPL forms a complex with Drp1

Endogenous MAPL immunoprecipitated from HeLa cell lysates using anti-MAPL serum, was able to precipitate endogenous DRP1.

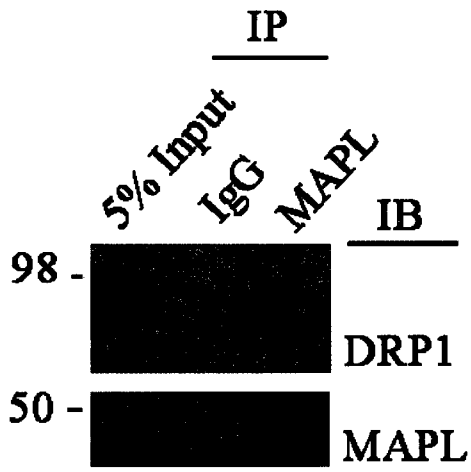
IP
5% Input
IgG
MAPL
IB
98 -
DRP1
50 -
MAPL

II.4 Material and methods

Antibodies, cDNA and general reagents

Anti-SUMO1 monoclonal antibodies were obtained from Zymed laboratories (Invitrogen, Burlington, ON, Canada); anti-SUMO1 polyclonal, and anti-ubiquitin were purchased from Biomol International (Cedarlane, Burlington, ON, Canada). Anti-HSP70 was obtained from Stressgen (Cedarlane, Burlington, ON, Canada), the anti-HSP60 from Sigma-Aldrich (Oakville, ON, Canada), and anti-Histone H3 from Upstate Biotechnologies (Etobicoke, ON, Canada). Anti-DRP1 and anti-TOM20 were from BD bioscience (Mississauga, ON, Canada), anti-Flag:HRP was purchased from Sigma-Aldrich (Oakville, ON, Canada) and anti-FP was from Clonetech (Burlington, ON, Canada). The anti-MAPL antibody was described previously (16). cDNA encoding $MAPL_{(257-352)}$:GST, MAPL:YFP, CFP:MAPL, OCT:YFP and OCT:CFP have been previously described (16). pEYFP (Clontech), and PCMV-Tag4A (Stratagene, La Jolla, CA, USA) were used to subclone Ubc9 and MAPL, using standard techniques.

General chemicals were obtained from Sigma-Aldrich (Oakville, ON, Canada) unless otherwise stated. The protease inhibitor cocktail was purchased from Roche, (Mississauga, ON, Canada). Recombinant SUMO, the biotinylated consensus peptide and control, the SUMO E1 heterodimer and Ubc9, were obtained from Boston Biochemicals (Cambridge, MA, USA). The recombinant ubiquitin E1 and ubiquitin were obtained from Biomol International (Cedarlane, Burlington, ON, Canada) and Ubc4 from Upstate Biotechnologies (Etobicoke, ON, Canada).

Cell culture and stable cell lines

HeLa cells were maintained in Dulbecco's Modified Eagle Medium (GIBCO Invitrogen, Burlington, ON, Canada) supplemented with 10% fetal bovine serum, penicillin, streptomycin and 2 mM L-glutamine. Transfections were performed overnight with HeLa cells at 70% confluency, using Lipofectamine 2000 (Invitrogen, Burlington, ON, Canada). shRNA was performed using the prepared sh-activated mRNA silencing system (Open Biosystems, Huntsville, AL, USA). To silence MAPL shRNA were transfected into HeLa cells using Arrest-In (Open Biosystems, Huntsville, AL, USA), and selected with 5 μg/ml puromycin.

PEG fusion assay

The PEG assay was performed as previously described (22). Briefly, HeLa cells were seeded on coverslips or in 10cm dishes and transfected for 6h00 with each of 4 markers; OCT:CFP, OCT:YFP, CFP:MAPL and MAPL:YFP. The cells transfected in 10cm dishes were then trypsinized and 50,000 cells were seeded on top of the transfected coverslips expressing the corresponding marker constructs. After 16 hours, cells were incubated for 1h00 with 20ug/mL cycloheximide to arrest the translation of each marker pair. Following this, 50% PEG solution (Sigma-Aldrich) was added for 60 seconds, washed off thoroughly and then replaced by with fresh media containing 20ug/mL cycloheximide. Following 4h00 to 6h00 incubation, the cells were fixed using 4% paraformaldehyde and analyzed with an Olympus FV1000 microscope fitted with a 100X objective lens. Images were acquired using sequential laser acquisition using a solid state diode 440nm and a 515nm argon laser lines. 10 heterokaryons were analyzed for each condition in three independent experiments.

Immunoprecipitations

HeLa cells were transfected with 15ug MAPL:Flag and Ubc9:YFP overnight. Following the transfection, cells were collected and solubilized in 50mM Tris pH 7.5, 100mM NaCl, 5mM $MgCl_2$, 1% Triton, 20mM *N*-methylmaleimide and protease inhibitor cocktail for 60 minutes. Insoluble material was removed by centrifugation at 9,300 x g for 20 minutes. The supernatant was assayed for protein concentration, and 1 mg per IP point was incubated overnight at 4 degrees with either 20 uL 1:1 Flag resin (Sigma-Aldrich) or 2.5 μg G-protein agarose-coupled mouse IgG (Sigma-Aldrich). After washing three times, the beads were mixed with loading sample buffer, separated on 4-20% acrylamide gels, and blotted with the indicated antibodies. Alternatively, for the endogenous MAPL immunoprecipitations, 20uL of anti-MAPL serum or 2.5ug rabbit IgG (Sigma-Aldrich) were incubated with Protein A agarose. NTA-Agarose pull down experiments to isolate His_6-SUMO conjugates have been previously described (13).

siRNA

The siGENOME SMARTpool reagent directed against MAPL (siMAPL) and the siCONTROL non-targeting (siNT) were obtained from Dharmacon (Lafayette, CO). Transfection of cells was performed using Dharmacon siGENOME SMARTpool transfection reagent according to manufacturer's protocol. Briefly, HeLa cells were seeded in 6 well dishes at ~50% confluency and were transfected with siRNA using Dharmafect 3. The cells were transfected 3 different times every 72h.

Recombinant protein expression

GST or GST-$MAPL_{(257-352)}$ expression was induced in E. coli BL21 strain with 0.3mM IPTG for 3 hours. Bacteria were recovered by centrifugation, resuspended in 20mM Hepes pH 7.4, 200 mM NaCl, 2 mM $MgCl_2$, 5 mM β-mercaptoethanol, protease inhibitor cocktail, and lysed at 2000 psi using a French press. The lysate was centrifuged at 100,000 x g for 40 minutes in a Ti55.2 rotor (Beckman Coulter, Mississauga, ON, Canada). The supernatant was then incubated with glutathione-Sepharose beads for 2h00 at 4 degrees (Amersham Biosciences, Piscataway, NJ, USA). Following the washing with the above buffer supplemented with 500mM NaCl then 1% Triton X-100, the amount of purified protein per bead volume was calculated. The fusion proteins were then either eluted with 15 mM glutathione in 50 mM Tris pH 8.0, 200 mM NaCl, or the RING domain of $MAPL_{257-352}$ was cleaved from GST using thrombin, overnight at 4 degrees, following manufacturers instructions (Sigma-Aldrich).

SUMOylation and ubiquitination assay

The SUMO conjugation assay was performed in 20 uL using 50 nM SUMO E1, 250 nM Ubc9, 10 uM His6-SUMO1, 20 uM of a consensus peptide in Buffer A (50 mM Tris pH 8.0, 100 mM NaCl, 5 mM $MgCl_2$, 1m M DTT), and either an ATP regenerating system (2.5 U creatine kinase, 125 nM creatine phosphate, 5 mM ATP) or 0.1U apyrase. Reactions were incubated for 90 minutes at 30 degrees. Streptavidin-coupled magnetic beads (Dynal, Invitrogen) were washed in buffer A supplemented with 2 mg/ml BSA and 1 % Triton X-100 using a magnetic particle concentrator (Dynal, Invitrogen), then incubated with the conjugation reaction for 60 minutes at 25 degrees, and finally washed in buffer A supplemented with 500 mM NaCl and 1 % Triton X-100. The beads were then incubated

with loading buffer and run by SDS electrophoresis using 4-20% acrylamide gels. Alternatively, bovine heart mitochondria were centrifuged at 800 x g for 15 minutes and resuspended in Tris mitochondria Buffer (50mM Tris, pH 7.4, 220 mM mannitol, 68 mM Sucrose, 80 mM KCl, 0.5 mM EGTA, 2 mM $Mg(Ac)_2$). 100 ug of these mitochondria were then used as substrate. 50 nM SUMO E1, 250 nM UBC9, 10 uM His_6-SUMO1 and the ATP regeneration system described above were added to the reaction in addition to Buffer A. Following 90 minutes incubation at 30 degrees, loading buffer was added to terminate the reaction, which were run by SDS electrophoresis using 4-20% acrylamide gels. The *in vitro* ubiquitination reaction was performed using Buffer A with the conditions previously described (17) (0.5 uM E1, 5 uM Ubc4, 30 uM GST-RING), or with the following conditions: 50 nM Ubiquitin E1, 250 nM Ubc4, 10 uM Ubiquitin and 500 nM MAPL-GST were incubated in Buffer A for 90 min at 30 C in the presence of the ATP regenerating system or apyrase. Loading buffer was added to terminate the reaction, then run by SDS electrophoresis using 4-20% acrylamide gels.

Fractionation

HeLa cells stably transfected with a short hairpin directed against MAPL (shMAPL) or a vector control (shVector) were plated in 6 x 20cm dishes each with 2.5ug/mL puromycin. After 16 hours, cells were trypsinized, washed in phosphate buffer and resuspended in 1 ml homogenization buffer (220 mM mannitol, 68 mM sucrose, 20 mM Hepes, pH 7.4, 80 mM KCl, 0.5 mM EGTA, 2 mM Mg_2Ac, protease inhibitors, 20mM *N*-methylmaleimide). Cells were broken in a cell cracker (EMBL-Heidelberg, Germany, 8.004 ball). The nuclear fraction was removed by centrifuging at 800 x g for 10 min. at 4°C. Then nuclear pellet was resuspended in 15mM Tris pH7.4, 60mM KCl, 15mM NaCl, 250mM

Sucrose, 1.5% NP40. Nuclear extracts were homogenized once again and purified nuclei were retrieved by centrifuging 5 min at 800g. The post-nuclear supernatant was centrifuged at 9,300 x g for 20 minutes at 4 degrees to pellet mitochondria. Mitochondria were washed in homogenization buffer and re-isolated to remove contaminants. The post-mitochondrial supernatant was centrifuged at 100,000 x g to clear the cytosolic fraction of light membranes. Total extracts, mitochondrial and cytosolic fractions were normalized for protein content, and 50μg loaded for electrophoresis and western blotting.

Purification of mitochondria from cow heart

A bovine heart freshly collected from the abattoir was minced, washed and decanted in PBS until little traces of blood were remaining. Two volumes of buffer A were added (20 mM Hepes, pH 7.4, 220 mM mannitol, 68 mM Sucrose, 80 mM KCl, 0.5 mM EGTA, 2 mM $Mg(Ac)_2$, 1 mM DTT, protease inhibitor). The tissue was placed in a Waring blender and homogenized. The lysate was centrifuged at 900 x g at 4 degrees for 20 minutes. The supernatant was transfered to a new tube for a second low speed spin, as above. The second supernatant was centrifuged at 10,000 x g for 20 minutes at 4 degrees. The pellet was washed with a large volume of buffer (500 ml) and recentrifugated at 10,000 x g for 20 minutes at 4 degrees. The mitochondria pellet was resupended in 100 ml of Buffer A (minus DTT and protease inhibitors) supplemented with 10% glycerol and snap frozen in liquid nitrogen for storage at –80 C.

Electron microscopy

Cells were fixed in 1.6% glutaraldehyde at room temperature for 1 hour to 2 hour before centrifugation at 10,000 x g. The fixed pellet was resuspended in 0.3% low melting

agarose before post fixation and embedding in Spurr epoxy resin, as described previously (22). Images were obtained using a JEOL 1230 TEM microscope, at 60kV, using a Hammamatsu Digital 2k x 2k camera (JEOL, Montreal, PQ).

II.4.2 Quantification and statistical analysis

All Western Blot analysis was performed using the FluorChem Imaging system and software (Cell Biosciences, Santa Clara, CA). Automatic background adjustment was selected for densitometry analysis. The Sigma Plot software (Systat Software Inc, Chicago, IL, USA) was used for statistical analysis and Student's t-test to evaluate statistical significance.

II.5 Discussion

The data presented here identify MAPL as the first mitochondrial SUMO E3 ligase. MAPL supports SUMOylation on a synthetic peptide containing the SUMO consensus sequence, on isolated mitochondrial proteins and on native Drp1. Our previous data have shown that MAPL stimulates mitochondrial fragmentation (16), and this study provides new mechanistic insight into the role of MAPL in regulating the SUMOylation of Drp1. In SUMOylating Drp1, MAPL functions as a positive regulator of mitochondrial fission, however the silencing data indicates that MAPL is not an essential component of the division machinery (16). The complex pattern of SUMO conjugates found on the mitochondria that are formed upon incubation with excess MAPL indicates that MAPL

likely also functions in additional mitochondrial processes via targets distinct from Drp1, including potential regulators of the fusion machinery.

Our data confirm that MAPL is also capable of facilitating ubiquitination. However, the MAPL-catalyzed ubiquitination was supported only when the concentrations of the enzymes were in the micromolar range. Since the cellular concentrations of ubiquitin and SUMO do not enter the micromolar range, it is unlikely that MAPL provides significant ubiquitination activity in vivo. Moreover, MAPL knockdown did not affect the mitochondrial ubiquitination pattern, and the addition of MAPL-RING to isolated mitochondria did not stimulate the ubiquitination reaction on native mitochondrial targets. Therefore, although MAPL may exhibit ubiquitination activity under some conditions, the data demonstrates that MAPL functions in vivo as an efficient SUMO E3 ligase.

Finally, the identification of a mitochondrial SUMO E3 ligase significantly expands the repertoire of SUMOylation enzymes, confirms the importance of non-nuclear SUMOylation, and provides a new platform from which to study the function of SUMOylation outside of the nucleus. Although some of the changes in the global SUMOylation upon silencing of MAPL might be indirect, it is clear that MAPL plays an important role in cellular SUMOylation. The localization of the RING domain on the cytosolic side of the mitochondrial outer membrane may also result in the SUMOylation of targets on closely apposed organelles such as the endoplasmic reticulum or peroxisomes via transfer of mitochondrial derived vesicles (16), as well as of other cytosolic factors. Characterization of the MAPL-specific SUMO proteome will clarify these possibilities and help define the role of MAPL in both mitochondrial dynamics and a broader cellular biological context.

II.6 References

1. Geiss-Friedlander, R., and F. Melchior. 2007. Concepts in sumoylation: a decade on. *Nat Rev Mol Cell Biol* 8:947-956.
2. Martin, S., K.A. Wilkinson, A. Nishimune, and J.M. Henley. 2007. Emerging extranuclear roles of protein SUMOylation in neuronal function and dysfunction. *Nat Rev Neurosci* 8:948-959.
3. Kahyo, T., T. Nishida, and H. Yasuda. 2001. Involvement of PIAS1 in the sumoylation of tumor suppressor p53. *Mol Cell* 8:713-718.
4. Bischof, O., K. Schwamborn, N. Martin, A. Werner, C. Sustmann, R. Grosschedl, and A. Dejean. 2006. The E3 SUMO ligase PIASy is a regulator of cellular senescence and apoptosis. *Mol Cell* 22:783-794.
5. Kagey, M.H., T.A. Melhuish, and D. Wotton. 2003. The polycomb protein Pc2 is a SUMO E3. *Cell* 113:127-137.
6. Pichler, A., A. Gast, J.S. Seeler, A. Dejean, and F. Melchior. 2002. The nucleoporin RanBP2 has SUMO1 E3 ligase activity. *Cell* 108:109-120.
7. Ivanov, A.V., H. Peng, V. Yurchenko, K.L. Yap, D.G. Negorev, D.C. Schultz, E. Psulkowski, W.J. Fredericks, D.E. White, G.G. Maul, M.J. Sadofsky, M.M. Zhou, and F.J. Rauscher, 3rd. 2007. PHD domain-mediated E3 ligase activity directs intramolecular sumoylation of an adjacent bromodomain required for gene silencing. *Mol Cell* 28:823-837.
8. Johnson, E.S., and G. Blobel. 1999. Cell cycle-regulated attachment of the ubiquitin-related protein SUMO to the yeast septins. *J Cell Biol* 147:981-994.
9. Rajan, S., L.D. Plant, M.L. Rabin, M.H. Butler, and S.A. Goldstein. 2005. Sumoylation silences the plasma membrane leak K+ channel K2P1. *Cell* 121:37-47.
10. Makhnevych, T., C. Ptak, C.P. Lusk, J.D. Aitchison, and R.W. Wozniak. 2007. The role of karyopherins in the regulated sumoylation of septins. *J Cell Biol* 177:39-49.
11. Dadke, S., S. Cotteret, S.C. Yip, Z.M. Jaffer, F. Haj, A. Ivanov, F. Rauscher, 3rd, K. Shuai, T. Ng, B.G. Neel, and J. Chernoff. 2007. Regulation of protein tyrosine phosphatase 1B by sumoylation. *Nat Cell Biol* 9:80-85.
12. Kang, J.S., E.F. Saunier, R.J. Akhurst, and R. Derynck. 2008. The type I TGF-beta receptor is covalently modified and regulated by sumoylation. *Nat Cell Biol* 10:654-664.
13. Harder, Z., R. Zunino, and H. McBride. 2004. Sumo1 conjugates mitochondrial substrates and participates in mitochondrial fission. *Curr. Biol.* 14:340-345.
14. Wasiak, S., R. Zunino, and H.M. McBride. 2007. Bax/Bak promote sumoylation of DRP1 and its stable association with mitochondria during apoptotic cell death. *J Cell Biol* 177:439-450.

15. Zunino, R., A. Schauss, P. Rippstein, M. Andrade-Navarro, and H.M. McBride. 2007. The SUMO protease SENP5 is required to maintain mitochondrial morphology and function. *J Cell Sci* 120:1178-1188.

16. Neuspiel, M., A.C. Schauss, E. Braschi, R. Zunino, P. Rippstein, R.A. Rachubinski, M.A. Andrade-Navarro, and H.M. McBride. 2008. Cargo-selected transport from the mitochondria to peroxisomes is mediated by vesicular carriers. *Curr Biol* 18:102-108.

17. Li, W., M.H. Bengtson, A. Ulbrich, A. Matsuda, V.A. Reddy, A. Orth, S.K. Chanda, S. Batalov, and C.A. Joazeiro. 2008. Genome-Wide and Functional Annotation of Human E3 Ubiquitin Ligases Identifies MULAN, a Mitochondrial E3 that Regulates the Organelle's Dynamics and Signaling. *PLoS ONE* 3:e1487.

18. Tang, Z., C.M. Hecker, A. Scheschonka, and H. Betz. 2008. Protein interactions in the sumoylation cascade: lessons from X-ray structures. *Febs J* 275:3003-3015.

19. Karbowski, M., A. Neutzner, and R.J. Youle. 2007. The mitochondrial E3 ubiquitin ligase MARCH5 is required for Drp1 dependent mitochondrial division. *J Cell Biol* 178:71-84.

20. Yonashiro, R., S. Ishido, S. Kyo, T. Fukuda, E. Goto, Y. Matsuki, M. Ohmura-Hoshino, K. Sada, H. Hotta, H. Yamamura, R. Inatome, and S. Yanagi. 2006. A novel mitochondrial ubiquitin ligase plays a critical role in mitochondrial dynamics. *EMBO J* 25:3618-3626.

21. Nakamura, N., Y. Kimura, M. Tokuda, S. Honda, and S. Hirose. 2006. MARCH-V is a novel mitofusin 2- and Drp1-binding protein able to change mitochondrial morphology. *EMBO Rep* 7:1019-1022.

22. Neuspiel, M., R. Zunino, S. Gangaraju, P. Rippstein, and H.M. McBride. 2005. Activated Mfn2 signals mitochondrial fusion, interferes with Bax activation and reduces susceptibility to radical induced depolarization. *J Biol Chem* 280:25060-25070.

Chapter III MAPL interacting column and mitochondria SUMO proteome

III.1 Significance and author contributions

The research presented in the following chapter includes the identification of MAPL interacting partners and of the mitochondrial SUMO proteome. This data has not been published, and will provide invaluable tools to better understand the physiological functions of MAPL and of mitochondrial SUMOylation. I performed most of the experimental procedures, with the exception of the Mass Spectrometry analysis, which was performed by Brian Raught (Ontario Cancer Institute, Toronto, Canada) for the SUMO proteome and by Daniel Figeys (Ottawa Institute for Systems Biology, Canada) for the affinity column.

III.2 Introduction

Numerous mitochondrial proteins are SUMOylated, although Drp1 is the only identified mitochondrial SUMO substrate so far (1). Specifically, the SUMOylation of Drp1 enhances mitochondrial fragmentation (1). Although the morphology of the mitochondria has important physiological functions, the high number of mitochondrial substrates indicates that mitochondrial SUMOylation may have other physiological roles. Importantly, the identification of MAPL, the first mitochondrial SUMO E3 ligase, is an important step to better understand the physiological functions of mitochondrial SUMOylation (2). In particular, MAPL could SUMOylate mitochondrial substrates, which could then have

another function. MAPL could also SUMOylate recruited cytosolic factors, triggering their translocation to other cellular compartments or modulating their function. Therefore, uncovering the interacting partners of MAPL and the mitochondrial SUMO proteome will hopefully shed light onto the physiological functions of MAPL and of mitochondrial SUMOylation.

III.3 Results

III.3.1 MAPL affinity column

Different methods can be used for the unbiased detection of interacting partners, including yeast-two hybrid analysis and affinity columns. In the yeast two hybrid system, the protein of interest, called the bait, is fused to the DNA-binding domain of a transcription factor, usually Gal4. A library of genes fused to the activation domain of Gal4 is selected. The bait and the library are then transfected into yeast cells. If protein-protein interaction occurs, the activation and DNA binding domains of Gal4 are in close proximity and are able to activate a reporter gene downstream of a Gal4 responsive promoter element. This method relies on the un-physiological targeting of proteins in the yeast nucleus, which is a problem when studying membrane anchored proteins. On the other hand, it is a sensitive method to detect weak interactions, and, unlike the affinity columns, purification of the protein is not required.

Affinity columns rely on the ability to efficiently purify the protein of interest or a specific domain. The protein is then incubated with extracts from the tissues of choice. The purified proteins and interacting partners are subsequently eluted and identified by Mass

Spectrometry. The advantage of this technique is that the protein can be incubated with any extracts, including different cellular fractions (nuclear, cytosolic, mitochondrial, etc.), different tissues (neurons, heart, muscles, etc.), or even normal versus carcinogenic cell extracts etc. In addition, the proteins from the isolated tissues will have been processed normally and should retain post-translational modifications. For example, if phosphorylation is required for the interaction, an affinity column is the method of choice.

We were interested in identifying interacting partners of the cytosolic RING domain of MAPL, since it is the enzymatic domain, and can be easily purified. In addition, by using the affinity column approach, we hoped to isolate interacting proteins from cytosolic fractions or mitochondrial enriched fractions specifically. We therefore purified GST:MAPL-RING, and incubated the recombinant proteins with cytosol and solubilized mitochondrial extracts isolated from human placenta. The RING and potential binding partners were then eluted from the GST using a thrombin cleavage site, and were resolved by SDS page. Following Coomassie staining, specific bands present in the GST:MAPL-RING elutions, but not in the GST control elutions, were cut and sent for Mass Spectrometry analysis at the University of Ottawa. The cytosolic fraction yielded eight specific bands *(Figure 3.1)*, unlike the mitochondrial fraction, which did not yield any specific bands. The results obtained from the cytosolic preparation are listed in *Table 3.1*. We decided to use a conservative approach and only proteins identified with a minimum of five peptides are listed.

Figure III-1 MAPL affinity column

5mg of bacterially purified GST:MAPL-RING or GST alone were incubated with 50 mg of human placenta cytosol. The RING domain and potential binding partners were subsequently eluted upon cleavage by thrombin. After staining with Coomassie blue, bands were excised and sent for mass spectrometry analysis. Molecular weights are shown in kDa.

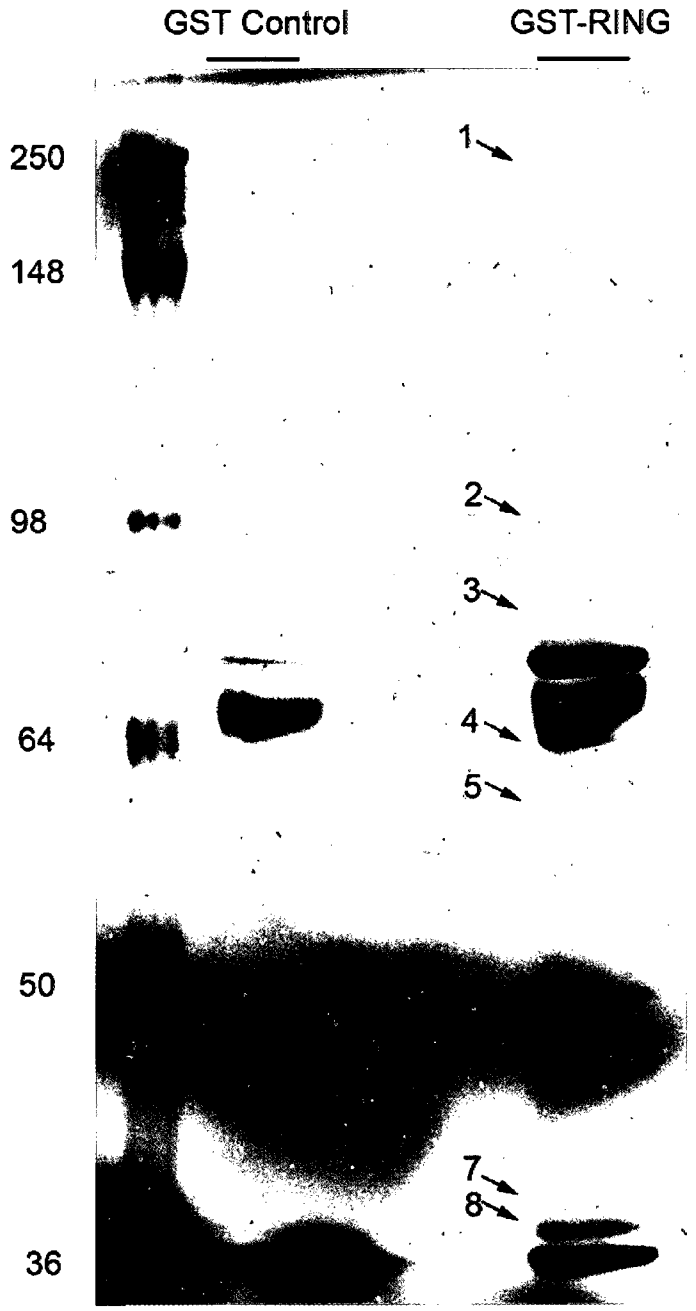
GST Control
GST-RING
250
148
98
64
50
36
1
2
3
4
5
7
8

Table III-1 MAPL affinity column

List of proteins that were identified as MAPL:RING interacting partners by Mass Spectrometry by at least five peptides. The "bands" column corresponds to the bands from the Coomassie gel that were cut and analyzed by Mass Spectrometry *(see Figure 3.1)*. Although only two peptides were recovered form SNX9, it was added to the list since it could play a role in MDV formation *(see Chapter 5)*.

Band	Protein	Function
1	Filamin A	Cytoskeleton organization
1	Filamin B	Cytoskeleton organization
2	IQ motif containing GTPase activating protein 1	Cytoskeleton organization
2	IQ motif containing GTPase activating protein 2	Cytoskeleton organization
2	vacuolar sorting protein 35	Vesicular trafficking
5	Dead box, X isoform	RNA helicase
5	Dead box polypeptide X-linked 3 (DDX3)	RNA helicase
6	Lamin A	Nuclear lamina
6	Lamin B2	Nuclear lamina
6	β-actin	Cytoskeleton
7	Anexin2	Phospholipid binding
7	CapZ α 1	Actin capping protein
7	CapZ α 2	Actin capping protein
7	protein disulfide isomerase-related protein 5, 6	Protein folding
5	SNX9 – 2 peptides only	Endocytosis

To select the potential interacting partners listed in *Table 3.1*, a stringent cutoff was used. It remains important to first validate a potential interacting protein by probing the elutions with antibodies raised against that specific protein. This has been done for the IQ motif containing GTPase activating protein 1 (IQGAP1) and Vps35 *(Figure 3.2)*. The next step is to validate the interaction by co-immunoprecipitation, which were performed for IQGAP1, Vps35, and the Sorting Nexin 9 (SNX9). SNX9 was identified as a potential MAPL interacting partner by only two peptides, and is therefore not listed in *Table 3.1*. However, since SNX9 is involved in vesicle formation *(see Chapter 5)*, and since MAPL is incorporated into vesicles, we decided to confirm whether it is co-precipitated with MAPL. MAPL:Flag was overexpressed in HeLa cells and immunoprecipitated using anti-Flag resin. The co-immunoprecipitation of overexpressed IQGAP1, Vps35 and SNX9, or of endogenous IQGAP1 and Vps35 was revealed using specific antibodies *(Figure 3.3)*. These results indicate that IQGAP1, Vps35 and SNX9 are in a complex with MAPL in HeLa cells.

Figure III-2 Confirmation of the MAPL affinity column by western blot analysis

50μg of post mitochondrial supernatant (PMS), along with the elutions from the affinity column were probed with α-IQGAP1 and α-Vps35 antibodies, as indicated.

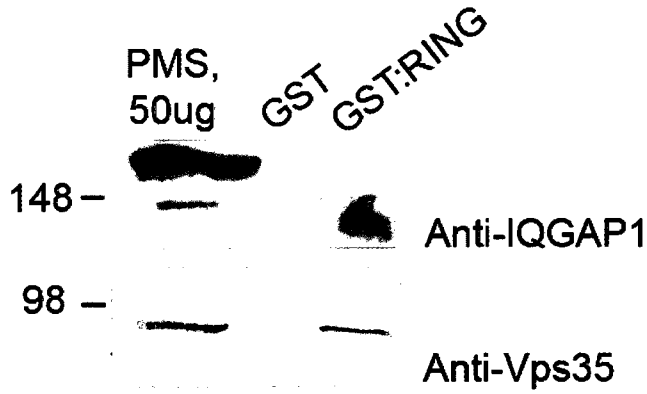
PMS,
50ug
GST
GST:RING
148 –
98 –
Anti-IQGAP1
Anti-Vps35

Figure III-3 Confirmation of interacting partners by co-immunoprecipitation

A) IQGAP1:myc and MAPL:Flag, were co-transfected into HeLa cells before cells were solubilized and immunoprecipitated with α-Flag-agarose beads. The western blots were decorated with α-myc to detect IQGAP1, and α-Flag to visualize MAPL. B) MAPL:Flag was overexpressed in HeLa cells and immunoprecipitated with α-Flag agarose beads. The co-immunoprecipitation of endogenous IQGAP1 was revealed using α-IQGAP1 antibodies. C) Vps35:YFP and MAPL:Flag, were co-transfected into HeLa cells before cells were solubilized and immunoprecipitated with α-Flag-agarose beads. The western blots were decorated with α-FP to detect Vps35, and α-Flag to visualize MAPL. D) MAPL:Flag was overexpressed in HeLa cells and immunoprecipitated with α-Flag agarose beads. The co-immunoprecipitation of endogenous Vps35 was revealed using α-Vps35 antibodies. E) SNX9:GFP and MAPL:Flag, were co-transfected into HeLa cells before cells were solubilized and immunoprecipitated with α-Flag-agarose beads. The western blots were probed with α-FP to detect SNX9, and α-Flag to visualize MAPL.

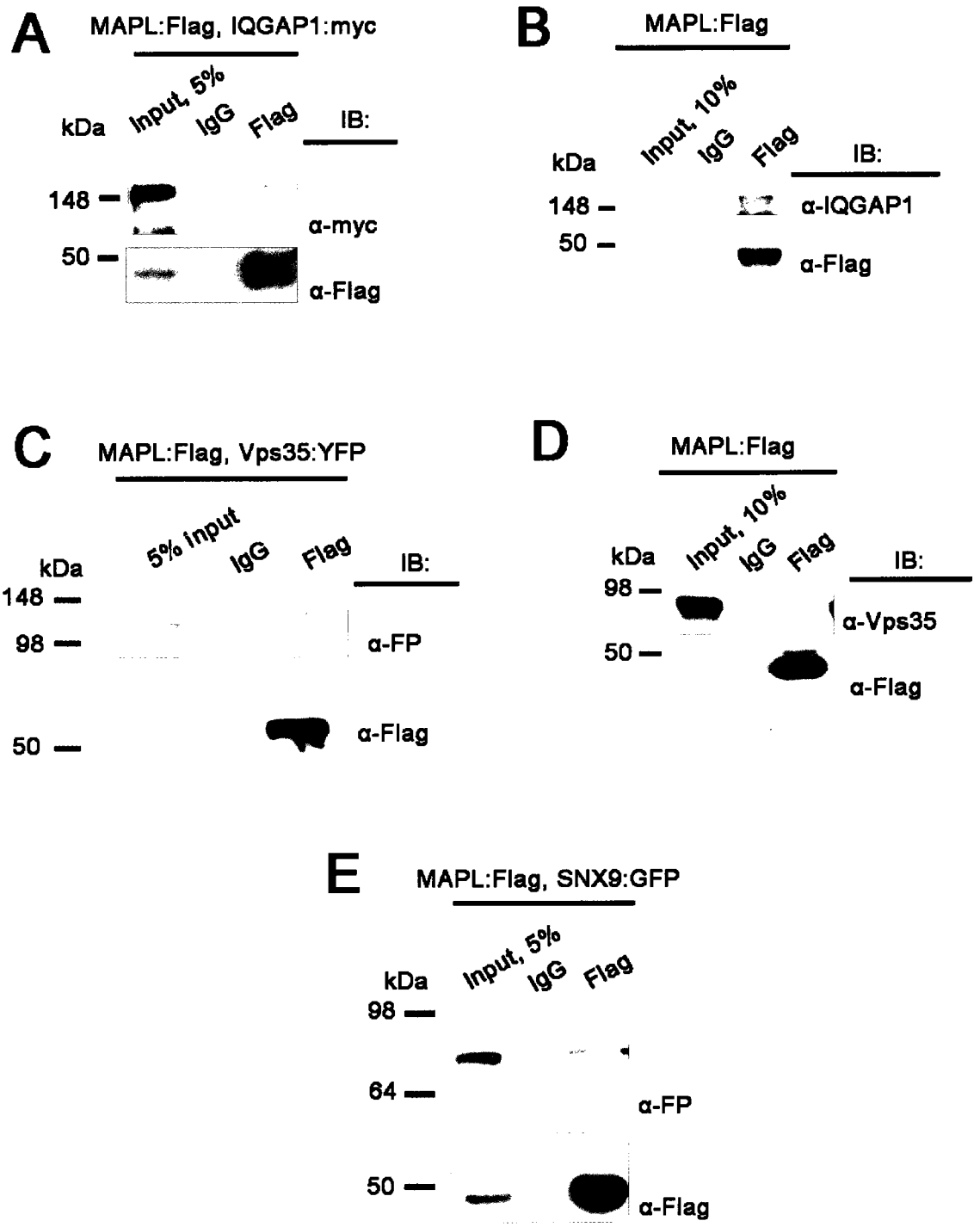
A
MAPL:Flag, IQGAP1:myc
kDa
Input, 5%
IgG
Flag
IB:
148
50
α-myc
α-Flag
B
MAPL:Flag
kDa
Input, 10%
IgG
Flag
IB:
148
50
α-IQGAP1
α-Flag
C
MAPL:Flag, Vps35:YFP
kDa
5% Input
IgG
Flag
IB:
148
98
50
α-FP
α-Flag
D
MAPL:Flag
kDa
Input, 10%
IgG
Flag
IB:
98
50
α-Vps35
α-Flag
E
MAPL:Flag, SNX9:GFP
kDa
Input, 5%
IgG
Flag
98
64
50
α-FP
α-Flag

III.3.2 Mitochondrial SUMO proteome

Different SUMO proteomes have been published, yielding valuable information. However, these screens either used whole cell extracts or enriched nuclear preparations. Given that most of the SUMOylation happens in the nucleus, these screens were not geared at identifying mitochondrial SUMO substrates. We therefore decided to characterize the mitochondrial SUMO proteome specifically. In order to design our experimental approach, we took into consideration problems that had previously been encountered when identifying proteomes.

A common problem, the lack of sensitivity, has been documented by Rosas-Acosta *et al.* In their study, a tagged SUMO was overexpressed in HEK293 cells; conjugated substrates were affinity-purified and identified by Mass Spectrometry. Although novel SUMO substrates were identified, they were unable to isolate by Mass Spectrometry the known SUMOylated proteins, that they had used for a Western-blot validation of their screen (3). To circumvent this problem of sensitivity, the SUMOylated substrates can be enriched by using fractions with a high level of SUMOylation, such as nuclear fractions (4), or by using treatments that enhance overall cellular SUMOylation. For example, the SUMOylation of both SUMO1 and SUMO2 is increased with the proteosome inhibitor MG132 and heat shock treatments (3, 5).

Another problem commonly encountered is the lack of specificity. To address this problem, two main approaches have been used: denaturing buffers, and Tandem Affinity Purification (TAP). Denaturing buffers prevent the purifications of non-SUMOylated proteins and of proteins that bind SUMO without being covalently modified. In addition,

denaturing buffers inactivate SUMO proteases, and have the benefit of improving the signal to noise ratio. On the other hand, TAP uses a SUMO construct fused to two different tags. A first purification is performed with the first tag, for example protein G (6). The SUMO is then recovered using agarose beads conjugated to immuno-globulins (6). The SUMO-conjugated substrates are then subsequently eluted using a protease cleavage site followed by a second purification step, for example using the streptavidin binding protein (6). In that case, the SUMO substrates are purified using beads conjugated to streptavidin and eluted with biotin (6). This method reduces the amount of non specific proteins co-isolated with the SUMOylated proteins, but also leads to a significant loss of sensitivity (6).

We chose to isolate mitochondria, conjugate mitochondrial proteins with a tagged SUMO by using an *in-vitro* SUMOylation reaction, and isolate the SUMO substrates by affinity purification. We elected to use a one step affinity chromatography purification, since the *in-vitro* SUMOylation reaction is inefficient, and by using a double affinity process we could have reached the limits of detection by Mass Spectrometry. Also, since our main aim was to understand the physiological function of mitochondrial SUMOylation, we were interested in identifying mitochondrial SUMO-binding partners in addition to the covalently modified SUMO conjugates, and decided to use non-denaturing buffers. To address the problem of specificity, we used a control reaction, with only mitochondria, to determine which proteins were isolated in a non-specific manner.

Following a pilot experiment using mitochondria freshly isolated from spinner HeLa (sHeLa) cells we realized that these mitochondria were able to sustain a strong *in-vitro* SUMOylation. We therefore performed two other independent experiments using mitochondria freshly isolated from sHeLa cells. Following Mass Spectrometry analysis, we

were able to isolate 97 SUMO substrates common to these two experiments, with a log(e) value below -2. The log(e) score takes into consideration the number of peptides recovered and the specificity of the peptides, and a score of -2 or less is usually considered significant. In this list, 12 proteins had previously been identified as common non-specific contaminants, and were removed, yielding 85 proteins (5). These are listed in *Table 3.2*. In addition, we also compiled the list of proteins that were common to the pilot experiment and to the following two experiments. We consider that these 9 proteins, listed in *Table 3.3,* which were identified in three independent experiments, are the most robust potential mitochondrial SUMO substrates.

Table III-2 Mitochondrial SUMO proteome, compiled from two independent experiments

Mitochondria from sHeLa cells were incubated in the presence of His_6-SUMO1, SUMO E1, Ubc9 and an ATP regenerating system. The mitochondria were then solubilized and proteins conjugated to His_6-SUMO1 were isolated by metal affinity chromatography, eluted, and analyzed by Mass Spectrometry. The experiment was performed two independent times, and the proteins which were recovered from these two experiments, and with a log(e) value bellow -2, are listed in *Table 3.2.*

log(e)	Description
-45.2	BICD1, Protein bicaudal D homolog 1
-34.7	PABPC1, Polyadenylate-binding protein 1
-24.7	PABPC4, Polyadenylate-binding protein 4
-19.9	METT11D1, Protein RSM22 homolog, mitochondrial Precursor
-17.4	BUD13, BUD13 homolog
-17.2	CBX4, E3 SUMO-protein ligase CBX4
-15.6	ILF2, Interleukin enhancer-binding factor 2
-15.5	GPBP1L1, Vasculin-like protein 1
-14.9	XRCC5, ATP-dependent DNA helicase 2
-14.2	WDR68, WD repeat-containing protein 68
-9	TTBK2, Tau-tubulin kinase 2
-8.9	GNAI3, Guanine nucleotide-binding protein G(k) subunit alpha
-8.4	PRR4, Proline-rich protein 4 Precursor
-7.8	TMEM33, Transmembrane protein 33
-7.4	CST1, Cystatin-SN Precursor
-7.2	MYLK2, Myosin light chain kinase 2
-7.1	PC, Pyruvate carboxylase
-6.5	TPM3, Tropomyosin alpha-3 chain
-4.8	MYCBP2, Probable E3 ubiquitin-protein ligase MYCBP2
-4.7	NKTR, NK-tumor recognition protein
-4.7	SLC4A2, Anion exchange protein 2
-4.5	HAL, Histidine ammonia-lyase
-4.5	MRPS2, 28S ribosomal protein S2, mitochondrial
-4.3	GNB2L1, Guanine nucleotide-binding protein subunit beta-2-like 1
-4.2	GNL3, Guanine nucleotide-binding protein
-4.1	BAIAP2L1, Brain-specific angiogenesis inhibitor 1-associated protein 2 like protein 1
-3.9	MNT, Max-binding protein
-3.7	RALY, RNA-binding protein Raly
-3.6	PRPF4B, Serine/threonine-protein kinase
-3.6	HSPG2, Basement membrane-specific heparan sulfate proteoglycan core protein
-3.5	PTPLAD1, Protein tyrosine phosphatase-like protein
-3.5	NFIC, Nuclear factor 1 C-type
-3.3	MRPS9, 28S ribosomal protein S9, mitochondrial Precursor
-3.3	AGPS, Alkyldihydroxyacetonephosphate synthase, peroxisomal Precursor
-3.3	MRPL41, 39S ribosomal protein L41, mitochondrial Precursor
-3.2	PABPC3, Polyadenylate-binding protein 3
-3.2	SYNCRIP, Heterogeneous nuclear ribonucleoprotein Q
-3.2	BMPR2, Bone morphogenetic protein receptor type-2 Precursor
-3.2	PAFAH1B1, Platelet-activating factor acetylhydrolase IB subunit alpha
-3.1	C19orf44, Uncharacterized protein C19orf44
-3.1	ATP13A2, Probable cation-transporting ATPase 13A2
-3	CYP4B1, Cytochrome P450 4B1
-3	FSCN2, Fascin-2
-3	C19orf21, Uncharacterized protein C19orf21
-3	MRPS23, 28S ribosomal protein S23, mitochondrial
-3	CITED2, Cbp/p300-interacting transactivator 2
-2.9	CLSTN3, Calsyntenin-3 Precursor
-2.8	PHTF2, Putative homeodomain transcription factor 2
-2.8	RBMX2, RNA-binding motif protein, X-linked 2
-2.8	GSX1, GS homeobox 1
-2.8	HP1BP3, Heterochromatin protein 1-binding protein 3
-2.8	GPR179, Probable G-protein coupled receptor 179
-2.6	PRKDC, DNA-dependent protein kinase catalytic subunit
-2.6	MICAL1, NEDD9-interacting protein with calponin homology and LIM domains
-2.6	SERBP1, Plasminogen activator inhibitor 1 RNA-binding protein
-2.5	DOCK4, Dedicator of cytokinesis protein 4
-2.5	ASCC3, Activating signal cointegrator 1 complex subunit 3
-2.5	PTGER3, Prostaglandin E2 receptor EP3 subtype
-2.4	ITGA7, Integrin alpha-7 Precursor
-2.4	SP6, Transcription factor Sp6
-2.4	SYNJ2, Synaptojanin-2
-2.4	KIF21B, Kinesin-like protein KIF21B
-2.3	BEX5, Protein BEX5
-2.3	PHLDA1, Pleckstrin homology-like domain family A member 1
-2.3	MARCH4, E3 ubiquitin-protein ligase MARCH4
-2.3	LINS1, Protein Lines homolog 1
-2.3	CALD1, Caldesmon
-2.3	FRY, Protein furry homolog
-2.2	FILIP1, Filamin-A-interacting protein 1
-2.2	NAT10, N-acetyltransferase 10
-2.2	MLH1, DNA mismatch repair protein Mlh1
-2.2	GIMAP4, GTPase IMAP family member 4
-2.2	ADAM21, ADAM 21 Precursor
-2.2	APPL1, DCC-interacting protein 13-alpha
-2.2	ATN1, Atrophin-1
-2.2	DPP6, Dipeptidyl aminopeptidase-like protein 6
-2.2	LANCL3, LanC-like protein 3
-2.2	LRRC30, Leucine-rich repeat-containing protein 30
-2.1	RASGRP4, RAS guanyl-releasing protein 4
-2.1	CPD, Carboxypeptidase D Precursor
-2.1	CCBL2, Kynurenine--oxoglutarate transaminase 3
-2.1	NAV3, Neuron navigator 3
-2.1	DEPDC2, Phosphatidylinositol 3,4,5-trisphosphate-dependent Rac exchanger 2 protein
-2.1	PFKP, 6-phosphofructokinase type C
-2.1	FCAMR, High affinity immunoglobulin alpha and immunoglobulin mu Fc receptor Precursor

Table III-3 Mitochondria SUMO proteome, compiled from three independent experiments

Mitochondria from sHeLa cells were incubated in the presence of His_6-SUMO1, SUMO E1, Ubc9 and an ATP regenerating system. The mitochondria were then solubilized and proteins conjugated to His_6-SUMO1 were isolated by metal affinity chromatography, eluted, and analyzed by Mass Spectrometry. The experiment was performed once as a pilot experiment, and two other independent times, and the proteins which were recovered from these three experiments are listed in *Table 3.3.*

Protein	Function
Protein bicaudal D homolog 1	Cellular trafficking
Uncharacterized protein C19orf21	Unknown
Cytochrome P450 4B1	Fatty acid metabolism
Furry	Cytoskeleton organization
MycBP2/Pam/highwire/rpm-1	E3 ubiquitin-protein ligase
Pleckstrin homology-like domain family A member 1	Cell death
Transmembrane protein 33	Unknown
WD repeat-containing protein 68	Unknown
ATP-dependent DNA helicase 2 subunit 2, Lupus Ku autoantigen protein p86, XRCC5	DNA repair

III.4 Materials and Methods

Reagents

Antibodies were purchased from the following providers: anti-Flag HRP, Sigma-Aldrich (Oakville, ON, Canada), monoclonal anti-Vps35, Abnova (Walnut, CA, USA), monoclonal anti-FP, Clonetech (Burlington, ON, Canada), monoclonal anti-IQGAP1, BD Bioscience (Mississauga, ON, Canada). General chemicals were obtained from Sigma-Aldrich (Oakville, ON, Canada) unless otherwise stated. The protease inhibitor cocktail was purchased from Roche, (Mississauga, ON, Canada). cDNA encoding $MAPL_{(257-352)}$:GST, have been previously described (7). PCMV-Tag4A (Stratagene, La Jolla, CA, USA) was used to subclone MAPL, using standard techniques. Recombinant SUMO, the SUMO E1 and Ubc9, were obtained from Boston Biochemicals (Cambridge, MA, USA). sHeLa cells were purchased from American Type Culture Collection (Manassas, VA).

Tissue culture

HeLa and sHeLa cells were maintained in Dulbecco's Modified Eagle Medium (GIBCO, Invitrogen, Burlington, ON, Canada) supplemented with 10% fetal bovine serum, penicillin, streptomycin and 2 mM L-glutamine. For subcellular fractionation, sHeLa cells were grown in 4 Fernbach flasks (Fisher Scientific) for 5–6 days until reaching a density of 100,000/ml, in 1 liter of Minimal Essential Media for suspension culture (Sigma-Aldrich, Oakville, ON, Canada) supplemented with 0.1 mM nonessential amino acids. All media used were supplemented with 10% FBS and antibiotics.

MAPL-GST fusion proteins and affinity column

GST or GST-$MAPL_{(257-352)}$ expression was induced in E. coli BL21 strain with 0.3mM IPTG for 3 hours. Bacteria were recovered by centrifugation, resuspended in 20mM Hepes pH 7.4, 200 mM NaCl, 2 mM $MgCl_2$, 5 mM β-mercaptoethanol, protease inhibitor cocktail, and lysed at 2000 psi using a French press. The lysate was centrifuged at 100,000 x g for 40 minutes in a Ti55.2 rotor (Beckman Coulter, Mississauga, ON, Canada). The supernatant was then incubated with glutathione-Sepharose beads for 2h00 at 4 degrees (Amersham Biosciences, Piscataway, NJ, USA). Following the washing with the above buffer supplemented with 500mM NaCl then 1% Triton X-100, the amount of purified protein per bead volume was calculated. The placenta cytosol was thawed, supplemented with protease inhibitor and centrifuged at 190,000 x g for 40 minutes. 50mg of the supernatant was then incubated with 5mg of GST for 2h00. The GST beads were removed by centrifugation and the pre-cleared cytosol was incubated with 5mg of GST or GST-$MAPL_{(257-352)}$ overnight. The beads were then washed extensively and the fusion proteins were cleaved from GST using thrombin, overnight at 4 degrees, following manufacturer's instructions (Sigma-Aldrich, Oakville, ON, Canada).

Fractionation of placenta cytosol

A human placenta was collected with consent, minced, washed and decanted in phosphate buffer until little traces of blood were remaining. Two volumes of buffer A were added (20mM Hepes, pH 7.4, 220mM mannitol, 68mM Sucrose, 80mM KCl, 0.5mM EGTA, 2mM $Mg(Ac)_2$, 1mM DTT, protease inhibitor). The tissue was placed in a Waring blender and homogenized. The lysate was centrifuged at 900 x g at 4 degrees for 20 minutes. The supernatant was transferred to a new tube for a second low speed spin, as above. The

second supernatant was centrifuged at 10,000 x g for 20 minutes at 4 degrees and snap frozen. Before the experiment, the placenta cytosol was thawed, supplemented with protease inhibitor and centrifuged at 190,000 x g for 40 minutes.

Immunoprecipitations

HeLa cells were transfected with the appropriate plasmids overnight. Following the transfection, cells were collected and solubilized in 50mM Tris pH 7.5, 100mM NaCl, 5mM $MgCl_2$, 1% Triton, 20mM *N*-methylmaleimide and protease inhibitor cocktail for 60 minutes. Insoluble material was removed by centrifugation at 13,000 x g for 20 min. The supernatant was assayed for protein concentration, and 1 mg per IP point was incubated overnight at 4 degrees with either 20 uL 1:1 Flag resin (Sigma-Aldrich, Oakville, ON, Canada) or 2.5 µg G-protein agarose-coupled mouse IgG (Sigma-Aldrich, Oakville, ON, Canada). After washing three times, the beads were mixed with loading sample buffer, separated on 4-20% acrylamide gels, and analyzed with the indicated antibodies.

Purification of mitochondria from spinner HeLa cells

sHeLa cells were harevested and washed in phosphate buffer by centrifugation, followed by a final wash in mitochondria isolation buffer (20mM Hepes, pH 7.4, 220mM mannitol, 68mM Sucrose, 80mM KCl, 0.5mM EGTA, 2mM $Mg(Ac)_2$, protease inhibitor). The cell pellets were resuspended in a minimal volume of mitochondria isolation buffer. Cells were broken in a cell cracker (EMBL-Heidelberg, Germany, 8.004 ball) and the nuclear fraction was separated by centrifugation at 800 x g for 10 minutes at 4 degrees. The post-nuclear supernatant was centrifuged at 9,300 x g for 20 min at 4 degrees to pellet mitochondria. Mitochondria were resuspended in 1mL homogenization buffer. Nuclear

contaminants were further removed by centrifugation at 800 x g for 10 minutes. Finally, the mitochondria were isolated following 9,300 x g centrifugation for 20 minutes at 4 degrees and resuspended in a minimal volume of mitochondria isolation buffer.

In vitro SUMO assay

10-12 mg of mitochondria were used for each assay. Isolated mitochondria were centrifuged at 8,000 x g for 15 min and resuspended in Tris mitochondria Buffer (50mM Tris, pH 7.4, 220mM mannitol, 68mM Sucrose, 80mM KCl, 0.5mM EGTA, 2mM $Mg(Ac)_2$). The SUMO conjugation assay was performed in 2mL per 10mg of mitochondria using 50nM SUMO E1, 250nM Ubc9, 10uM his_6-SUMO1, and 1mM ATP, 25mM Na Succinate, 4mM ADP, 10mM K_2HPO_4 in 50mM Tris pH 8.0, 100mM NaCl, 5mM $MgCl_2$, 1M DTT. Following 90 minutes incubation at 30 degrees, the mitochondria were solubilized in 500mM Salt, 1% Triton X-100, 50mMTris pH 8.0, 20mM *N*-methylmaleimide in twice their volume. The mitochondria were solubilized for 2h00 at 4 degrees, centrifuged at 13,000 x g for 30 minutes and pre-cleared with plastic beads for 1h00. 50uL of Ni-NTA-Agarose (Qiagen, Mississauga, ON, Canada) were added to the extract, which was incubated overnight. Beads were washed in solubilization buffer and the his_6-SUMO1 was eluted in solubilization buffer with increasing concentrations of Imidazole: 20mM, 50mM, 150mM and 250mM Imidazole, 10 minutes at 37 degrees. 10% of the elusions were analyzed by SDS electrophoresis using 4-20% acrylamide gels to confirm the efficiency of the SUMOylation reaction. The rest was used for Mass Spectrometry analysis at the University of Toronto, to be analyzed in the laboratory of Brian Raught.

III.5 Discussion

III.5.1 MAPL affinity column

Using an affinity column approach, we were able to successfully isolate a number of potential MAPL binding partners *(Table 3.1)*. However, one weakness of the column is that we only identified MAPL partners recruited to the RING domain. In fact, another set of partners might be recruited to the predicted conserved intermembrane space domain of MAPL. Unfortunately, the BAM domain is slightly hydrophobic and therefore not easy to purify. In addition, it is normally inserted into the mitochondrial outer membrane, and using a two-hybrid approach to find interacting partners, which would artificially target it to the yeast nucleus, might not give reliable results. Another option would be to use large scale immunoprecipitations, since we now have an antibody which immunoprecipitates MAPL efficiently (2). On the other hand, one of the strengths of using an affinity column approach is that one can use extracts from different tissues to determine specific sets of binding partners. Therefore, if MAPL were to have an important role in the cerebellum, we could repeat the affinity column using brain extracts to isolate brain-specific MAPL interacting partners.

Importantly, following the validation of a binding partner with co-immunoprecipitations (*see Results section)*, another important step is to verify that the two proteins colocalize with microscopy studies. If two proteins interact or are in the same complex *in-vivo*, they should be localized to the same cellular compartment. Finally, once a potential binding partner has been confirmed, the physiological relevance of the interaction should be explored. Since MAPL is a SUMO E3 ligase, the partner might be SUMOylated,

which could change its cellular functions. Alternatively, MAPL might serve as a receptor to recruit the protein to the mitochondria where it might regulate mitochondrial function.

III.5.2 Mitochondrial SUMO proteome

SUMOylation is a transient modification, and at any time only a small percent of the substrates are SUMOylated. Considering this, isolating a SUMO proteome is not trivial. Characterizing the mitochondrial SUMO proteome was even more challenging, since mitochondria represent a minor (yet important) source of SUMOylated proteins, the nucleus being where the bulk of the SUMOylation occurs. Using a stringent approach, we have identified 9 potential mitochondrial SUMO1 substrates *(Table 3.3)*.

Once a substrate will have been chosen, important considerations should be kept in mind. For example, the mitochondrial proteomes were isolated under non-denaturing conditions. Since our aim was to better understand the physiological pathways in which mitochondrial SUMOylation might be involved, we decided to isolate both conjugated substrates and SUMO binding partners. Once a substrate will have been chosen, it will therefore be important to determine whether it is covalently modified by SUMO. This can be achieved by immunoprecipitating the substrate in denaturing conditions and probing for the covalent association with SUMO. Future steps could then include the mutation of SUMO sites to understand the functional consequences of SUMOylation.

In addition, it is possible that our proteome is not entirely MAPL specific. Indeed, we do not exclude the existence of other mitochondrial SUMO E3 ligases, and, unlike ubiquitin E2 enzymes, the SUMO E2, Ubc9, possesses catalytic activity. This implies that the substrates SUMOylated during the *in-vitro* SUMO reaction could have been

SUMOylated by Ubc9. Genetic data from *S. cerevisiae* indicates that Ubc9 might SUMOylate specific substrates, not shared by known SUMO E3 ligases (8). Using tissues from the MAPL *knock-out* mouse will therefore be essential to determine which SUMO substrates are MAPL specific.

Importantly, we have focused our study on SUMO1. However, it is possible that SUMO 2 and 3 play an important role in mitochondrial processes. Studies comparing the conjugation of SUMO1 versus SUMO2/3 reported a low degree of overlap between them, indicating that these two modifications fulfill independent physiological functions. For example, Rosas-Acosta *et al.* reported that only 22% of the proteins that they identified as SUMO1 substrates were modified by both (3), and, similarly, in the study published by Makhnevych *et al.*, only 25% of the targets of SUMO1 were shared with SUMO2/3 (8). Comparing the mitochondrial SUMO1 proteome to the mitochondrial SUMO2/3 proteome might therefore yield interesting information.

Finally, a new quantitative approach to detect SUMO substrates, which relies on the use of different isotopes, has recently been described: Stable Isotope Labeling With Amino Acids in Cell culture (SILAC). Two proteomes have been published using this technique (4). One proteome isolated SUMO1 versus SUMO2 substrates. Three different conditions were used (1) Normal HeLa, which were unlabelled, (2) HeLa stably transfected with His_6-SUMO1, and labeled with $^{13}C_6$, $^{14}N_4$-arginine, (3) HeLa stably transfected with His_6-SUMO2, and labeled with $^{13}C_6$, $^{15}N_4$-arginine (4). Nuclear lysates from each conditions were mixed in a 1:1:1 ratio and His_6-SUMO isolated. Contaminants originating from outside of the experiment (keratine, albumin..) were only found in the unlabelled form. Non specific contamination that occurred during the purification process, were equally found in all

isotopes. This study used a conservative approach, and were considered SUMO substrates, proteins identified with at least two peptides and enriched in the heavy arginine by 1.5 fold. By comparing the levels of $^{13}C_6$, $^{14}N_4$-arginine to $^{13}C_6$, $^{15}N_4$-arginine for each peptide, the authors were able to compare the relative amounts of SUMOylation by SUMO1 and 2 (4).

The other study using SILAC compared SUMOylated substrates in steady state or heat shock conditions. This study used the following conditions: (1) HeLa cells, isotopically normal and grown in normal conditions, (2) HeLa cells transfected with TAP-tagged SUMO2, labeled with 4,4,5,5-D_4-lysine and $^{13}C_6$-arginine, and grown in normal conditions, and (3) HeLa cells transfected with TAP-tagged SUMO2, labeled with $^{13}C_6$ $^{15}N_2$-lysine and $^{13}C_6$ $^{15}N_6$-arginine and grown during 30 minutes at 42 degrees (8). SUMO2 substrates were isolated in denaturing conditions (2% SDS). The double labeling of the proteins increased sensitivity since the authors were able to identify hits that contained either heavy lysine or heavy arginine isotopes. Hits were identified by one peptide or more.

These studies are interesting for a number of reasons. They highlight the difficulties of identifying SUMO proteomes. The first study enhanced the starting amounts of SUMO substrates by utilizing a nuclear-enriched fraction. In addition, although the authors disposed of the isotope labeling to increase the specificity of their purification, both used stringent approaches: the first study used a high cutoff, and the second study used TAP and denaturing conditions.

Importantly, SILAC could be used to refine a MAPL-specific proteome. For example MEFs isolated from *wild-type* or MAPL *knock-out* animals could be labeled with different isotopes in order to isolate MAPL specific substrates. In addition, we have shown that Drp1 is SUMOylated during cell death (9). HeLa cells could be labeled with one isotope and

apoptotic HeLa cells with another to compare differential mitochondrial SUMOylation during cell death.

III.5.3 Current and future directions

By identifying MAPL interacting partners and the SUMO proteome, our main objective was to better understand the physiological function of MAPL. Using an affinity column approach, we identified one potential interacting partner, Vps35, which is a component of the retromer coat complex (10). Since MAPL is transported to peroxisomes in a vesicular pathway, I have chosen to focus my research on this particular protein. This work is described in the next chapter *(Chapter 4)*.

Future work will focus on studying other interacting partners and substrates. Unfortunately, there was no overlap between the mitochondria SUMO proteome and the MAPL affinity column. This could be caused by a number of reasons, including the fact that different tissues were used for the two assays. In addition, for the MAPL affinity column, analyzed bands were cut at specific molecular weights, and interacting partners of other molecular weights could have been missed. Finally, a strong interacting partner might only be SUMOylated by MAPL following specific cellular cues, and would not be isolated in the *in-vitro* SUMO assay. However, it appears that different proteins from the affinity column and the mitochondrial SUMO proteome are linked to the cytoskeleton. These will be expanded upon in the general discussion *(Chapter 5)*. Importantly, once the phenotypes of the MAPL *knock-out* mouse will have been determined, it will be interesting to re-explore the proteins identified in the affinity column and the SUMO proteome to examine if any of these could explain certain phenotypes.

III.6 References

1. Harder, Z., R. Zunino, and H. McBride. 2004. Sumo1 conjugates mitochondrial substrates and participates in mitochondrial fission. *Curr Biol* 14:340-345.
2. Braschi, E., R. Zunino, and H.M. McBride. 2009. MAPL is a new mitochondrial SUMO E3 ligase that regulates mitochondrial fission. *EMBO Rep* 10:748-754.
3. Rosas-Acosta, G., W.K. Russell, A. Deyrieux, D.H. Russell, and V.G. Wilson. 2005. A universal strategy for proteomic studies of SUMO and other ubiquitin-like modifiers. *Mol Cell Proteomics* 4:56-72.
4. Vertegaal, A.C., J.S. Andersen, S.C. Ogg, R.T. Hay, M. Mann, and A.I. Lamond. 2006. Distinct and overlapping sets of SUMO-1 and SUMO-2 target proteins revealed by quantitative proteomics. *Mol Cell Proteomics* 5:2298-2310.
5. Golebiowski, F., I. Matic, M.H. Tatham, C. Cole, Y. Yin, A. Nakamura, J. Cox, G.J. Barton, M. Mann, and R.T. Hay. 2009. System-wide changes to SUMO modifications in response to heat shock. *Sci Signal* 2:ra24.
6. Gregan, J., C.G. Riedel, M. Petronczki, L. Cipak, C. Rumpf, I. Poser, F. Buchholz, K. Mechtler, and K. Nasmyth. 2007. Tandem affinity purification of functional TAP-tagged proteins from human cells. *Nat Protoc* 2:1145-1151.
7. Neuspiel, M., A.C. Schauss, E. Braschi, R. Zunino, P. Rippstein, R.A. Rachubinski, M.A. Andrade-Navarro, and H.M. McBride. 2008. Cargo-selected transport from the mitochondria to peroxisomes is mediated by vesicular carriers. *Curr Biol* 18:102-108.
8. Makhnevych, T., Y. Sydorskyy, X. Xin, T. Srikumar, F.J. Vizeacoumar, S.M. Jeram, Z. Li, S. Bahr, B.J. Andrews, C. Boone, and B. Raught. 2009. Global map of SUMO function revealed by protein-protein interaction and genetic networks. *Mol Cell* 33:124-135.
9. Wasiak, S., R. Zunino, and H.M. McBride. 2007. Bax/Bak promote sumoylation of DRP1 and its stable association with mitochondria during apoptotic cell death. *J Cell Biol* 177:439-450.
10. Bonifacino, J.S., and J.H. Hurley. 2008. Retromer. *Curr Opin Cell Biol* 20:427-436.

Chapter IV Vps35 mediates the vesicular transport between the mitochondria and peroxisomes

IV.1 Significance and author contributions

One of the interacting partners of MAPL identified using the affinity column, Vps35, is part of the retromer coat complex (1). Since we have recently shown that MAPL is incorporated into vesicles, we therefore hypothesized that Vps35 could mediate mitochondrial to peroxisomal transport. This study provides mechanistic insights onto the formation of MDVs and places the retromer complex within a novel transport route. This manuscript is currently under revision in journal "*Current Biology*".

I performed and designed most of the experiments, with the exception of the Mass Spectrometry analysis, which was performed by D. Figeys (Ottawa Institute for Systems Biology). I was also helped by V. Goyon and R. Zunino for the fractionation in Figure 4.4, and by A. Mohanty, L. Xu for Figure 4.2A, and 4,2B. I wrote the manuscript in conjunction with my supervisor, and thank members of the lab and L. Pellegrini (University of Laval) for critical reading of the manuscript.

IV.2 Introduction

Mitochondrial Derived Vesicles (MDVs) have been shown to transport cargo from the mitochondria to the peroxisomes (2). Mitochondria and peroxisomes share common functions in the oxidation of fatty acids and the reduction of damaging peroxides (3, 4).

Their biogenesis is also linked through both the activation of master transcription factors such as PGC1α (5, 6), and the common use of fission machinery, including DRP1, Mff and hFis1 (7-10). We have previously shown that MDVs are formed independently of the known mitochondrial fission GTPase Drp1, and are enriched for a mitochondrial SUMO E3 ligase called MAPL (2). The existence of a vesicle transport route suggests the presence of specific machinery that regulates cargo enrichment, vesicle budding, transport and fusion with the peroxisomes. Here, we demonstrate that the retromer complex, a known component of vesicle transport from the endosome to the Golgi apparatus (11-14), regulates the transport of MAPL from mitochondria to peroxisomes. An unbiased screen has led us to show that Vps35 and Vps26A are found in complex with MAPL, and confocal imaging reveals Vps35 recruitment to mitochondrial vesicles. Silencing of Vps35 or Vps26A leads to a significant reduction in the delivery of MAPL to peroxisomes, placing the retromer within a novel intracellular trafficking route and providing insight into the formation of MAPL positive MDVs.

IV.3 Results

In the search for mechanisms that regulate mitochondrial fission, we recently uncovered MAPL as a novel mitochondrial SUMO E3 ligase that positively regulates the mitochondrial fission GTPase Drp1 (2, 15). Upon silencing of Drp1 to block mitochondrial fragmentation, the resulting fused mitochondrial reticulum allowed us to visualize the presence of small vesicular profiles that carried selected cargo. One population of these vesicles carried MAPL, but lacked the outer membrane marker Tom20 (2). These structures were then shown to fuse with a sub-population of peroxisomes, providing the first evidence

for a novel vesicular transport route between these organelles. In an effort to better understand the function of MAPL in mitochondria and peroxisomes, we searched for interacting partners using an affinity chromatography approach.

MAPL is a mitochondrial membrane protein containing two hydrophobic regions that separate two domains, a BAM domain of unknown function within the intermembrane space (16), and a RING finger motif exposed to the cytosol. We have previously demonstrated that the cytosolic RING domain is an active SUMO E3 ligase (15). In order to identify cytosolic binding partners and potential SUMO substrates for MAPL, we fused the C-terminal cytosolic domain of MAPL, which includes the RING finger motif, to GST and incubated the immobilized protein with cytosolic extracts derived from human placenta. Coomassie stained proteins that specifically bound GST:$MAPL_{(257-352)}$ were then analyzed by mass spectrometry *(Figure 4.1A, B)*. In one of the bands, we identified 8 peptides matching a component of the mammalian retromer complex, Vps35 *(Figure 4.1B)*. This interacting partner was of interest since Vps35, in addition to the other components of the retromer complex, Vps26 and Vps29, is known to be involved in the selection of cargo into vesicles (1, 17, 18), a process that we had also observed in mitochondrial vesicle formation. Western blot analysis confirmed the specificity of Vps35 binding to the purified RING domain of MAPL *(Figure 1C)*. Although we did not identify peptides derived from Vps26A or Vps29 in the mass spectrometry analysis, we confirmed the binding of Vps26A to the MAPL:RING domain by Western blot analysis, consistent with the retromer functioning as a heterotrimeric complex *(Figure 4.1C)*.

We then tested whether MAPL and Vps35 may interact in transfected cells. MAPL:Flag and Vps35:YFP were co-transfected in HEK293T cells and MAPL:Flag was

immunoprecipitated using α-Flag agarose beads. Immunodetection with α-FP antibodies revealed that Vps35:YFP co-precipitates with MAPL:Flag *(Figure 4.1D, right panels)*. In addition to transfected proteins, the endogenous Vps35 was also seen to co-precipitate with MAPL:Flag from transfected HeLa cells *(Figure 4.1E)*. Interestingly, the interaction with Vps35 was unaffected by the inactivation of the RING domain using an H319L mutation *(Figure 4.1E)*. This was not unexpected since the transport of MAPL to the peroxisomes does not depend on a functional SUMO E3 ligase activity, suggesting that the incorporation into vesicles is not directly related to its catalytic activity (2). Finally, to further validate this interaction, we performed cross-linking studies on post-nuclear supernatants to examine the interaction of endogenous MAPL with Vps35 and Vps26A. The addition of Bis-maleimidohexane (BMH) to post-nuclear supernatant led to the appearance of a high molecular weight cross-linked product, immunoreactive for bothVps26A and Vps35 (+ BMH input lanes, visualized with a 4-20% acrylamide gel *(Figure 4.1F, G)*. Importantly, these high molecular weight species co-immunoprecipitated with endogenous MAPL, indicating that MAPL binds to the Vps26A/Vps35 retromer complex in HeLa cells *(Visualized with an 8 % gel, arrows in Figure 4. 1F,G)*.

Figure IV-1 MAPL and Vps35 are in a complex

A) 5mg of bacterially purified GST:MAPL-RING or GST alone were incubated with 50 mg of human placenta cytosol. The RING domain and binding partners were subsequently eluted upon cleavage by thrombin. After staining with Coomassie blue, bands were excised and sent for mass spectrometry analysis. B) LC-MS/MS analysis identified 8 peptides matching Vps35, as listed in the table. Mascot scores and probabilities are indicated. C) 50μg of human placental post-mitochondrial supernatant, along with the elutions from the affinity column, were probed with α-Vps35 and α-Vps26A antibodies, as indicated. D) Vps35:YFP and MAPL:Flag, or MAPLH319L:Flag were co-transfected into HEK293T cells for 16 hours before cells were solubilized and immunoprecipitated with α-Flag-agarose beads. The Western blots were decorated with α-FP to detect Vps35, and α-Flag to visualize MAPL. The arrow indicates Vps35:YFP. E) MAPL:Flag or MAPLH319L:Flag were transfected into HeLa cells and immunoprecipitated with α-Flag agarose beads. The co-immunoprecipitation of endogenous Vps35 was revealed using α-Vps35 antibodies. F) and G) The post-nuclear supernatant of HeLa cells were collected and then incubated with or without 1mM of the Bis-maleimidohexane cross-linker (BMH), as indicated. After quenching the crosslinker with DTT and solubilizing the extacts endogenous MAPL was immunoprecipitated from the BMH-treated samples. Inputs without crosslinker were analyzed by SDS-PAGE using a 4-20% acrylamide gel, whereas the inputs and immunoprecipitations with crosslinker were an analyzed using 8% SDS-PAGE. Western Blot analysis was performed to reveal Vps26A (F), or Vps35 (G). The arrow indicates the cross-linked products.

The retromer complex has not been localized to mitochondria, so we next tested whether Vps35 may be recruited to mitochondria. Over-expressed Vps35:YFP is mainly cytosolic with a few punctuate structures, consistent with its established endosomal localization (1). However, when CFP:MAPL was co-expressed with Vps35:YFP, a fraction of the Vps35:YFP was recruited to MAPL positive vesicular structures *(Figure 4.2A white circle)*, or to sub-domains along the mitochondria *(Figure 4.2A, white arrows)*. To confirm the colocalization of Vps35:YFP and CFP:MAPL, time-lapse imaging was used to test whether the two structures move coordinately within the cell *(Figure 4.2B)*. In the acquired video, a tubulated MAPL-positive structure labeled with Vps35:YFP at the tip is seen to pinch off and move upward through the cell. We then quantified the number of cells where Vps35:YFP was visibly recruited to mitochondria using confocal microscopy. The data show that Vps35:YFP was recruited to mitochondria in 10% of cells transfected with OCT:CFP as a mitochondrial marker. This recruitment was increased in cells transfected with CFP:MAPL, where 25% of the cells contain mitochondria labeled with Vps35:YFP (Student's t-test, $p<0.05$). This indicates that the recruitment of Vps35:YFP to the mitochondria is enhanced upon MAPL expression, consistent with a functional interaction (Figure 4.2C). Finally, we further confirmed the presence of endogenous Vps35 on mitochondria by both immunofluorescence and electron microscopy (EM) *(Figure 4.2D, E)*. The specificity of the Vps35 antibody was demonstrated using RNAi treated cells silenced for Vps35, where the staining was reduced to background *(Figure 4.3)*. Both by EM and fluorescence, the Vps35 antibody labeled numerous structures within the cell, consistent with previous studies *(Figure 4.2D, E)*. In addition to this label, we also observed

enrichment for endogenous Vps35, either by gold or by immunofluorescence, on mitochondria, in agreement with the overexpression studies.

Figure IV-2 Vps35 is recruited to emerging MDVs enriched for MAPL

A) CFP:MAPL and Vps35:YFP were co-transfected into HeLa cells for 16 hours. Representative confocal images acquired to visualize the transfected proteins are indicated. The white circle highlights Vps35:YFP recruitment to MAPL-positive vesicular structures and the white arrows to the mitochondria. Scale bar: 20 microns B) Confocal time-lapse imaging of CFP:MAPL and Vps35:YFP transfected into HeLa cells shows the recruitment of Vps35:YFP to the CFP:MAPL labeled mitochondria, and the movement of the vesicle through the cell. Scale bar: 1 micron. C) Quantification of the recruitment of Vps35:YFP to the mitochondria. Cells were transfected with OCT:CFP or CFP:MAPL and Vps35:YFP. The number of cells with Vps35:YFP positive structures co-localizing with the mitochondrial marker was quantified. 60 cells were analyzed from three independent experiments. The graph represents the mean and standard error around the mean. D) To observe endogenous Vps35 recruitment to mitochondria, HeLa cells were transfected with MAPL:YFP, fixed and stained for endogenous Vps35. The white arrow highlights the recruitment of Vps35:YFP to the mitochondria. Scale bar: 20 microns. E) Cells expressing CFP-MAPL were immunolabeled with anti-Vps35 for analysis by EM. Panel i) shows the global decoration of Vps35 on endocytic structures. In ii) and iii), arrows highlight the specific label of Vps35 associated with mitochondria (M). Additional structures are seen with strong Vps35 labeling as well. Scale bars are 500nm.

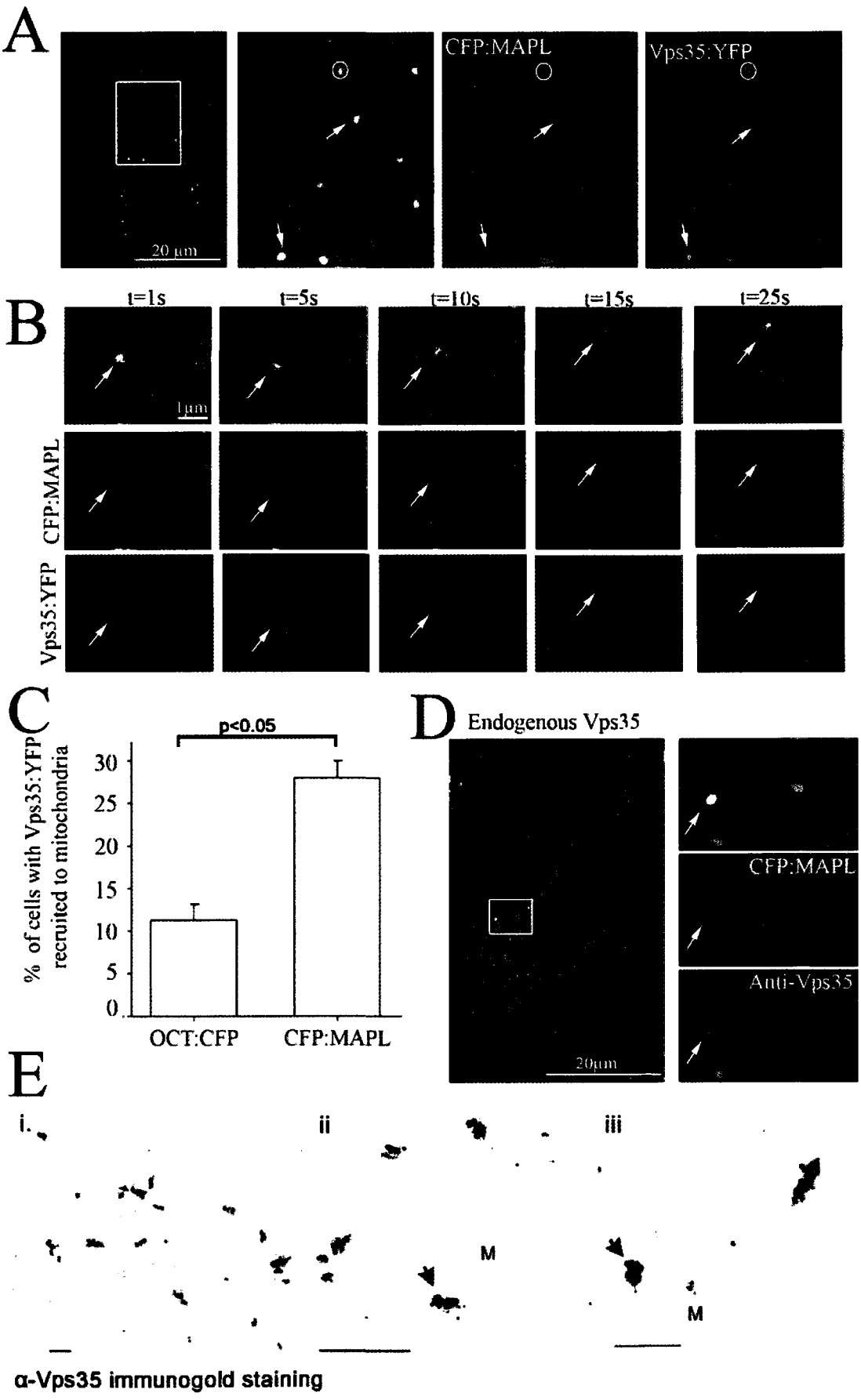
A
CFP:MAPL
Vps35:YFP
20 μm
B
t=1s
t=5s
t=10s
t=15s
t=25s
1μm
CFP:MAPL
Vps35:YFP
C
p<0.05
% of cells with Vps35:YFP recruited to mitochondria
30
25
20
15
10
5
0
OCT:CFP
CFP:MAPL
D
Endogenous Vps35
CFP:MAPL
Anti-Vps35
20μm
E
i.
ii
iii
M
M
α-Vps35 immunogold staining

Figure IV-3 Specificity of theVps35 antibody

HeLa cells were transfected with Vps35 RNAi or a Non Targeted control for 72 hours. The cells were then fixed and stained with antibodies against PRDX3, as a mitochondrial marker, and Vps35.

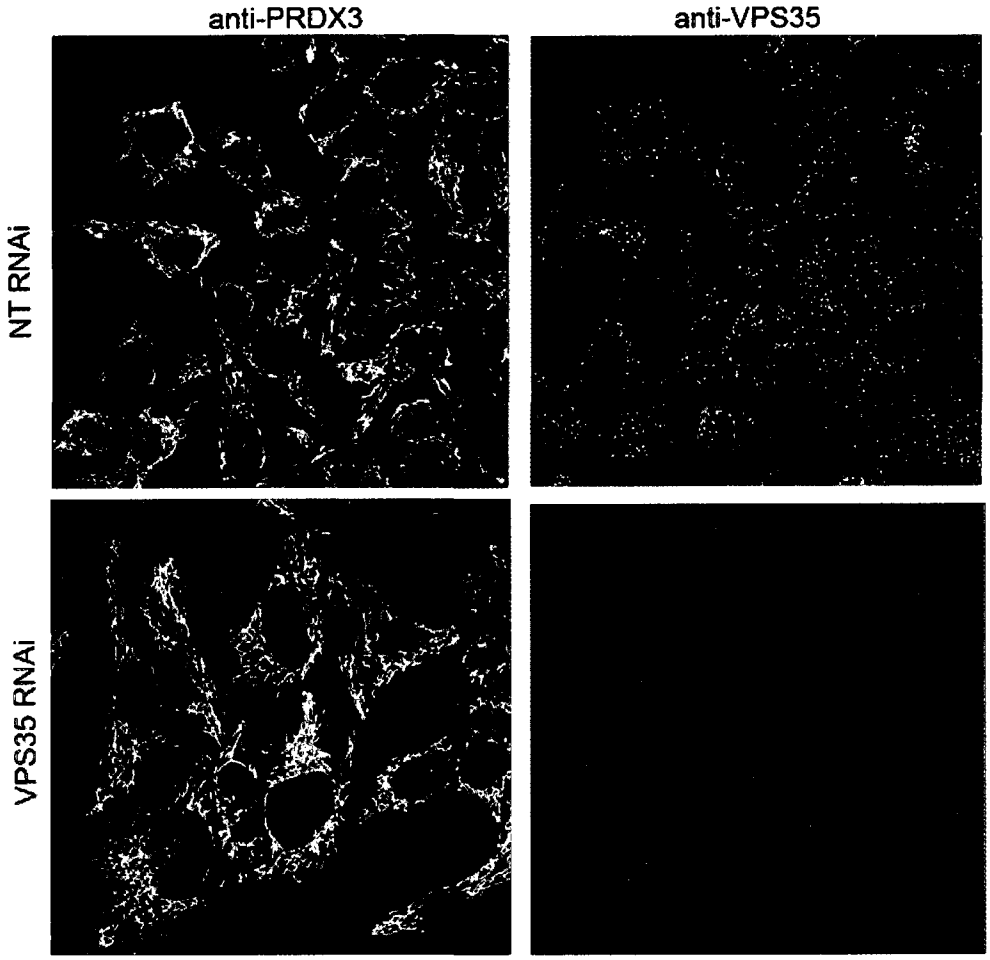
anti-PRDX3
anti-VPS35
NT RNAi
VPS35 RNAi

Since MAPL over-expression increased the recruitment of Vps35 to the mitochondria, we next wanted to confirm endogenous Vps35 recruitment to mitochondria using biochemical fractionation, and test whether its recruitment required the presence of MAPL *(Figure 4.4A)*. We used siRNA to transiently knock-down MAPL (or non-targeted siRNA) in HeLa cells *(Figure 4.4A)* for 60 hours. Mitochondria from these two cell lines were fractionated using differential centrifugation and further purified using a percoll gradient. The whole cell extract (WCE), cytosolic and mitochondrial fractions were probed for a number of markers. The purity of the mitochondrial fractions was demonstrated by the enrichment of mitochondrial markers VDAC and MAPL, and the absence of markers for the early endosomes, golgi apparatus and cytosol. Consistent with our previous results, endogenous Vps35 was present in the mitochondrial fractions. The retromer complex has been associated with retrograde transport of cargo from Rab5-positive, early endosomes (12, 18-20), so the absence of the Early Endosome Antigen 1 (EEA1) in the fractions indicates that the recruitment of Vps35 to mitochondria is not due to contaminating early endosomes. We did observe the presence of the Lysosomal Associated Protein 1 (LAMP1), a lysosomal marker, cofractionating within our mitochondrial preparations. However, the extent of lysosomal proteins within these fractions was variable between the three independent runs *(Figure 4.5)*, whereas the levels of Vps35 were unchanged *(Figure 4.4B)*. This indicates that the Vps35 signal in the mitochondrial fraction corresponds to Vps35 recruited to mitochondria and not to the contaminating late endosomes/lysosomes. Importantly, the silencing of MAPL did not affect the level of Vps35 recruitment to mitochondria *(Figure 4.4B)*, suggesting that other mitochondrial binding partners must exist for Vps35.

Figure IV-4 Vps35 recruitment to mitochondria is MAPL-independent

A) Whole cell extract (WCE), cytosolic, and percoll purified mitochondrial fractions from $45x10^6$ HeLa cells treated either with siRNA directed against MAPL or a Non-Targeted (NT) siRNA control were separated by SDS-PAGE. Western blots were stained with α-Vps35, α-MAPL, α-Giantin (Golgi marker), α-EEA1 (Endosomal marker), α-Calnexin (ER marker), α-tubulin (cytosolic marker), and α-VDAC (mitochondrial marker). B) Quantification of the amount of mitochondrial Vps35 in cells treated with Non-Targeted or treated with RNAi directed against MAPL. The data was quantified from 3 independent experiments. The graph represents the mean and the standard error around the mean.

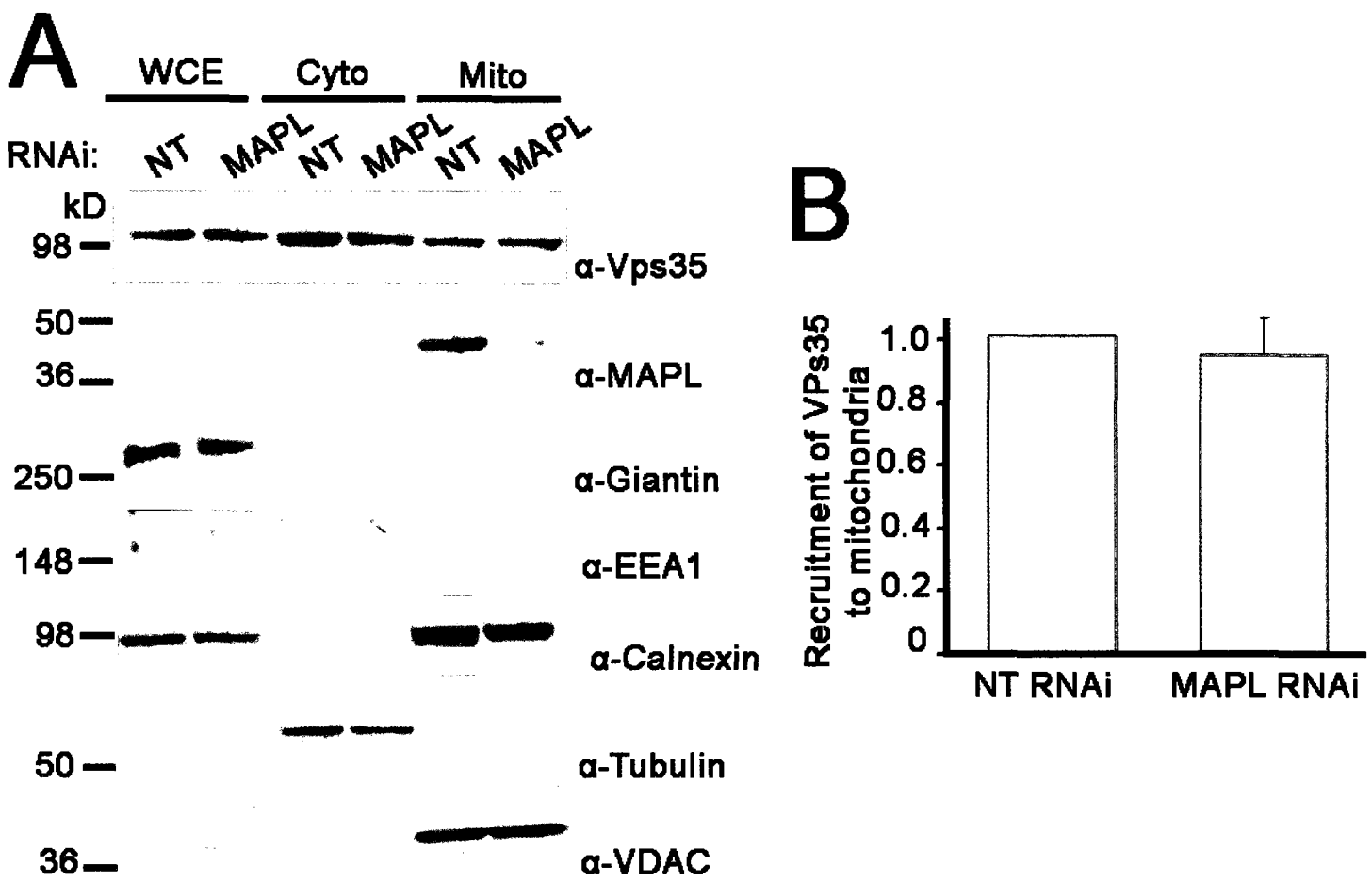
A
WCE
Cyto
Mito
RNAi:
NT
MAPL
NT
MAPL
NT
MAPL
kD
98
50
36
250
148
98
50
36
α-Vps35
α-MAPL
α-Giantin
α-EEA1
α-Calnexin
α-Tubulin
α-VDAC
B
Recruitment of VPs35 to mitochondria
1.0
0.8
0.6
0.4
0.2
0
NT RNAi
MAPL RNAi

Figure IV-5 Lysosomal contamination of the mitochondrial preparations

Western blots from the three independent experiments described in Figure 3A) and 3B) reveal the variation in Lamp1 association with mitochondria isolated from the percoll gradients. The star indicates a non-specific band.

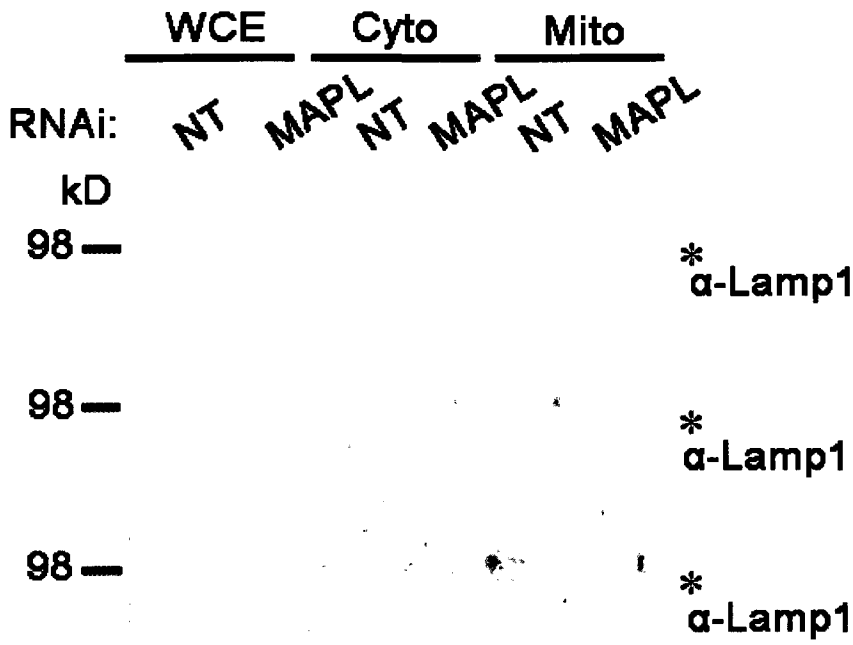
WCE
Cyto
Mito
RNAi:
NT
MAPL
NT
MAPL
NT
MAPL
kD
98
*
α-Lamp1
98
*
α-Lamp1
98
*
α-Lamp1

Since MAPL is present on vesicular profiles and Vps35 is part of the retromer complex, we considered that Vps35 may be required for the formation of MAPL-containing MDVs. To track the fate of newly synthesized MAPL en route to the peroxisomes, we employed an inducible Tet-On system to study YFP:MAPL MDV transport. Vps35 was silenced for 48 hours in MCF7 cells expressing a doxycycline responsive transactivator. The cells were then transiently transfected with the inducible plasmid encoding YFP:MAPL. The cells were treated with doxycycline for 3 hours to induce expression. This pulse of new synthesis was chased forward by the addition of cycloheximide for another 2 hours. The peroxisome delivery of YFP:MAPL was then analyzed by immunofluorescence *(Figure 4.6A)*. We quantified YFP:MAPL positive peroxisomes stained with the integral membrane protein Pmp70 in cells silenced for Vps35 relative to control cells *(Figure 4.6B)*. The data shows that there is a 50% reduction in the number of YFP:MAPL peroxisomes per cell in the cells treated with Vps35 RNAi compared to the cells treated with the non-targeted RNAi, indicating that the downregulation of Vps35 leads to a significant reduction in the rates of YFP:MAPL transport to peroxisomes (Student's t-test, $p<0.05$, n=52-54) *(Figure 4.6 B, C)*. The loss of Vps35 leads to the destabilization of the other components of the retromer complex (12, 19, 21). We confirmed that the downregulation of Vps35 leads to reduced levels of Vps26A, and that the loss of Vps26A leads to a partial destabilization of Vps35 by Western blot analysis, with MAPL and Hsp70 levels unaffected *(Figure 4.7A)*. Consistent with these results, the loss of Vps26A also led to a significant reduction in the number of YFP:MAPL positive peroxisomes per cell (Student's t-test, $p<0.05$) *(Figure 4.7B)*.

Finally, we have previously shown that different populations of MDVs are present in cultured cells. To determine whether the retromer may function in multiple MDV transport routes, we quantified the number of TOM20 positive, cytochrome c negative vesicles per cell in the presence or absence of Vps35 *(Figure 4.6C)*. Interestingly, the number of TOM20 positive MDVs is increased upon the downregulation of Vps35 *(Figure 4.6C)*, indicating that the retromer complex is not required for the generation of TOM20-containing MDVs. It is currently unclear why TOM 20 MDVs are increased upon Vps35 silencing; one possibility is that the loss of the mitochondrial to peroxisomal transport may lead to a metabolic stress that triggers the formation of TOM20 MDVs.

Figure IV-6 Vps35 is required for the formation of MAPL MDVs

A) Stable MCF7 cells expressing the Tet-ON Advanced plasmid treated with Non-Targeted (NT) or Vps35 RNAi for 48 hours, were then transfected with the inducible YFP:MAPL plasmid. YFP:MAPL expression was induced with doxycycline for 3 hours, followed by a cycloheximide chase for 2 hours. Cells were then fixed and stained for peroxisomal Pmp70 and the mitochondrial cytochrome c marker, and confocal images were obtained, as indicated. Circles indicate the colocalization of MAPL with a sub-population of peroxisomes, which are reduced upon Vps35 silencing. B) Quantification of the number of YFP:MAPL-positive peroxisomes per cell in each condition were obtained from 52-54 cells from 3 independent experiments. The graph represents the mean and standard error around the mean. To confirm efficient Vps35 silencing in these experiments, whole cell extracts were probed with α-Vps35 and α-Hsp70 (loading control) as indicated. D) HeLa cells were treated with Non-Targeted RNAi (NT) or Vps35 RNAi for 72 hours and the number of TOM20-positive, cytochrome c negative MDVs per cell were counted. 60 cells from 3 independent experiments were analyzed. The graph represents the mean and standard error around the mean. To confirm efficient Vps35 silencing in these experiments, whole cell extracts were probed with α-Vps35 and α-Hsp70 (loading control) as indicated.

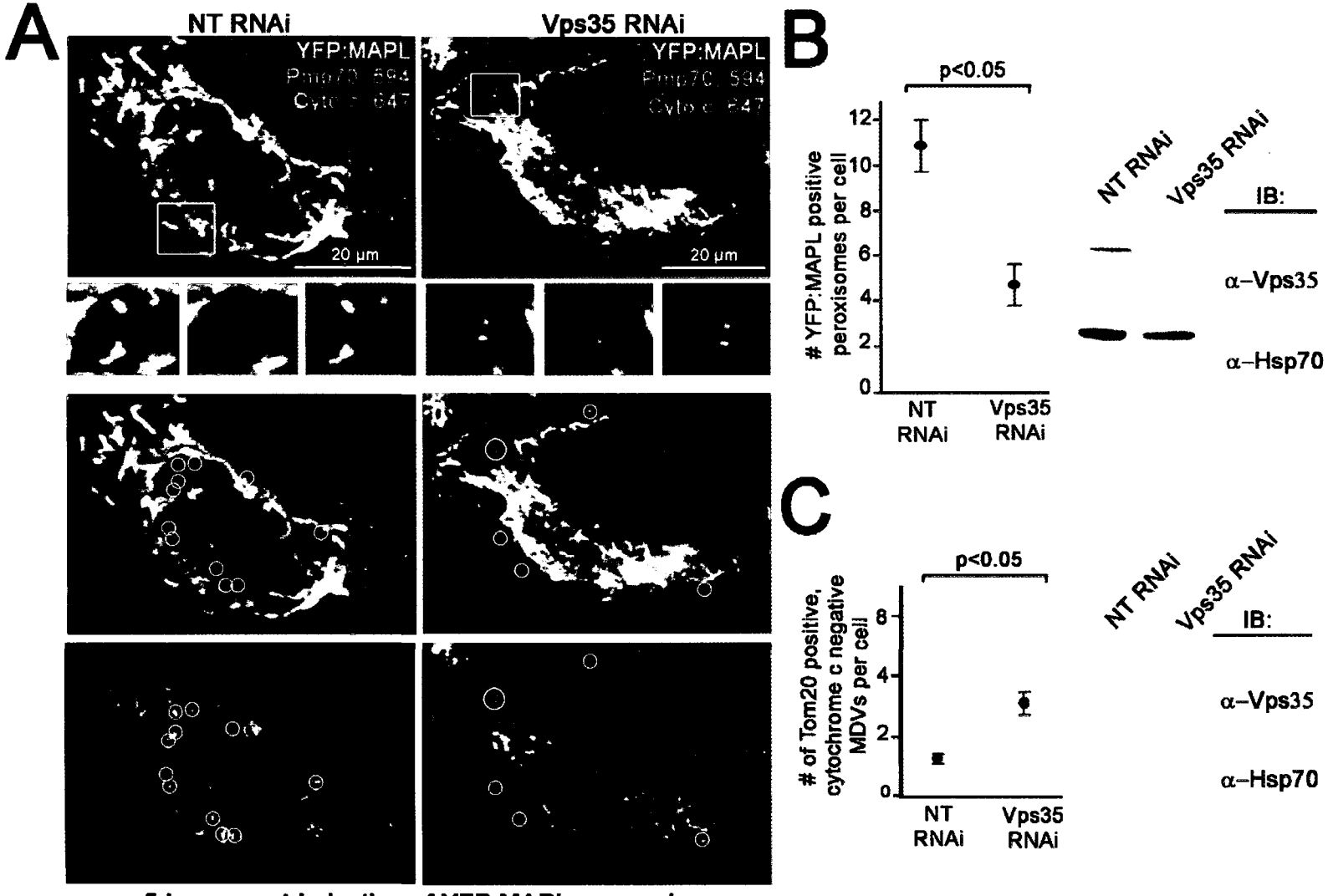

5 hours post-induction of YFP:MAPL expression.

Figure IV-7 Vps26A is required for the formation of MAPL MDVs

A) As in Figure 4, stable MCF7 cells expressing the Tet-ON Advanced plasmid treated with Non-Targeted (NT), Vps26A RNAi, or Vps35 RNAi for 48 hours, were then transfected with the inducible YFP:MAPL plasmid. YFP:MAPL expression was induced with doxycycline for 3 hours, followed by a cycloheximide chase for 2 hours. Cells were then fixed and stained for peroxisomal Pmp70 and the mitochondrial Cytochrome c marker. The quantification of the number of YFP:MAPL-positive peroxisomes per cell in each condition were obtained from 45 cells from 3 independent experiments. The graph represents the mean and standard error around the mean. B) To confirm efficient silencing in these experiments, whole cell extracts were probed with α-Vps35, α-Vps26 and α-Hsp70 (loading control) as indicated. The immuno-detection of MAPL shows that the levels endogenous of MAPL are not changed upon the downregulation of Vps35 or Vps26A.

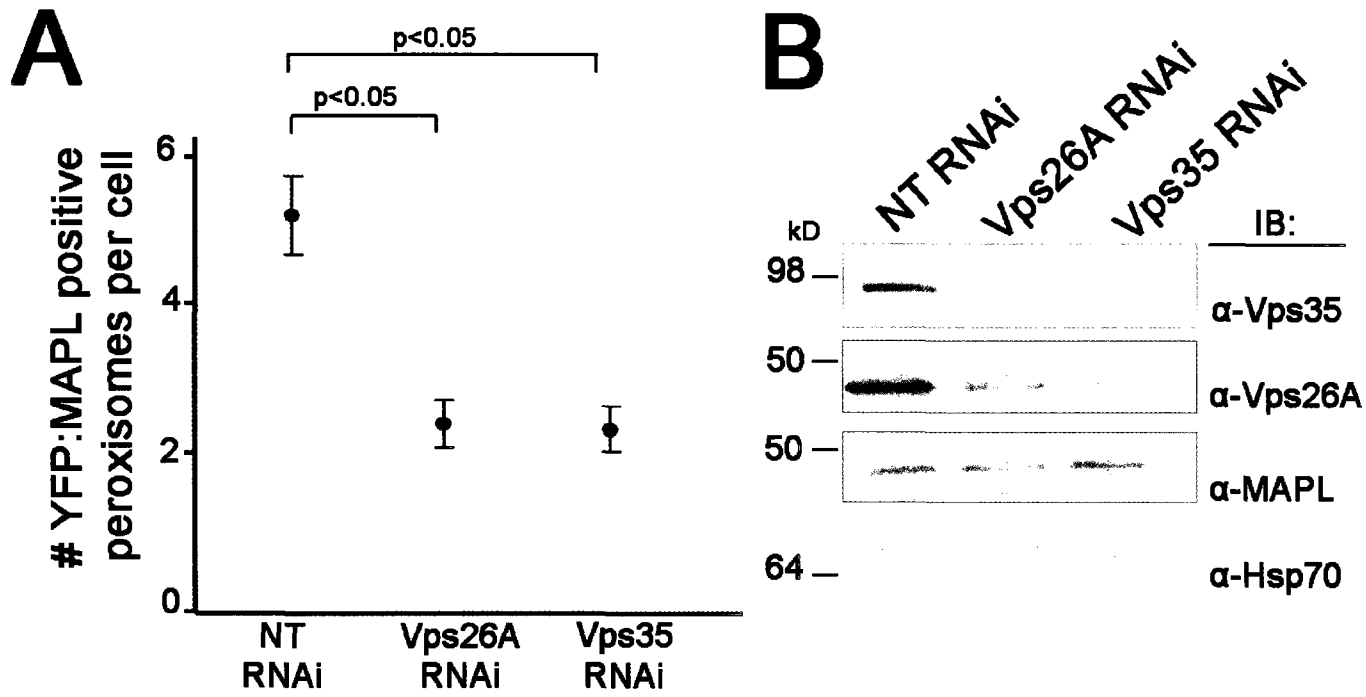
A
p<0.05
p<0.05
YFP:MAPL positive peroxisomes per cell
6
4
2
0
NT RNAi
Vps26A RNAi
Vps35 RNAi
B
NT RNAi
Vps26A RNAi
Vps35 RNAi
kD
IB:
98
α-Vps35
50
α-Vps26A
50
α-MAPL
64
α-Hsp70

IV.4 Materials and Methods

Antibodies and constructs

Antibodies were purchased from the following providers: mouse anti-cytochrome c, mouse anti-tubulin and mouse anti-EEA1 from BD Bioscience (Mississauga, ON, Canada), anti-Flag HRP from Sigma-Aldrich (Oakville, ON, Canada), mouse anti-Vps35 and mouse anti-Vps26A from Abnova (Walnut, CA, USA), mouse anti-FP from Clonetech (Burlington, ON, Canada), mouse anti-HSP70 and rabbit calnexin from Stressgen (Cedarlane, Burlington, ON, Canada), mouse anti-Lamp1 and rabbit anti-TOM20, from Santa Cruz Biotechnology (Santa Cruz, CA, USA), rabbit anti-giantin and rabbit anti-pmp70 from Abcam (Cambridge, MA, USA), anti-MAPL was previously described (2). Secondary goat anti-mouse- or goat anti-rabbit-conjugated antibodies were from Molecular Probes (Invitrogen, Burlington, ON, CA). General chemicals were obtained from Sigma-Aldrich (Oakville, ON, Canada) unless otherwise stated. The protease inhibitor cocktail was purchased from Roche, (Mississauga, ON, Canada).

MAPL:Flag, MAPL:YFP, CFP:MAPL and GST-MAPL$_{(257-352)}$ have been described (2). Vps35:YFP was a generous gift from Dr. R. Teasdale (University of Queensland, Australia). To clone the pTRE-Tight YFP:MAPL plasmid, MAPL was first inserted in a pEYFP C3 vector using the following primers: 5' GAA GAT CTG ATG GAG AGC GGA GGG CGG 3' and 5'CCC AAG CTT TTA GCT CTT GTA CAG GGG TAT 3', containing the BglII and HindIII sites. The YFP:MAPL construct was then isolated using the Nhe1 and HindIII sites and inserted into the pTRE-tight vector (Clonetech, Burlington, ON, Canada).

YFP:MAPL induction

The MCF7 Tet-ON Advanced Cell Line (Clonetech, Burlington, ON, Canada) was maintained in Dulbecco's Modified Eagle Medium (GIBCO Invitrogen, Burlington, ON, Canada) supplemented with 10% tetracycline-free fetal bovine serum (Clonetech, Burlington, ON, Canada), 2mM L-glutamine and 250ug/mL G418. MCF7 cells were seeded in 6 well plates coated with 50ug/mL fibronectin at ~50% confluency. The cells were then transfected in media free of G418 with 100nM ON Target siRNA (Dharmacon, Lafayette, Colorado) for 48 hours using DharmaFECT transfection reagent 1 (Dharmacon, Lafayette, Colorado). The cells were then washed and transfected with 4ug per well of the pTight YFP:MAPL plasmid using Lipofectamine 2000 (Invitrogen, Burlington, ON, Canada). Following 24 hours of transfection the cells were washed and the expression of YFP:MAPL was induced using 2ug/mL doxycycline (Clonetech, Burlington, ON, Canada) for 3 hours. The cells were then washed and incubated with 20ug/mL cycloheximide for 2 hours before fixing and staining using a standard protocol.

Immunoprecipitations

Immunoprecipitations were performed using HeLa or HEK293 cells (ATCC, Manassas, VA, USA). HeLa and HEK293T cells were maintained in Dulbecco's Modified Eagle Medium (GIBCO Invitrogen, Burlington, ON, Canada) supplemented with 10% fetal bovine serum and 2mM L-glutamine. Transfections were performed overnight at 70% confluency, using Lipofectamine 2000 (Invitrogen, Burlington, ON, Canada). HeLa cells were transfected in 15 cm^2 plates with 15ug of the indicated plasmids. HEK cells were transfected in 10cm^2 plates with 5ug of the indicated plasmids.

Following 16 hours, cells were collected and solubilized in 50mM Tris pH 7.5, 100mM NaCl, 5mM $MgCl_2$, 1% Triton and protease inhibitor cocktail for 60 minutes. Insoluble material was removed by centrifugation at 16,000 x g for 20 minutes. The supernatant was assayed for protein concentration, and 1-1.5 mg per IP point was incubated overnight at 4 degrees with either 20 uL 1:1 Flag resin (Sigma-Aldrich, Oakville, ON, Canada) or 2.5 μg G-protein agarose coupled mouse IgG (Sigma-Aldrich, Oakville, ON, Canada). After washing three times, the beads were mixed with loading sample buffer, separated on 4-20% acrylamide gels, and blotted with the indicated antibodies.

For the crosslinking experiments, HeLa cells plated at ~80% confluency were washed in PBS, and recovered by scraping in 1mL of Mitochondria Isolation Buffer (MRB: 225mM Manitol, 75mM Sucrose, 20mM Hepes pH 7.4, protease inhibitor tablets). The cells were recovered by centrifugation at 600 x g for 5 minutes, and resuspended in a minimal volume of MRB. The cells were then broken on ice with a ball-bearing cell breaker. The cell lysate was then centrifugated at 800 x g for 1.5 minutes using an eppendorf microcentrifuge, and the post-nuclear supernatant (PNS) was subjected to another centrifugation at 800 x g for 1.5 minutes. The concentration of the PNS was calculated, adjusted to 1mg/mL, and 1mg was subsequently used for each IP point. EDTA was added to a final concentration of 5mM before the addition of 1mM of Bis-maleimidohexane (BMH: Pierce, distributed by Sigma-Aldrich, Oakville, ON, Canada). Following 1 hour incubation at 25 degrees, the BMH was quenched with the addition of 10mM DTT final for 15 minutes at 25 degrees. The PNS was diluted 2.5 times with MRB and Triton was added to a final concentration of 1%. The PNS was solubilized for 45 minutes at 4 degrees. Insoluble material was removed by centrifugation for 30 minutes at 16,000 x g. The cell lysate was then incubated overnight

with either 20uL 1:1 protein A agarose (Upstate distributed by Millipore, Billerica, MA, USA) and 50uL serum directed against MAPL or 10ug of Rabbit IgG (Sigma-Aldrich, Oakville, ON, Canada). After washing three times in MRB supplemented with 1% Triton, the beads were mixed with loading sample buffer, separated on 8% or 4-20% acrylamide gels, and blotted with the indicated antibodies.

Immunofluorescence

For immunofluorescence, cells previously seeded onto coverslips were washed three times with phosphate-buffer and fixed in 4% paraformaldehyde in PBS for 15 minutes at 37 degrees. Cells were permeabilized and blocked in 10% fetal bovine serum, 0.1% Triton X-100 in PBS for 30 minutes at room temperature. Cells were then incubated with primary antibody for 1 hour at 1:1000 dilution. Following extensive washes in 5% fetal bovine serum in PBS cells were incubated with goat anti-mouse- or goat anti-rabbit conjugated secondary antibodies (Molecular Probes). Cells were then washed with PBS, mounted and imaged using an FV1000 laser scanning confocal microscope (IX80, Olympus) equipped with a 100X objective 133 NA 1.4. All images were obtained using sequential image acquisition, and the figures were assembled in Adobe Photoshop. A 1 pixel Gaussian blur filter was applied within Photoshop in Figure 4 to better define the signals relative to the noise.

Subcellular Fractionation

The mitochondria isolation protocol was developed using established methods (22). Briefly, $3x10^6$ HeLa cells were plated in $15cm^2$ dishes. 6 hours after seeding, the cells were transected with 50nM of ON Target siRNA pool directed against MAPL or a non-targeted siRNA control pool using DarmaFECT transfection reagent 1 (Dharmacon, Lafayette,

Colorado). 15 dishes were used for each condition. 72 hours after the transfection, cells were trypsinized, washed in PBS and resuspended in a minimal volume of Isolation Buffer (IB: 225mM Manitol, 75mM Sucrose, 20mM Hepes pH=7.4, 0.1mM EGTA). The cells were then homogenized using a Telfon Potter homogenizer (Wheaton Industries Inc., Millville, NJ, USA) at 3,000 rpm, until ~80% of cell breakage. MRB was added to the cell homogenate to a final volume of 20mL, which was then centrifugated at 600 x g for 5 minutes in a SS34 rotor (Sorvall, Fisher Scientific Company, Toronto ON, Canada) to remove nuclear contaminants. The supernatant was once again centrifugated at 600 x g for 5 minutes, followed by a centrifugation at 7,000 x g for 10 minutes in a SS34 rotor to isolate mitochondria. The supernatant was centrifugated at 200,000 x g in a TLA 110 rotor (Beckman Coulter, Mississauga, ON, Canada) to collect the cytosolic fraction. The mitochondrial pellet was washed in 20mL IB, centrifugated at 7,000 x g for 10 minutes, resuspended in 20mL IB, centrifugated at 10,000 x g for 10 minutes and finally resuspended in 2 mL Resuspention Buffer (RB: 225mM Manitol, 5mM hepes pH 7.4, 0.5mM EGTA). Using clear Polyallomer ultracentrifuge tubes (Beckman Coulter, Mississauga, ON, Canada), the mitochondrial fraction was overlaid on top of 7mL Percoll medium (225mM manitol, 25mM Hepes pH 7.4, 1mM EGTA and 30% Percoll (vol/vol)). 2.5mL MRB was added on top of the mitochondrial layer, followed by centrifugation at 95,000 x g in a SW41 rotor for 30 minutes at 4 degrees (Beckman Coulter, Mississauga, ON, Canada). The mitochondrial fraction was collected using a spinal needle (TSK Laboratory international Inc., Vancouver, BC, CA), resuspended in 20mL MRB buffer and centrifugated 10 minutes at 6,300 x g using a SS34 rotor. The pellet was resuspended in 1mL MRB buffer, centrifugatd at 6,300 x g in an Eppendorf microcentifuge for 2 minutes. 30ug of each

fractions was then loaded on a 4-20% polyacrylamide gel and subjected SDS-PAGE and western blot analysis.

Affinity Chromatography

A freshly collected human placenta was obtained with ethics approval. The tissue was minced, washed and decanted in PBS until little traces of blood were remaining. Two volumes of mitochondria isolation buffer were added (20 mM Hepes, pH 7.4, 220 mM mannitol, 68 mM Sucrose, 80 mM KCl, 0.5 mM EGTA, 2 mM Mg(Ac)2, 1 mM DTT, protease inhibitors). The tissue was placed in a Waring blender and homogenized. The lysate was centrifuged at 900 x g at 4 degrees for 20 minutes to remove nuclei and unbroken cells in a Sorvall SS34 rotor (Fisher Scientific Company, Toronto ON, CA). The supernatant was then transferred to a new tube for a second low speed centrifugation, as above. The second supernatant was cleared at 10,000 x g for 20 minutes at 4 degrees in a Sorvall SS34 rotor (Fisher Scientific Company, Toronto ON, CA) to isolate mitochondria, and the post-mitochondrial supernatant was snap frozen at -80 degrees C. Immediately prior to the affinity column, this supernatant was thawed, dialyzed in 50mM NaCl, 20mM Hepes pH 7.4, 2mM $MgCl_2$, 2mM β-mercaptoethanol and protease inhibitors, centrifugated at 100,000 x g for 30 minutes at 4 degrees using a Ti55.2 rotor (Beckman Coulter, Mississauga, ON, Canada) and the final protein concentration was calculated.

GST or GST-MAPL(257-352) expression was induced in E. coli BL21 strain with 0.3mM IPTG for 3 hours. Bacteria were recovered by centrifugation, resuspended in 20mM Hepes pH 7.4, 200 mM NaCl, 2 mM MgCl2, 5 mM β-mercaptoethanol, protease inhibitor cocktail, and lysed at 2000 psi using a French press. The lysate was centrifuged at 100,000 x g for 40 minutes in a Ti55.2 rotor (Beckman Coulter, Mississauga, ON, Canada). The

supernatant was then incubated with glutathione-sepharose beads for 2 hours at 4 degrees (Amersham Biosciences, Piscataway, NJ, USA). Following washes with the above buffer supplemented with 500mM NaCl then 1% Triton X-100, the amount of purified protein per bead volume was calculated. 50mg of the placenta cytosol was then incubated with 5mg of GST coupled to gluthathione-sepharose beads for 2 hours. The beads were removed by centrifugation and the pre-cleared cytosol was incubated with 5mg of GST or GST-MAPL(257-352) overnight at 4 degrees. The beads were then washed extensively and the fusion proteins were cleaved from GST using recombinant thrombin, overnight at 4 degrees, following manufacturer's instructions (Sigma-Aldrich, Oakville, ON, Canada).

Immunogold labeling by EM

HeLa cells plated on glass coverslips were left either untransfected or transfected with CFP:MAPL using Lipofectamine 2000, for 16 hours. Cells were then fixed in 4% paraformaldehyde and 0.1% glutaraldehyde in PBS. The cells were then quenched in 0.05M glycine in PBS (pH 7.4) for 15 minutes, washed thoroughly in PBS and permeabilized in 0.25% saponin and 5% bovine serum albumin (BSA) for 30 minutes. Immunolabelling was then performed using anti-Vps35 in 1% BSA, 0.05% saponin for 1 hour. Following washes in 1% BSA, 0.05% saponin, the cells were incubated with a-mouse immunoglobin G (IgG) that was conjugated to colloidal gold (1.4 nm diameter) for 1 hour (Invitrogen, Burlington, ON, Canada). Cells were washed extensively with PBS, post-fixed with 1% glutaraldehyde in PBS for 10 minutes, washed thoroughly in distilled water, before intensifying the gold labelling with a silver enhancement kit (Nanoprobes, Yaphank, NY, USA) for 5 minutes at 20 degrees, following the manufacturer's instructions. The cells were then washed extensively in distilled water and stored in 1.6% glutaraldehyde. Cells were postfixed in

0.5% OsO4 for 90 minutes at 4 degrees, washed with distilled water, incubated with 50% ethanol for 10 minutes, and stained with 2% uranyl acetate in 70% ethanol for 2 hours. The cells were further dehydrated with a graded series of ethanol and then embedded in Spurr epoxy resin. Ultrathin sections were counterstained with uranyl acetate and lead citrate. Digital images were taken with a JEOL 1230 TEM at 60kV adapted with a 2000 x 2000 pixel bottom mount CCD digital camera (Hamamatsu, Japan) and AMT software.

Statistical analysis

All Western Blot analysis was performed using the FluorChem Imaging system and software (Cell Biosciences, Santa Clara, CA). Automatic background adjustment was selected for densitometry analysis. The Sigma Plot software (Systat Software Inc, Chicago, IL, USA) was used for statistical analysis and Student's t-test to evaluate statistical significance.

IV.5 Discussion

With the identification of mitochondrial derived vesicles, we have expanded the mechanisms by which the mitochondria communicate with the peroxisomes (2, 16). This transport pathway has not yet been functionally characterized, however, our data show that the delivery of MAPL is specific to only a sub-population of peroxisomes within the cell (2) *(Figure 4.6)*. We are exploring potential functions in peroxisome biogenesis, fatty acid catabolism and potential signaling pathways that could relate to the SUMOylation activity of MAPL on the peroxisomes (16). However, an obvious first step in our ability to examine the functional impact of mitochondria to peroxisome transport is the identification of the

machinery that governs this event. In an unbiased screen for MAPL interacting proteins, we have identified the retromer complex as a candidate coat protein to facilitate MDV formation. Experiments presented here demonstrate that Vps35, Vps26A and MAPL are found in a complex *(Figure 4.1)*, and both EM and confocal imaging techniques have confirmed the presence of endogenous Vps35 in association with sub-domains of the mitochondria *(Figure 4.2)*. Although MAPL is a SUMO E3 ligase (15), its enzymatic activity does not appear to be requisite for efficient Vps35 binding to MAPL. Functionally, we have demonstrated that silencing Vps35 or Vps26A inhibits the formation of MAPL-MDVs and their subsequent delivery of MAPL to the peroxisome. Importantly, we had previously been unable to modulate vesicle delivery to peroxisomes (2), so the inhibition of this transport route is an important further validation of the pathway.

The function of the retromer complex on mitochondria might suggest the presence of mitochondrial sorting nexins, clathrin and related chaperones like RME-8 and Rab GTPases that could also participate in retromer-dependent MDV transport (20, 21, 23). Although a role for these types of proteins at the mitochondria has not yet been widely considered, our data may be consistent with emerging studies suggesting that the retromer complex may function in multiple intracellular transport pathways. It has been proposed, for example, that the combinatorial use of paralogues of the retromer components, and different adaptor sorting nexin proteins may help to explain a wide range of cargo selectivity and localizations of this complex (14, 24-26). It is not unprecedented that the mitochondria utilize structural adaptors and enzymes in common with the endocytic and biosynthetic pathways (27). Proteins like synaptojanin 2A (28), endophilin B1(29, 30), Rab32 (31), WAVE-1 (32), and a mitochondrial phospholipase D (33) are known to affect mitochondrial function and

dynamics. Together, these data demonstrate that the transport and morphology of mitochondrial membranes share many features with the more established pathways in cell biology. With the identification of some of the machinery required for MDV transport to peroxisomes, we have a tool to help us dissect this pathway and further characterize the regulatory machinery.

IV.6 References

1. Bonifacino, J.S., and J.H. Hurley. 2008. Retromer. Curr Opin Cell Biol 20:427-436.
2. Neuspiel, M., A.C. Schauss, E. Braschi, R. Zunino, P. Rippstein, R.A. Rachubinski, M.A. Andrade-Navarro, and H.M. McBride. 2008. Cargo-selected transport from the mitochondria to peroxisomes is mediated by vesicular carriers. Curr Biol 18:102-108.
3. Poirier, Y., V.D. Antonenkov, T. Glumoff, and J.K. Hiltunen. 2006. Peroxisomal beta-oxidation--a metabolic pathway with multiple functions. Biochim Biophys Acta 1763:1413-1426.
4. Schrader, M., and H.D. Fahimi. 2006. Peroxisomes and oxidative stress. Biochim Biophys Acta 1763:1755-1766.
5. Wu, Z., P. Puigserver, U. Andersson, C. Zhang, G. Adelmant, V. Mootha, A. Troy, S. Cinti, B. Lowell, R.C. Scarpulla, and B.M. Spiegelman. 1999. Mechanisms controlling mitochondrial biogenesis and respiration through the thermogenic coactivator PGC-1. Cell 98:115-124.
6. Mandard, S., M. Muller, and S. Kersten. 2004. Peroxisome proliferator-activated receptor alpha target genes. Cell Mol Life Sci 61:393-416.
7. Koch, A., Y. Yoon, N.A. Bonekamp, M.A. McNiven, and M. Schrader. 2005. A role for Fis1 in both mitochondrial and peroxisomal fission in mammalian cells. Mol Biol Cell 16:5077-5086.
8. Kobayashi, S., A. Tanaka, and Y. Fujiki. 2007. Fis1, DLP1, and Pex11p coordinately regulate peroxisome morphogenesis. Exp Cell Res 313:1675-1686.
9. Delille, H.K., and M. Schrader. 2008. Targeting of hFis1 to peroxisomes is mediated by Pex19p. J Biol Chem 283:31107-31115.
10. Gandre-Babbe, S., and A.M. van der Bliek. 2008. The novel tail-anchored membrane protein Mff controls mitochondrial and peroxisomal fission in mammalian cells. Mol Biol Cell 19:2402-2412.
11. Popoff, V., G.A. Mardones, D. Tenza, R. Rojas, C. Lamaze, J.S. Bonifacino, G. Raposo, and L. Johannes. 2007. The retromer complex and clathrin define an early endosomal retrograde exit site. J Cell Sci 120:2022-2031.
12. Arighi, C.N., L.M. Hartnell, R.C. Aguilar, C.R. Haft, and J.S. Bonifacino. 2004. Role of the mammalian retromer in sorting of the cation-independent mannose 6-phosphate receptor. J Cell Biol 165:123-133.
13. Seaman, M.N., J.M. McCaffery, and S.D. Emr. 1998. A membrane coat complex essential for endosome-to-Golgi retrograde transport in yeast. J Cell Biol 142:665-681.
14. Haft, C.R., M. de la Luz Sierra, R. Bafford, M.A. Lesniak, V.A. Barr, and S.I. Taylor. 2000. Human orthologs of yeast vacuolar protein sorting proteins Vps26, 29, and 35: assembly into multimeric complexes. Mol Biol Cell 11:4105-4116.

15. Braschi, E., R. Zunino, and H.M. McBride. 2009. MAPL is a new mitochondrial SUMO E3 ligase that regulates mitochondrial fission. EMBO Rep 10:748-754.

16. Andrade-Navarro, M.A., L. Sanchez-Pulido, and H.M. McBride. 2009. Mitochondrial vesicles: an ancient process providing new links to peroxisomes. Curr Opin Cell Biol 21:560-567.

17. Seaman, M.N. 2005. Recycle your receptors with retromer. Trends Cell Biol 15:68-75.

18. Johannes, L., and V. Popoff. 2008. Tracing the retrograde route in protein trafficking. Cell 135:1175-1187.

19. Seaman, M.N. 2004. Cargo-selective endosomal sorting for retrieval to the Golgi requires retromer. J Cell Biol 165:111-122.

20. Rojas, R., T. van Vlijmen, G.A. Mardones, Y. Prabhu, A.L. Rojas, S. Mohammed, A.J. Heck, G. Raposo, P. van der Sluijs, and J.S. Bonifacino. 2008. Regulation of retromer recruitment to endosomes by sequential action of Rab5 and Rab7. J Cell Biol 183:513-526.

21. Popoff, V., G.A. Mardones, S.K. Bai, V. Chambon, D. Tenza, P.V. Burgos, A. Shi, P. Benaroch, S. Urbe, C. Lamaze, B.D. Grant, G. Raposo, and L. Johannes. 2009. Analysis of articulation between clathrin and retromer in retrograde sorting on early endosomes. Traffic 10:1868-1880.

22. Wieckowski, M.R., C. Giorgi, M. Lebiedzinska, J. Duszynski, and P. Pinton. 2009. Isolation of mitochondria-associated membranes and mitochondria from animal tissues and cells. Nat Protoc 4:1582-1590.

23. Shi, A., L. Sun, R. Banerjee, M. Tobin, Y. Zhang, and B.D. Grant. 2009. Regulation of endosomal clathrin and retromer-mediated endosome to Golgi retrograde transport by the J-domain protein RME-8. Embo J 28:3290-3302.

24. Collins, B.M., S.J. Norwood, M.C. Kerr, D. Mahony, M.N. Seaman, R.D. Teasdale, and D.J. Owen. 2008. Structure of Vps26B and mapping of its interaction with the retromer protein complex. Traffic 9:366-379.

25. Kim, E., J.W. Lee, D.C. Baek, S.R. Lee, M.S. Kim, S.H. Kim, K. Imakawa, and K.T. Chang. 2008. Identification of novel retromer complexes in the mouse testis. Biochem Biophys Res Commun 375:16-21.

26. Carlton, J., M. Bujny, A. Rutherford, and P. Cullen. 2005. Sorting nexins--unifying trends and new perspectives. Traffic 6:75-82.

27. McBride, H.M., M. Neuspiel, and S. Wasiak. 2006. Mitochondria: more than just a powerhouse. Curr Biol 16:R551-560.

28. Nemoto, Y., and P. De Camilli. 1999. Recruitment of an alternatively spliced form of synaptojanin 2 to mitochondria by the interaction with the PDZ domain of a mitocondrial outer membrane protein. EMBO J. 18:2991-3006.

29. Pierrat, B., M. Simonen, M. Cueto, J. Mestan, P. Ferrigno, and J. Heim. 2001. SH3GLB, a new endophilin-related protein family featuring an SH3 domain. Genomics 71:222-234.

30. Karbowski, M., S.Y. Jeong, and R.J. Youle. 2004. Endophilin B1 is required for the maintenance of mitochondrial morphology. J Cell Biol 166:1027-1039.

31. Alto, N.M., J. Soderling, and J.D. Scott. 2002. Rab32 is an A-kinase anchoring protein and participates in mitochondrial dynamics. J Cell Biol 158:659-668.

32. Sung, J.Y., O. Engmann, M.A. Teylan, A.C. Nairn, P. Greengard, and Y. Kim. 2008. WAVE1 controls neuronal activity-induced mitochondrial distribution in dendritic spines. Proc Natl Acad Sci U S A 105:3112-3116.

33. Choi, S.Y., P. Huang, G.M. Jenkins, D.C. Chan, J. Schiller, and M.A. Frohman. 2006. A common lipid links Mfn-mediated mitochondrial fusion and SNARE-regulated exocytosis. Nat Cell Biol 8:1255-1262.

Chapter V General conclusion

V.1 The emerging mitochondria

V.1.1 From in-vitro assays to mitochondrial dynamics

The study of mitochondria can be divided into different historical periods. The biochemistry regulating oxidative phosphorylation was initially dissected using *in vitro* assays. These provided invaluable insights into the mechanisms to produce energy, but also contributed to the image of an isolated organelle. This conception of the mitochondria was then changed as live microscopy techniques improved (1). *In vivo*, the mitochondria formed a highly interconnected network, constantly remodeled by fusion and fission events. Further studies documented the importance of mitochondrial dynamics for the proper functioning of cells (2), which is highlighted by the fact that losing core mitochondrial morphology proteins is embryonic lethal in mice, and mutations in their genes cause human diseases (3). In addition, changes in mitochondrial dynamics play important roles during different cellular events, including metabolism (4), the cell cycle (5), migration (6) and cellular stress (7). In some cases an imbalance in the fusion or fission rates of the mitochondria can interfere with these cellular processes, one example being the protection against apoptosis conferred by mitochondrial fusion (8).

The response of the mitochondrial reticulum to the cellular environment supposes that signaling cascades are able to modulate the fusion and fission rates of the mitochondria. One way in which this can be achieved is through the post-translational modification of core

mitochondrial morphology proteins, and in fact, Drp1 has been shown to be modified by a variety of post-translational modifications, including SUMOylation (9), phosphorylation (10), ubiquitination (11) and S-nitrosylation (12). Importantly, whether signaling cascades affect the rates of mitochondrial fission or fusion can lead to very different outcomes. For example, mitochondrial fragmentation impairs insulin secretion and eventually induces cell death only when fragmentation is caused by the overexpression of Fis1, and not by when it is caused by a reduction of fusion by overexpressing a dominant negative Mfn1 (13). This example highlights the great care that must be taken when interpreting mitochondrial morphology.

In addition to regulating the morphology of the mitochondrial reticulum, signaling cascades are also responsible for the coordination of mitochondrial positioning and movement. This is well illustrated in neurons, where mitochondrial dynamics are coupled to transport, and where the activation of signaling cascades promotes the docking of mitochondria to the actin cytoskeleton for short range movements (14, 15). Finally, mitochondrial dynamics can impact mitochondrial function, and, for example, in hyperglycemic conditions, the fragmentation of the mitochondria is necessary for increased oxidative phosphorylation (4).

Importantly, since the mitochondria were shown to share content during fusion events, it was often assumed that they formed a homogenous population. However, a recent study has shown that mitochondrial fission can be asymmetrical to produce one mitochondrion with high potential and a high probability of re-fusing with the network, and another mitochondrion with low potential and low levels of Opa1, preventing fusion back into the reticulum (16). The subsequent discovery that dysfunctional mitochondria are

targeted to lysosomes by Parkin, highlights the relevance of this pathway for diseases like Parkinson's (17). These studies are also important since they suggest that proteins can be enriched into selected mitochondria. This raises the possibility that specific mitochondria can be produced to respond to specific subcellular environments, for example at the synapse in neurons.

In other words, from static, isolated organelles, the mitochondria are now considered dynamic, heterogeneous organelles responsive to changes in their cellular environment. Over the course of my doctoral studies, I have further explored the idea that mitochondria are integral components of signaling networks.

V.1.2 Mitochondria as signaling organelles

Numerous examples highlight the active response of mitochondria to changes in their cellular environment. An attractive hypothesis, which would expand the role of mitochondria in the cell, is the idea that mitochondrial proteins fulfill active signaling functions.

This hypothesis is supported by studies that have demonstrated that some mitochondrial proteins can modulate signaling cascades, and is best illustrated by the fusion GTPase Mfn2. Unlike Mfn1, Mfn2 possesses low rates of hydrolysis and a high affinity for GTP, the characteristics of a signaling GTPase, as opposed to a mechanoenzyme (18). Interestingly, in a PEG fusion assay, mitochondria expressing a GTP bound, dominant active, Mfn2 were able to signal to, recruit and fuse with cells expressing *wild-type* Mfn2 (18). Since Mfn2 is a membrane anchored protein, this result implies that Mfn2 initiates signaling cascades to trigger these events (18). Interestingly, the intermembrane space

domain of Mfn2 possesses a conserved tryptophan residue, and the mutation of this residue impairs the activation of Mfn2 (18). Altogether these results suggest that the fusion capacity of Mfn2 can be regulated by intra-mitochondrial information through its conserved tryptophan residue, and by the nucleotide state of its cytoplasmic GTPase domain, which could be post-translationally modified by signaling cascades. Once activated, Mfn2 is able to signal to, and recruit other mitochondria to initiate fusion events (18).

In addition, Mfn2 has been shown to possess fusion-independent signaling functions. For example, Mfn2 is able to negatively impact cell proliferation (19), and its overexpression increases membrane potential and rates of glucose utilization (20). Importantly, although these signaling functions of Mfn2 can be isolated from its role as a fusion GTPase, in a physiological setting, fusion and signaling could fulfill complementary functions. In addition, the signaling events downstream of Mfn2 have not yet been elucidated. Mfn2 has been proposed to sequester Ras, preventing growth-factor induced G_1 progression (19). However, the signals that would trigger Ras recruitment to and release from the mitochondria are currently unknown (19). The overexpression of Mfn2 has also been shown to increase the expression of mitochondrial proteins involved in oxidative phosphorylation, and a potential role for the PGC1α signaling pathway has been suggested, although not demonstrated (21). Further studies will hopefully shed light onto the signaling pathways modulated by Mfn2, upstream regulatory events, and downstream signal transduction mechanisms. It will also be interesting to explore how mitochondrial function modulates Mfn2-mediated signaling.

In addition to the signaling function of Mfn2, different signaling cascades have had components shown to be mitochondrial residents. The innate immunity protein, the

Mitochondrial Antiviral Signaling Protein (MAVS), is an integral mitochondrial protein (22). MAVS acts downstream of the viral RNA receptor Retinoid Inducible Gene 1 (RIG1) and is essential for the activation of the Interferon Regulatory Factor 3 (IRF3), and the Nuclear Factor kappa-light-chain-enhancer of activated B cells (NF-kB) pathways (22-25). Since the discovery of MAVS, other mitochondrial proteins, including Mfn2 have also been shown to modulate innate immunity (26). However, the advantages of the mitochondrial localization of MAVS have not been elucidated yet, although a role in promoting cell death during viral infection has been proposed (27). Finally, the mammalian Target of Rapamycin (mTOR) pathway has also been linked to the mitochondria. The FK506 binding protein 8 (FKBP38), an integral mitochondrial protein, has been suggested to modulate the mTOR pathway, although this result is controversial (28, 29). mTOR itself has been localized on the mitochondria (30). It is therefore possible that mitochondria play a greater role in the modulation of this pathway then previously envisioned.

V.1.3 Discovery of MAPL and MDVs

The discovery that a number of mitochondrial proteins are SUMOylated (9) raises the possibility that SUMOylation plays a central role in mitochondrial signaling. In fact, the SUMOylation of substrates can be used to relay signaling events, by changing protein conformation, promoting or disassembling complexes (31). SUMO has mostly been studied as a nuclear modification, but an increasing number of cytoplasmic SUMO substrates have been reported (32). In most of the cases, the SUMO E3 ligase is often hypothesized to be one of the characterized nuclear SUMO E3 ligases, since no primarily cytoplasmic ligase has been characterized so far (32, 33). In addition, none of the known SUMO E3 ligases

have been localized to the mitochondria. To better understand the role of mitochondrial SUMOylation, it was therefore important to uncover the mitochondrial SUMO machinery.

To uncover a potential mitochondrial SUMO E3 ligase, a bioinformatics approach was used, which led to the characterization of MAPL (34). Over the course of my doctoral studies, I have demonstrated that MAPL SUMOylates mitochondrial proteins, including Drp1 (35) *(Chapter 2)*. In addition, to better understand the physiological function of MAPL and of mitochondrial SUMOylation, I have isolated MAPL interacting partners and characterized the mitochondrial SUMO proteome *(Chapter 3)*. My and other lab member's current research is now focused on understanding the physiological function of MAPL. Downregulating the expression of MAPL in HeLa cells, does not lead to obvious morphological cellular or mitochondrial phenotypes (34), and the function of MAPL remains elusive. However, further research with the MAPL *knock-out* mice will hopefully shed light onto the physiological functions of MAPL. The first part of my discussion will therefore focus on known roles of mitochondrial SUMOylation within cellular signaling networks.

The characterization of MAPL also led to the unexpected discovery of Mitochondrial Derived Vesicles (MDVs) (34). One population of MDVs, enriched for MAPL, are targeted to the peroxisomes, uncovering a previously uncharacterized transport mechanism between these two organelles (34). In addition, one of the interacting partners of MAPL, Vps35, is a component of a coat complex (36). I have shown that Vps35 regulates the delivery of MAPL from the mitochondria to peroxisomes, although it does not participate in the formation of TOM20 containing MDVs *(Chapter 4)*. The second part of this discussion will therefore focus on MDVs, which expand the integration of mitochondria within their cellular

environment to the exchange of content with other organelles. Finally the third part of my discussion will try to integrate the discovery that MAPL is a mitochondrial SUMO E3 ligase to its transport to peroxisomes, to formulate a unifying hypothesis.

V.2 MAPL is the first mitochondrial SUMO E3 ligase

V.2.1 Insights from the characterization of MAPL, its substrates, and partners

V.2.1.1 SUMOylation versus Ubiquitination

Using both *in-vitro* and *in-vivo* studies, I have shown that MAPL is the first mitochondrial SUMO E3 ligase (35). Not only does MAPL add to a small list of characterized SUMO E3 ligases, MAPL also represents a new type of E3 ligase, since it is anchored to a membrane and cytosolic. In addition, the characterization of MAPL was important in that it highlighted the importance of the experimental design when testing ubiquitin or SUMO E3 ligase activity. In fact, the RING domain of MAPL can act both as a ubiquitin and a SUMO E3 ligase *in-vitro* (34). However, only micromolar concentrations of MAPL will drive an *in-vitro* ubiquitination reaction, whereas MAPL is able to effectively act as a SUMO E3 ligase within nanomolar concentrations (34). In addition, unlike known ubiquitin E2 conjugating enzymes, the SUMO E2 conjugating enzyme, Ubc9, possesses catalytic activity and can conjugate SUMO by itself (34). When Ubc9 is used in excess, the SUMOylation reaction will proceed primarily in a Ubc9-dependent fashion. Only when lower concentrations of Ubc9 are used, can one detect the increased SUMOylation due to the presence of a SUMO E3 ligase. These examples highlight the care that must be taken

when characterizing a novel E3 ligase. In addition, it cannot be excluded that some SUMO E3 ligases, including MAPL, can function as ubiquitin E3 ligases under specific conditions (37). For example, the topoisomerase I binding arginine/serine-rich (TOPORS) can act both as a SUMO and a ubiquitin E3 ligase (38, 39), depending on its phosphorylation state (40).

V.2.1.2 Substrates and interacting partners

We have not yet uncovered the cellular phenotypes triggered by the down-regulation of MAPL, and the only known mitochondrial SUMO substrate is Drp1 (35).The characterization of MAPL's substrates and interacting partners was therefore important to better understand its physiological function. To identify MAPL interacting partners, we chose an affinity chromatography approach using the bacterially purified RING domain of MAPL and human placenta cytosol. Using this method, we have isolated a protein involved in vesicle formation, Vps35 (36), and proteins linked to the actin cytoskeleton, including IQGAP1 (41) and Filamin (42, 43).

To characterize the mitochondrial SUMO proteome, we isolated mitochondria and incubated them with the SUMOylation enzymes and His_6-SUMO1. Substrates conjugated or binding to His_6-SUMO1 were then isolated by metal affinity chromatography and identified by Mass Spectrometry in collaboration with Brian Raught at the University of Toronto. Obtaining SUMO proteomes can be very challenging, since there is a fine balance between specificity and sensitivity. I have performed the mitochondrial SUMO proteome three times using cow heart mitochondria at different scales and three times using fresh sHeLa mitochondria. Fresh sHeLa mitochondria gave the most robust *in-vitro* SUMO reaction and we therefore chose to focus on the proteins identified from this source. Specifically, using this method, we have successfully identified 7 potential mitochondrial SUMO substrates,

which will be invaluable to better understand the physiological function of mitochondrial SUMOylation.

V.2.2 Physiological roles of mitochondrial SUMOylation

V.2.2.1 SUMO and mitochondrial fission

One of the earliest roles attributed to mitochondrial SUMOylation has been mitochondrial fission (9). In fact, the overexpression of SUMO1 promotes mitochondrial fission, a phenotype which can be rescued by the overexpression of a dominant negative form of Drp1 (9). In solubilized extracts, Drp1 is rapidly degraded, a phenomenon which can be reversed by the overexpression of SUMO1 or by the inhibition of SUMO proteases by the cysteine alkylating agent N-Ethylmaleimide (9). These results led to the idea that SUMOylation stabilizes the protein by a yet unknown mechanism (9).

Supporting this hypothesis, I have shown that MAPL SUMOylates Drp1 *in-vitro*, and that the downregulation of MAPL leads to a 20% reduction of Drp1 protein levels (35). Finally, the overexpression of MAPL triggers mitochondrial fragmentation, which is consistent with increased Drp1 SUMOylation and stabilization (34).

V.2.2.2 The G2/M transition

SENP5 is a SUMO protease involved in the deSUMOylation of Drp1 (44). The overexpression of SENP5 rescues the fragmentation triggered by SUMO1 overexpression, unlike the overexpression of another protease, SENP2 (44). SENP5 is a primarily nucleolar enzyme, which is recruited to the mitochondria during mitosis (5). Importantly, the downregulation of SENP5 leads to a cell cycle arrest at mitosis, precisely when it should be

recruited to the mitochondria (5). In addition, mitochondria isolated from cells arrested at G_1/S are able to sustain a much stronger *in-vitro* SUMOylation reaction than mitochondria isolated from cells arrested at G_2/M (5). These results indicate that the deSUMOylation of mitochondrial substrates during mitosis might be an important function of SENP5 during the cell cycle (5) *(Figure 5.1).*

It is possible that during mitosis, in addition to the recruitment of a SUMO protease to the mitochondria, there is also a reduction in mitochondrial SUMOylation. In other words, the activity of MAPL could be decreased during mitosis. Alternatively, the activity of MAPL could be increased, such that the cycle of SUMOylation-deSUMOylation is enhanced. This could drive the formation or disassembly of Drp1 oligomers to promote mitotic mitochondrial fission.

Figure V-1 SENP5 is recruited to the mitochondria during mitosis

Blue dots represent SENP5. The yellow circles represent SUMO. During interphase, the SUMO protease SENP5 is a primarily nucleolar enzyme with a cytoplasmic pool regulating the deSUMOylation of Drp1. During mitosis, prior to the breakdown of the nuclear envelop, SENP5 is recruited to the mitochondria. This event is accompanied by a loss of mitochondrial SUMOylation and mitochondrial fragmentation.

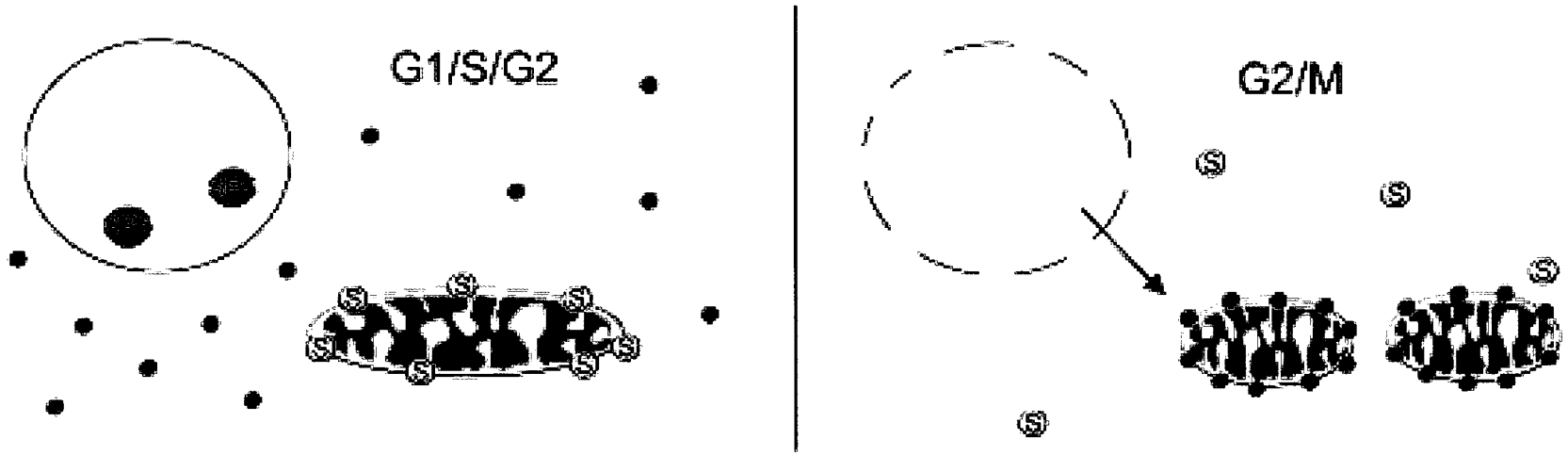
G1/S/G2
G2/M

V.2.2.3 SUMOylation of Drp1, model

The role of Drp1 during mitochondrial fission is not fully understood. In the cytosol, Drp1 forms dimers (45). These are recruited to the mitochondria by an unknown mechanism, which might include modified lipids or proteins acting as receptors. Once recruited, Drp1 oligomerizes to form ring structures at fission sites (45). In mammalian cells Drp1 is modified by phosphorylation (10), ubiquitination (11), SUMOylation (9) and S-nitrosylation (12). These modifications either affect Drp1's GTPase activity, its recruitment to the mitochondria, or unknown mechanisms. In the absence of *in-vitro* assays to study the conformational changes of Drp1 and its mitochondrial recruitment it is difficult to understand the precise role of Drp1 SUMOylation.

However, since the downregulation of MAPL does lead to a fused mitochondrial phenotype (34), it is unlikely that SUMOylation is required for the activity of Drp1. On the other hand, increasing mitochondrial SUMOylation by overexpressing SUMO (9), or MAPL (34), or downregulating SENP5 (44) does promote fragmentation. SUMOylation therefore seems pro-fission. However, complicating this analysis, SENP5's recruitment to the mitochondria during mitosis is accompanied by mitochondrial fragmentation (5). The SUMOylation of Drp1 might therefore fulfill two independent roles: It might act as a chaperone to prevent Drp1 degradation on the one hand, or the cycle of SUMO-deSUMOylation may drive conformational changes that could facilitate the production of functional oligomers at constriction sites *(Figure 5.2)*.

Figure V-2 SUMOylation of Drp1

Figure modified from: Zunino R, Braschi E, Xu L, McBride HM. (2009) Translocation of SenP5 from the nucleoli to the mitochondria modulates DRP1-dependent fission during mitosis. *J Biol Chem.* 284(26):17783-95, with permission.

Model explaining the role of SUMOylation in the fission activity of Drp1. The downregulation of MAPL does not lead to mitochondrial elongation, indicating that the SUMOylation of Drp1 is not required for the fission cycle. However, SUMOylation promotes fission, in part by preventing the degradation of Drp1. SUMO might therefore have a chaperone function, in addition to a regulatory role by promoting the formation of Drp1 oligomers.

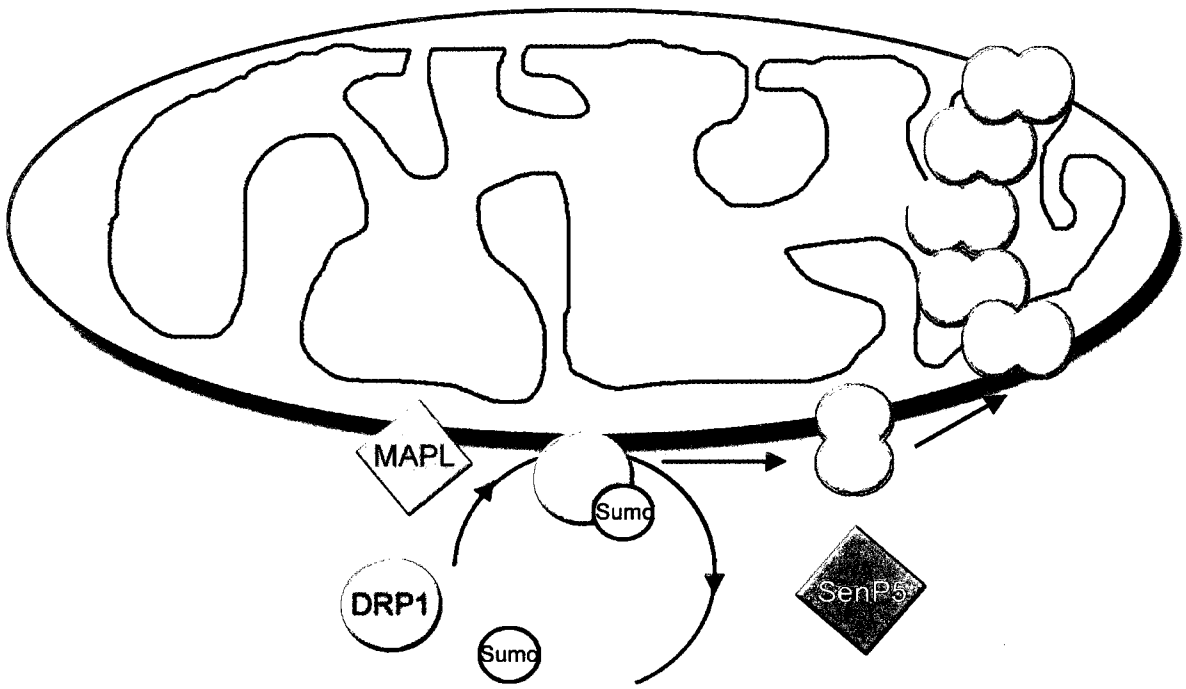
MAPL
Sumo
DRP1
Sumo
SenP5

V.2.2.4 SUMOylation of DRP1 during cell death

In steady state, fluorescence recovery after photobleaching (FRAP) studies have demonstrated that the mitochondrial enrichments of Drp1:YFP are dynamic and that Drp1 cycles on and off the mitochondrial membrane (46). Following a cell death trigger, before the release of cytochrome c but after the activation of Bax and its recruitment to the mitochondria, the recycling of Drp1:YFP is stopped (46). Drp1:YFP becomes stably associated with the mitochondrial membrane in immobile enrichments (46). Importantly, this shift in the activity of Drp1:YFP during cell death is accompanied by the SUMOylation of Drp1 in a Bax/Bak-dependent manner (46). Whether this SUMOylation event is required for cell death is still unknown. However, since we have demonstrated that MAPL SUMOylates Drp1, we can now modulate the SUMOylation of Drp1 by changing the expression levels of MAPL, and examine the role of Drp1's SUMOylation during cell death *(Figure 5.3)*.

Figure V-3 SUMOylation and cell death

Drp1 are red puncta, SUMO yellow puncta, cytochrome c blue puncta. In steady state, Drp1 cycles on and off the mitochondrial membrane. During apoptosis, its behavior dramatically changes as it stops recycling and becomes stably associated on the mitochondria. This event is accompanied by a Bak/Bax dependent SUMOylation of Drp1.

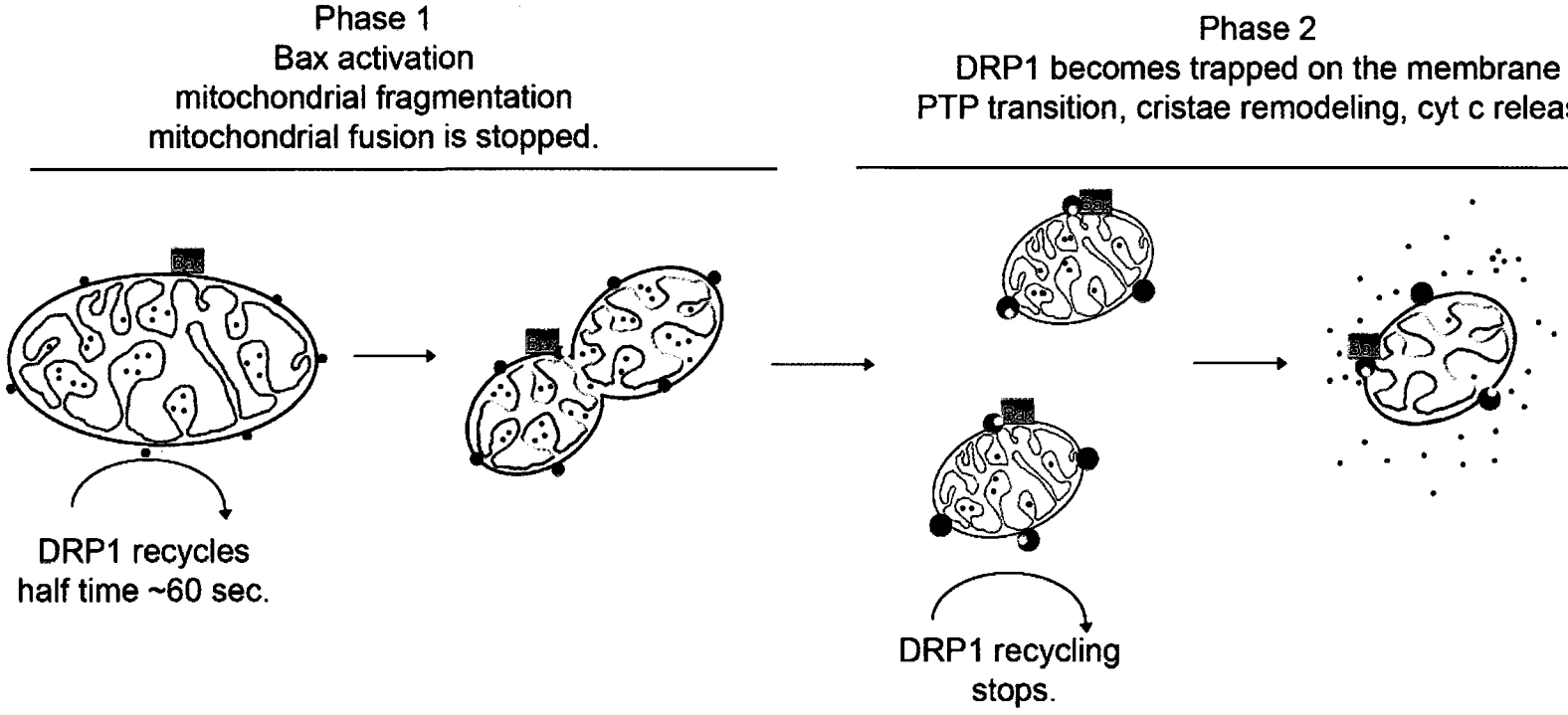
Phase 1
Bax activation
mitochondrial fragmentation
mitochondrial fusion is stopped.
Phase 2
DRP1 becomes trapped on the membrane
PTP transition, cristae remodeling, cyt c release
Bax
DRP1 recycles
half time ~60 sec.
DRP1 recycling
stops.

V.2.2.5 MAPL expands SUMOylation to peroxisomes

Future work using the MAPL *knock-out* mice will shed light onto the physiological functions of MAPL and mitochondrial SUMOylation. In addition, although MAPL is primarily mitochondrial, it is transported to peroxisomes in MDVs (34). The SUMOylation of peroxisomal proteins has not been reported but it will be interesting to determine whether SUMOylation plays an important role in peroxisomal functions.

V.3 Mitochondrial Derived Vesicles

V.3.1 Different cargos, different fates

MDVs are small, uniform structures, 100 nanometers in size. They contain selected cargo and unlike classical fission events, are formed in a Drp1-independent manner, from the lateral segregation of cargo (34). The MDVs first characterized were enriched for MAPL and fused with a sub-population of peroxisomes (34). Importantly, different vesicular structures, formed in a Drp1-independent manner, and containing selected cargos have been reported, raising the possibility that different mitochondrial vesicular pathways exist with distinct cargos and fates (34). In fact, generating ROS at a sub-toxic dose in HeLa cells stimulates the formation of vesicles by up to two fold, when compared to non treated cells *(unpublished, Appendix 4)*. These ROS-induced structures are formed independently of Drp1, which is consistent with them being MDVs as opposed to simple fragments *(unpublished, Appendix 4)*. Importantly, ROS-induced vesicles deliver oxidized mitochondrial cargo to the lysosomes, highlighting a novel route for mitochondrial protein

turnover, and Parkin appears to be selectively recruited to these vesicles *(unpublished, Appendix 4)*. This places MDVs and Parkin on a novel intracellular route regulating mitochondrial quality control. Since Parkin is a ubiquitin E3 ligase, it could select damaged cargo through its ubiquitination activity *(unpublished, Appendix 4)*.

We do not exclude that other MDVs containing different cargos could be targeted to other sub-cellular compartments *(Figure 5.4)*. MDVs therefore highlight the intimate integration of the mitochondria within their cellular environment. Not only are mitochondria able to respond to signaling cascades, they can also share content with other cellular organelles.

Importantly, one of the interacting partners of MAPL identified using the affinity column approach, Vps35, is a component the retromer coat complex (47). We therefore hypothesized that Vps35 could be involved in the formation of MAPL MDVs. And indeed, we have shown that Vps35 and MAPL form a complex *in-vivo*, that Vps35 is localized to MAPL positive MDVs, and that it regulates the vesicular transport of MAPL to peroxisomes *(Chapter 4)*. In addition to providing insights into the formation of MDVs, this study might give valuable tools to better understand the functional consequences that may result from the lack of this transport event.

Figure V-4 MDVs enriched for specific cargo have specific fates

Different vesicles enriched for different cargoes have different fates. MAPL positive MDVs are targeted to peroxisomes, and ROS-induced vesicles are targeted to lysosomes for degradation. Other vesicles with different cargos might have yet unspecified fates.

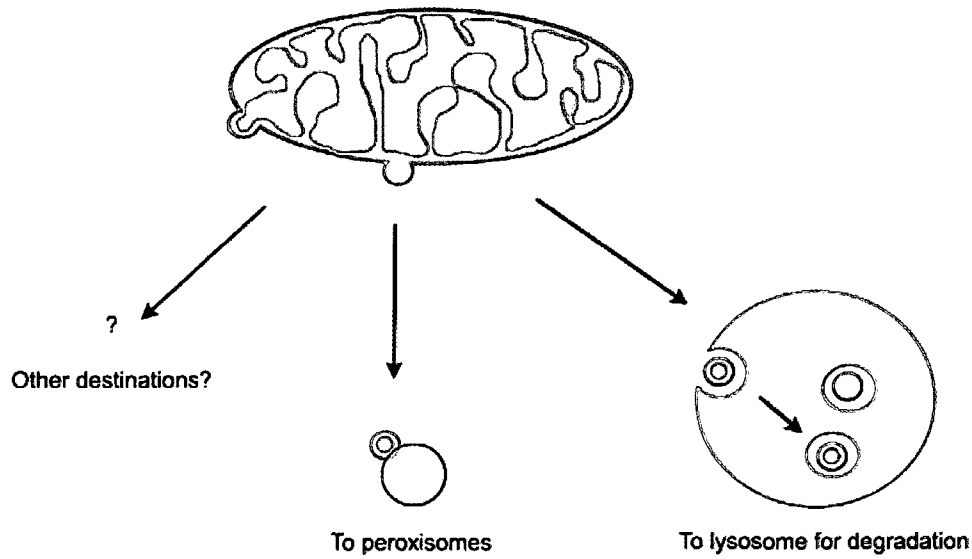
?
Other destinations?
To peroxisomes
To lysosome for degradation

V.3.2 Mitochondrial to peroxisome transport

V.3.2.1 The retromer complex

The yeast retromer is composed of two main subcomplexes that are thought to fulfill independent functions. The first subcomplex, composed of Vps35, Vps26 and Vps29, recognizes and binds to the cargo. The second sub-complex, composed of Vps5 and Vps7 assembles onto the clustered cargo via interactions with the Vps35 subcomplex and membrane lipids (48, 49). It has been hypothesized that the self assembly of Vps5 promotes the formation of the vesicle although the mechanism of vesicle formation is still unknown (50). The human homologues of Vps35, Vps26 and Vps29 also form a complex involved in cargo selectivity (47). However, it is unclear whether the human homologues of Vps5 and Vps7, SNX1, 2 and SNX 5, 6 respectively are involved in the mechanical formation of the vesicle (51) *(Figure 5.5)*.

The SNXs form a heterogeneous family of proteins defined by the presence of a phox homology (PX) domain, which binds to phosphatidylinositol phosphates (52). To date, 29 mammalian SNXs have been identified; different members having different domains, including Bin, Amphiphysin, Rvs (BAR) domains, which sense membrane curvature, Src homology 3 (SH3) domains for protein-protein interaction, kinesin motors, microtubule-interacting domains, and transmembrane domains (52). It is possible that instead of a single retromer complex, different complexes with unique components could participate in specific retromer functions (53), and that the combinatorial use of SNXs with different retromer subunits could modulate the recruitment of the retromer to specific cargos (47). In fact, SNX3 was recently shown to be in a complex with the retromer and to play a role in

preventing the degradation of the *S. Cerevisiae* reductive iron transporter when cells are starved for iron (54).

Figure V-5 The retromer complex

The retromer complex is composed of two sub-complexes. The Vps35, Vps26, Vps29 complex is involved in cargo recognition with the Vps35 complex binding to a transmembrane receptor in this case (for example, the mannose 6-phosphate receptor). The SNX1 and SNX2 are thought to fulfill a structural role and to promote membrane deformation thanks to their BAR domain. In addition, SNX1 and 2's specific binding to modified phospholipids promote their recruitment to specific membranes.

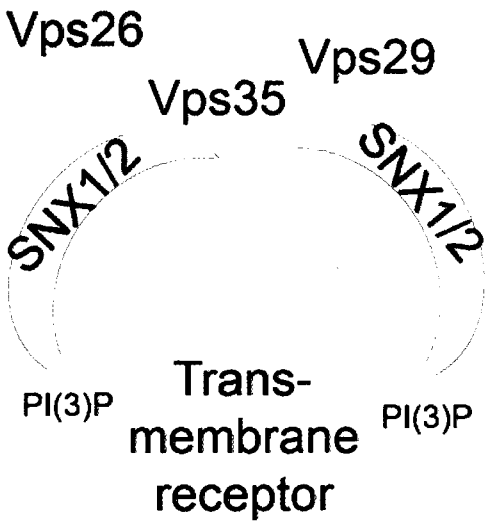
Vps26
Vps29
Vps35
SNX1/2
SNX1/2
PI(3)P
Trans-
membrane
receptor
PI(3)P

In addition, a recently uncovered component of the retromer, Vps26b is mainly found in the cytoplasm, at regions of actin polymerization, and at low levels on the plasma membrane (55).

SNX9 is a potential MAPL interacting partner identified from the affinity column *(Chapter 3)*. Only two peptides were recovered from SNX9, and it was therefore not added to *Table 3.1*. SNX9 localizes to clathrin coated pits where it couples actin dynamics to clathrin-mediated endocytosis (56). SNX9 binds to dynamins, and is able to enhance their assembly on liposomes by stimulating their GTPase activity (56). Consistent with its role in endocytosis, the *knock-down* of SNX9 inhibits transferrin internalization in HeLa cells (57). Given that SNX9 is a potential interacting partner of MAPL, it might participate in the retromer mediated mitochondrial to peroxisome vesicular transport. Alternatively, SNX9 could play a role in regulating mitochondrial fission, since this process, which is mediated by Drp1, is also modulated by MAPL (34).

V.3.2.2 Typical and atypical functions of the retromer

The yeast retromer was originally identified as a coat complex involved in endosome to Golgi retrograde transport in yeast, and a well-characterized cargo is the acid-hydrolase receptor, Vps10 (49). Hydrolase precursors bind to transmembrane receptors like Vps10 in the Golgi and are delivered to endosomes in clathrin-coated vesicles. The acidic pH of the maturing endosome triggers the release of the hydrolases, which are then carried to the lysosome. Vps35 directly binds the cytosolic tail of Vps10 and mediates its retrograde transport to the trans-Golgi network (49). Interfering with this process by mutating components of the retromer complex leads to the transport of Vps10 to the vacuole, where it is degraded, and to the impairment of vacuolar function. Like its yeast counterpart, the

mammalian retromer is required for the recycling of the mannose 6-phosphate receptor. This receptor recognizes newly synthesized hydrolytic enzymes, which are modified in the Golgi by the addition of a mannose 6-phosphate tag (48).

Although the retrieval of the mannose 6-phosphate receptor is a well characterized function of the retromer, other roles have been emerging. The loss of Vps26 is embryonic lethal and Vps26 *knock-out* mice die during the gastrulation stage (58, 59), indicating that although the retromer is not required for proliferation *in-vivo*, it is essential for developmental functions. However, since Vps26 yeast mutants only have mild defects in protein processing at the vacuole (60), it is unlikely that the Vps26 *knock-out* mice die because of problems in lysosomal functions. In addition, humans suffering from the Inclusion-cell disease are unable to properly generate the mannose-6-phosphate tag, but still survive through early adolescence (61, 62). An emerging hypothesis is that the retromer is required for the synthesis, transport, or secretion of other molecules (63). Defects in some of these processes would cause lethality (63). For example, the retromer has been implicated in the establishment of polarity (64, 65), transcytosis (66, 67), Wnt signaling (68-70), cytoskeletal remodeling (71), and the mTOR pathway (72). Altogether these examples highlight the numerous physiological functions of the retromer.

V.3.2.3 Mitochondrial to peroxisome transport

Peroxisomes are single-membrane organelles, which play important roles in oxygen and lipid metabolism (73, 74). Peroxisomes oxidize a large collection of substrates, leading to the formation of H_2O_2, which is then decomposed by a peroxisomal catalase (74). Peroxisomes are also the sites of β-oxidation, and of the biosynthesis of ether lipids, a central component of myelin sheets (75). Different hypotheses could be explored to

understand the function of the transport of MDVs from mitochondria to peroxisomes. Importantly, MAPL could coordinate signaling events between mitochondria and peroxisomes through its SUMOylation activity. In addition, the BAM domain, which is highly conserved and of unknown function, could facilitate processes important to these two organelles.

Biogenesis

The overexpression of MAPL leads to mitochondrial fragmentation, indicating that MAPL is a positive regulator of mitochondrial fission (34). Since mitochondria and peroxisomes share the same components of the fission machinery, it is possible that MAPL also regulates peroxisomal fission. In fact, tubular peroxisomes have been shown to divide into smaller fractions, a process dependent on Drp1, Fis1 and Mff (76, 77). However, the downregulation of any of these proteins leads to elongated peroxisomes, unlike the downregulation of MAPL, which does not lead to fused mitochondrial nor peroxisomal phenotypes (34). In addition, MAPL is targeted to a subpopulation of peroxisomes and it is therefore unlikely that its primary role is to regulate peroxisomal morphology (34).

β-oxidation

Mitochondria and peroxisomes share specific and interrelated functions in the degradation of fatty acids. Peroxisomes oxidize more complex fatty acids, and some mono and polyunsaturated fatty acids (73). On the other hand, mitochondria degrade short chain fatty acids which are then used in the tricarboxylic acid (TCA) cycle. The peroxisomal β-oxidation system does not degrade fatty acids completely, and these have to be shuttled back to the mitochondria for complete oxidation (73). Although each organelle have their

own set of enzymes with specific targeting sequences, MDV transport could facilitate the coordination of the two processes or allow for the transport of mistargeted lipids/proteins. In addition, the transport of MAPL could coordinate the metabolic functions of these two organelles through SUMOylation (78).

Formation of peroxisomes de-novo

The mistargeting of peroxisomal proteins to the mitochondria has already been reported. Peroxisomes can be formed by growth, elongation and fragmentation. They can also be formed *de novo* from the endoplasmic reticulum (79). A loss of the peroxisomal biogenesis proteins leads to a complete absence of peroxisomes (79). Their reintroduction triggers their formation *de novo* from the endoplasmic reticulum (79). It is possible that this endoplasmic reticulum-mediated *de novo* synthesis provides the peroxisomes with essential lipids and proteins. However, when peroxisomal membrane insertion is affected, some peroxisomal proteins have been shown to target to the mitochondria (80, 81). If peroxisomes benefit from material originating from the endoplasmic reticulum, a similar mechanism could be envisioned for the mitochondria (78). Alternatively, MDVs could be required for the biogenesis of specific peroxisomes needed for specialized cellular functions.

V.4 SUMO, MAPL and MDVs

One of the challenges of understanding complex biological systems is to approach the available information from a global perspective, and to examine the different aspects of a problem, which are generally studied independently, to find a unifying perspective. In the case of MAPL and mitochondrial SUMOylation, this is complicated by the fact that the

physiological roles of both are largely unknown. However, we do know that MAPL is a mitochondrial SUMO E3 ligase, I have identified potential MAPL-binding partners and substrates, and MAPL is transported to peroxisomes. With these few elements, I have tried to propose a unifying hypothesis.

V.4.1 Membrane remodeling

V.4.1.1 Actin and migration

A number of potential MAPL interacting partners and SUMO substrates are functionally linked to the cytoskeleton. β-actin, the capping protein muscle Z-line (CapZ), Filamin and IQGAP1 are components of the actin cytoskeleton (42, 43). Furry and the Myc binding protein 2 (MycBP2) have also been linked to membrane remodeling (82).

Specifically, among MAPL interacting partners, β-actin forms the building block of the actin cytoskeleton, and the growth of actin filaments is stopped by capping proteins like CapZ (83). Filamin is a high molecular weight dimeric protein that cross-links actin filaments and binds effectors of the Rho family of GTPases (42, 43). It plays an essential role during mammalian cell locomotion (42, 43). IQGAP1 is a multi-domain protein also important for cytoskeletal remodeling. Like Filamin, IQGAP1 cross-links actin filaments and binds effector molecules, including Cell division cycle 42 (Cdc42) and Rac1 (41). IQGAP1 does not function as a GTPase activator protein, and instead it stabilizes Cdc42 and Rac1 in their GTP bound form, acting as an atypical GTP exchange factor (84). In addition, IQGAP1 coordinates the actin and microtubule cytoskeleton by binding the Adenomatosis Polyposis Coli (APC) (85-87). The downregulation of IQGAP1 leads to a loss of cellular migration, due to the failure of microtubules to polarize and to the inappropriate position of

the microtubule organizing center. On the other hand, overexpressing IQGAP1 enhances cellular migration by activating Cdc42 and Rac1 (86). Finally, IQGAP1 has other domains binding β-catenin, calmodulin, ERK and the MAP kinase-ERK kinase (MEK) (88). In particular, IQGAP1 acts as a scaffold to regulate MAP kinase signaling by binding both ERK and MEK (89).

Interestingly, other proteins in the mitochondrial SUMO proteome have also been linked to membrane remodeling. Furry is a large multidomain protein, which regulates the actin cytoskeleton in yeast (90, 91) and which binds microtubules (82). It was originally identified in *D. melanogaster* as a gene important for the formation and maintenance of polarized cellular extensions (92). MycBP2 is another large multi-domain protein, with a GTP effector domain and a RING domain (93). The *D. melanogaster* homologue, Protein Associated with myc (Pam), regulates the mTOR pathway by ubiquitinating tuberin (94, 95). Interestingly, the *C. elegans* homologue, Regulator of Presynaptic Morphology 1 (RPM-1), regulates axon termination through the Gut granule Loss 1 (GLO-1) (96), a homologue of Rab32, which has been localized to the mitochondria where it regulates mitochondrial morphology (97).

An important link between the mitochondria and the actin cytoskeleton has been described during the chemotaxis of lymphocytes (6). During polarization, most of the machinery for actin polymerization is concentrated in the anterior part of the cell, called the leading edge, whereas the posterior part of the cell, the uropod, contains the adhesion molecules, the microtubule organizing center, and the majority of the cellular organelles and cytosol, including the mitochondria (6). Importantly, the formation of a mitochondrial network prevents migration, although global levels of ATP are unchanged (6).

Mitochondrial fragmentation seems to be required for the specific positioning of mitochondria in sub-cellular domains with high energy requirements, since using creatine to enhance mitochondrial oxidative phosphorylation, rescues the migration defects triggered by Opa1 overexpression (6).

The requirement for mitochondria at the uropod was traced to the phosphorylation of the Myosin Light Chain (MLC) by the Myosin Light Chain Kinase (MLCK) (98). Phosphorylation activates myosins, which contract actin filaments, providing the tension for cellular movements (98). In fact, MLC phosphorylation is more prominent at the uropod than at the leading edge, and when mitochondrial ATP production is inhibited by oligomycin treatment, MLC phosphorylation is lost at the uropod specifically (6). Importantly, although most of the actin polymerization machinery is localized at the leading edge, the role of mitochondria in regulating the actin cytoskeleton seems to play a more important role at the uropod.

During chemotaxis, mitochondria are transported along microtubules (6). An attractive hypothesis is that interactions with the cytoskeleton, which could occur through direct or indirect binding to β-actin, Filamin, or IQGAP1, could ensure that mitochondria are properly positioned once they have reached the uropod. Importantly, these interactions might not be direct and these proteins might form a complex important for the anchorage of mitochondria to the cytoskeleton, with only one of them specifically binding to MAPL. Proteins like IQGAP1 or Furry, which seem to coordinate the actin and the microtubule cytoskeleton, could also play a role in the initial microtubule mediated polarized transport of mitochondria. Finally, MycBP2 could promote mitochondrial fission through Rab32, a process which seems important for the localization of mitochondria in specific sub-cellular

domains (6). Importantly, if MAPL plays a role in coordinating mitochondrial to cytoskeleton interactions, one could expect migration problems in the MAPL *knock-out* mouse, leading to improper development or neuronal defects.

V.4.1.2 Lipid metabolism and migration

Another important function of MAPL might be related to its transport to peroxisomes. Importantly, peroxisomal dysfunctions lead to Zellweger syndrome, which is characterized by a striking increase in very long fatty acids and an almost complete loss of plasmogens, one of the most important class of phospholipids (99). In addition to these metabolic disorders, other characteristic features of the Zellweger syndrome are neuronal migration defects (100-102).

Interestingly, numerous studies indicate that these migration problems are not caused by the known metabolic abnormalities triggered by the loss of peroxisomal function. In fact, one study using mice lacking the second enzyme of the β-oxidation pathway, the hydrate-dehydrogenase, showed no impairment in neuronal migration, although the authors reported a complete block of peroxisomal β-oxidation (101). However, mice lacking Pex11β, a protein involved in peroxisomal biogenesis, have the neuronal migration defects characteristic of the Zellweger syndrome (99). Unlike most Zellweger models, Pex11β *knock-out* mice only have mild defects in β-oxidation and ether lipid synthesis and no alterations in the levels of the brain very long chain fatty acids (99). In other words, the Pex11β null mice mimic the developmental pathological features of Zellweger syndrome, but lack the cellular and biochemical features. It is therefore unlikely that the migration defects in Zellweger syndrome are triggered by decreased β-oxidation (99).

Emerging evidence points to complex differences in lipid profiles between control cells and cells lacking peroxisomal function (103). For example, differences in cholesterol biosynthesis in peroxisomal disorders have been reported (104). However, because the localization of certain enzymes involved in lipid metabolism is controversial, it is hard to understand which of these effects are direct (105, 106). Importantly, lipid profile changes in peroxisomal pathologies could trigger changes in the fluidity of membranes. This in turn could affect cellular migration (107, 108), and at least partially explain the neuronal migration defects of peroxisomal disorders (109). In fact, different studies have reported changes in membrane fluidity due to peroxisomal dysfunction, although the results vary, some demonstrating an increase in fluidity, others a decrease (103, 109). Future work will hopefully clarify the changes triggered by peroxisomal defects on the membrane lipid composition and properties.

V.4.1.3 Possible regulation of actin and lipid metabolism by MAPL during migration

A number of MAPL-interacting partners and potential SUMO substrates regulate migration by modulating the cytoskeleton. In addition, MAPL is transported to peroxisomes (34) and an important phenotype triggered by peroxisomal dysfunction is improper neuronal migration (100-102). An attractive speculation is that MAPL coordinates migration and mitochondrial metabolism by facilitating the localization of mitochondria at sites of high ATP consumption. In addition, MAPL could influence cellular fluidity by modulating lipid metabolism thanks to its transport to peroxisomes. Interestingly, a number of enzymes involved in lipid metabolism have been shown to be SUMOylated in yeast (110), and SUMO could act as a global coordinator of this pathway. Future studies will determine if

MAPL regulates cytoskeletal changes and lipid metabolism through its SUMOylation activity, and whether this could modulate migration *(Figure 5.6)*.

Figure V-6 MAPL and migration

During cell migration MAPL could promote migration by two mechanisms. The interaction of MAPL with actin binding proteins like Filamin, actin or IQGAP1, MAPL could facilitate the localization of mitochondria at sites of high ATP consumption. MAPL could also regulate lipid metabolism through its SUMOylation activity or by modulating peroxisomal function. This in turn could affect membrane viscosity and migration.

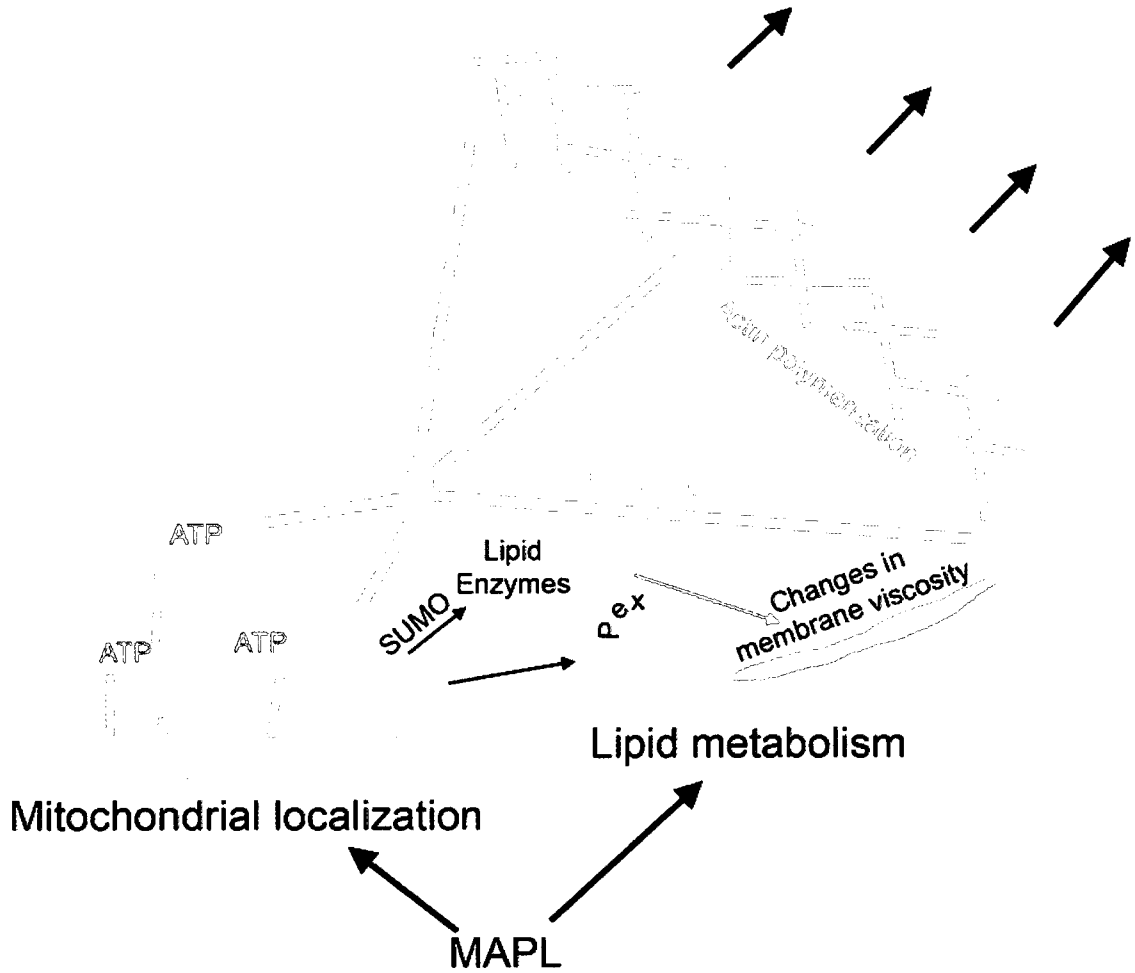
ATP
ATP
ATP
SUMO
Lipid
Enzymes
Pex
Changes in
membrane viscosity
Lipid metabolism
Mitochondrial localization
MAPL

V.4.2 Apoptosis

Our lab has previously demonstrated that the behavior of Drp1 during cell death is strikingly altered (46). This event is accompanied by the SUMOylation of Drp1 in a Bax/Bak-dependent manner (46). It is unclear whether the SUMOylation of Drp1 is required for the progression of cell death. If this is the case, MAPL could modulate cell death by regulating this SUMOylation event. Ongoing studies are exploring whether Drp1 is SUMOylated by MAPL during cell death, and whether this plays a role during the progression of apoptosis.

In addition, the molecular events leading to the block in the dynamic behavior of Drp1 during cell death are currently unknown. Drp1 could become associated to the cytoskeleton, which could stabilize mitochondrial Drp1 enrichments. MAPL, by modulating the activity of IQGAP1 or Filamin, both actin cross linkers, could facilitate this process. In addition, MAPL could modulate changes in the lipid composition of the mitochondria. In fact, during cell death, the fission machinery and the apoptotic machinery appear to be recruited to specific microdomains, which have been shown to play an important role during cell death (111). In particular, two lipids which have been shown to be enriched in mitochondrial lipid microdomains during cell death are ceramide and cholesterol (112, 113).

The synthesis of ceramide occurs following a number of apoptotic stimuli (114). Ceramide can be generated *de novo* from the endoplasmic reticulum (115) and mitochondria (116), or from the hydrolysis of sphingomyelin by sphingomyelinase (114). Mitochondria isolated from apoptotic cells have a two to three-fold increase in the levels of ceramide (117), preceding cytochrome c release (118). Importantly, targeting sphingomyelinase to the

mitochondria leads to cytochrome c release and apoptosis, highlighting a specific role for mitochondrial ceramide (119). The apoptotic function of ceramide has been proposed to be mediated by its ability to form channels in lipid bilayers (120). In addition, an increase in ceramide and cholesterol in mitochondrial detergent resistant microdomains, has been reported in post-ischemic hearts (121-123). Since detergent-resistant mitochondrial microdomains are enriched in Bax (123), ceramide and cholesterol might participate in the stable recruitment of proteins, including Drp1, to the mitchondria during cell death.

There are currently no reports demonstrating a function for peroxisomes during cell death and no clear, well-accepted, involvement of peroxisomes in ceramide or cholesterol synthesis. However, it is be possible that some of the changes in lipid metabolism associated with apoptosis are initiated in peroxisomes. MAPL could be involved in coordinating mitochondrial and peroxisomal function during cell death. Alternatively, steady state changes in mitochondrial lipid composition could lead to differential responses during apoptosis. For example, a decrease in mitochondrial cholesterol has been shown to delay Bax activation (124, 125), possibly due to a reduction in the formation of lipid microdomains during cell death.

Interestingly, MAPL could have a more profound role in the formation of mitochondrial lipid microdomains by coordinating lipid metabolism and cytoskeletal changes during cell death. In fact, the formation of lipid rafts at the immunological synapse during T cell stimulation, requires cytoskeletal changes (42). In particular, it has been hypothesized that Filamin stabilizes and cross-links actin filaments at the immunological synapse, leading to the accumulation of lipid microdomains (42). A similar mechanism could be envisioned on the mitochondrial outer membrane during cell death. In other words,

one could speculate that changes in lipid composition and the cross-linking of actin filaments by Filamin or IQGAP1, which could potentially be orchestrated by MAPL, might contribute to the dramatic shift in the behavior of Drp1 during cell death *(Figure 5.7)*.

Figure V-7 MAPL and cell death

During cell death, the mitochondrial SUMO substrate, Drp1 is stably recruited to the mitochondria. This event is accompanied by its SUMOylation. MAPL could therefore modulate cell death by SUMOylating Drp1. In addition, the stable association of Drp1 on the mitochondrial membrane could be promoted by the formation of cholesterol containing microdomains, which could be stabilized by the cross linking of actin filaments. In fact, two potential MAPL binding partners, Filamin and IQGAP1 cross-link actin filaments.

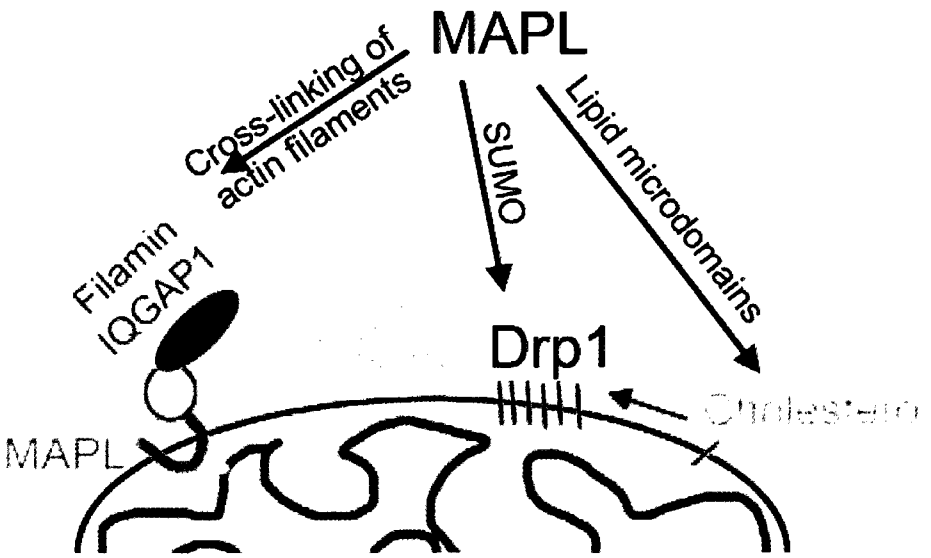
MAPL
Cross-linking of actin filaments
SUMO
Lipid microdomains
Filamin
IQGAP1
Drp1
Cholesterol
MAPL

V.4.3 Conclusion

MAPL is the first mitochondrial SUMO E3 ligase. As a cytoplasmic SUMO E3 ligase, MAPL might coordinate global cellular SUMOylation. In particular, MAPL could SUMOylate mitochondrial, cytoplasmic and peroxisomal proteins. In addition, the BAM domain of MAPL is conserved from bacteria to higher eukaryotes (78). Although the function of this domain is unknown, a common function between bacteria and modern eukaryotes could be metabolic sensing. The addition of the RING domain in higher eukaryotes could relay metabolic information through the SUMOylation of cytoplasmic factors. If the RING domain were to be modified by cellular signaling molecules, MAPL could integrate both intra-mitochondrial and intra-cellular signaling to modulate downstream signaling cascades accordingly *(Figure 5.8)*. Finally, thanks to its transport to peroxisomes, MAPL might coordinate broad metabolic processes common to peroxisomes and mitochondria. Future work will focus on studying the phenotypes of the MAPL *knock-out* mouse to elucidate the physiological functions of MAPL. Importantly, the research presented here, uncovering the function of MAPL as a SUMO E3 ligase, substrates and interacting partners, and the discovery that Vps35 mediates the transport of MAPL from the mitochondria to peroxisomes, will provide invaluable tools to further explore the physiological function of MAPL.

Figure V-8 MAPL is an attractive modulator of cellular signaling

MAPL possesses a highly conserved intermembrane space domain, which could sense or regulate mitochondrial metabolism. Conformational changes in the BAM domain could modulate the activity of the RING finger of MAPL. In addition, kinases activated by signaling cascades could phosphorylate the RING domain since it faces the cytoplasm. Through its SUMOylation activity, MAPL might therefore be able to integrate both the intra-mitochondrial and the intra-cellular environments. SUMOylation of mitochondrial targets could promote a new mitochondrial function, and the SUMOylation of recruited mitochondrial factors could modulate downstream signaling cascades.

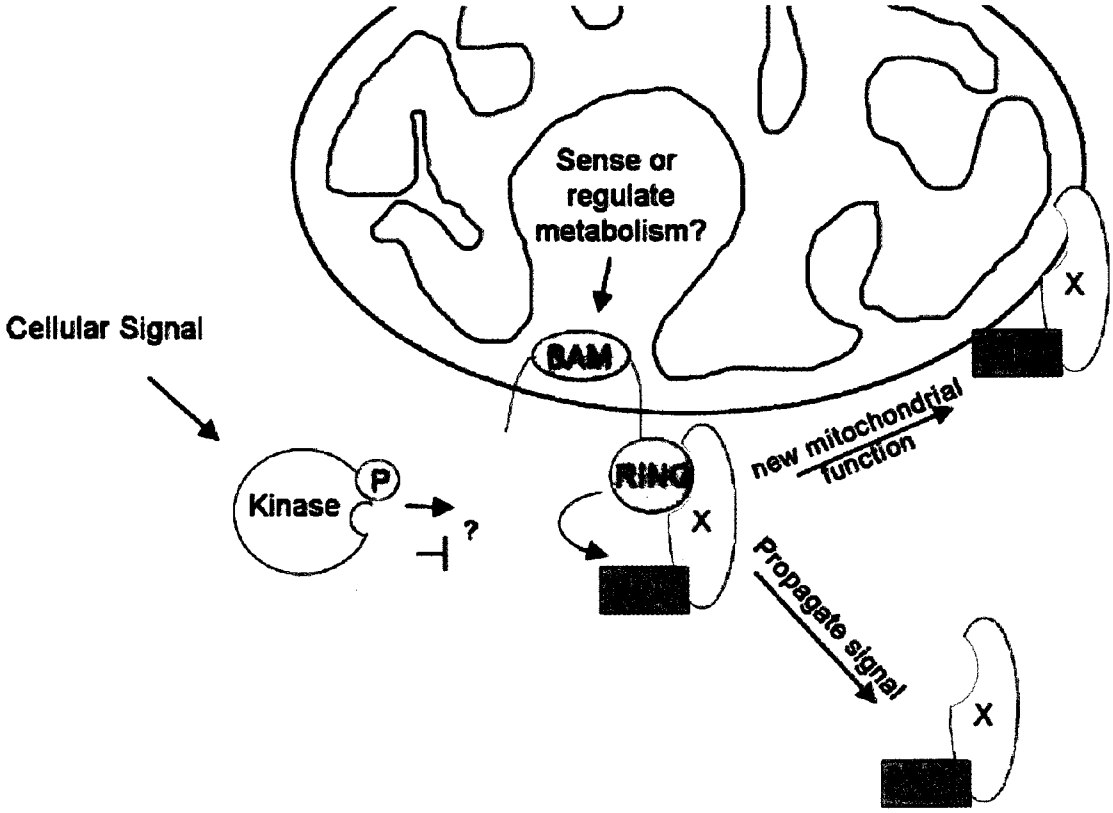
Sense or
regulate
metabolism?
Cellular Signal
BAM
X
Kinase
P
?
RING
X
new mitochondrial
function
Propagate signal
X

V.5 References

1. Cortese, J.D., L.A. Voglino, and C.R. Hackenbrock. 1998. Novel fluorescence membrane fusion assays reveal GTP-dependent fusogenic properties of outer mitochondrial membrane-derived proteins. *Biochim Biophys Acta* 1371:185-198.

2. Nakada, K., K. Inoue, T. Ono, K. Isobe, A. Ogura, Y.I. Goto, I. Nonaka, and J.I. Hayashi. 2001. Inter-mitochondrial complementation: Mitochondria-specific system preventing mice from expression of disease phenotypes by mutant mtDNA. *Nat Med* 7:934-940.

3. Chan, D.C. 2006. Mitochondria: dynamic organelles in disease, aging, and development. *Cell* 125:1241-1252.

4. Yu, T., J.L. Robotham, and Y. Yoon. 2006. Increased production of reactive oxygen species in hyperglycemic conditions requires dynamic change of mitochondrial morphology. *Proc Natl Acad Sci U S A* 103:2653-2658.

5. Zunino, R., E. Braschi, L. Xu, and H.M. McBride. 2009. Translocation of SenP5 from the nucleoli to the mitochondria modulates DRP1-dependent fission during mitosis. *J Biol Chem* 284:17783-17795.

6. Campello, S., R.A. Lacalle, M. Bettella, S. Manes, L. Scorrano, and A. Viola. 2006. Orchestration of lymphocyte chemotaxis by mitochondrial dynamics. *J Exp Med* 203:2879-2886.

7. Tondera, D., S. Grandemange, A. Jourdain, M. Karbowski, Y. Mattenberger, S. Herzig, S. Da Cruz, P. Clerc, I. Raschke, C. Merkwirth, S. Ehses, F. Krause, D.C. Chan, C. Alexander, C. Bauer, R. Youle, T. Langer, and J.C. Martinou. 2009. SLP-2 is required for stress-induced mitochondrial hyperfusion. *Embo J* 28:1589-1600.

8. Lee, Y.J., S.Y. Jeong, M. Karbowski, C.L. Smith, and R.J. Youle. 2004. Roles of the mammalian mitochondrial fission and fusion mediators Fis1, Drp1, and Opa1 in apoptosis. *Mol Biol Cell* 15:5001-5011.

9. Harder, Z., R. Zunino, and H. McBride. 2004. Sumo1 conjugates mitochondrial substrates and participates in mitochondrial fission. *Curr Biol* 14:340-345.

10. Cribbs, J.T., and S. Strack. 2007. Reversible phosphorylation of Drp1 by cyclic AMP-dependent protein kinase and calcineurin regulates mitochondrial fission and cell death. *EMBO Rep* 8:939-944.

11. Karbowski, M., A. Neutzner, and R.J. Youle. 2007. The mitochondrial E3 ubiquitin ligase MARCH5 is required for Drp1 dependent mitochondrial division. *J Cell Biol* 178:71-84.

12. Cho, D.H., T. Nakamura, J. Fang, P. Cieplak, A. Godzik, Z. Gu, and S.A. Lipton. 2009. S-nitrosylation of Drp1 mediates beta-amyloid-related mitochondrial fission and neuronal injury. *Science* 324:102-105.

13. Park, K.S., A. Wiederkehr, C. Kirkpatrick, Y. Mattenberger, J.C. Martinou, P. Marchetti, N. Demaurex, and C.B. Wollheim. 2008. Selective actions of mitochondrial fission/fusion genes on metabolism-secretion coupling in insulin-releasing cells. *J Biol Chem* 283:33347-33356.

14. Chada, S.R., and P.J. Hollenbeck. 2004. Nerve growth factor signaling regulates motility and docking of axonal mitochondria. *Curr Biol* 14:1272-1276.

15. Chada, S.R., and P.J. Hollenbeck. 2003. Mitochondrial movement and positioning in axons: the role of growth factor signaling. *J Exp Biol* 206:1985-1992.

16. Twig, G., A. Elorza, A.J. Molina, H. Mohamed, J.D. Wikstrom, G. Walzer, L. Stiles, S.E. Haigh, S. Katz, G. Las, J. Alroy, M. Wu, B.F. Py, J. Yuan, J.T. Deeney, B.E. Corkey, and O.S. Shirihai. 2008. Fission and selective fusion govern mitochondrial segregation and elimination by autophagy. *Embo J* 27:433-446.

17. Kitada, T., S. Asakawa, N. Hattori, H. Matsumine, Y. Yamamura, S. Minoshima, M. Yokochi, Y. Mizuno, and N. Shimizu. 1998. Mutations in the parkin gene cause autosomal recessive juvenile parkinsonism. *Nature* 392:605-608.

18. Neuspiel, M., R. Zunino, S. Gangaraju, P. Rippstein, and H. McBride. 2005. Activated mitofusin 2 signals mitochondrial fusion, interferes with Bax activation, and reduces susceptibility to radical induced depolarization. *J Biol Chem* 280:25060-25070.

19. Chen, K.H., X. Guo, D. Ma, Y. Guo, Q. Li, D. Yang, P. Li, X. Qiu, S. Wen, R.P. Xiao, and J. Tang. 2004. Dysregulation of HSG triggers vascular proliferative disorders. *Nat Cell Biol* 6:872-883.

20. Pich, S., D. Bach, P. Briones, M. Liesa, M. Camps, X. Testar, M. Palacin, and A. Zorzano. 2005. The Charcot-Marie-Tooth type 2A gene product, Mfn2, up-regulates fuel oxidation through expression of OXPHOS system. *Hum Mol Genet* 14:1405-1415.

21. Soriano, F.X., M. Liesa, D. Bach, D.C. Chan, M. Palacin, and A. Zorzano. 2006. Evidence for a mitochondrial regulatory pathway defined by peroxisome proliferator-activated receptor-gamma coactivator-1 alpha, estrogen-related receptor-alpha, and mitofusin 2. *Diabetes* 55:1783-1791.

22. Seth, R.B., L. Sun, C.K. Ea, and Z.J. Chen. 2005. Identification and characterization of MAVS, a mitochondrial antiviral signaling protein that activates NF-kappaB and IRF 3. *Cell* 122:669-682.

23. Xu, L.G., Y.Y. Wang, K.J. Han, L.Y. Li, Z. Zhai, and H.B. Shu. 2005. VISA is an adapter protein required for virus-triggered IFN-beta signaling. *Mol Cell* 19:727-740.

24. Meylan, E., J. Curran, K. Hofmann, D. Moradpour, M. Binder, R. Bartenschlager, and J. Tschopp. 2005. Cardif is an adaptor protein in the RIG-I antiviral pathway and is targeted by hepatitis C virus. *Nature* 437:1167-1172.

25. Ishii, K.J., C. Coban, H. Kato, K. Takahashi, Y. Torii, F. Takeshita, H. Ludwig, G. Sutter, K. Suzuki, H. Hemmi, S. Sato, M. Yamamoto, S. Uematsu, T. Kawai, O.

Takeuchi, and S. Akira. 2006. A Toll-like receptor-independent antiviral response induced by double-stranded B-form DNA. *Nat Immunol* 7:40-48.

26. Yasukawa, K., H. Oshiumi, M. Takeda, N. Ishihara, Y. Yanagi, T. Seya, S. Kawabata, and T. Koshiba. 2009. Mitofusin 2 inhibits mitochondrial antiviral signaling. *Sci Signal* 2:ra47.

27. Lei, Y., C.B. Moore, R.M. Liesman, B.P. O'Connor, D.T. Bergstralh, Z.J. Chen, R.J. Pickles, and J.P. Ting. 2009. MAVS-mediated apoptosis and its inhibition by viral proteins. *PLoS One* 4:e5466.

28. Bai, X., D. Ma, A. Liu, X. Shen, Q.J. Wang, Y. Liu, and Y. Jiang. 2007. Rheb activates mTOR by antagonizing its endogenous inhibitor, FKBP38. *Science* 318:977-980.

29. Wang, X., B.D. Fonseca, H. Tang, R. Liu, A. Elia, M.J. Clemens, U.A. Bommer, and C.G. Proud. 2008. Re-evaluating the roles of proposed modulators of mammalian target of rapamycin complex 1 (mTORC1) signaling. *J Biol Chem* 283:30482-30492.

30. Clements, D., R.J. Mayer, and S.R. Johnson. 2007. Subcellular distribution of the TSC2 gene product tuberin in human airway smooth muscle cells is driven by multiple localization sequences and is cell-cycle dependent. *Am J Physiol Lung Cell Mol Physiol* 292:L258-266.

31. Meulmeester, E., and F. Melchior. 2008. Cell biology: SUMO. *Nature* 452:709-711.

32. Geiss-Friedlander, R., and F. Melchior. 2007. Concepts in sumoylation: a decade on. *Nat Rev Mol Cell Biol* 8:947-956.

33. Takahashi, Y., M. Iwase, A.V. Strunnikov, and Y. Kikuchi. 2008. Cytoplasmic sumoylation by PIAS-type Siz1-SUMO ligase. *Cell Cycle* 7:1738-1744.

34. Neuspiel, M., A.C. Schauss, E. Braschi, R. Zunino, P. Rippstein, R.A. Rachubinski, M.A. Andrade-Navarro, and H.M. McBride. 2008. Cargo-selected transport from the mitochondria to peroxisomes is mediated by vesicular carriers. *Curr Biol* 18:102-108.

35. Braschi, E., R. Zunino, and H.M. McBride. 2009. MAPL is a new mitochondrial SUMO E3 ligase that regulates mitochondrial fission. *EMBO Rep* 10:748-754.

36. Bonifacino, J.S., and J.H. Hurley. 2008. Retromer. *Curr Opin Cell Biol* 20:427-436.

37. Li, W., M.H. Bengtson, A. Ulbrich, A. Matsuda, V.A. Reddy, A. Orth, S.K. Chanda, S. Batalov, and C.A. Joazeiro. 2008. Genome-wide and functional annotation of human E3 ubiquitin ligases identifies MULAN, a mitochondrial E3 that regulates the organelle's dynamics and signaling. *PLoS One* 3:e1487.

38. Weger, S., E. Hammer, and R. Heilbronn. 2005. Topors acts as a SUMO-1 E3 ligase for p53 in vitro and in vivo. *FEBS Lett* 579:5007-5012.

39. Pungaliya, P., D. Kulkarni, H.J. Park, H. Marshall, H. Zheng, H. Lackland, A. Saleem, and E.H. Rubin. 2007. TOPORS functions as a SUMO-1 E3 ligase for chromatin-modifying proteins. *J Proteome Res* 6:3918-3923.

40. Park, H.J., H. Zheng, D. Kulkarni, J. Kerrigan, P. Pungaliya, A. Saleem, and E.H. Rubin. 2008. Identification of phosphorylation sites of TOPORS and a role for serine 98 in the regulation of ubiquitin but not SUMO E3 ligase activity. *Biochemistry* 47:13887-13896.

41. Bashour, A.M., A.T. Fullerton, M.J. Hart, and G.S. Bloom. 1997. IQGAP1, a Rac- and Cdc42-binding protein, directly binds and cross-links microfilaments. *J Cell Biol* 137:1555-1566.

42. Tavano, R., R.L. Contento, S.J. Baranda, M. Soligo, L. Tuosto, S. Manes, and A. Viola. 2006. CD28 interaction with filamin-A controls lipid raft accumulation at the T-cell immunological synapse. *Nat Cell Biol* 8:1270-1276.

43. Mammoto, A., S. Huang, and D.E. Ingber. 2007. Filamin links cell shape and cytoskeletal structure to Rho regulation by controlling accumulation of p190RhoGAP in lipid rafts. *J Cell Sci* 120:456-467.

44. Zunino, R., A. Schauss, P. Rippstein, M. Andrade-Navarro, and H.M. McBride. 2007. The SUMO protease SENP5 is required to maintain mitochondrial morphology and function. *J Cell Sci* 120:1178-1188.

45. Ingerman, E., E.M. Perkins, M. Marino, J.A. Mears, J.M. McCaffery, J.E. Hinshaw, and J. Nunnari. 2005. Dnm1 forms spirals that are structurally tailored to fit mitochondria. *J Cell Biol* 170:1021-1027.

46. Wasiak, S., R. Zunino, and H.M. McBride. 2007. Bax/Bak promote sumoylation of DRP1 and its stable association with mitochondria during apoptotic cell death. *J Cell Biol* 177:439-450.

47. Haft, C.R., M. de la Luz Sierra, R. Bafford, M.A. Lesniak, V.A. Barr, and S.I. Taylor. 2000. Human orthologs of yeast vacuolar protein sorting proteins Vps26, 29, and 35: assembly into multimeric complexes. *Mol Biol Cell* 11:4105-4116.

48. Arighi, C.N., L.M. Hartnell, R.C. Aguilar, C.R. Haft, and J.S. Bonifacino. 2004. Role of the mammalian retromer in sorting of the cation-independent mannose 6-phosphate receptor. *J Cell Biol* 165:123-133.

49. Nothwehr, S.F., S.A. Ha, and P. Bruinsma. 2000. Sorting of yeast membrane proteins into an endosome-to-Golgi pathway involves direct interaction of their cytosolic domains with Vps35p. *J Cell Biol* 151:297-310.

50. Seaman, M.N., and H.P. Williams. 2002. Identification of the functional domains of yeast sorting nexins Vps5p and Vps17p. *Mol Biol Cell* 13:2826-2840.

51. Wassmer, T., N. Attar, M.V. Bujny, J. Oakley, C.J. Traer, and P.J. Cullen. 2007. A loss-of-function screen reveals SNX5 and SNX6 as potential components of the mammalian retromer. *J Cell Sci* 120:45-54.

52. Carlton, J., M. Bujny, A. Rutherford, and P. Cullen. 2005. Sorting nexins--unifying trends and new perspectives. *Traffic* 6:75-82.

53. Kim, E., J.W. Lee, D.C. Baek, S.R. Lee, M.S. Kim, S.H. Kim, K. Imakawa, and K.T. Chang. 2008. Identification of novel retromer complexes in the mouse testis. *Biochem Biophys Res Commun* 375:16-21.

54. Strochlic, T.I., B.C. Schmiedekamp, J. Lee, D.J. Katzmann, and C.G. Burd. 2008. Opposing activities of the Snx3-retromer complex and ESCRT proteins mediate regulated cargo sorting at a common endosome. *Mol Biol Cell* 19:4694-4706.

55. Collins, B.M., S.J. Norwood, M.C. Kerr, D. Mahony, M.N. Seaman, R.D. Teasdale, and D.J. Owen. 2008. Structure of Vps26B and mapping of its interaction with the retromer protein complex. *Traffic* 9:366-379.

56. Soulet, F., D. Yarar, M. Leonard, and S.L. Schmid. 2005. SNX9 regulates dynamin assembly and is required for efficient clathrin-mediated endocytosis. *Mol Biol Cell* 16:2058-2067.

57. Yarar, D., C.M. Waterman-Storer, and S.L. Schmid. 2007. SNX9 couples actin assembly to phosphoinositide signals and is required for membrane remodeling during endocytosis. *Dev Cell* 13:43-56.

58. Radice, G., J.J. Lee, and F. Costantini. 1991. H beta 58, an insertional mutation affecting early postimplantation development of the mouse embryo. *Development* 111:801-811.

59. Lee, J.J., G. Radice, C.P. Perkins, and F. Costantini. 1992. Identification and characterization of a novel, evolutionarily conserved gene disrupted by the murine H beta 58 embryonic lethal transgene insertion. *Development* 115:277-288.

60. Bachhawat, A.K., J. Suhan, and E.W. Jones. 1994. The yeast homolog of H < beta > 58, a mouse gene essential for embryogenesis, performs a role in the delivery of proteins to the vacuole. *Genes Dev* 8:1379-1387.

61. Futerman, A.H., and G. van Meer. 2004. The cell biology of lysosomal storage disorders. *Nat Rev Mol Cell Biol* 5:554-565.

62. Dittmer, F., E.J. Ulbrich, A. Hafner, W. Schmahl, T. Meister, R. Pohlmann, and K. von Figura. 1999. Alternative mechanisms for trafficking of lysosomal enzymes in mannose 6-phosphate receptor-deficient mice are cell type-specific. *J Cell Sci* 112 (Pt 10):1591-1597.

63. Verges, M. 2007. Retromer and sorting nexins in development. *Front Biosci* 12:3825-3851.

64. Jaillais, Y., M. Santambrogio, F. Rozier, I. Fobis-Loisy, C. Miege, and T. Gaude. 2007. The retromer protein VPS29 links cell polarity and organ initiation in plants. *Cell* 130:1057-1070.

65. Jaillais, Y., and T. Gaude. 2007. Sorting out the sorting functions of endosomes in Arabidopsis. *Plant Signal Behav* 2:556-558.

66. Verges, M., F. Luton, C. Gruber, F. Tiemann, L.G. Reinders, L. Huang, A.L. Burlingame, C.R. Haft, and K.E. Mostov. 2004. The mammalian retromer regulates transcytosis of the polymeric immunoglobulin receptor. *Nat Cell Biol* 6:763-769.

67. Verges, M., I. Sebastian, and K.E. Mostov. 2007. Phosphoinositide 3-kinase regulates the role of retromer in transcytosis of the polymeric immunoglobulin receptor. *Exp Cell Res* 313:707-718.

68. Franch-Marro, X., F. Wendler, S. Guidato, J. Griffith, A. Baena-Lopez, N. Itasaki, M.M. Maurice, and J.P. Vincent. 2008. Wingless secretion requires endosome-to-Golgi retrieval of Wntless/Evi/Sprinter by the retromer complex. *Nat Cell Biol* 10:170-177.

69. Port, F., M. Kuster, P. Herr, E. Furger, C. Banziger, G. Hausmann, and K. Basler. 2008. Wingless secretion promotes and requires retromer-dependent cycling of Wntless. *Nat Cell Biol* 10:178-185.

70. Belenkaya, T.Y., Y. Wu, X. Tang, B. Zhou, L. Cheng, Y.V. Sharma, D. Yan, E.M. Selva, and X. Lin. 2008. The retromer complex influences Wnt secretion by recycling wntless from endosomes to the trans-Golgi network. *Dev Cell* 14:120-131.

71. Korolchuk, V.I., M.M. Schutz, C. Gomez-Llorente, J. Rocha, N.R. Lansu, S.M. Collins, Y.P. Wairkar, I.M. Robinson, and C.J. O'Kane. 2007. Drosophila Vps35 function is necessary for normal endocytic trafficking and actin cytoskeleton organisation. *J Cell Sci* 120:4367-4376.

72. Scott, K.L., O. Kabbarah, M.C. Liang, E. Ivanova, V. Anagnostou, J. Wu, S. Dhakal, M. Wu, S. Chen, T. Feinberg, J. Huang, A. Saci, H.R. Widlund, D.E. Fisher, Y. Xiao, D.L. Rimm, A. Protopopov, K.K. Wong, and L. Chin. 2009. GOLPH3 modulates mTOR signalling and rapamycin sensitivity in cancer. *Nature* 459:1085-1090.

73. Poirier, Y., V.D. Antonenkov, T. Glumoff, and J.K. Hiltunen. 2006. Peroxisomal beta-oxidation--a metabolic pathway with multiple functions. *Biochim Biophys Acta* 1763:1413-1426.

74. Schrader, M., and H.D. Fahimi. 2006. Peroxisomes and oxidative stress. *Biochim Biophys Acta* 1763:1755-1766.

75. Camoes, F., N.A. Bonekamp, H.K. Delille, and M. Schrader. 2009. Organelle dynamics and dysfunction: A closer link between peroxisomes and mitochondria. *J Inherit Metab Dis* 32:163-180.

76. Kobayashi, S., A. Tanaka, and Y. Fujiki. 2007. Fis1, DLP1, and Pex11p coordinately regulate peroxisome morphogenesis. *Exp Cell Res* 313:1675-1686.

77. Gandre-Babbe, S., and A.M. van der Bliek. 2008. The novel tail-anchored membrane protein Mff controls mitochondrial and peroxisomal fission in mammalian cells. *Mol Biol Cell* 19:2402-2412.

78. Andrade-Navarro, M.A., L. Sanchez-Pulido, and H.M. McBride. 2009. Mitochondrial vesicles: an ancient process providing new links to peroxisomes. *Curr Opin Cell Biol* 21:560-567.

79. Hoepfner, D., D. Schildknegt, I. Braakman, P. Philippsen, and H.F. Tabak. 2005. Contribution of the endoplasmic reticulum to peroxisome formation. *Cell* 122:85-95.

80. Sacksteder, K.A., J.M. Jones, S.T. South, X. Li, Y. Liu, and S.J. Gould. 2000. PEX19 binds multiple peroxisomal membrane proteins, is predominantly cytoplasmic, and is required for peroxisome membrane synthesis. *J Cell Biol* 148:931-944.

81. Soukupova, M., C. Sprenger, K. Gorgas, W.H. Kunau, and G. Dodt. 1999. Identification and characterization of the human peroxin PEX3. *Eur J Cell Biol* 78:357-374.

82. Chiba, S., M. Ikeda, K. Katsunuma, K. Ohashi, and K. Mizuno. 2009. MST2- and Furry-mediated activation of NDR1 kinase is critical for precise alignment of mitotic chromosomes. *Curr Biol* 19:675-681.

83. Pollard, T.D., and G.G. Borisy. 2003. Cellular motility driven by assembly and disassembly of actin filaments. *Cell* 112:453-465.

84. Hart, M.J., M.G. Callow, B. Souza, and P. Polakis. 1996. IQGAP1, a calmodulin-binding protein with a rasGAP-related domain, is a potential effector for cdc42Hs. *Embo J* 15:2997-3005.

85. Kuroda, S., M. Fukata, M. Nakagawa, K. Fujii, T. Nakamura, T. Ookubo, I. Izawa, T. Nagase, N. Nomura, H. Tani, I. Shoji, Y. Matsuura, S. Yonehara, and K. Kaibuchi. 1998. Role of IQGAP1, a target of the small GTPases Cdc42 and Rac1, in regulation of E-cadherin- mediated cell-cell adhesion. *Science* 281:832-835.

86. Fukata, M., T. Watanabe, J. Noritake, M. Nakagawa, M. Yamaga, S. Kuroda, Y. Matsuura, A. Iwamatsu, F. Perez, and K. Kaibuchi. 2002. Rac1 and Cdc42 capture microtubules through IQGAP1 and CLIP-170. *Cell* 109:873-885.

87. Watanabe, T., S. Wang, J. Noritake, K. Sato, M. Fukata, M. Takefuji, M. Nakagawa, N. Izumi, T. Akiyama, and K. Kaibuchi. 2004. Interaction with IQGAP1 links APC to Rac1, Cdc42, and actin filaments during cell polarization and migration. *Dev Cell* 7:871-883.

88. Johnson, M., M. Sharma, and B.R. Henderson. 2009. IQGAP1 regulation and roles in cancer. *Cell Signal* 21:1471-1478.

89. Roy, M., Z. Li, and D.B. Sacks. 2005. IQGAP1 is a scaffold for mitogen-activated protein kinase signaling. *Mol Cell Biol* 25:7940-7952.

90. Du, L.L., and P. Novick. 2002. Pag1p, a novel protein associated with protein kinase Cbk1p, is required for cell morphogenesis and proliferation in Saccharomyces cerevisiae. *Mol Biol Cell* 13:503-514.

91. Kanai, M., K. Kume, K. Miyahara, K. Sakai, K. Nakamura, K. Leonhard, D.J. Wiley, F. Verde, T. Toda, and D. Hirata. 2005. Fission yeast MO25 protein is localized at SPB and septum and is essential for cell morphogenesis. *Embo J* 24:3012-3025.

92. Cong, J., W. Geng, B. He, J. Liu, J. Charlton, and P.N. Adler. 2001. The furry gene of Drosophila is important for maintaining the integrity of cellular extensions during morphogenesis. *Development* 128:2793-2802.

93. Grill, B., W.V. Bienvenut, H.M. Brown, B.D. Ackley, M. Quadroni, and Y. Jin. 2007. C. elegans RPM-1 regulates axon termination and synaptogenesis through the Rab GEF GLO-4 and the Rab GTPase GLO-1. *Neuron* 55:587-601.

94. Murthy, V., S. Han, R.L. Beauchamp, N. Smith, L.A. Haddad, N. Ito, and V. Ramesh. 2004. Pam and its ortholog highwire interact with and may negatively regulate the TSC1.TSC2 complex. *J Biol Chem* 279:1351-1358.

95. Han, S., R.M. Witt, T.M. Santos, C. Polizzano, B.L. Sabatini, and V. Ramesh. 2008. Pam (Protein associated with Myc) functions as an E3 ubiquitin ligase and regulates TSC/mTOR signaling. *Cell Signal* 20:1084-1091.

96. Wildonger, J., L.Y. Jan, and Y.N. Jan. 2008. The Tsc1-Tsc2 complex influences neuronal polarity by modulating TORC1 activity and SAD levels. *Genes Dev* 22:2447-2453.

97. Alto, N.M., J. Soderling, and J.D. Scott. 2002. Rab32 is an A-kinase anchoring protein and participates in mitochondrial dynamics. *J Cell Biol* 158:659-668.

98. Tan, J.L., S. Ravid, and J.A. Spudich. 1992. Control of nonmuscle myosins by phosphorylation. *Annu Rev Biochem* 61:721-759.

99. Li, X., E. Baumgart, J.C. Morrell, G. Jimenez-Sanchez, D. Valle, and S.J. Gould. 2002. PEX11 beta deficiency is lethal and impairs neuronal migration but does not abrogate peroxisome function. *Mol Cell Biol* 22:4358-4365.

100. Janssen, A., P. Gressens, M. Grabenbauer, E. Baumgart, A. Schad, I. Vanhorebeek, A. Brouwers, P.E. Declercq, D. Fahimi, P. Evrard, L. Schoonjans, D. Collen, P. Carmeliet, G. Mannaerts, P. Van Veldhoven, and M. Baes. 2003. Neuronal migration depends on intact peroxisomal function in brain and in extraneuronal tissues. *J Neurosci* 23:9732-9741.

101. Baes, M., P. Gressens, S. Huyghe, N.K. De, C. Qi, Y. Jia, G.P. Mannaerts, P. Evrard, V.P. Van, P.E. Declercq, and J.K. Reddy. 2002. The neuronal migration defect in mice with Zellweger syndrome (Pex5 knockout) is not caused by the inactivity of peroxisomal beta-oxidation. *J Neuropathol Exp Neurol* 61:368-374.

102. Gressens, P. 2006. Pathogenesis of migration disorders. *Curr Opin Neurol* 19:135-140.

103. Nagura, M., M. Saito, M. Iwamori, Y. Sakakihara, and T. Igarashi. 2004. Alterations of fatty acid metabolism and membrane fluidity in peroxisome-defective mutant ZP102 cells. *Lipids* 39:43-50.

104. Kovacs, W.J., J.E. Shackelford, K.N. Tape, M.J. Richards, P.L. Faust, S.J. Fliesler, and S.K. Krisans. 2004. Disturbed cholesterol homeostasis in a peroxisome-deficient PEX2 knockout mouse model. *Mol Cell Biol* 24:1-13.

105. Krisans, S.K. 1996. Cell compartmentalization of cholesterol biosynthesis. *Ann N Y Acad Sci* 804:142-164.

106. Olivier, L.M., and S.K. Krisans. 2000. Peroxisomal protein targeting and identification of peroxisomal targeting signals in cholesterol biosynthetic enzymes. *Biochim Biophys Acta* 1529:89-102.

107. Vasanji, A., P.K. Ghosh, L.M. Graham, S.J. Eppell, and P.L. Fox. 2004. Polarization of plasma membrane microviscosity during endothelial cell migration. *Dev Cell* 6:29-41.

108. Ghosh, P.K., A. Vasanji, G. Murugesan, S.J. Eppell, L.M. Graham, and P.L. Fox. 2002. Membrane microviscosity regulates endothelial cell motility. *Nat Cell Biol* 4:894-900.

109. Hermetter, A., B. Rainer, E. Ivessa, E. Kalb, J. Loidl, A. Roscher, and F. Paltauf. 1989. Influence of plasmalogen deficiency on membrane fluidity of human skin fibroblasts: a fluorescence anisotropy study. *Biochim Biophys Acta* 978:151-157.

110. Makhnevych, T., Y. Sydorskyy, X. Xin, T. Srikumar, F.J. Vizeacoumar, S.M. Jeram, Z. Li, S. Bahr, B.J. Andrews, C. Boone, and B. Raught. 2009. Global map of SUMO function revealed by protein-protein interaction and genetic networks. *Mol Cell* 33:124-135.

111. Garofalo, T., A.M. Giammarioli, R. Misasi, A. Tinari, V. Manganelli, L. Gambardella, A. Pavan, W. Malorni, and M. Sorice. 2005. Lipid microdomains contribute to apoptosis-associated modifications of mitochondria in T cells. *Cell Death Differ* 12:1378-1389.

112. Dobrowsky, R.T. 2000. Sphingolipid signalling domains floating on rafts or buried in caves? *Cell Signal* 12:81-90.

113. Grassme, H., A. Jekle, A. Riehle, H. Schwarz, J. Berger, K. Sandhoff, R. Kolesnick, and E. Gulbins. 2001. CD95 signaling via ceramide-rich membrane rafts. *J Biol Chem* 276:20589-20596.

114. Siskind, L.J. 2005. Mitochondrial ceramide and the induction of apoptosis. *J Bioenerg Biomembr* 37:143-153.

115. Mandon, E.C., I. Ehses, J. Rother, G. van Echten, and K. Sandhoff. 1992. Subcellular localization and membrane topology of serine palmitoyltransferase, 3-dehydrosphinganine reductase, and sphinganine N-acyltransferase in mouse liver. *J Biol Chem* 267:11144-11148.

116. Bionda, C., J. Portoukalian, D. Schmitt, C. Rodriguez-Lafrasse, and D. Ardail. 2004. Subcellular compartmentalization of ceramide metabolism: MAM (mitochondria-associated membrane) and/or mitochondria? *Biochem J* 382:527-533.

117. Garcia-Ruiz, C., A. Colell, M. Mari, A. Morales, and J.C. Fernandez-Checa. 1997. Direct effect of ceramide on the mitochondrial electron transport chain leads to generation of reactive oxygen species. Role of mitochondrial glutathione. *J Biol Chem* 272:11369-11377.

118. Dai, Q., J. Liu, J. Chen, D. Durrant, T.M. McIntyre, and R.M. Lee. 2004. Mitochondrial ceramide increases in UV-irradiated HeLa cells and is mainly derived from hydrolysis of sphingomyelin. *Oncogene* 23:3650-3658.

119. Birbes, H., S. El Bawab, Y.A. Hannun, and L.M. Obeid. 2001. Selective hydrolysis of a mitochondrial pool of sphingomyelin induces apoptosis. *Faseb J* 15:2669-2679.

120. Siskind, L.J., R.N. Kolesnick, and M. Colombini. 2006. Ceramide forms channels in mitochondrial outer membranes at physiologically relevant concentrations. *Mitochondrion* 6:118-125.

121. Rouslin, W., J. MacGee, S. Gupte, A. Wesselman, and D.E. Epps. 1982. Mitochondrial cholesterol content and membrane properties in porcine myocardial ischemia. *Am J Physiol* 242:H254-259.

122. Venter, H., S. Genade, R. Mouton, B. Huisamen, I.S. Harper, and A. Lochner. 1991. Myocardial membrane cholesterol: effects of ischaemia. *J Mol Cell Cardiol* 23:1271-1286.

123. Martinez-Abundis, E., F. Correa, N. Pavon, and C. Zazueta. 2009. Bax distribution into mitochondrial detergent-resistant microdomains is related to ceramide and cholesterol content in postischemic hearts. *Febs J* 276:5579-5588.

124. Lucken-Ardjomande, S., S. Montessuit, and J.C. Martinou. 2008. Bax activation and stress-induced apoptosis delayed by the accumulation of cholesterol in mitochondrial membranes. *Cell Death Differ* 15:484-493.

125. Martinez-Abundis, E., N. Garcia, F. Correa, M. Franco, and C. Zazueta. 2007. Changes in specific lipids regulate BAX-induced mitochondrial permeability transition. *Febs J* 274:6500-6510.

Appendix 1 Curriculum Vitae

EMELIE BRASCHI

EDUCATION

University of Ottawa — 2006 - present
PhD in Biochemistry
McGill University — 2003-2006
Bachelor of Science

PUBLICATIONS

Braschi E. McBride H. Vps35 mediates the vesicular transport between mitochondria and peroxisomes. Under revision in *Current Biology*

Braschi E., Zunino R., McBride H.M (2009) MAPL is a new mitochondrial SUMO E3 ligase that regulates mitochondrial fission. *EMBO Rep.* 10(7):748-54.
*Article highlighted with Commentary in EMBO Reports.
*Article selected for Faculty of 1000 "must read".

Zunino R, Braschi E., McBride H.M (2009) Translocation of SenP5 from the nucleoli to the mitochondria modulates DRP1-dependent fission during mitosis. *J Biol Chem.* 26;284(26):17783-95.

Neuspiel M, Schauss AC, Braschi E, Zunino R, Rippstein P, Rachubinski RA, Andrade-Navarro MA, McBride HM. (2008) Cargo-selected transport from the mitochondria to peroxisomes is mediated by vesicular carriers. *Curr Biol.* 18(2):102-8.
*Article chosen as a Research Highlight in Nature Reviews Molecular Cell Biology 9, 186-187 (March 2008)
*Article selected for Faculty of 1000 "must read".
*Article subject to a commentary in Trends in Cell Biology 18(6):253-6, 2008

Soubannier, V., McLelland, G.-L., Braschi, E., Rippstein, P., Kaufman, B., Shoubridge, E.A., Fon, E.A, and McBride, H.M. Parkin selectively modulates the delivery of oxidized cargo to the lysosomes through a novel vesicular transport pathway. *In preparation*

PUBLISHED ABSTRACTS

Keystone Symposia 2009. MAPL is a novel SUMO E3 ligase that regulates mitochondrial fission. Emelie Braschi, Rodolfo Zunino, Heidi McBride.

Keystone Symposia 2009, Mitochondrial vesicles carry damaged cargo to the lysosomes. Vincent Soubannier, Emelie Braschi, Peter Rippstein Brett Kauffman, Eric Shoubridge, and Heidi M. McBride.

Cold Spring Harbor 2008, The Cell Cycle Meeting. Mitochondrial SUMOylation is a novel cell cycle check point. Emelie Braschi, Rodolfo Zunino, Heidi McBride.

2007 FASEB Summer Research Conference. Characterization of cargo selected, DRP1 independent mitochondria derived vesicles. Vincent Soubannier, Margaret Neuspiel, Emelie Braschi, Rodolfo Zunino, Peter Rippstein, Heidi McBride.

ACADEMIC AWARDS/FUNDING

F. Banting and C. Best Ca. Graduate Scholarships, Doctoral Award *Canadian Institute of Health Research*	2008-present
University of Ottawa Excellence Scholarship *University of Ottawa*	2007-present
F. Banting and C. Best Ca. Graduate Scholarships, Master's Award *Canadian Institute of Health Research*	2007-2008
Ontario Graduate Scholarship in Science and Technology *University of Ottawa*	2006/2007
Strategic Areas of Development Award *University of Ottawa*	2006
Admission Scholarship *University of Ottawa*	2006
John D. Schultz Scholarship *Heart and Stroke Foundation of Ontario*	Summer 2006
Emily Crawford Scholarship *McGill University*	2005/2006
Dean's Honour List *McGill University*	2004/2005

Appendix 2 Cargo-selected transport from the mitochondria to peroxisomes is mediated by vesicular carriers

Current Biology 18, 102–108, January 22, 2008 ©2008 Elsevier Ltd All rights reserved DOI 10.1016/j.cub.2007.12.038

Report

Cargo-Selected Transport from the Mitochondria to Peroxisomes Is Mediated by Vesicular Carriers

Margaret Neuspiel,[1,4] Astrid C. Schauss,[1,4] Emelie Braschi,[1] Rodolfo Zunino,[1] Peter Rippstein,[1] Richard A. Rachubinski,[2] Miguel A. Andrade-Navarro,[3] and Heidi M. McBride[1,*]

[1]Lipoproteins and Atherosclerosis Group
University of Ottawa Heart Institute
40 Ruskin St.
Ottawa, Ontario K1Y 4W7
Canada

[2]Department of Cell Biology
University of Alberta
Medical Sciences Building 5-14
Edmonton, Alberta T6G 2H7
Canada

[3]Max Delbrück Center for Molecular Medicine
Robert-Rössle-Strasse 10
13125 Berlin
Germany

Summary

Mitochondria and peroxisomes share a number of common biochemical processes, including the β oxidation of fatty acids and the scavenging of peroxides. Here, we identify a new outer-membrane mitochondria-anchored protein ligase (MAPL) containing a really interesting new gene (RING)-finger domain. Overexpression of MAPL leads to mitochondrial fragmentation, indicating a regulatory function controlling mitochondrial morphology. In addition, confocal- and electron-microscopy studies of MAPL-YFP led to the observation that MAPL is also incorporated within unique, DRP1-independent, 70–100 nm diameter mitochondria-derived vesicles (MDVs). Importantly, vesicles containing MAPL exclude another outer-membrane marker, TOM20, and vesicles containing TOM20 exclude MAPL, indicating that MDVs selectively incorporate their cargo. We further demonstrate that MAPL-containing vesicles fuse with a subset of peroxisomes, marking the first evidence for a direct relationship between these two functionally related organelles. In contrast, a distinct vesicle population labeled with TOM20 does not fuse with peroxisomes, indicating that the incorporation of specific cargo is a primary determinant of MDV fate. These data are the first to identify MAPL, describe and characterize MDVs, and define a new intracellular transport route between mitochondria and peroxisomes.

Results

Identification of a Novel Mitochondrial RING-Finger-Containing Protein

We were interested in identifying candidate mitochondrial proteins that participate in the regulation of mitochondrial morphology. It has been shown that mitochondrial morphology can be regulated both by ubiquitination and SUMOylation (SUMO: small ubiquitin-related modifier) [1–6]. We therefore performed a bioinformatics screen to identify candidate mitochondrially anchored ubiquitin or SUMO E3 ligases containing conserved really interesting new gene (RING)-finger motifs. One of these sequences was a mitochondrially targeted, ubiquitously expressed, unidentified open reading frame, FLJ12875, which encoded a protein that we have named MAPL, for mitochondria-anchored protein ligase (Figure S1 available online). The translated protein contains 352 amino acids with both the N-terminal and the C-terminal RING domains exposed to the cytosol and with two predicted transmembrane helices (Figures S1A and S1B). Transient transfection of MAPL-YFP (YFP: yellow fluorescent protein) in HeLa or COS7 cells resulted in a partially fragmented mitochondrial phenotype (Figures 1A and 1E). This was in contrast to the tubular morphology of the TOM20-labeled mitochondria in neighboring, untransfected control cells (Figure 1A, top middle). Mitochondrial fragmentation was dependent upon the RING-finger domain of MAPL because transfection of $MAPL_{1-296}$-YFP lacking the RING-finger domain did not induce this phenotype (Figure 1A, bottom). To determine whether this phenotype required the mitochondrial fission GTPase, DRP1, we cotransfected cells with the dominant interfering mutant, DRP1(K38E)-CFP (CFP: cyan fluorescent protein) [7–9]. The fragmentation induced by MAPL expression was blocked in the presence of the DRP1 mutant, and the resulting mitochondria were highly fused (Figure 1B). These data indicate that MAPL participates in the regulation of mitochondrial fragmentation. However, in cells expressing both dominant-negative DRP1 and either wild-type MAPL or $MAPL_{(1-296)}$, a pool of very small MAPL- or TOM20-positive fragments remained within the otherwise highly interconnected mitochondrial reticulum (Figure 1B, circles). Electron microscopy (EM) analysis of cells transfected with MAPL-YFP revealed the presence of highly distinct structures, 70–100 nm in diameter, emanating from the sides of the mitochondria expressing MAPL-YFP (Figure 1C, arrows). These profiles contained either one or both mitochondrial membranes and showed an increase in electron density around the surface. Preembedded immunogold labeling of MAPL-YFP revealed small, ~100 nm structures resembling intracellular-transport vesicles that were not attached to the larger mitochondria (Figure 1D, top left). They often contained inner mitochondrial membrane; however, cristae were rarely observed and, instead, the outer and inner membranes appeared as two concentric circles (Figure 1D, top left). Standard immunogold labeling of fixed sections also revealed multiple enrichments of MAPL-YFP along mitochondria (Figure 1D, top right, bottom left, and bottom right, arrows).

To follow the formation of the small MAPL-containing fragments in real time, we employed time-lapse confocal microscopy. In addition to the expected general fragmentation of the mitochondria in cells expressing MAPL-CFP, we also observed a few unique fission events consistent with the EM analysis. In the time series presented in Figure 1E (Movie S1), we first observed a lateral enrichment of MAPL-CFP along the tubular mitochondria (Figure 1E, arrow). This enriched region of the mitochondria was then seen to pinch off from the side of the organelle, liberating a spherical mitochondrial

*Correspondence: hmcbride@ottawaheart.ca
[4]These authors contributed equally to this work.

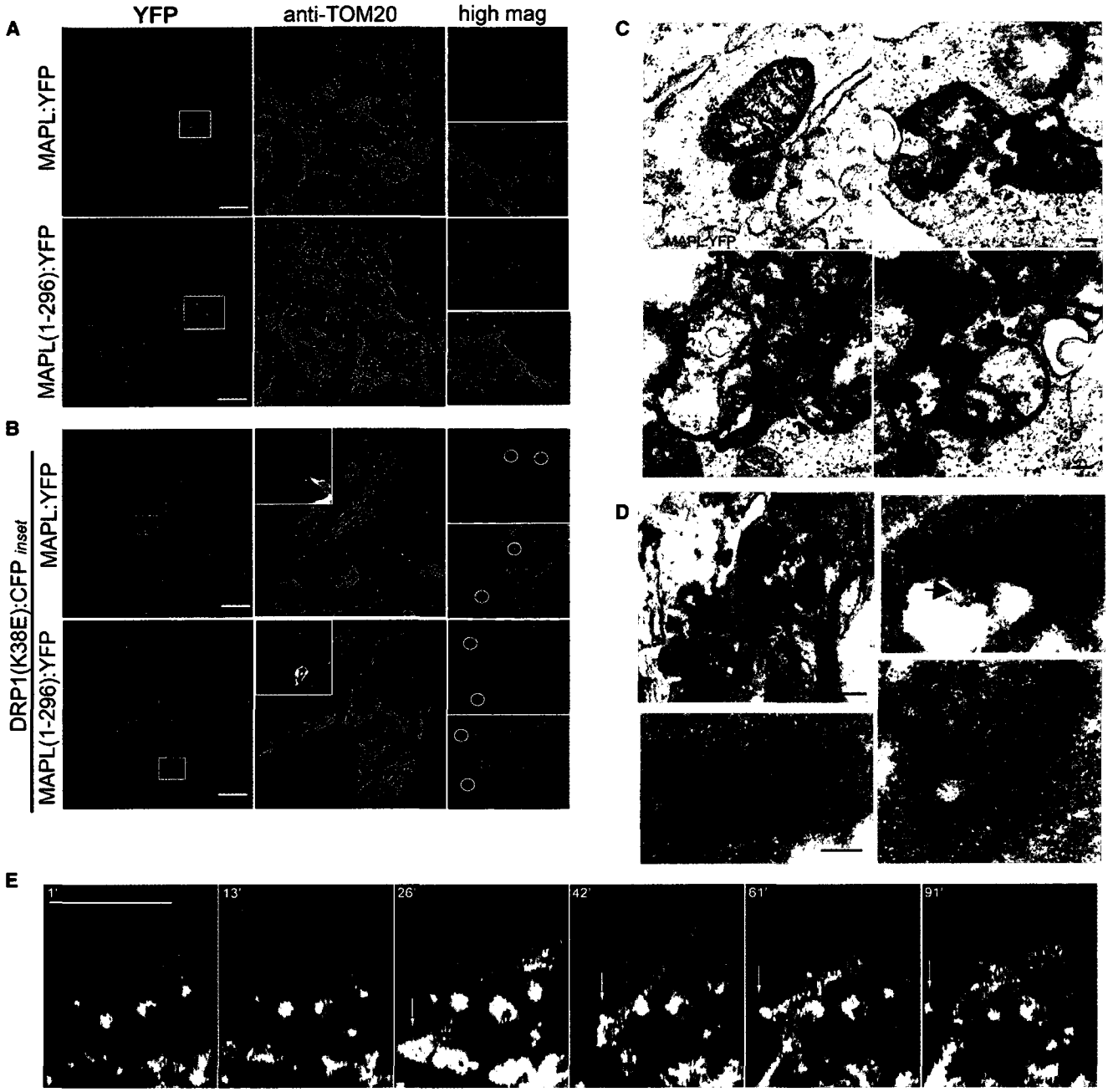

Figure 1. MAPL Induces Mitochondrial Fragmentation and Marks Unique Mitochondrial Structures

(A) Mitochondria in HeLa cells were transfected with either MAPL-YFP (top panels) or MAPL(1-296)YFP (lower panels), and fixed cells were stained with anti-TOM20 and imaged by confocal microscopy. Boxed regions were enlarged. Scale bars represent 20 μm.

(B) As in (A), except that cells were cotransfected with DRP1(K38E)-CFP, which is shown in the insets (gray). Some small fragmented structures are circled.

(C) COS7 cells transfected with MAPL-YFP were fixed and prepared for electron microscopy. Arrows highlight vesicular profiles. Scale bars represent 100 nm.

(D) The top left panel shows COS7 cells transfected with MAPL-YFP were fixed on coverslips, permeabilized with saponin, and labeled with YFP antibodies and then goat anti-rabbit gold secondary antibodies. The top right, bottom left, and bottom right panels show standard immunogold labeling with FP antibodies on thin sections. Scale bars represent 100 nm. Arrows highlight enrichments of MAPL.

(E) Confocal time-lapse imaging of MAPL-CFP transfected into COS7 cells shows the formation of a mitochondrial vesicle. Arrows highlight the enrichment of MAPL-CFP along the side of a mitochondrial tubule that eventually separates into an individual vesicle. Note the mixture of the rod-like and spherical mitochondrial fragments. The scale bar represents 5 μm, and the time stamp is in seconds.

fragment. This event was qualitatively distinct from previously documented mitochondrial fission, which instead involves a constriction along the tubule mediated by DRP1, leading to a smooth separation of the two halves of the mitochondrion (Movie S2). Taken together, the EM and confocal analysis of MAPL-CFP indicate that MAPL is incorporated within small mitochondria-derived vesicles (MDVs) that form in a distinct, DRP1-independent manner.

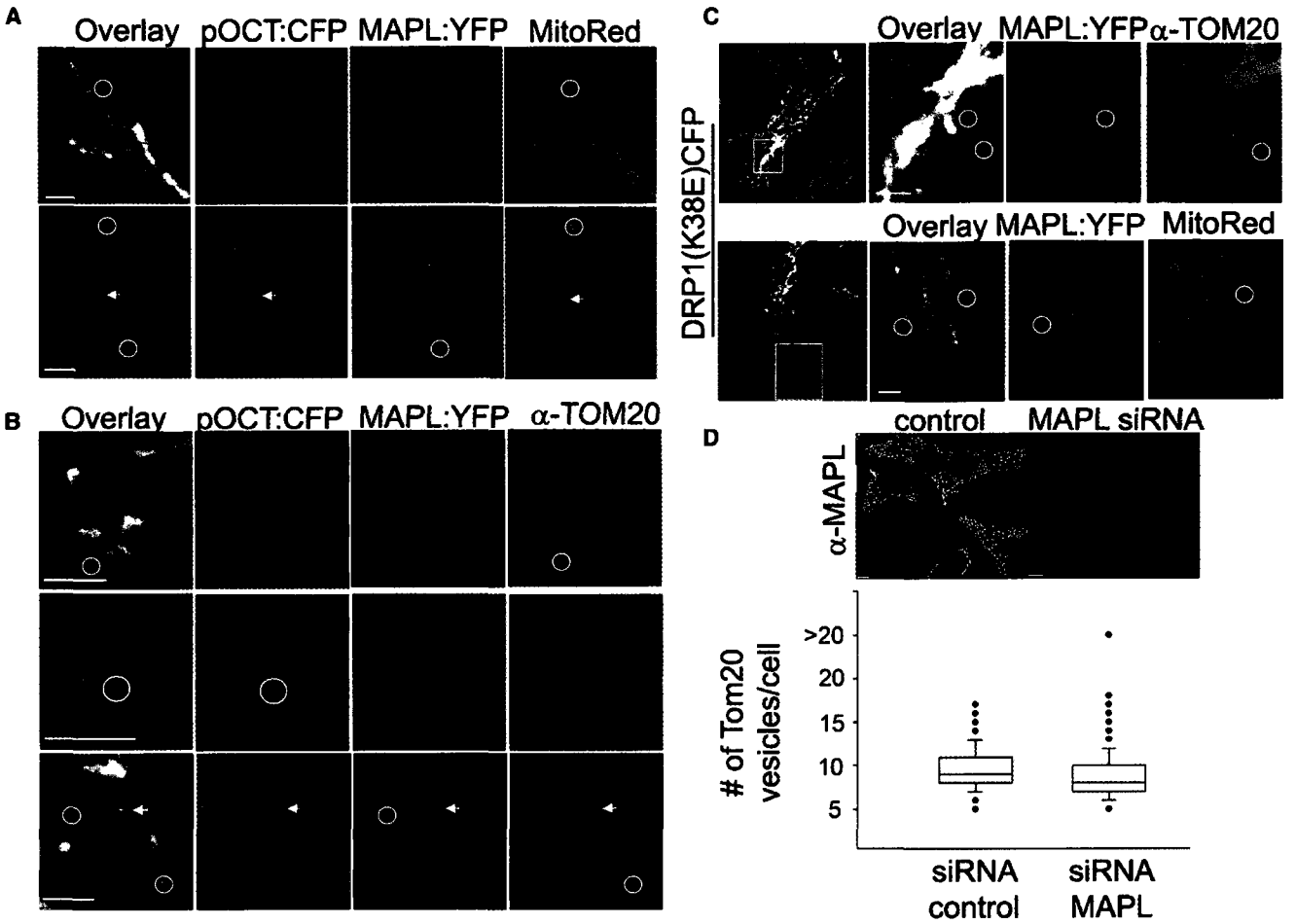

Figure 2. Evidence of Cargo Selection within Mitochondrial Vesicles

(A–C) HeLa cells were cotransfected with MAPL-YFP and pOCT-CFP, loaded with MitoFluorRed 633, and imaged live (A) or fixed and stained with anti-TOM20 antibodies (B). In (C), HeLa cells were cotransfected with DRP1(K38E)-CFP (magenta) and MAPL-YFP and either loaded with MitoFluorRed 633 (bottom panels) or fixed and stained with anti-TOM20 antibodies (top panels). Circles indicate mitochondrial structures that carry a single label, and arrows indicate vesicles carrying more than one label. Scale bars represent 2 μm.

(D) Nontargeting siRNA or MAPL siRNA were transfected into HeLa cells that were fixed and stained with MAPL antibodies (top panels) or TOM20 antibodies. The quantification of the number of TOM20-positive structures in 150 cells from three independent experiments is shown in the vertical box plot. The median of the data is set by the horizontal line, and the whiskers indicate the maximum and minimum values. Asterisks indicate the data points lying beyond two standard deviations from the mean.

MDVs Exhibit Cargo Selection

EM and video examination suggested that there might be an enrichment or selection of specific mitochondrial cargo within these structures. To test this directly, we cotransfected MAPL-YFP with a mitochondrial matrix marker, pOCT-CFP, and performed either live-cell experiments with the potentiometric dye, MitoFluorRed633, or fixed cells and stained them with antibodies against the outer-membrane import receptor, TOM20 (Figures 2A and 2B). Surprisingly, we observed multiple combinations of cargo incorporated within very small mitochondrial fragmented structures. Representative images reflecting the diversity of cargo within these structures are shown in Figure 2. For example, in the bottom panel of Figure 2A, there are structures containing MAPL-YFP that do not contain $\Delta\Psi$, and other potential-containing vesicles that do not contain MAPL-YFP (circles). One structure is seen to contain both OCT-CFP and $\Delta\Psi$ but to lack MAPL-YFP (arrows). In fixed cells stained with TOM20 antibodies, we observed a similar mixture of vesicular profiles (Figure 2B, circles). These images also reveal small mitochondrial profiles containing all three markers, which is expected from the generation of DRP1-dependent fragments (Figure 2B, bottom panels, arrows). Coexpression of MAPL-YFP with DRP1(K38E)-CFP resulted in a highly interconnected mitochondrial reticulum (Figures 1B and 2C, left panels). However, careful examination of the remaining fragments revealed that they also contained either MAPL-YFP or TOM20 (Figure 2C, top panels, circles) or $\Delta\Psi$ (Figure 2C, bottom panels, circles) with few, if any, fragments labeled for both markers. Although microscopy might not eliminate the possibility of undetectable amounts of each cargo present, the data show that the vesicles selectively exclude, and are significantly enriched for, specific cargo. This indicates that mitochondria have the capacity to segregate specific cargo even within a single membrane. Therefore, we suggest that in addition to their DRP1-independence and uniform size of 70–100 nm, another criterion to define a MDV is evidence of cargo selectivity.

Although MAPL expression stimulates mitochondrial fragmentation and is incorporated within these small vesicles, it

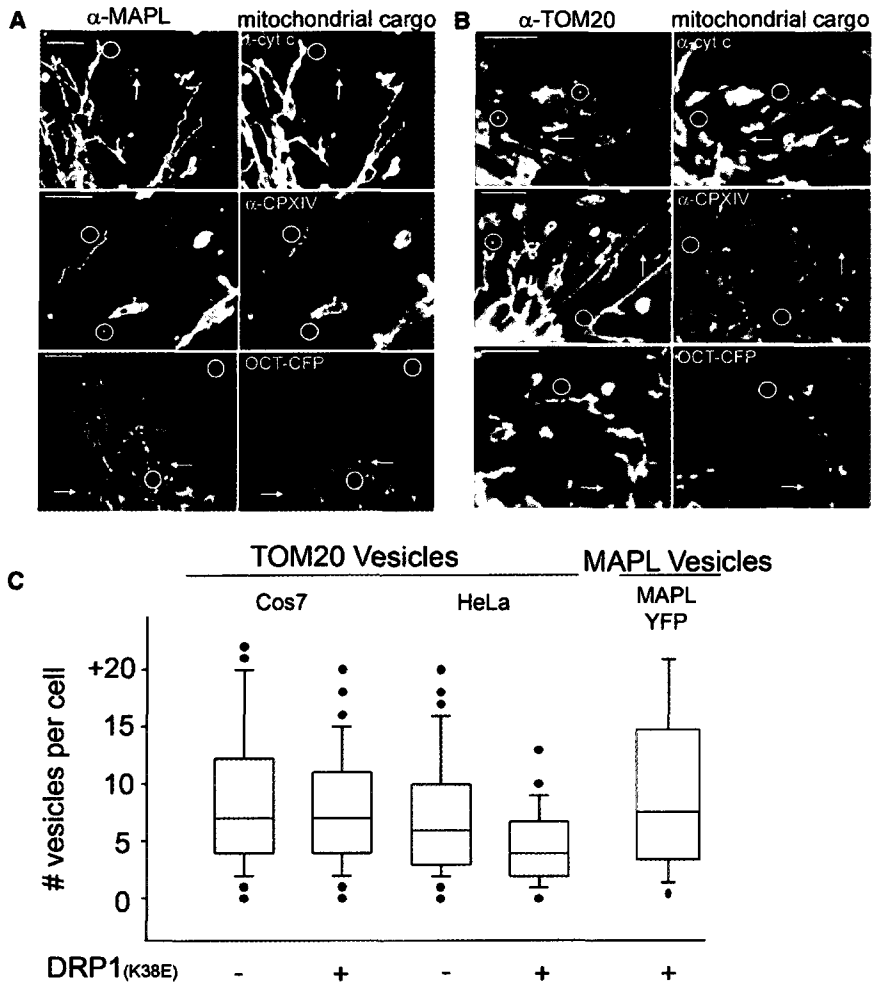

Figure 3. Quantification of Cargo Selectivity and DRP1-Independent Vesicle Formation

(A) COS7 cells were fixed and stained with MAPL polyclonal antibodies and antibodies to cytochrome c (top panels), anti-subunit 1 of complex IV (middle panels), or the matrix marker, OCT-CFP marker (bottom panels). Circles illustrate vesicles positive for only MAPL, and arrows point to vesicles containing both cargoes. Scale bars represent 1 μm.

(B) As in (A), except decoration is with antibodies to the outer-membrane marker, TOM20.

(C) COS7 or HeLa cells untransfected or transfected with DRP1(K38E)-CFP were fixed and stained for anti-TOM20. The number of MAPL-positive vesicles within HeLa cells expressing DRP1(K39E)-CFP and MAPL-YFP are quantified in the last lane. The total number of vesicles was counted per cell from 150 cells from three independent experiments and plotted in the vertical box plot shown. To confirm that the DRP1(K38E)-CFP was functionally blocking DRP1 activity, only cells expressing the CFP-tagged protein and that also contained highly fused, interconnected mitochondria were included. The median of the data is set by the horizontal line, and the whiskers indicate the maximum and minimum values. Asterisks indicate the data points lying beyond two standard deviations from the mean.

was unclear whether MAPL was a regulator of vesicle formation. To test this, we quantified the number of small TOM20-positive structures in cells expressing endogenous or silenced MAPL (Figure 2D). Analysis showed that the overall mitochondrial morphology was not dramatically altered (Figure S2) and that the number of TOM20-labeled mitochondrial vesicular structures was similar in cells lacking MAPL compared to control cells (Figure 2D). This indicates that although MAPL can be incorporated within vesicles and stimulates DRP1-dependent mitochondrial fragmentation (Figures 1, 2A, 2B, and 2C), it is not a core component of the machinery required for MDV formation.

We next quantified both the extent of MDV cargo selectivity (Figures 3A, and 3B, Table 1) and the total number of vesicles within cells (Figure 3C) by using endogenous markers. Immunofluorescence of endogenous MAPL revealed a number of distinct, very small punctate vesicular structures in addition to a mitochondrial location (Figure 3A, left panels). This antibody staining was specific because the silencing of MAPL through small interfering RNA (siRNA) abolished this signal (Figure 2D, top panels). To further investigate the cargo selection observed above (Figures 2A and 2B) with endogenous markers, we costained the untransfected cells with either MAPL or TOM20 antibodies together with one of the following markers: cytochrome *c* of the intermembrane space (Figures 3A and 3B, top panels), subunit 1 of complex IV of the inner mitochondrial membrane (Figures 3A and 3B, middle panels), and a matrix-targeted CFP (Figures 3A and 3B, bottom panels). Quantification revealed that only 33%–50% of vesicles containing either TOM20 or MAPL also contained a second mitochondrial marker (Table 1).

We next quantified the number of vesicles in cells expressing the dominant interfering mutant of DRP1, DRP1(K38E)-CFP, in COS7 and HeLa cells. Quantification showed that cells expressing DRP1(K38E)-CFP and showing completely interconnected mitochondria exhibited nearly the same number of vesicles as did controls (Figure 3C). The slight reduction observed within HeLa cells upon inhibition of DRP1 likely reflects the inclusion of some DRP1-dependent fragments with vesicles during the counting in control cells. Quantification of the number of MAPL-YFP-positive vesicles in DRP1(K38E)-CFP-expressing cells indicated that they are present in numbers similar to TOM20-labeled vesicles (Figure 3C). Together, the data confirm that both TOM20- and MAPL-positive MDVs are formed by a mechanism distinct from DRP1-mediated mitochondrial fission.

Table 1. Quantification of the Percentage Colocalization of Each Marker Pair

Label	MAPL	TOM20
cytochrome c	33 ± 9.0	38.0 ± 11.1
sub1-complexIV	50 ± 8.0	37.3 ± 7.5
OCT-CFP	48 ± 11.3	42 ± 7.2

Data are taken from 50 vesicles from each of three independent experiments.

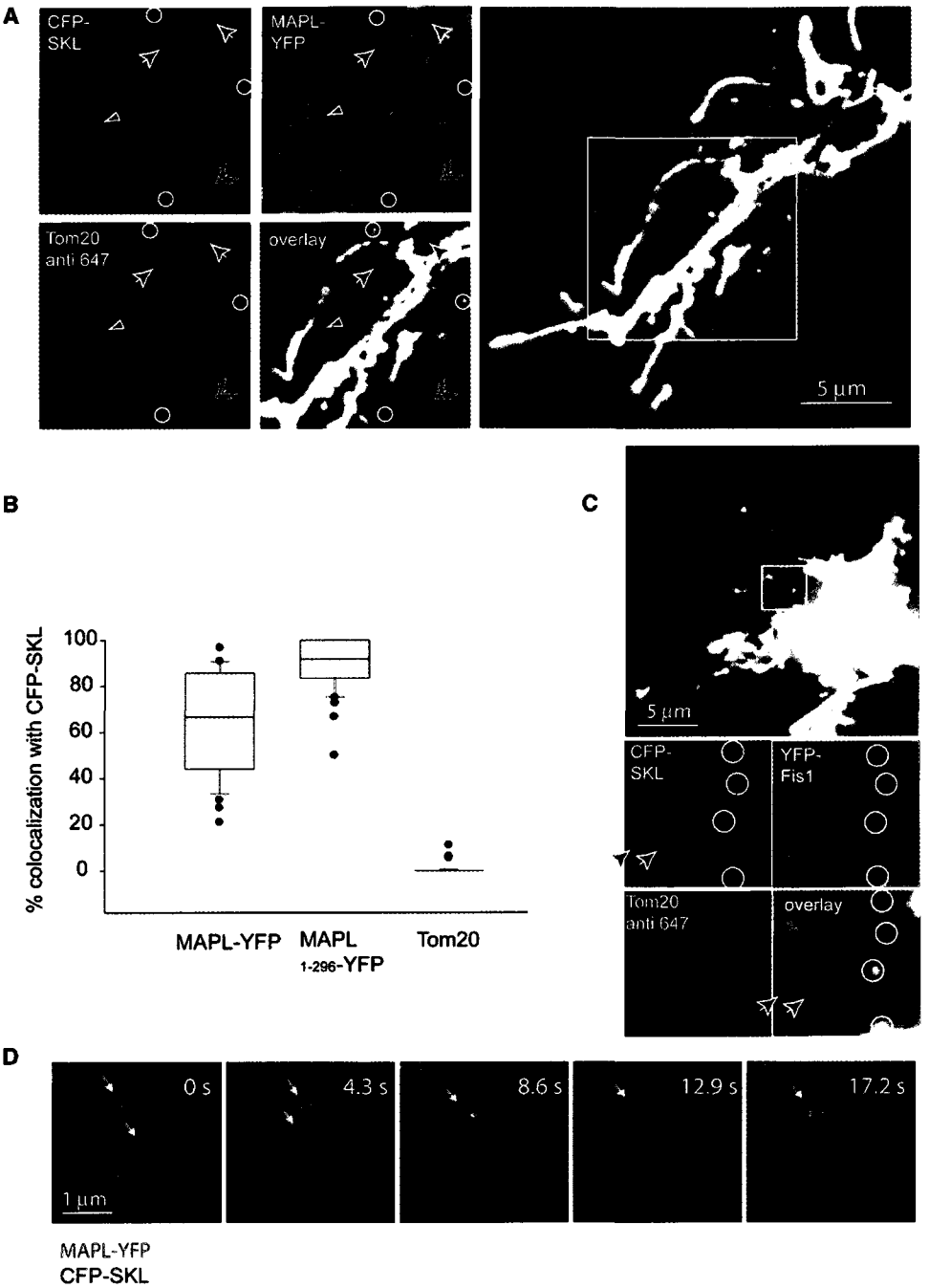

Figure 4. MAPL-Containing Vesicles Are Targeted to the Peroxisomes

(A) HeLa cells were cotransfected with CFP-SKL and MAPL-YFP and, after 16 hr, were fixed and stained with polyclonal TOM20 antibodies. A representative confocal image shows the colocalization of MAPL-YFP-positive vesicles (green) with peroxisomes (red). The magenta TOM20 signal is excluded from the peroxisomal structures. Red arrowheads depict peroxisomes that do not contain MAPL, green arrowheads designate MAPL-positive vesicles that do not contain CFP-SKL or TOM20, and magenta arrowheads reveal TOM20-positive vesicles that do not colocalize with either MAPL or CFP-SKL. Circles reveal vesicles that are labeled for both CFP-SKL and MAPL-YFP but exclude TOM20.

(B) HeLa cells cotransfected with MAPL-YFP or $MAPL_{1-296}$-YFP and CFP-SKL were fixed and immunostained for TOM20 (anti-Alexa 647). The percentage of colocalization of MAPL-positive or TOM20-positive vesicles with CFP-SKL (n = 42 for each data set) is shown in the vertical box plot. The median of the data is set by the horizontal line, and the whiskers indicate the maximum and minimum values. Asterisks indicate the data points lying beyond two standard deviations from the mean.

(C) As in (A), except that HeLa cells were transfected with YFP-Fis1 (green) and CFP-SKL (red) and stained for Tom20 (magenta). The scale bar represents 5 µm.

(D) Confocal time-lapse series showing MAPL-YFP-labeled vesicles (in green) and CFP-SKL-labeled peroxisomes. Time scale is indicated in seconds. Arrows point to two independent structures that are shown to fuse in the last three panels. The scale bar represents 1 µm.

MAPL-Containing MDVs Are Targeted to Peroxisomes

In order to determine the fate of MDVs, we tested a number of cellular markers. Surprisingly, we found that the MAPL-positive vesicles were targeted to peroxisomes, whereas TOM20-containing vesicles did not share this fate (Figure 4A). We quantified the colocalization of MAPL-YFP-positive, TOM20-negative vesicles with peroxisomes and found that a mean of 65% of MAPL-containing vesicles colocalize with CFP-SKL-labeled peroxisomes (Figure 4B). The targeting of MAPL vesicles to the peroxisome was independent of the RING-finger motif because in cells expressing $MAPL_{1-296}$-YFP lacking the RING motif, a mean of 91% of MAPL-positive vesicles colocalized with peroxisomes (Figure 4B). Importantly, vesicles positive for TOM20 and negative for MAPL did not colocalize with peroxisomes, further demonstrating the specificity for the cargo incorporation and the transport event (Figure 4B). As shown earlier, the total number of DRP1-independent MAPL vesicles within a given cell is relatively low, between 5 and 15 vesicles per cell. This is far below the number of peroxisomes per cell, which ranges between 50 and a few hundred, indicating that most peroxisomes do not contain MAPL. The fact that MAPL is not equally found in all peroxisomes, unlike CFP-SKL, indicates that MAPL is not imported into peroxisomes. Another mitochondrial outer-membrane protein, Fis1, has been dually localized to peroxisomes. As previously shown [10], YFP-Fis1 is found in the vast majority of peroxisomes (Figure 4C), which is distinct from the restricted localization of MAPL-YFP in only a few peroxisomes. This is consistent with an import mechanism of targeting for YFP-Fis1. However, we did note the presence of some peroxisomes that were devoid of YFP-Fis1 (Figure 4C, arrows), further suggesting the presence of distinct subpopulations of peroxisomes. Given that peroxisomes grow and divide [11], we also considered that very low levels of MAPL within the entire peroxisomal population might have been missed by our confocal analysis. Indeed, by using higher sensitivities of both excitation and detection, we could observe low amounts of MAPL within many additional peroxisomes, although this still represented a subpopulation of peroxisomes (Figure S3). Therefore, we consider that the initial delivery of the bright, MAPL-containing vesicles to peroxisomes would target a bulk of protein to a subset of these organelles. After this, the MAPL protein might then become diluted throughout the peroxisomal population over time. To further confirm the direct transport of MDVs to peroxisomes, we performed time-lapse imaging, and we observed a MAPL-positive MDV fusing directly with a peroxisome labeled with CFP-SKL (Figure 4D, Movie S3). Together, these data indicate that MDVs specifically containing MAPL are targeted to, and fuse with, a subpopulation of peroxisomes.

Discussion

We have identified a novel mitochondrial outer-membrane protein, MAPL, that participates in the regulation of DRP1-mediated mitochondrial fission in a RING-finger-dependent manner. In addition, our study is the first to report the novel observation that mitochondrial cargo, including MAPL, is sorted into previously uncharacterized mitochondrially derived vesicles. We define MDVs with four independent criteria: (1) They are formed in a DRP1-independent manner, (2) they are highly uniform 70–100 nm structures, (3) they form from the lateral segregation of mitochondrial membrane in a manner distinct from previously characterized whole-organelle constriction, and (4) they incorporate selected mitochondrial cargo. Importantly, our data reveal that MAPL-containing vesicles are targeted to fuse with a subset of peroxisomes. In contrast, TOM20-containing vesicles do not share this fate, providing evidence that the incorporated cargo is an important determinant of vesicle fate. Peroxisomes share common metabolic functions with the mitochondria, as well as their fission machinery, DRP1 and Fis1 [10, 12–16]. However, the expression or silencing of MAPL did not visibly alter peroxisomal morphology (Figure S2), indicating a more subtle role, if any, in peroxisome fission. Many examples of metabolite shuttling between the mitochondria and peroxisomes, including ammonium, carnitine, and the flux of metabolites involved in the TCA cycle, have been reported [17, 18]. In addition, the mitochondria-specific lipid, cardiolipin, has been found in significant levels within peroxisomes [19, 20]. Our work represents the first report of vesicular transport and communication between the mitochondria and peroxisomes. Future work will determine the precise function of MAPL within peroxisomes and the nature of the peroxisomal population that fuses with MDVs. For now, we have identified an unexpected intracellular transport route that provides a direct link between two organelles that are known to operate in a highly coordinated manner. In addition, the observation that there are multiple MDVs containing specific subsets of cargo represents an important new aspect of mitochondrial dynamics. The function and fates of MDVs carrying TOM20 and other specific cargo are the focus of ongoing studies.

Supplemental Data

Experimental Procedures, three figures, and three movies are available at http://www.current-biology.com/cgi/content/full/18/2/102/DC1/.

Acknowledgments

This work was supported by the Heart and Stroke Foundation of Ontario and a Canadian Institutes of Health Research (CIHR) New Investigator Award to H.M.M. M.N and E.B. were supported by an Ontario Heart and Stroke Doctoral and an Ontario Graduate Scholarship in Science and Technology, respectively. A.C.S was supported by a CIHR Postdoctoral Fellowship. M.A.A. is Canada Research Chair in Bioinformatics. R.A.R. is a Canada Research Chair in Cell Biology and an International Research Scholar of the Howard Hughes Medical Institute. We would like to thank Alex Stewart (University of Ottawa Heart Institute) for technical help, Gordon Shore (McGill University) for TOM20 antibodies, Richard Youle (National Institutes of Health [NIH]) for YFP-Fis1 complementary DNA (cDNA), and Jeremy Simpson (European Molecular Biology Laboratories [EMBL]) for sharing plasmids. We thank members of the Group, Luca Pellegrini (Laval University), Robert Screaton (Apoptosis Research Center [ARC], University of Ottawa), and Gordon Shore for stimulating discussions and insightful comments on the manuscript.

Received: October 9, 2007
Revised: November 29, 2007
Accepted: December 7, 2007
Published online: January 17, 2008

References

1. Yonashiro, R., Ishido, S., Kyo, S., Fukuda, T., Goto, E., Matsuki, Y., Ohmura-Hoshino, M., Sada, K., Hotta, H., Yamamura, H., et al. (2006). A novel mitochondrial ubiquitin ligase plays a critical role in mitochondrial dynamics. EMBO J. *25*, 3618–3626.
2. Nakamura, N., Kimura, Y., Tokuda, M., Honda, S., and Hirose, S. (2006). MARCH-V is a novel mitofusin 2- and Drp1-binding protein able to change mitochondrial morphology. EMBO Rep. *7*, 1019–1022.
3. Karbowski, M., Neutzner, A., and Youle, R.J. (2007). The mitochondrial E3 ubiquitin ligase MARCH5 is required for Drp1 dependent mitochondrial division. J. Cell Biol. *178*, 71–84.
4. Harder, Z., Zunino, R., and McBride, H. (2004). Sumo1 conjugates mitochondrial substrates and participates in mitochondrial fission. Curr. Biol. *14*, 340–345.

5. Wasiak, S., Zunino, R., and McBride, H.M. (2007). Bax/Bak promote sumoylation of DRP1 and its stable association with mitochondria during apoptotic cell death. J. Cell Biol. *177*, 439–450.
6. Zunino, R., Schauss, A., Rippstein, P., Andrade-Navarro, M., and McBride, H.M. (2007). The SUMO protease SENP5 is required to maintain mitochondrial morphology and function. J. Cell Sci. *120*, 1178–1188.
7. Smirnova, E., Griparic, L., Shurland, D.L., and van Der Bliek, A.M. (2001). Dynamin-related protein drp1 is required for mitochondrial division in mammalian cells. Mol. Biol. Cell *12*, 2245–2256.
8. Yoon, Y., Pitts, K.R., and McNiven, M.A. (2001). Mammalian dynamin-like protein dlp1 tubulates membranes. Mol. Biol. Cell *12*, 2894–2905.
9. Hoppins, S., Lackner, L., and Nunnari, J. (2007). The machines that divide and fuse mitochondria. Annu. Rev. Biochem. *76*, 751–780.
10. Koch, A., Yoon, Y., Bonekamp, N.A., McNiven, M.A., and Schrader, M. (2005). A role for Fis1 in both mitochondrial and peroxisomal fission in mammalian cells. Mol. Biol. Cell *16*, 5077–5086.
11. Fagarasanu, A., Fagarasanu, M., and Rachubinski, R.A. (2007). Maintaining peroxisome populations: A story of division and inheritance. Annu. Rev. Cell Dev. Biol. *23*, 321–344.
12. Koch, A., Thiemann, M., Grabenbauer, M., Yoon, Y., McNiven, M.A., and Schrader, M. (2003). Dynamin-like protein 1 is involved in peroxisomal fission. J. Biol. Chem. *278*, 8597–8605.
13. Koch, A., Schneider, G., Luers, G.H., and Schrader, M. (2004). Peroxisome elongation and constriction but not fission can occur independently of dynamin-like protein 1. J. Cell Sci. *117*, 3995–4006.
14. Tanaka, A., Kobayashi, S., and Fujiki, Y. (2006). Peroxisome division is impaired in a CHO cell mutant with an inactivating point-mutation in *dynamin-like protein* 1 *gene*. *Exp. Cell Res. 312, 1671–1684.*
15. Kobayashi, S., Tanaka, A., and Fujiki, Y. (2007). Fis1, DLP1, and Pex11p coordinately regulate peroxisome morphogenesis. Exp. Cell Res. *313*, 1675–1686.
16. Schrader, M. (2006). Shared components of mitochondrial and peroxisomal division. Biochim. Biophys. Acta *1763*, 531–541.
17. Linka, M., and Weber, A.P. (2005). Shuffling ammonia between mitochondria and plastids during photorespiration. Trends Plant Sci. *10*, 461–465.
18. Scott, I., Sparkes, I.A., and Logan, D.C. (2007). The missing link: Interorganellar connections in mitochondria and peroxisomes? Trends Plant Sci. *12*, 380–381.
19. Wriessnegger, T., Gubitz, G., Leitner, E., Ingolic, E., Cregg, J., de la Cruz, B.J., and Daum, G. (2007). Lipid composition of peroxisomes from the yeast *Pichia pastoris* grown on different carbon sources. Biochim. Biophys. Acta *1771*, 455–461.
20. Leber, R., Zinser, E., Zellnig, G., Paltauf, F., and Daum, G. (1994). Characterization of lipid particles of the yeast, *Saccharomyces cerevisiae*. Yeast *10*, 1421–1428.

Appendix 3 Translocation of SENP5 from the nucleoli to the mitochondria modulates Drp1-dependent fission during mitosis

THE JOURNAL OF BIOLOGICAL CHEMISTRY VOL. 284, NO. 26, pp. 17783–17795, June 26, 2009

Translocation of SenP5 from the Nucleoli to the Mitochondria Modulates DRP1-dependent Fission during Mitosis*

Received for publication, March 23, 2009 Published, JBC Papers in Press, May 1, 2009, DOI 10.1074/jbc.M901902200

Rodolfo Zunino, Emélie Braschi[1], Liqun Xu, and Heidi M. McBride[2]

From the University of Ottawa Heart Institute, Ottawa, Ontario K1Y 4W7, Canada

The mechanisms that ensure an equal inheritance of cellular organelles during mitosis are an important area of study in cell biology. For the mitochondria fragment during mitosis, however, the cellular links that signal these changes are largely unknown. We recently identified a SUMO protease, SenP5, that deSUMOylates a number of mitochondrial targets, including the dynamin-related fission GTPase, DRP1. In interphase, SenP5 resides primarily within the nucleoli, in addition to a cytosolic pool. Here we report the relocalization of SenP5 from the nucleoli to the mitochondrial surface at G_2/M transition prior to nuclear envelope breakdown. The recruitment of SenP5 results in a significant loss in mitochondrial SUMOylation, and a concomitant increase in the labile pool of DRP1 that drives mitochondrial fragmentation. Importantly, silencing of SenP5 leads to an arrest in the cell cycle precisely at the time when the protease is translocated to the mitochondria. These data indicate that transition of SenP5 to the mitochondria plays an important role in mitochondrial fragmentation during mitosis. The altered intracellular localization of SenP5 represents the first example of the mitochondrial recruitment of a SUMO protease and provides new insights into the mechanisms of interorganellar communication during the cell cycle.

The regulation of the cell cycle is based upon a number of critical checkpoints that ensure the cell is healthy, the DNA is correctly replicated, there is sufficient metabolic energy, and that the organelles are properly partitioned during mitosis. Each of the cell cycle checkpoints are maintained through precise signaling cascades, whose activities determine whether the cycle proceeds, remains quiescent, or whether the cell may enter into apoptotic death. A complete understanding of all cell cycle checkpoints is critical for the identification of new therapeutic targets for both cancer and for the development of regenerative technologies. Recently, genetic models in *Drosophila melanogaster* have identified at least two novel retrograde signaling pathways that ensure sufficient metabolic capacity and health at the G_1/S checkpoint (1, 2). Mutations in a component of electron transport chain complex IV led to a 60% decrease in cellular ATP, thereby activating AMP-activated protein kinase and p53-dependent degradation of cyclin E (1). In a parallel pathway, the increased production of cellular ROS through mutations in a component of complex I led to the activation of the c-Jun NH_2-terminal kinase (JNK)-FOXO cascade that up-regulates the cyclin E inhibitor Dacapo, causing cell cycle arrest at G_1/S (2). These two pathways highlight the emerging importance of the mitochondria as an essential component of intracellular signaling cascades and cell cycle regulation.

The mitochondria cannot be formed *de novo*, therefore the proliferation and segregation of these organelles during mitosis may be just as important to cellular survival as their role in signaling the health of the cell during G_1. Mitochondrial segregation during mitosis has been investigated in yeast model organisms where the active delivery of the organelles into the growing bud is essential (3, 4). However, the regulation of mitochondrial segregation in mammalian cell division has attracted less attention because it is generally considered to be a primarily stochastic event. This idea has been challenged recently by studies investigating mitochondrial morphology during each cell cycle phase. Notably, the fragmentation of mitochondria requires a member of the dynamin family of GTPases, the dynamin-related protein 1 (DRP1),[3] which was recently found to be phosphorylated by the cell cycle-specific kinase Cdk1/cyclin B1 during mitosis (5). The phosphorylation of DRP1 increased fission activity of the protein specifically during anaphase, further hinting that morphology and distribution of the mitochondria may be tightly controlled to ensure equal segregation into the daughter cells. On a molecular level, these findings support the idea that activity of the mitochondrial shaping proteins is modulated by cellular signaling cascades.

In addition to the phosphorylation of DRP1, we have previously documented that this fission GTPase is also subject to covalent conjugation by the small ubiquitin-like modifier, SUMO1 (6–8). SUMOylation requires the sequential action of the ATP-dependent E1 enzyme heterodimer Aos1/SAE1 that forms a thioester bond with the terminal diglycine motif in SUMO, followed by its transfer to Ubc9, the E2 ligating enzyme (reviewed in Refs. 9 and 10). After this, a tightly localized SUMO E3 ligase is required to provide substrate specificity and facilitate the transfer of SUMO to the final target protein. The SUMOylated targets are thought to acquire a new conformation, leading to alternate protein interactions, cellular loca-

* This work was supported in part by Canadian Institutes of Health Research Grant 68833.

[1] Recipient of a Canadian Institutes of Health Research Frederick Banting and Charles Best Canada Graduate Scholarship.

[2] To whom correspondence should be addressed: Rm. H445A, 40 Ruskin St., Ottawa, Ontario K1Y 4W7, Canada. Tel.: 613-761-4701; Fax: 613-761-5281; E-mail: hmcbride@ottawaheart.ca.

[3] The abbreviations used are: DRP1, dynamin-related protein 1; ERK, extracellular signal-regulated kinase; BrdUrd, bromodeoxyuridine; YFP, yellow fluorescent protein; CYP, cyan fluorescent protein; shRNA, short hairpin RNA; FACS, fluorescence-activated cell sorter; PBS, phosphate-buffered saline; E1, ubiquitin-activating enzyme; E2, ubiquitin carrier protein.

tions, or protein stability (9). In the case of DRP1, SUMOylation appears to stabilize the protein from degradation, leading to an increase in mitochondrial fragmentation (6–8). Relative to the abundance of documented ubiquitin E3 ligases, there are only a few identified SUMO E3 ligases that are primarily localized within the nucleus. Those identified to date include the Siz1/PIAS (protein inhibitor of activated STAT (signal transducer and activator of transcription)) family that contains the SP-RING motif (11), the nuclear pore component RanBP2 (12), the polycomb2 protein (13), the dual ubiquitin and SUMO E3 ligase TOPORS (14–16), and the transcriptional corepressor KAP1/TIF1β, which contains a RING-related PHD domain (17). These ligases do not function enzymatically, and instead provide a scaffold for the SUMO E2 ligase, Ubc9, to conjugate SUMO to the substrate (18). Importantly, SUMOylation is a transient, substoichiometric modification that is removed by the action of SUMO (or Sentrin) proteases. The yeast *Saccharomyces cerevisiae* has two ubiquitin like proteases, Ulp1 and Ulp2, whereas the mammalian genome encodes 6, named Sentrin protease SenP1–3 and SenP5–7. SUMO proteases bind directly to the SUMO protein, and not the substrate, which allows their broad specificity. These proteases are differentially localized and thought to have specific cellular functions, including regulation of cell cycle progression (19–22). To date, no SUMO E3 ligases or proteases function directly on the mitochondrial membranes, although many mitochondrial SUMO targets, including DRP1, have been reported.

In an effort to understand the function of mitochondrial SUMOylation, we recently identified a specific SUMO protease, SenP5, which is responsible for the deSUMOylation of DRP1 in steady state (8). SenP5 is localized primarily to the nucleoli, but there is also a substantial amount of the endogenous protein found within the cytosol, where we proposed that it functions to deSUMOylate DRP1 (8). SenP1, SenP5, and SenP3 were the first SUMO proteases to demonstrate a preference to deSUMOylate SUMO2 and SUMO3 from substrates relative to SUMO1 (23, 24). However, recent data has shown that the conformation of SUMO within the substrate can lead to differential deSUMOylation. For example, SenP5 could remove SUMO1 from Lys^{65} of promyelocytic leukemia, but not Lys^{160} or Lys^{490} of the same substrate (24). Interestingly, SenP5 could remove the two SUMO1 paralogues, SUMO2 and SUMO3, from their conjugation at Lys^{160} or Lys^{490}. This, combined with evidence that mixed chains containing all three paralogues are found on native substrates (25), strongly suggests that there is a much higher level of complexity and specificity in the SUMOylation pathways than previously suspected. Indeed, SUMO2/3 were shown to specifically conjugate to a microtubule motor protein CENP-E, which was required to target it to kinetochores during mitosis (26). In contrast, SUMO1 was shown to conjugate proteins that bind directly to the spindles, indicating very distinct functional roles for the SUMO proteins. Finally, SUMO proteins have also been shown to be themselves subject to regulated phosphorylation (27), although the extent and functional consequences of this are still under investigation.

One of the most common general functions for SUMOylation appears to be in the regulation of the cell cycle. The loss of the SUMO proteases in yeast (called Ulp1 and Ulp2) led to a cell cycle arrest, suggesting that deSUMOylation is important for cell cycle progression (28). Similar studies in mammalian cells have shown that global SUMOylation tends to favor cellular senescence rather than proliferation (29). Because SUMOylation plays a global role in cell cycle-dependent regulation of many different proteins (19, 20, 29, 30), and that SenP5 was specifically shown to be essential for cell cycle progression (21), we have examined the localization of SenP5 throughout the cell cycle. We here report its relocation from the nucleoli to the mitochondria specifically at the G_2/M transition. This movement leads to an increase in the labile pool of DRP1 that drives mitochondrial fragmentation and significantly decreases total mitochondrial SUMOylation. Our data provide the first insights into the role of SenP5 in facilitating a change in global mitochondrial SUMOylation during cell cycle progression.

EXPERIMENTAL PROCEDURES

Materials—COS-7 and sHeLa cells were purchased from American Type Culture Collection (Manassas, VA). Polyclonal anti-SenP5 serum was obtained from rabbit immunization with recombinant SenP5-His_6 (pQE31:SenP5) as described (8). Polyclonal anti-SenP5 directed against the first 124 amino acids (mitochondrial targeting signal) of the total sequence of 756 of the SenP5 protein was obtained from immunizing rabbits with recombinant MTS-His_6 (pQE30:MTS), at 21st Century Biochemicals (Marlboro, MA). Polyclonal anti-TOM20 was a generous gift from Dr. Gordon Shore (McGill University, Canada). Rabbit monoclonal anti-ERK1 was obtained from Cell Signaling (Danvers, MA). Monoclonal anti-cyclin B1, anti-DRP1, and anti-cytochrome *c* were obtained from BD Biosciences. Monoclonal anti-cyclin A was obtained from Transduction Laboratories. Monoclonal anti-bromodeoxyuridine (BrdUrd)-Alexa Fluor 594 conjugated was obtained from Molecular Probes (Eugene, OR). Monoclonal anti-SUMO1 (anti GMP1) was obtained from Zymed Laboratories Inc., polyclonal anti-SUMO1 was obtained from Cell Signaling. Monoclonal, anti-KI-67 was obtained from DAKO (Denmark). Monoclonal anti-HSP60 was obtained from Sigma and monoclonal anti-HSP70 from Stressgen (Victoria, Canada). Anti-MFN2 serum was obtained by immunizing rabbits with recombinant MFN2-glutathione *S*-transferase as described (31). Anti-rabbit Alexa Fluor 514 and anti-mouse Alexa Fluor 647 secondary antibodies were obtained from Invitrogen. Thymidine, nocodazole, puromycin, ATP, BrdUrd, and *N*-methylmaleimide were obtained from Sigma. Dulbecco's modified Eagle's medium, suspension minimum essential medium, Hoechst 33258, Lipofectamine 2000, and DNase I were obtained from Invitrogen. Arrest-In transfection lipid was obtained from Open Biosystems (Huntsville, AL). Protease inhibitor mixture was obtained from Roche (Switzerland). Trypsin was obtained from Fluka Biochemika (Buchs, Switzerland), and Triton X-100 was obtained from Bio-Rad. Fetal bovine serum was obtained from HyClone.

DNA Constructs—pOCT:CFP, SenP5:YFP, and pQE31:SenP5 were described previously (6, 8). To obtain pQE30:MTS (for recombinant protein expression and antibody production)

MTS:FLAG was digested with BamHI and HindIII. The fragment was ligated to pQE30, cut with BamHI and HindIII.

Cell Culture and Synchronization—COS-7 cells were cultured in Dulbecco's modified Eagle's medium (Invitrogen) containing 10% heat-inactivated fetal bovine serum (HyClone), 2 mM L-glutamine, penicillin, and streptomycin. Transfections with OCT:CFP and SenP5:YFP were performed overnight with COS-7 cells at 80–90% confluence, using Lipofectamine 2000 (Invitrogen). Synchronization experiments were performed as described (32). Briefly, cells were incubated with 2 mM thymidine for 12 h to block DNA replication, followed by a release in thymidine-free medium for 9 h. A second incubation with 2 mM thymidine for 12 h was performed to bring most cells to synchrony. For synchronization of cells in mitosis (prophase) a double thymidine block followed by 100 ng/ml nocodazole incubation for 14 h was performed. For sHeLa cells, suspension minimum essential medium was used, and cells were incubated in Fernbach flasks (Fisher Scientific) for at least 5 days, until reaching a density of 100,000/ml. Then thymidine (2 mM) or Nocodazole (100 ng/ml) was added to the flasks and cells were incubated for 20 h, to become synchronized, and finally harvested and subjected to fractionation.

Cell Proliferation Assay—Approximately 400,000 COS-7 stable cells of either pSHAG-MAGIC2 vector alone or pSHAG-MAGIC2-SenP5 shRNA, were seeded on 6-well plates, in triplicate, in Dulbecco's modified Eagle's medium + 10% fetal calf serum containing 20 μg/ml puromycin. At days 3, 5, and 7 cells were counted and reseeded. Vector stable cells were reseeded 1:4 at day 3, and 1:3 at day 5, to avoid confluence, to keep the cells growing in logarithmic phase (for the final cell numbers dilution factors were considered in the calculations).

Flow Cytometry—HeLa cells stably silenced for vector-shRNA, SenP5-shRNA I or SenP5-shRNA II were grown in complete culture medium + 2 μg/ml puromycin as a selective agent. To optimize the silencing of SenP5 for cell cycle studies (DNA content), the cells were grown in 20 μg/ml puromycin and samples (100,000 cells aliquots) were taken at day 3, then fixed with cold ethanol for 20 min and stained with 50 μg/ml propidium iodide (Sigma) + 100 μg/ml RNase A for 20 min at room temperature. Cells were then analyzed for DNA content by FACS using the 488 nm laser (FACSAria, BD Biosciences).

Immunofluorescence and Microscopy Studies—For immunofluorescence, cells previously seeded onto coverslips were washed 3 times with PBS and fixed in 4% paraformaldehyde/PBS for 15 min at 37 °C. Cells were then quenched with 50 mM ammonium chloride in PBS for 10 min at room temperature, and permeabilized with 0.1% Triton X-100/PBS for 10 min. Cells were then blocked with 5% FBS in PBS for 1 h at room temperature, then incubated with primary antibody for 2 h followed by 3 washes in blocking solution. Cells were next incubated with goat anti-mouse or goat anti-rabbit conjugated (515 or 647 nm) Alexa Fluor secondary antibodies (Invitrogen) for 45 min at room temperature followed by 3 washes with PBS. A final incubation with 2.5 μg/ml Hoechst in PBS (to observe DNA) was performed, followed by 3 PBS washes and finally mounting onto slides. For anti-BrdUrd staining, cells grown on coverslips and previously transfected with OCT-CFP + SenP5-YFP were incubated with 20 μM BrdUrd for 30 min at 37 °C. Cells were then fixed, washed, and permeabilized, followed by incubation with a mixture containing 0.15 M NaCl, 4.2 mM $MgCl_2$, 10 μM HCl, 5000 units/ml DNase I (Invitrogen), for 30 min at 37 °C. Cell were then washed and incubated with 1 N HCl for 10 min at room temperature, followed by PBS washes. The 2 latest incubation steps are to make the chromatin accessible to the antibody. Cells were then blocked and stained with monoclonal anti-BrdUrd conjugated to Alexa Fluor 594, washed with PBS, and mounted for microscopy. Fixed cells transfected with fluorescence constructs or stained with antibodies were imaged on Olympus IX70 microscope with a ×100 objective U Plan Apochromat, NA 1.35–0.50 objective, excited at 514 (YFP), 434 (CFP), and 350 nm (Hoechst), with the Polychrome IV monochrometer (Till Photonics, Grafelfing, Germany). The emitted light was filtered through either Till double CFP/YFP or Fura filters. Confocal images were obtained with a ×100 objective NA1.4 on an Olympus IX81 inverted microscope with appropriate lasers (440 nm for CFP 434, 515 nm Argon for YFP 515, and 633 nm for Alexa Fluor 647), using Olympus FV1000 confocal scanning microscope. Images acquired were saved as tiff images and overlaid in Adobe Photoshop for image assembly.

To quantify the recruitment of DRP1 to mitochondrial membranes, synchronized cells were fixed and stained with monoclonal anti-DRP1 and polyclonal anti-TOM20. The cytosolic pool of DRP1 is visible by the antibody and appears as small, granular staining. Therefore, in each cell 10 short line scans were plotted across the cytosolic DRP1 signal and an additional 10 scans were taken crossing DRP1 foci that were aligned along the TOM20-labeled mitochondria. This was done for 7 cells in the G_1/S- and G_2/M-synchronized cells, with care taken to maintain the confocal scanning conditions below saturation and constant for each coverslip (including the laser power, PMT voltage, and scanning pixel resolution). The maximum pixel intensity across the line scans on mitochondrial DRP1 foci were averaged per cell and divided by the maximum pixel intensities across the scans taken from the cytosolic DRP1 signals within the same cell. This provides a ratio defining the relative increase in endogenous DRP1 recruitment to the mitochondrial membranes compared with the cytosolic signal. The standard deviation of this ratio was then calculated and graphed accordingly.

Fluorescence recovery after photobleaching was done as described (7). Briefly, HeLa cells grown on coverslips were transfected with DRP1-YFP, and the following day, were synchronized with either a double thymidine block or with an additional 12-h incubation with nocodazole. Cells were loaded into a live imaging chamber and incubated with Mitofluor Red 633 for 15 min to label the mitochondria. Using the Olympus FV1000, the DRP1-YFP signal within a region of interest was bleached with 3 scans using the 514-nm laser line at 50% power. 50 images of the entire cell were then taken every 6 s, and the percentage of DRP-YFP fluorescence within the region of interest relative to the entire cell was calculated as described (7), and the average of the recovery plotted with standard deviations indicated. The initial slopes were calculated from the data obtained in the first 40 s following the bleach, and S.E. obtained with their associated p values. Given the very rounded shape of cells following nocodazole incubation, we released the cells for

1 h in complete medium before imaging. In this way the fluorescence recovery after photobleaching analysis from nocodazole-treated cells were limited to prophase.

Cell Fractionation and Trypsin Digestion—Unsynchronized and synchronized cells were washed in PBS and harvested by trypsinization and centrifugation (HeLa) or centrifugation (sHeLa), followed by 2 washes in cold PBS and centrifugation. The cell pellets were resuspended in 1 ml of homogenization buffer (220 mM mannitol, 68 mM sucrose, 20 mM Hepes, pH 7.4, 80 mM KCl, 0.5 mM EGTA, 2 mM $MgOAc_2$, protease inhibitors). Cells were broken in a cell cracker (10 passages, 8.002 ball) and after taking an aliquot of the total fraction, the nuclear fraction was separated by centrifugation at 800 × *g* for 10 min at 4 °C. The post-nuclear supernatant was centrifuged at 9,300 × *g* for 20 min at 4 °C to pellet mitochondria. Post-mitochondrial supernatant was centrifuged at 200,000 × *g* to clear the cytosolic fraction of light membranes. Total, mitochondrial, and cytosolic fractions were normalized for protein content, and around 50 μg were loaded for electrophoresis and Western blotting. For the trypsin digestion experiment, mitochondria were isolated from synchronized sHeLa suspension cultured cells and 20-μg aliquots were incubated on ice for 30 min with 100 μg/ml trypsin (Fluka Biochemika), or buffer containing trypsin plus 1% Triton X-100 (Bio-Rad), then processed for electrophoresis and Western blotting.

shRNA Studies—shRNA was performed using the prepared sh-activated mRNA silencing system (Open Biosystems). Two different shRNAs inserted into pSHAG-MAGIC2 vectors were as follows: (shRNAI) 5′-TGCTGTTGACAGTGAGCGACCAGTTTACTTGGAATAGACAGTAGTGAAGCCACAGATGTA-3′, and (shRNAII) 5′-TGCTGTTGACAGTGAGCGCGCGCAGATGGTTTGTTACTTGAATAGTGAAGCCACAGATGTAT-3′. COS-7 cells were transfected using Arrest-In transfection reagent (Open Biosystems) and incubated for 48 h. Transfectants were selected in 3 μg/ml puromycin (Sigma) for 12 days. Control cells were transfected with pSHAG-MAGIC2 vector.

In Vitro SUMO Conjugation Assay—The SUMO conjugation assay was performed in 20-μl volumes containing 100 nM SUMO activating enzyme (Boston Biochem), 250 nM UBC9 (Biomol), 10 μM His_6-SUMO1 (Boston Biochem), buffer A (50 mM Tris-HCl, pH 8.0, 100 mM NaCl, 5 mM $MgCl_2$), 1 mM dithiothreitol, and either an ATP regenerating system (2.5 units creatine kinase, 125 nM creatine phosphate, 5 mM ATP) or 0.1 unit of apyrase in the ATP minus control; and finally, 100 μg (per reaction) of synchronized and purified sHeLa mitochondria. Reactions were incubated for 90 min at 30 °C. Streptavidin-coupled magnetic beads (Dynal) were washed in buffer B (buffer A with 2 mg/ml bovine serum albumin and 1% Triton X-100) using a magnetic particle concentrator (Dynal). For each reaction, 20 μl of packed beads were suspended in 180 μl of buffer B and incubated with the SUMO1 conjugation reaction for 35 min, rocking at 25 °C. The beads were then subjected to several washing cycles with buffer C (buffer A with 500 mM NaCl and 1% Triton X-100). The mixture was finally subjected to SDS-polyacrylamide gel electrophoresis on 4–20% gels, followed by standard immunoblotting procedures using SUMO1 antibody.

Cross-linking and Immunoprecipitation—For cross-linking studies, HeLa cells synchronized either for the G_1/S or G_2/M borders were harvested, washed, and a fractionation was performed in mitochondrial extraction buffer containing 20 mM *N*-methylmaleimide and protease inhibitors. After normalization, post-nuclear supernatants (containing both cytosolic and mitochondrial fractions) were then treated or not (controls) with 0.2, 1, 2, or 10 mM of the BMH (bis(maleimido)hexane) cross-linker, in mitochondrial buffer, for 2 h at 4 °C, to freeze protein-protein interactions. The reaction was then stopped by incubation with 10 mM dithiothreitol for 15 min at 4 °C, followed by SDS-PAGE running and inmunoblotting for DRP1, as well as controls for loading and synchronization efficiency.

For immunoprecipitation experiments, HeLa cells were synchronized for either the G_1/S or G_2/M border and fractionated for total, cytosolic, and mitochondrial fractions, in mitochondrial extraction buffer containing 20 mM *N*-methylmaleimide and protease inhibitors, as previously indicated. Each fraction (totals, cytosol, and mitochondria), from each condition, was then solubilized by adding Triton X-100 to a final concentration of 1%, for 30 min, at 4 °C, followed by ultracentrifugation at 200,000 × *g* for 40 min, at 4 °C. Supernatants were normalized for protein content and incubated with either a nonspecific mouse IgG or with monoclonal anti-DRP1 (2.5 μg for each mg of protein per IP point), conjugated to protein G-Sepharose beads, for 12 h, at 4 °C. After centrifugation at 10,000 × *g* to spin down the protein G-Sepharose-immune complexes, 3 bead washes were made in mitochondrial buffer containing 1% Triton X-100. Beads were then run by SDS-PAGE electrophoresis followed by immunoblots with either monoclonal SUMO1 or monoclonal DRP1 antibodies.

Quantification and Statistical Analysis—Quantification of blots was performed using the Scion Image program (Scion Image Corporation). Graphs with data from blots quantification or microscopy counts and statistical analysis (*p* values) using unpaired *t* test were obtained using Sigma Plot.

RESULTS

SenP5 Translocates to Mitochondria during Mitosis—Previously it was reported that silencing the expression of SenP5 induces cell cycle arrest in cytokinesis (21). We confirmed this in COS7 cells stably transfected with SenP5-shRNA. As previously shown (8), the maximal loss of SenP5 in the targeted shRNA containing cells was 48%. The experiment shown in Fig. 1 demonstrates that a reduction in SenP5 levels led to cell cycle arrest relative to the control cells (Fig. 1*A*). To determine at which stage of the cycle the cells were arrested, we probed the lysates for two cell cycle markers, cyclin B1 (accumulates during mitosis) and cyclin A (accumulates in S and G_2). The loading control Tom20 confirmed equal protein amounts, however, SenP5-shRNA cells showed a higher relative level of cyclin B1 (Fig. 1*B*) and a lower level of cyclin A than control cells, indicating cell cycle arrest occurred at the G_2/M transition. Western blots of cell extracts also show no change in phospho-ERK, indicating that the G_1 growth phase of cells silenced for SenP5 was not affected relative to controls (33)(Fig. 1*B*). We confirmed this result using FACS sorting of HeLa cells expressing either the vector shRNA, or two different SenP5 shRNA stable

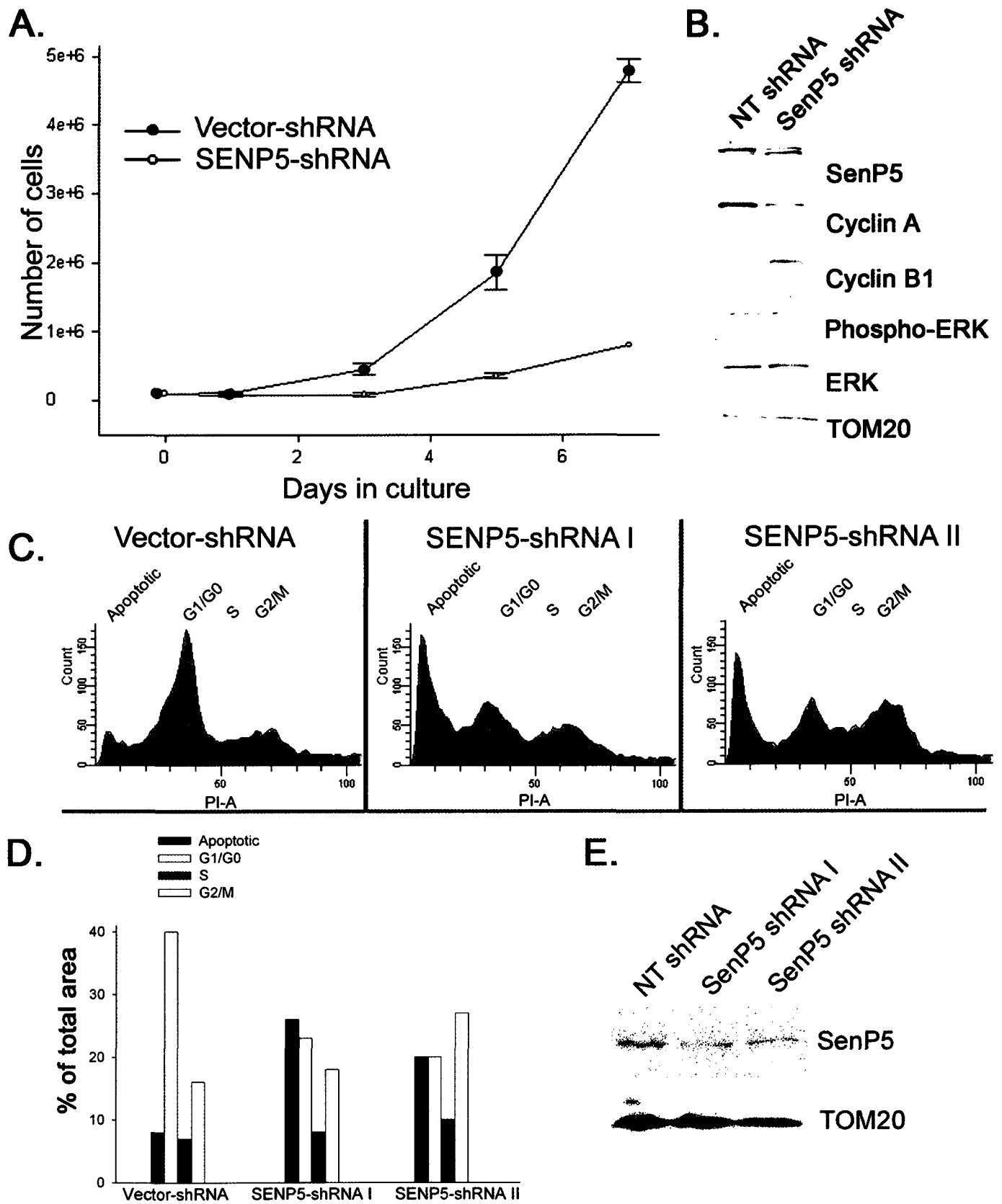

FIGURE 1. **Silencing of SenP5 leads to a cell cycle arrest at G_2/M.** *A*, COS-7 cells stably expressing non-targeted shRNA or SenP5 shRNA were cultured and cell numbers quantified. The graph plots the cell numbers obtained at 3, 5, and 7 days of culture. Results express the mean ± S.D. of two independent experiments. *B*, aliquots obtained at 7 days of the experiment in *A* were processed for electrophoresis and Western blots with the indicated antibodies. *C*, HeLa cells expressing vector-shRNA, SenP5-shRNA I, or SenP5-shRNA II were grown in 20 μg/ml puromycin for 3 days, harvested, stained with propidium iodide, and analyzed for DNA content by FACS. *D*, the peaks were quantified using Summit version 4.3 software and plotted, as indicated. *E*, an aliquot of the HeLa cells used for the FACS analysis were analyzed by Western blot to confirm the extent of SenP5 silencing using each hairpin.

lines targeting unique regions of the SenP5 message. The reduction in SenP5 in the HeLa cells was similar to the COS7 cell line (Fig. 1*E*). Cells expressing the vector control shRNA showed a majority of cells containing 1 N DNA (40%), and 16% containing 2 N DNA, which reflects cells at G_2/M (Fig. 1, *C* and *D*). In contrast, upon silencing of SenP5 with two independent shRNA, the cells showed an increase in 2 N DNA content after 3 days, consistent with biochemical data indicating a cell cycle arrest at G_2/M (Fig. 1, *C* and *D*). In addition, there was a significant increase in apoptotic fragments within the cells silenced for SenP5 (from 8% in control to 20–26% in shRNA cells), which is a common event when the cell cycle is delayed (34). Therefore, consistent with previous results (21), the reduction of SenP5 is sufficient to significantly affect cell proliferation and trigger cell death. The further loss of SenP5 is likely lethal and explains why we could not obtain lower expression levels in our stable shRNA cell lines.

Given that we have previously demonstrated a role for SenP5 in the regulation of mitochondrial dynamics and morphology (8), we examined whether cell cycle arrest induced in the absence of SenP5 may involve its mitochondrial function. Although over 90% of cells examined showed primarily nucleolar localization of SenP5 (Fig. 2*A*, *top panels*), we noticed a small percentage of cells that exhibited a different pattern of localization (Fig. 2*A*). We examined the mitochondria using the matrix marker pOCT-CFP (6) and followed SenP5-YFP localization in multiple cells. Interestingly, some cells showed a dual location for SenP5, both within the nucleoli and the mitochondria (Fig. 2*A*, *middle panels*), where in other cells SenP5 was recruited almost exclusively to the mitochondria (Fig. 2*A*, *bottom panels*). Finally, in the mitotic cells identified by the condensed chromosomes we could observe that SenP5-YFP was completely targeted to the mitochondria (Fig. 2*B*). To better characterize whether the shift of SenP5 to the mitochondria occurred in a cell cycle-dependent manner, we synchronized COS-7 cells either at the G_1/S boundary, or at G_2/M. We fractionated the cytosol and mitochondria and probed the fractions with antibodies against endogenous SenP5. The data revealed a shift of endogenous SenP5 to the mitochondria during mitosis (Fig. 2*C*), consistent with the SenP5-YFP translocation observed by microscopy. Although the total cellular levels of DRP1 did not change during the cell cycle, we observed a significant reduction in the stable association of DRP1 with mitochondrial membranes during mitosis (Fig. 2*C*). Interestingly, DRP1 appears as a doublet on the 6% SDS-PAGE, and in addition to an overall reduction in mitochondrial associated DRP1, the top band of the doublet is significantly reduced within the mitochondrial fraction at G_2/M, consistent with a shift in post-translational modifications at this time. The success of the synchronization was revealed by cell cycle markers cyclin B1, whose levels are maximal at G_2/M, and cyclin A, maximal at G_1/S. Western blot analysis of the mitochondrial SenP5 protein present at G_2/M revealed that it was completely degraded by the addition of trypsin, whereas the intermembrane space protein, cytochrome *c*, was protected (Fig. 2*D*). This demonstrates that SenP5 is not imported, but is recruited to the surface of the mitochondria. This localization would suggest that the majority of SenP5 substrates are either outer membrane or peripherally associated proteins such as DRP1.

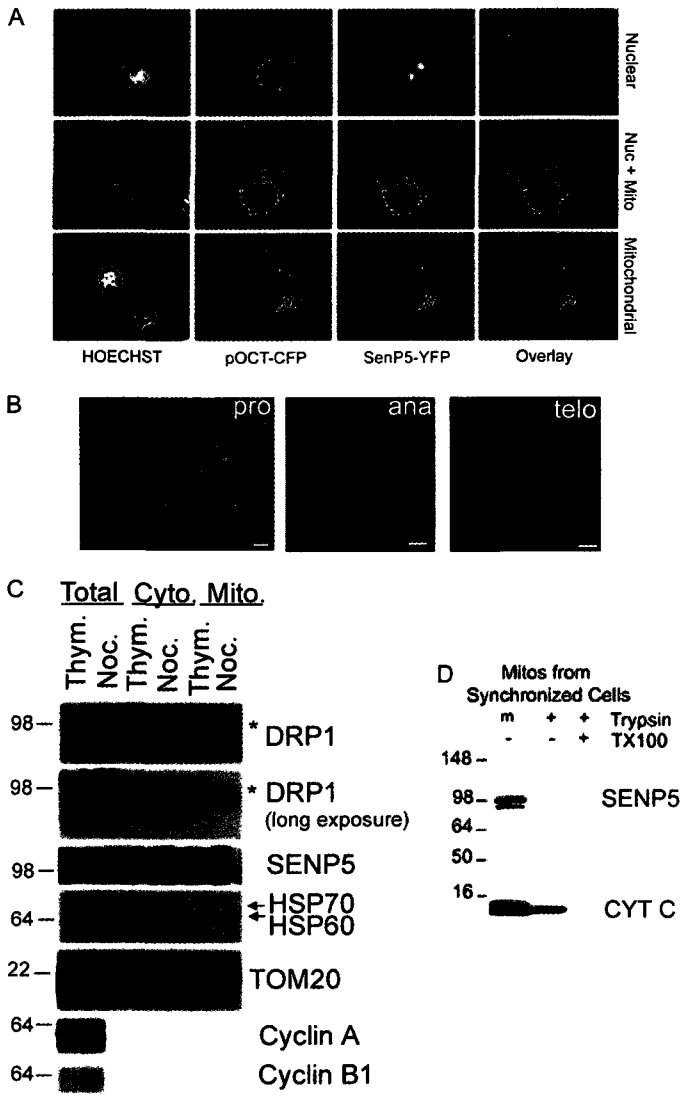

FIGURE 2. **SenP5 translocates to the mitochondrial membrane during the G_2/M phase.** *A*, COS-7 cells were transfected with OCT-CFP, SenP5-YFP, fixed, and stained with Hoechst, prior to analysis by fluorescence microscopy. *B*, mitotic cells at prophase, anaphase, and telophase, showing SenP5-YFP on the mitochondria (*red*). Chromatin distribution was revealed by Hoechst (*green*). Scale is 5 μm. *C*, COS-7 cells were synchronized with either a double thymidine block alone (G_1/S), or the thymidine block followed by a 12-h release in 100 ng/ml nocodazole (G_2/M). These cells were harvested, and total extracts, cytosolic and mitochondrial fractions were obtained. Then, 25 μg of protein from each fraction was loaded on the gel and processed for electrophoresis and Western analysis with antibodies against endogenous SenP5, DRP1, HSP60, TOM20, and HSP70, as shown. Cyclin A (G_1/S) and cyclin B1 (G_2/M) were probed as synchronization controls. *Asterisks* indicate the higher migrating form of DRP1 that is lost upon the delivery of SenP5 to the mitochondria in nocodazole-treated cells. *D*, COS-7 cells were synchronized with double thymidine block, followed by a 6-h release to enrich endogenous SenP5 on the mitochondria. Cells were harvested, mitochondria were isolated, and 20-μg aliquots were either left untreated (*lane 1*), or treated with 0.1 mg/ml trypsin in the presence or absence of 1% Triton X-100 (*second* and *third lanes 2*). Western blots were probed for endogenous SenP5, and cytochrome *c* as an internal control.

To precisely map the stage within the cell cycle when SenP5 transits outside of the nucleus to the mitochondria we stained COS-7 cells transfected with SenP5-YFP with a monoclonal antibody against the cell cycle marker KI-67, a nuclear protein

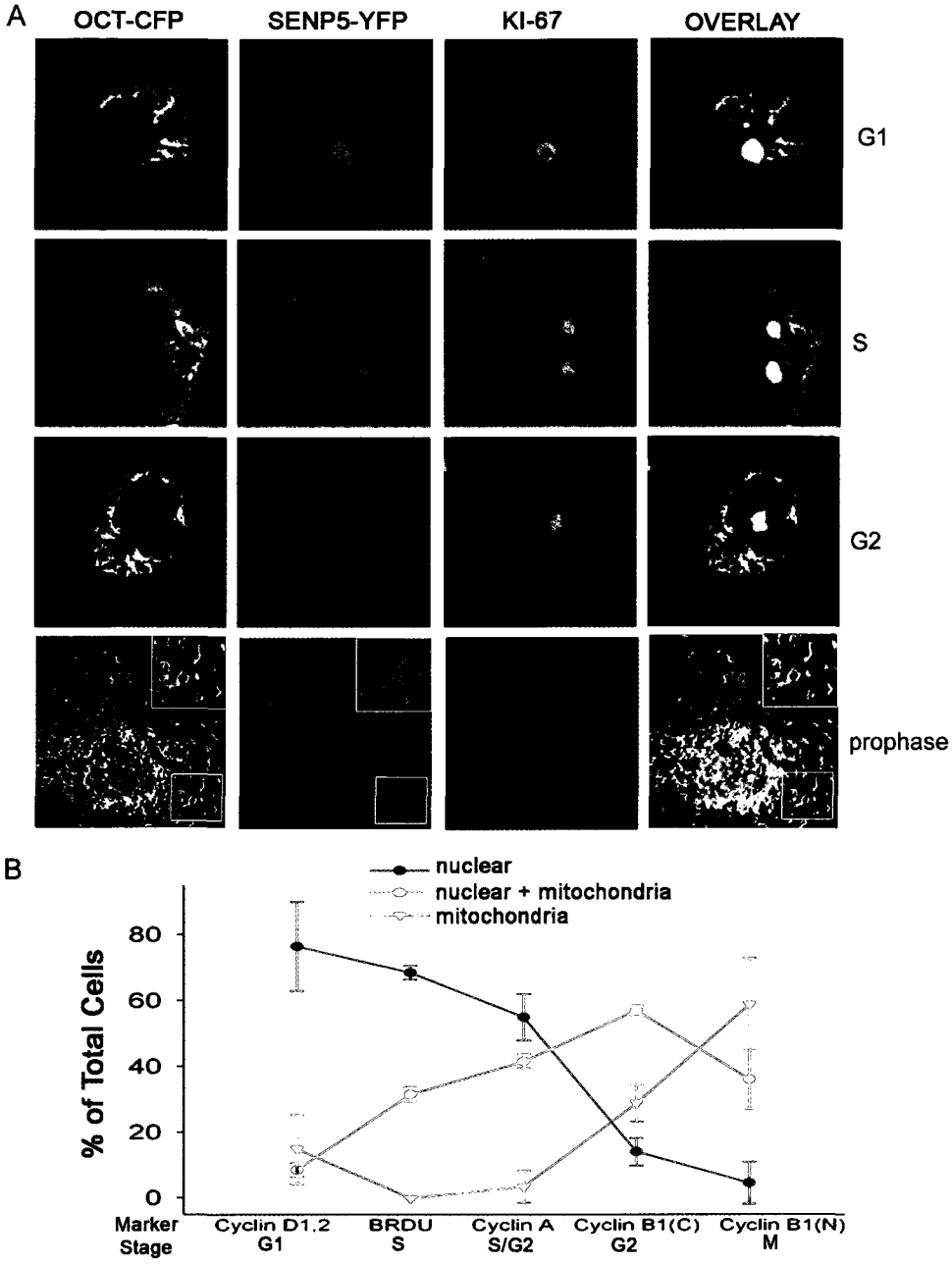

FIGURE 3. **Quantification of SenP5 recruitment to the mitochondria using multiple cell cycle markers.** *A*, unsynchronized COS-7 cells were transfected with OCT-CFP and SenP5-YFP overnight. The cells were then fixed and stained with an antibody against the cell cycle marker KI-67. Representative fluorescence microscopy pictures at different stages of the cell cycle are shown. *Insets* show colocalization of SenP5-YFP and the mitochondrial marker OCT-CFP. *Scale bar*, 5 μm. *B*, quantification of SenP5-YFP distribution along the cell cycle. COS-7 cells were transfected with OCT-CFP and SenP5-YFP overnight, then stained with monoclonal antibodies against different markers of the cell cycle: anti-cyclin D1 and -2 for G_1 phase, anti-BrdUrd for S phase, anti-cyclin A for S and G_2 phases, anti-cyclin B1 (cytosolic) for the G_2 phase, and nuclear cyclin B1 staining reflected the M phase. The distribution of SenP5-YFP was scored as nuclear, nuclear and mitochondrial, or mitochondrial, and determined as a percentage of total cells positive for both SenP5-YFP transfection and for the different cell cycle markers. Results express the mean ± S.D. of three independent experiments, with at least 50 cells examined in each case.

present in cycling cells that exhibits unique subnuclear localizations in each stage of the cell cycle (35). Based on these properties, we imaged the transiently transfected pOCT-CFP and SenP5-YFP, and observed that SenP5-YFP mostly colocalizes with nucleolar KI-67 in G_1 and S phases (Fig. 3*A*, *top two panels*). During G_2, when KI-67 is found in irregular nucleoli and nucleoplasm, SenP5 exhibits faint mitochondrial localization, additional to its colocalization with KI-67 in irregular nucleoli (Fig. 3*A*, *third panels*). At prophase, KI-67 associates with condensing chromosomes, whereas SenP5 migrates to the mitochondria (*bottom panels*). These results show that SenP5 starts to exit the nucleus at G_2, whereas the nuclear envelope is still intact. Upon disassembly of the nucleoli and nuclear envelope, SenP5 associates with mitochondria.

We expanded this approach by quantifying the localization of SenP5-YFP in cells stained with a number of established cell cycle markers, including cyclin D1 antibodies for G_1 phase, BrdUrd incorporation and anti-cyclin A staining for S phase, and cyclin B1 staining for G_2 (cytosolic) and prophase (nuclear). In each condition, cells were cotransfected with SenP5-YFP and the mitochondrial marker pOCT-CFP. Cells that showed bright cyclin D1 fluorescence had SenP5-YFP mainly within the nucleus (at the nucleoli) (Fig. 3*B*), cells that incorporated anti-BrdUrd fluorescence at the nucleus (S) had SenP5-YFP mainly at the nucleoli and a few cells showed faint mitochondrial staining. Cells with nuclear cyclin A fluorescence (S/G_2) had SenP5 in the nucleus and on the mitochondria. Cells that showed bright anti-cyclin B1 fluorescence in the cytosol (G_2) had SenP5-YFP mostly in the nucleus and recruited to the mitochondria and some of them only on the mitochondria, and cells showing bright cyclin B1 fluorescence in the nucleus (prophase) had SenP5-YFP mostly on the mitochondria. These results confirmed that SenP5 starts to actively move out of the nucleus between S and G_2, before being recruited to the mitochondria during mitosis.

SenP5 deSUMOylates Mitochondrial Targets and Alters Morphology—The presence of SenP5 on the mitochondria was accompanied by a reduction in the stable association of DRP1 with the mitochondrial membrane (Fig. 2*C*). Therefore we tested whether this was also accompanied by a change in mitochondrial morphology. COS7 cells were synchronized at G_1/S, or in mitosis, and morphology of the mitochondria in these cells was quantified. Consistent with

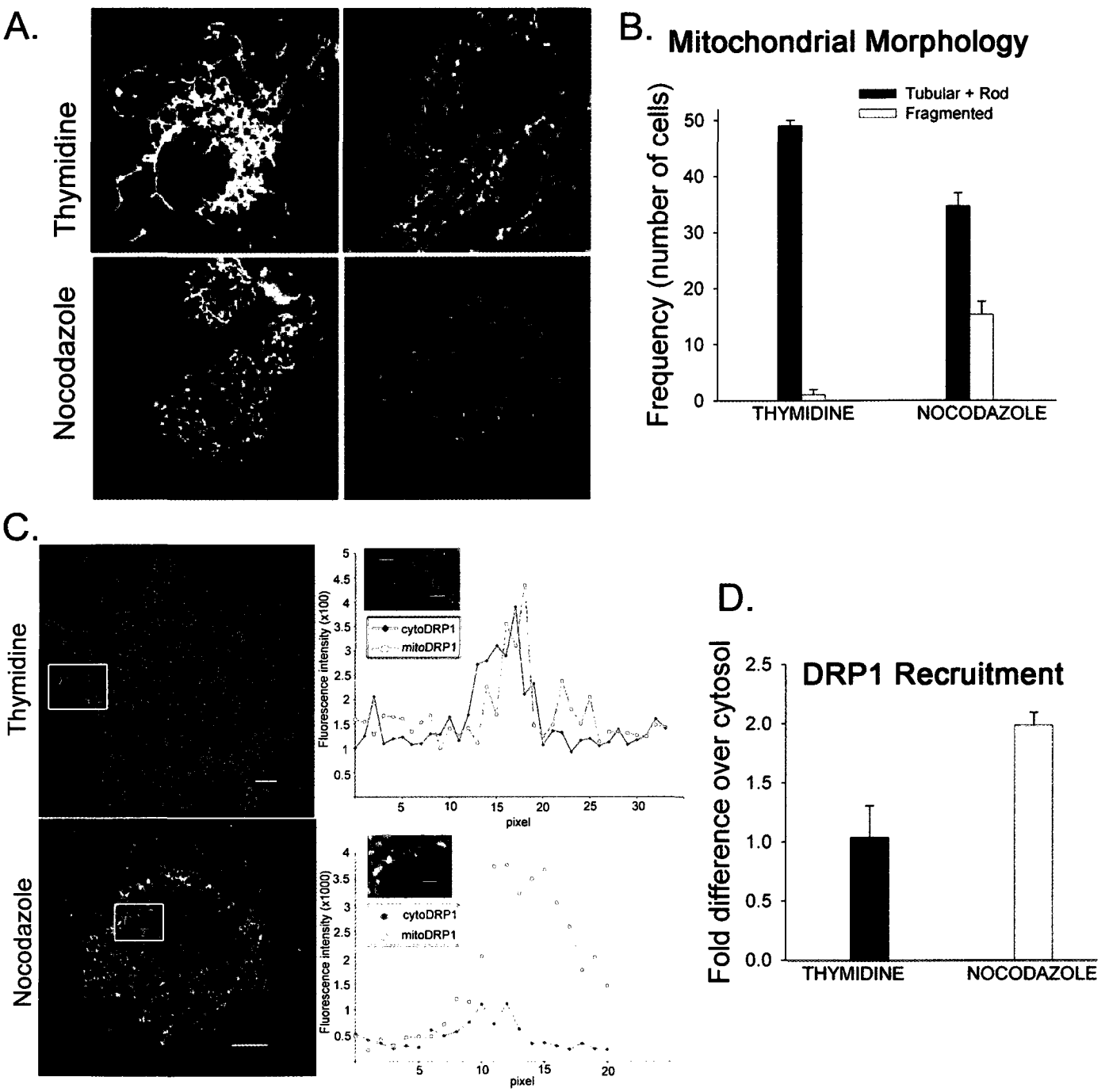

FIGURE 4. **Mitochondria fragment in mitosis and a more labile pool of DRP1 is enriched on the membranes.** *A*, panels showing cells synchronized as indicated, fixed, and stained with anti-Tom20 antibodies. *Scale bar*, 10 μm. *B*, graph showing the mitochondrial phenotype in G_1/S (thymidine) *versus* G_2/M (nocodazole)-synchronized cells (results are mean ± S.D. of 3 coverslips examined in each case, with 50 cells examined per coverslip). *C*, COS-7 cells were synchronized as indicated, then fixed and stained with monoclonal anti-DRP1 (*red*) and polyclonal anti-Tom20 (*green*), for analysis by confocal fluorescence microscopy. *Line scans* were drawn across DRP1 puncta that localized with mitochondria, and those that were found within the cytosol. Examples of these foci are shown for each condition (*inset*) and the line scans are indicated. *Scale bars*, 5 μm. *D*, the relative intensity of endogenous DRP1 foci along the mitochondrial tubules relative to the background cytosolic signal were quantified using line scans in cells synchronized in G_1/S (thymidine) and G_2/M (nocodazole). The results are the mean ± S.D. of 10 cytosolic DRP1 line scans *versus* 10 mitochondrial DRP1 line scans per cell with $n = 7$ cells examined for both G_1/S and G_2/M phases.

previously published data (5), the quantification revealed a significant increase in cells containing fragmented mitochondria at G_2/M (Fig. 4, *A* and *B*). To quantify the recruitment of endogenous DRP1 to the mitochondrial membrane, we stained cells with anti-DRP1 antibodies (Fig. 4*C*). In both thymidine- and nocodazole-treated cells, confocal imaging reveals DRP1 fluorescence within small foci localized in the cytosol, some of which may likely localize to microtubules, as previously described (36, 37). In addition, there are also DRP1 foci that colocalize with the mitochondria. To score for an enrichment of DRP1 recruitment, we performed line scans across the cytosolic and mitochondrial DRP1 foci and generated a ratio of

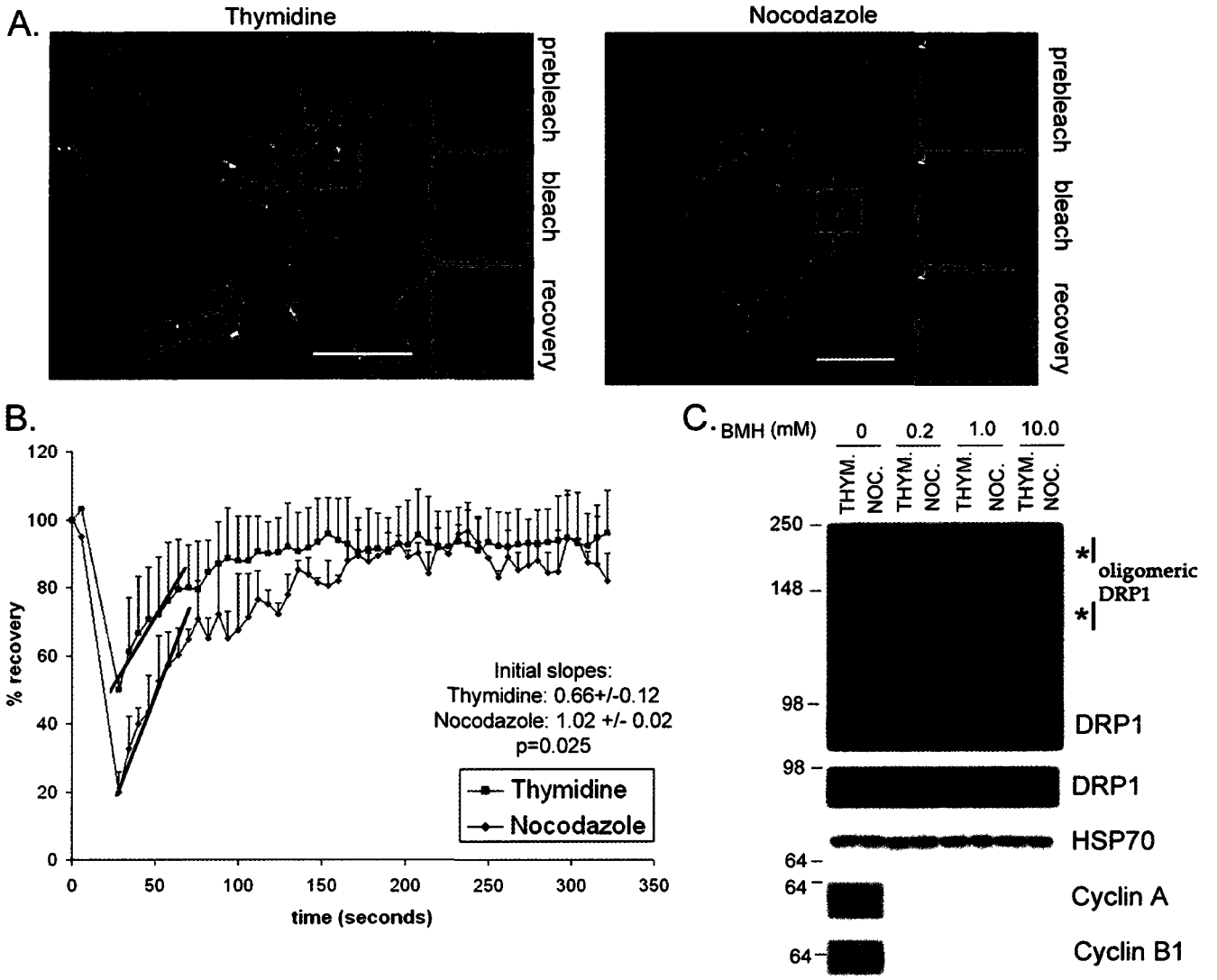

FIGURE 5. **DRP1 association with mitochondria is more labile, leading to an increase in functional oligomers during mitosis.** *A*, HeLa cells transfected with DRP1-YFP were synchronized with thymidine or nocodazole. The nocodazole was washed out for 60 min to facilitate a more complete attachment of the cells to the coverslips during imaging. Cells were labeled with Mitofluor Red 633 and the extent of DRP1-YFP recovery after photobleaching is equivalent in both thymidine- and nocodazole-synchronized cells. *B*, the quantification of fluorescence recovery after the bleach shows that the rates of recovery are distinct. The average curves are shown from ($n = 3$) thymidine- and ($n = 2$) nocodazole-treated cells. The *lines* indicate the initial slopes of DRP1-YFP recovery following the bleach. Quantification of the slopes are indicated along with the statistical significance (*inset*). *C*, HeLa cells synchronized with thymidine or nocodazole were harvested, and the post-nuclear supernatants were incubated with increasing concentrations of bis(maleimido)hexane (*BMH*) cross-linker, as indicated. Western blots with anti-DRP1 antibodies reveal the enrichment of oligomeric forms of DRP1, which is specific to the nocodazole-treated cells (*asterisks*). HSP70 antibodies control for equal loading in each lane, where cyclins A and B indicate the efficiency of synchronization.

fluorescence (Fig. 4, *C* and *D*). In thymidine-treated cells, the intensity of DRP1 fluorescence on the mitochondria is similar to those within the cytosol. However, in nocodazole-treated cells, the mitochondrial association is enriched by 2-fold relative to cytosolic DRP1 (Fig. 4*D*). Therefore, although biochemical fractionation demonstrated a reduction in the stable membrane-associated DRP1 (Fig. 2*C*), immunofluorescence staining of DRP1 indicated that within intact cells there is an increased amount of DRP1 localizing along the mitochondrial tubules during G_2/M (Fig. 4, *C* and *D*). This suggests that the association of DRP1 on the mitochondria is more labile during mitosis than at the G_1/S transition, and is more readily washed away from the mitochondria during biochemical fractionation, as seen in Fig. 2.

To confirm whether cycling of DRP1 recruitment to mitochondria is more labile during mitosis, we employed fluorescence recovery after photobleaching experiments (Fig. 5, *A* and *B*). HeLa cells were transfected with DRP1-YFP, and synchronized either in G_1/S or G_2/M. The data show that the recovery of DRP1-YFP onto mitochondria following photobleaching occurs in both conditions; however, the rates of recovery are increased nearly 2-fold in prophase (Fig. 5*B*). This is consistent with an increase in endogenous DRP1 recruitment (Fig. 4, *C* and *D*), but an increase in recycling rates is also consistent with the biochemical evidence that mitochondrial associated DRP1 is less stably associated with the membranes (Fig. 2*C*). To determine whether increased rates of recycling may correlate to an increase in functional fission activity, we performed cross-linking studies on post-nuclear supernatants to examine oligomerization of DRP1 (Fig. 5*C*). It has previously been shown that an increase in dynamin oligomerization reflects an increase in the fission-competent rings formed during constric-

tion (38–41). We observe a cell cycle-specific increase in DRP1 oligomers during mitosis (Fig. 5*C*), which is consistent with an increase in mitochondrial fission observed at this time (Fig. 4, *A* and *B*). Together these data show an increase in the lability of DRP1, which leads to an increased formation of functional oligomers during mitosis.

To test whether SenP5 delivery to the mitochondria directly affects mitochondrial targets of SUMOylation, including DRP1, we examined isolated mitochondria probed for endogenous SUMO conjugates. Western blots probing for endogenous SUMO1 conjugates revealed an overall reduction of mitochondrial SUMO targets during mitosis (Fig. 6*A*, *top panel*). As expected, we also saw a reduction in SUMO2/3 conjugates on the mitochondria (data not shown). These results demonstrate that the recruitment of SenP5 to the mitochondria during mitosis (Fig. 6*A*, *middle panel*) leads to a general reduction of mitochondrial SUMO1 targets. In addition, the data reveal that the global pattern of mitochondrial SUMOylated targets were reduced, consistent with the biochemical evidence that SUMO proteases do not exhibit substrate specificity, and instead bind to the SUMO1 protein within the conjugates (42, 43).

To further confirm whether active mitochondrial SUMOylation is reduced during G_2/M, we performed *in vitro* SUMOylation reactions on mitochondria isolated from synchronized cells. Mitochondria were isolated from suspension HeLa cells synchronized at G_1/S, or at G_2/M, then assayed for the energy-dependent conjugation of recombinant His_6-SUMO in the presence of E1 and E2 sumoylating enzymes. The efficiency of synchronization was confirmed using the cell cycle-specific markers cyclin A and cyclin B1 (Fig. 6*B*). Mitochondria isolated from G_1/S-synchronized cells were able to form SUMOylated conjugates in an energy-dependent manner (Fig. 6*C*, *first* and *second lanes*). This indicates that the isolated mitochondria must contain an endogenous SUMO E3 ligase sufficient to conjugate exogenously added His_6-SUMO to native substrates. In contrast, mitochondria isolated from cells synchronized at G_2/M are not able to efficiently SUMOylate their targets relative to interphase cells (Fig. 6*C*, *third lane versus first lane*). Quantification of these results revealed a 60% reduction in active SUMOylation targets on mitotic mitochondria (Fig. 6*D*), consistent with the recruitment of the protease SenP5.

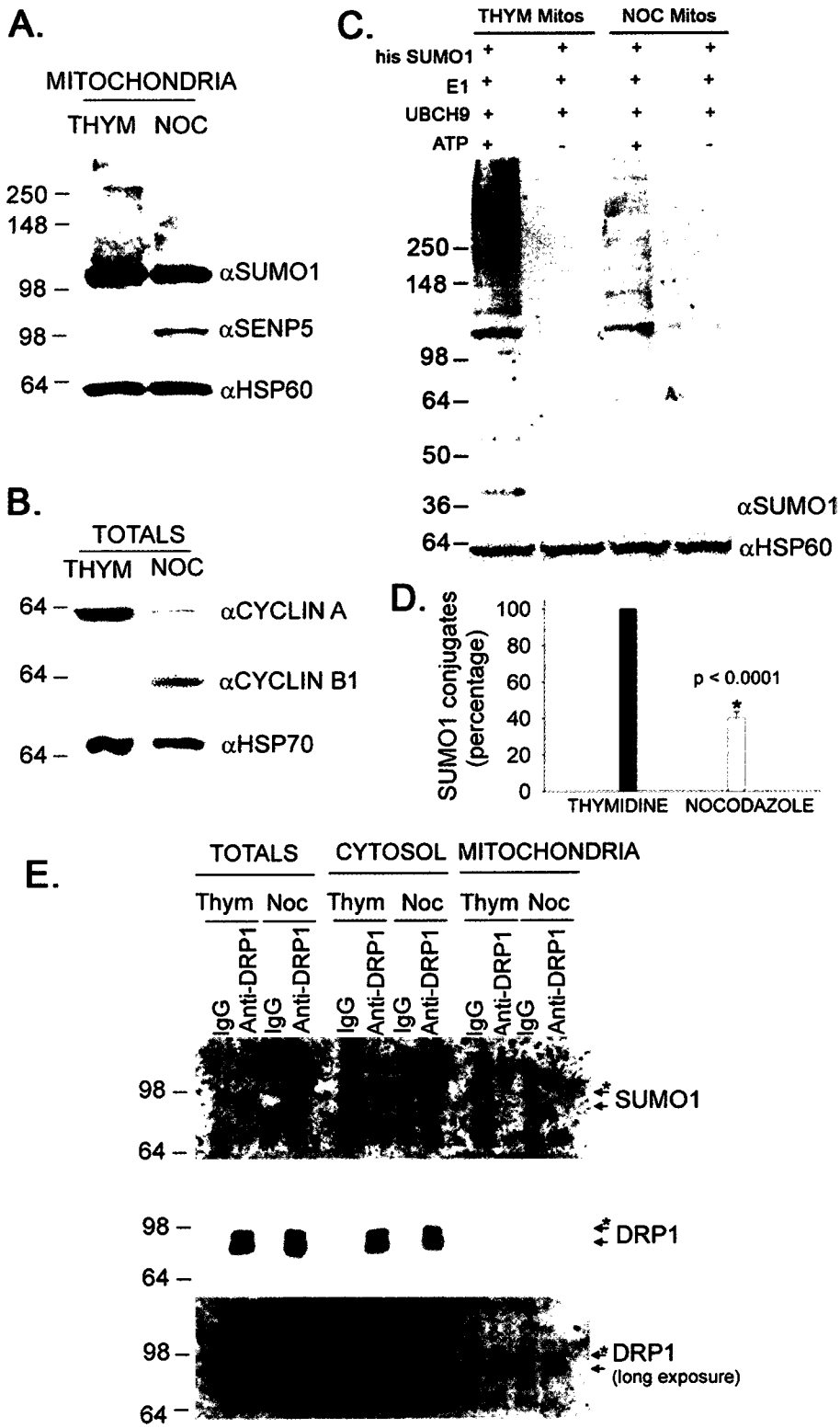

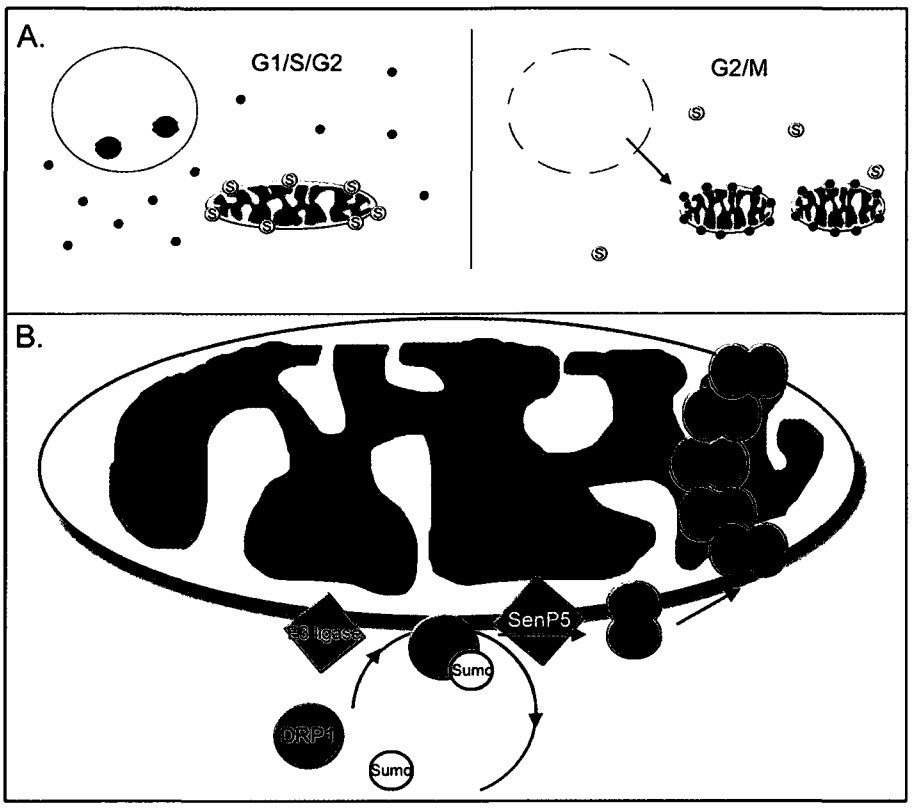

FIGURE 7. **Schematic of SenP5 transition and the DRP1 SUMOylation cycle.** *A*, illustrates the translocation of SenP5 from the nucleoli to the mitochondria at G_2/M, which coincides with the global deSUMOylation of mitochondrial targets and increase in mitochondrial fission. *B*, our data indicates that the SUMOylation cycle of DRP1 is enhanced upon delivery of SenP5 to the membrane. The deSUMOylation of DRP1 helps to drive the oligomerization of DRP1, which promotes mitochondrial fission during mitosis.

This data suggested that the mitochondrial associated DRP1 would also be efficiently deSUMOylated by SenP5 along with all other targets. To test this directly, we immunoisolated endogenous DRP1 from total cell extracts, fractionated cytosol and mitochondria synchronized in G_1/S or G_2/M. The data reveal that the doublet form of DRP1 is immunoreactive for SUMO1 at G_1/S, however, only the lower molecular weight band is SUMO positive at G_2/M, both from total extracts and cytosol (Fig. 6*E*). This is consistent with the release of SenP5 from the nucleoli, where it would deSUMOylate DRP1. Within the mitochondrial fraction, we again observe a reduction in the biochemical association of DRP1 with the membranes, but we also observe the selective loss of the upper, SUMOylated band of DRP1 at G_2/M. Interestingly, the cytosolic pool of DRP1 is found in doublet form in both conditions, yet only the lower band is SUMO positive. This may indicate a replacement of SUMOylated DRP1 with a phosphorylated or ubiquitinated form that could retain the same mobility (5, 44). Nevertheless, our data demonstrate the loss of a SUMOylated form of DRP1 during mitosis, which is consistent with the selective delivery of SenP5 to the mitochondrial membranes. That the lower molecular weight band of DRP1 remains SUMOylated indicates that the cycle of SUMOylation is retained during mitosis, consistent with our previous observation that the SUMOylation of DRP1 enhances its recruitment and fission activity (6–8). From this data, we consider that the delivery of SenP5 stimulates the cycle of DRP1 SUMOylation and deSUMOylation, which increases the rate of oligomerization, mitochondrial fission, and DRP1 recycling (Fig. 7).

DISCUSSION

Recent data has highlighted the importance of metabolic stability and mitochondrial function before cells commit to DNA synthesis in S phase (1, 2). This illustrates the high degree of cross-talk between the mitochondrial and cell signaling pathways (45). During mitosis, it is equally important that the intracellular organelles, including the mitochondria, be equally and efficiently segregated into the daughter cells. Work presented here provides new insights into how events within the nucleus can be communicated directly to the mitochondrial surface to initiate the morphological changes that accompany cell division. The use of SUMOylation as a means to translate these changes is consistent with its role in multiple aspects of cell cycle regulation. For example, it has been shown in yeast that translocation of the SUMO E3 ligase Siz1p from the nuclear envelope to the cleavage furrow facilitates septin SUMOylation and oligomerization during cytokinesis (46). Following this, the carefully timed release of the SUMO protease, Ulp1, from the nuclear envelope into the cytosol ensures the efficient deSUMOylation of the septin ring following cytokinesis (46).

FIGURE 6. **Mitochondrial SUMOylation is decreased during mitosis.** *A*, sHeLa cells were grown in suspension and synchronized for 20 h with either 2 mM thymidine or 100 ng/ml nocodazole, then harvested and processed for mitochondria purification. SUMO1-conjugated targets in G_1/S (thymidine) *versus* mitotic (nocodazole) mitochondria. Mitochondria isolated from the synchronized cells show a decrease in endogenous SUMO1 conjugates, concomitant with the recruitment of SenP5 during mitosis (HSP60 shown as internal loading control). *B*, aliquots of the total cell fractions were probed for cyclin A and cyclin B1 to monitor the synchronization efficiency (HSP70 was used as loading control). *C*, mitochondria were incubated in the indicated conditions ("Experimental Procedures") and probed for the association of conjugated His_6-SUMO1. The conjugation of SUMO1 to the mitochondrial targets is ATP dependent. HSP60 was probed to monitor mitochondrial loading. *D*, the data from three independent conjugation experiments, using mitochondria from two independent fractionations were quantified and, after subtraction of background signal (−ATP conditions), the percentage of total SUMO1 conjugates intensity are plotted in G_1/S and G_2/M. *E*, sHeLa cells synchronized as indicated were fractionated into cytosol or mitochondrial fractions, solubilized, and anti-DRP1 antibodies used to immunoprecipitate endogenous DRP1. Extracts were loaded on two independent gels, with one probed with anti-SUMO1 antibodies, and the other with DRP1 antibodies. The data shows that DRP1 immunoprecipitates are immunoreactive for SUMO1, with a higher migrating species being lost specifically when SenP5 is delivered to the mitochondria in nocodazole-synchronized cells (*asterisk*).

Therefore, cellular localization of the SUMOylation enzymes is emerging as a critical factor that controls cell cycle progression. Given this precedent, it is significant that the silencing of SenP5 leads to a cell cycle arrest at G_2/M, precisely at the point where the protein should be recruited to the mitochondria. This suggests that the gain of SenP5-mediated deSUMOylation activity on mitochondrial targets plays an important role in the G_2/M transition. Just as the mitochondria exert a cell cycle checkpoint at the G_1/S transition (1, 2), these data hint toward a second requirement for mitochondrial transitions at the G_2/M checkpoint.

The translocation of SenP5 to the mitochondria supports growing evidence that the changes in SUMOylation can be mediated, at least in part, through the regulated translocation of SUMO proteases and/or ligases between intracellular compartments. In addition, the specific recruitment of SenP5 to the mitochondrial surface highlights the emerging importance of this modification as a highly regulated tool to modulate mitochondrial behavior. At least one of the functional requirements for SenP5 recruitment to the mitochondria is to modulate the activity of its known target, DRP1 (8). Our previous studies have shown that conditions where SUMOylation becomes stabilized, through the silencing of SenP5 (8), overexpression of SUMO1 (6), or during apoptosis (7), lead to increased mitochondrial fragmentation. The data presented here show that movement of SenP5 to the mitochondria at the onset of mitosis appears to accelerate the binding and release cycles of DRP1, which also resulted in increased mitochondrial fragmentation. The ongoing presence of a SUMOylated form of DRP1 in both G_1/S and G_2/M (Fig. 6*E*) indicates that SUMOylation is not blocked during mitosis, rather that the timing of deSUMOylation is increased. Given the data presented here along with our previous studies, we consider that SUMOylation may play a chaperone-like function to drive DRP1 recruitment to the mitochondrial membrane (see *model*, Fig. 7). During apoptosis, DRP1 SUMOylation is stabilized in a Bax/Bak-dependent manner, and this stabilizes the protein on the membrane. The data here show that stimulating deSUMOylation of DRP1 on the mitochondrial membrane during mitosis enhances its incorporation into functional oligomers, and leads to an increase in overall recycling rates, a process that is required to facilitate membrane scission. In this way the deSUMOylation appears essential to complete the cycle and release DRP1 from the membrane (Ref. 7 and this study). Finally, because DRP1 also undergoes regulated ubiquitination, phosphorylation, and dephosphorylation, it is likely that the combinatorial use of post-translational modifications contributes to its recruitment, assembly, and constriction to drive mitochondrial fission (5, 44, 47–50). We observe a change in DRP1 SUMOylation during mitosis, however, the cytosolic pool of DRP1 continues to migrate as a doublet (Fig. 6*E*), suggesting the involvement of another modification at this time. Therefore, cell cycle-dependent changes in other post-translational modifications may also contribute to the labile properties of DRP1 during G_2/M (5). These data highlight the integration of mitochondrial morphology with cellular cues, and provide insight into the role of SUMOylation enzymes as a switch to modulate mitochondrial shape.

Importantly, our previous data (6, 8), along with this study (Fig. 5), reveal additional mitochondrial targets that likely also play important roles in the G_2/M transition. We are currently pursuing the mitochondrial SUMO proteome in an effort to understand the contribution of mitochondrial deSUMOylation to cell cycle transition. Because SenP5 also deSUMOylates SUMO2/3 (21, 24), it will be important to follow the potential function of these conjugates and the substrates of mixed chains between SUMO1, -2, and -3. For now, these data are the first to provide a direct molecular link between the breakdown of the nucleoli and the preparation of the mitochondria to complete the cell cycle. Future work will uncover the mechanisms that mediate SenP5 movement from the nucleoli to the mitochondria and provide further insights into how these two organelles are functionally integrated during progression of the cell cycle.

REFERENCES

1. Mandal, S., Guptan, P., Owusu-Ansah, E., and Banerjee, U. (2005) *Dev. Cell* **9,** 843–854
2. Owusu-Ansah, E., Yavari, A., Mandal, S., and Banerjee, U. (2008) *Nat. Genet.* **40,** 356–361
3. Yaffe, M. P. (1999) *Science* **283,** 1493–1497
4. Boldogh, I. R., Fehrenbacher, K. L., Yang, H. C., and Pon, L. A. (2005) *Gene* **354,** 28–36
5. Taguchi, N., Ishihara, N., Jofuku, A., Oka, T., and Mihara, K. (2007) *J. Biol. Chem.* **282,** 11521–11529
6. Harder, Z., Zunino, R., and McBride, H. (2004) *Curr. Biol.* **14,** 340–345
7. Wasiak, S., Zunino, R., and McBride, H. M. (2007) *J. Cell Biol.* **177,** 439–450
8. Zunino, R., Schauss, A., Rippstein, P., Andrade-Navarro, M., and McBride, H. M. (2007) *J. Cell Sci.* **120,** 1178–1188
9. Geiss-Friedlander, R., and Melchior, F. (2007) *Nat. Rev. Mol. Cell Biol.* **8,** 947–956
10. Martin, S., Wilkinson, K. A., Nishimune, A., and Henley, J. M. (2007) *Nat. Rev. Neurosci.* **8,** 948–959
11. Palvimo, J. J. (2007) *Biochem. Soc. Trans.* **35,** 1405–1408
12. Pichler, A., Gast, A., Seeler, J. S., Dejean, A., and Melchior, F. (2002) *Cell* **108,** 109–120
13. Kagey, M. H., Melhuish, T. A., and Wotton, D. (2003) *Cell* **113,** 127–137
14. Pungaliya, P., Kulkarni, D., Park, H. J., Marshall, H., Zheng, H., Lackland, H., Saleem, A., and Rubin, E. H. (2007) *J. Proteome Res.* **6,** 3918–3923
15. Hammer, E., Heilbronn, R., and Weger, S. (2007) *FEBS Lett.* **581,** 5418–5424
16. Rajendra, R., Malegaonkar, D., Pungaliya, P., Marshall, H., Rasheed, Z., Brownell, J., Liu, L. F., Lutzker, S., Saleem, A., and Rubin, E. H. (2004) *J. Biol. Chem.* **279,** 36440–36444
17. Ivanov, A. V., Peng, H., Yurchenko, V., Yap, K. L., Negorev, D. G., Schultz, D. C., Psulkowski, E., Fredericks, W. J., White, D. E., Maul, G. G., Sadofsky, M. J., Zhou, M. M., and Rauscher, F. J., 3rd (2007) *Mol. Cell* **28,** 823–837
18. Johnson, E. S. (2004) *Annu. Rev. Biochem.* **73,** 355–382
19. Li, S. J., and Hochstrasser, M. (1999) *Nature* **398,** 246–251
20. Taylor, D. L., Ho, J. C., Oliver, A., and Watts, F. Z. (2002) *J. Cell Sci.* **115,** 1113–1122
21. Di Bacco, A., Ouyang, J., Lee, H. Y., Catic, A., Ploegh, H., and Gill, G. (2006) *Mol. Cell. Biol.* **26,** 4489–4498
22. Mukhopadhyay, D., and Dasso, M. (2007) *Trends Biochem. Sci.* **32,** 286–295
23. Mukhopadhyay, D., Ayaydin, F., Kolli, N., Tan, S. H., Anan, T., Kametaka, A., Azuma, Y., Wilkinson, K. D., and Dasso, M. (2006) *J. Cell Biol.* **174,** 939–949
24. Gong, L., and Yeh, E. T. (2006) *J. Biol. Chem.* **281,** 15869–15877
25. Matic, I., van Hagen, M., Schimmel, J., Macek, B., Ogg, S. C., Tatham, M. H., Hay, R. T., Lamond, A. I., Mann, M., and Vertegaal, A. C. (2008) *Mol. Cell. Proteomics* **7,** 132–144
26. Zhang, X. D., Goeres, J., Zhang, H., Yen, T. J., Porter, A. C., and Matunis,

M. J. (2008) *Mol. Cell* **29,** 729–741
27. Matic, I., Macek, B., Hilger, M., Walther, T. C., and Mann, M. (2008) *J. Proteome Res.* **7,** 4050–4057
28. Felberbaum, R., and Hochstrasser, M. (2008) *Cell Cycle* **7,** 52–56
29. Bischof, O., Schwamborn, K., Martin, N., Werner, A., Sustmann, C., Grosschedl, R., and Dejean, A. (2006) *Mol. Cell* **22,** 783–794
30. Li, S. J., and Hochstrasser, M. (2003) *J. Cell Biol.* **160,** 1069–1081
31. Neuspiel, M., Zunino, R., Gangaraju, S., Rippstein, P., and McBride, H. M. (2005) *J. Biol. Chem.* **280,** 25060–25070
32. Stein, G. S., and Borun, T. W. (1972) *J. Cell Biol.* **52,** 292–307
33. Meloche, S., and Pouysségur, J. (2007) *Oncogene* **26,** 3227–3239
34. Blagosklonny, M. V. (2007) *Cell Cycle* **6,** 70–74
35. Scholzen, T., and Gerdes, J. (2000) *J. Cell. Physiol.* **182,** 311–322
36. Varadi, A., Johnson-Cadwell, L. I., Cirulli, V., Yoon, Y., Allan, V. J., and Rutter, G. A. (2004) *J. Cell Sci.* **117,** 4389–4400
37. Cereghetti, G. M., Stangherlin, A., Martins de Brito, O., Chang, C. R., Blackstone, C., Bernardi, P., and Scorrano, L. (2008) *Proc. Natl. Acad. Sci. U.S.A.* **105,** 15803–15808
38. Shin, H. W., Takatsu, H., Mukai, H., Munekata, E., Murakami, K., and Nakayama, K. (1999) *J. Biol. Chem.* **274,** 2780–2785
39. Fukushima, N. H., Brisch, E., Keegan, B. R., Bleazard, W., and Shaw, J. M. (2001) *Mol. Biol. Cell* **12,** 2756–2766
40. Bhar, D., Karren, M. A., Babst, M., and Shaw, J. M. (2006) *J. Biol. Chem.* **281,** 17312–17320
41. Ingerman, E., Perkins, E. M., Marino, M., Mears, J. A., McCaffery, J. M., Hinshaw, J. E., and Nunnari, J. (2005) *J. Cell Biol.* **170,** 1021–1027
42. Xu, Z., Chau, S. F., Lam, K. H., Chan, H. Y., Ng, T. B., and Au, S. W. (2006) *Biochem. J.* **398,** 345–352
43. Ihara, M., Koyama, H., Uchimura, Y., Saitoh, H., and Kikuchi, A. (2007) *J. Biol. Chem.* **282,** 16465–16475
44. Karbowski, M., Neutzner, A., and Youle, R. J. (2007) *J. Cell Biol.* **178,** 71–84
45. McBride, H. M., Neuspiel, M., and Wasiak, S. (2006) *Curr. Biol.* **16,** R551–560
46. Makhnevych, T., Ptak, C., Lusk, C. P., Aitchison, J. D., and Wozniak, R. W. (2007) *J. Cell Biol.* **177,** 39–49
47. Yonashiro, R., Ishido, S., Kyo, S., Fukuda, T., Goto, E., Matsuki, Y., Ohmura-Hoshino, M., Sada, K., Hotta, H., Yamamura, H., Inatome, R., and Yanagi, S. (2006) *EMBO J.* **25,** 3618–3626
48. Nakamura, N., Kimura, Y., Tokuda, M., Honda, S., and Hirose, S. (2006) *EMBO Rep.* **7,** 1019–1022
49. Chang, C. R., and Blackstone, C. (2007) *J. Biol. Chem.* **282,** 21583–21587
50. Cribbs, J. T., and Strack, S. (2007) *EMBO Rep* **8,** 939–944

Appendix 4 Parkin selectively modulates the delivery of oxidized cargo to the lysosomes through a novel vesicular transport pathway